

Western Australian School of Mines

**Adsorption of Gold from Thiosulfate Leaching Solutions
using Polyethylenimine Functionalised Magnetic
Nanoparticles**

Nirmala Damayanthi Ilankoon

**This thesis is presented for the degree of
Doctor of Philosophy
of
Curtin University**

March 2020

Author's Declaration

To the best of my knowledge and belief this thesis contains no material previously published by any other person except where due acknowledgement has been made.

This thesis contains no material which has been accepted for the award of any other degree or diploma in any university.

[Signature]

04/03/2020

[Date]

Abstract

For over a century, cyanidation was known to be the most established method for leaching gold from various ores. However, due to its toxicity and ineffectiveness in leaching gold from refractory carbonaceous ores, a need for an alternative lixiviant arose over time. In the search for an environmentally friendly alternative, thiosulfate seemed to show some promise as a lixiviant for leaching gold from refractory carbonaceous ores. Recently, a calcium thiosulfate and air based leaching system became an industrial reality at Barrick Gold's Goldstrike operation in Nevada, USA. This system is being used to treat double refractory (sulfidic and carbonaceous) gold ores after pre-oxidation in autoclaves.

Although gold leaching by thiosulfate is considerably well understood, gold recovery from pregnant leaching solutions has not been sufficiently explored. A gold thiosulfate complex shows only a very low affinity towards activated carbon (AC), making the well-established carbon in leach (CIL) and carbon in pulp (CIP) processes undesirable for use in gold recovery from thiosulfate leach solutions. Despite the inherent limitations associated with ion exchange (IX) resins, strong base anion exchange resins are able to recover gold from thiosulfate solutions. However, the elution of gold from IX resins is complicated and requires higher eluant concentrations. The use of resin beads necessitates filtration steps in the process. Therefore, the main objectives of this study were to prepare an adsorbent to recover an anionic gold complex from thiosulfate leach solutions that could then be eluted using a lower concentration of eluants. Furthermore characterisation of the adsorbent, reuse of the adsorbent and determination of the adsorption mechanism were accomplished.

To take advantage of magnetic separation process, iron oxide magnetic nanoparticles (MNPs) were chosen for use as the adsorbent core. This avoids many of the intermediate filtration steps which are currently used. In thiosulfate leaching solutions, gold exists as an $Au(S_2O_3)_2^{3-}$ anionic complex. However, adsorption of an anionic complex in an alkaline solution is challenging, due to the negative surface charge of many of the adsorbents at higher pH solutions. Magnetic iron oxide nanoparticles are not an exception in this scenario. Therefore, in order to retain a positive surface charge, even in alkaline solutions, suitable surface functionalisation was essential. Due to its high cationic charge density, availability of an ample amount of amine groups that could be protonated and due to its high point of zero charge (pH_{PZC}), polyethylenimine (PEI) was used as the surface functionalisation agent in the presence of citrate groups, as the intermediate coating layer. The one-pot functionalisation method used was simple and straightforward.

Deagglomeration of MNPs, prior to surface functionalisation form an important part of the uniform surface coating process. An ultrasonic dispersion technique was used for bare (uncoated) nanoparticle dispersion, and longer ultrasonication durations yielded lower hydrodynamic sizes, fairly closer to individual particle diameters. Well dispersed bare MNPs subsequently coated with trisodium citrate, followed by PEI.

The functionalised magnetic nanoparticles, hereinafter termed PEI-MNPs, were comprehensively characterised. X-ray diffraction (XRD), Fourier transform infrared spectroscopy (FTIR) and Raman spectroscopy results revealed the crystalline structure to be pure iron oxide, mainly consisting of magnetite (Fe_3O_4) and maghemite ($\gamma\text{-Fe}_2\text{O}_3$). Successful surface functionalisation with citrate and PEI was verified by X-ray photoelectron spectroscopy (XPS) and FTIR techniques. Following the PEI coating, the surface charge changed to positive, resulting in a significant increase in the point of zero charge (pH_{PZC}) to pH 11. This indicates the potential for using PEI-MNPs in anionic gold complex recovery. The saturation magnetisation of bare MNPs and PEI-MNPs was 60.5 and 52.3 emu/g respectively. Thermogravimetric analysis (TGA) revealed that approximately 10% (weight basis) of functional groups are available on the nanoparticle surfaces. Successful gold loading on to PEI-MNPs was verified by XPS and atom probe tomography (APT) analysis techniques.

A series of laboratory scale batch adsorption experiments was conducted to recover gold from synthetic leach solutions, as well as from a gold ore leachate. The effect of solution pH, temperature, free thiosulfate concentration, copper concentration and adsorbent dosage as well as gold adsorption isotherms, adsorption kinetics and thermodynamic properties were investigated in synthetic leaching solutions. Almost 100% gold adsorption was achieved in pure gold thiosulfate solutions using a 5 g/L adsorbent dosage, with 78% adsorption efficiency in simulated leach solutions using a 20 g/L adsorbent dosage. An adsorbent dosage equivalent to 75 g/L was able to adsorb almost 100% of the gold from a simulated leaching solution in less than 30 minutes. Low free thiosulfate concentrations and high adsorbent dosages yielded greater gold adsorption. The competitive adsorption of some copper and sulfur species was observed in simulated leach solutions. Gold adsorption kinetics were extremely fast, irrespective of the solution composition. The maximum adsorption capacity was 33.8 mg (gold)/g (PEI-MNPs) at 50 °C which was calculated using the Langmuir isotherm model. The adsorption process was spontaneous, exothermic and the adsorption mechanism was determined as physical adsorption through isotherm and thermodynamic approaches. Adsorption experiments with a gold ore leachate were performed based on a central composite design (CCD) and optimisation of the process parameters was carried out using a response surface methodology (RSM). The optimisation results revealed that higher adsorbent dosages

enhance gold adsorption efficiency. Successful gold adsorption from real ore leachates and effective gold elution were corroborated by these experiments.

Selective copper and gold elution was performed using a two-step elution process; copper pre-elution followed by gold elution. Almost 100% selective copper elution was accomplished with 0.02 M ethylenediaminetetraacetic acid (EDTA) solution, while 0.01 M NaOH was capable of eluting 100% gold in the following process. This level of elution enhances the potential for using this adsorbent for gold recovery from thiosulfate leaching systems. Elution kinetics were sufficiently fast to attain 100% in 15 minutes for both gold and copper in batch operations. The reuse of PEI-MNPs for adsorption was evaluated and only a 12-15% drop in adsorption efficiency was observed after six cycles.

In summary, this is the first time, as far as it is known, that the use of PEI coated iron oxide magnetic nanoparticles for anionic gold (I) adsorption from non-ammoniacal thiosulfate leaching solutions in alkaline pH solutions has been explored. This study hopes to lay the foundations for further exploration of the use of functionalised magnetic nanosorbents for gold recovery from thiosulfate leaching solutions in the future. The fast kinetics, simplicity of the metal elution process and ease of solid-liquid separation by magnetic separation are some of the main advantages with this adsorbent. The overall results of this study have revealed the possibility of considering PEI-MNPs as a potential adsorbent in gold recovery.

List of Abbreviations and Acronyms

AAS	Atomic absorption spectroscopy
AC	Activated Carbon
ANOVA	Analysis of variance
APT	Atom Probe Tomography
BDL	Below detection limit
BET	Brunauer-Emmett-Teller
CCD	Central composite design
CIL	Carbon in leach
CIP	Carbon in pulp
DI	De-ionised
DLS	Dynamic light scattering
D-R	Dubinin-Radushkevich
DSC	Differential scanning calorimetry
EDL	Electric double layer
EDTA	Ethylenediaminetetraacetic acid
emu	electromagnetic unit
FC	Field cooled
α -Fe ₂ O ₃	Hematite
γ -Fe ₂ O ₃	Maghemite
Fe ₃ O ₄	Magnetite
FTIR	Fourier transform infrared spectroscopy
FWHM	Full width half maximum
HPLC	High performance liquid chromatography
ICP-MS	Inductively coupled plasma mass spectroscopy
ICP-OES	Inductively coupled plasma optical emission spectroscopy
IX	Ion exchange
MNPs	Magnetic nanoparticles
NPs	Nanoparticles
Oe	Oersted
PDF	Powder diffraction file
PdI	Polydispersity index
PEI	Polyethylenimine
PZC	Point of zero charge

QXRD	Quantitative X-ray diffraction
RIL	Resin in leach
RIP	Resin in pulp
RSM	Response surface methodology
SEM	Scanning electron microscopy
SQUID	Superconducting quantum interference device
TEM	Transmission electron microscopy
TGA	Thermogravimetric analysis
TOMAC	trioctylmethylammonium chloride
TRAO	trialkyl amine oxide
US	ultrasonic
XPS	X-ray photoelectron spectroscopy
XRD	X-ray diffraction
XRF	X-ray fluorescence spectroscopy
ZFC	Zero field cooled

Acknowledgements

I would like to express my sincere gratitude to my supervisors, Professor Chris Aldrich and Professor Jacques Eksteen for their expertise, guidance, encouragement and patience throughout the last few years. I would especially like to thank Dr Elsayed Oraby for the guidance, suggestions and support that he has given me in conducting my experiments. Without the supervision of these esteemed persons, this work would not have been possible.

I would like to extend my gratitude to all the wonderful members of the WASM Gold technology group; Greg, Karen, Jim, Alireza, Bennson, Chong, Hazel, Mpinga, Peo, Huan, Deng, Jason, Yang and Irlina to name a few, for their helpful discussions, friendship and good company, which made the environment an interesting one in which to learn and grow.

I would also like to thank staff members of the John de Later centre (Ms Elaine Miller, Dr Jean-Pierre Veder, Ms Veronica Avery, Dr David Saxey, Dr Zakaria Quadir and staff members of the Curtin Chemistry Department (Dr Franca Jones, Dr Thomas Becker and Mr Peter Chapman) for assisting me with much of the particle characterisation and solution analysis. I would like to say thank to Ms Danielle Hewitt at CSIRO Minerals, Waterford for her great support in HPLC analysis. I would also like to thank Ms Felicity Lewis for her great help with language and grammar corrections in my thesis.

I should also mention that this research is supported by an Australian Government Research Training Program (RTP) Scholarship.

I wish to express my appreciation for all the help and support given by my friends Tharanga, Erandi (and family) and Indika (and family) in many ways.

Finally, I would like to express my wholehearted gratitude to my husband Nuwan for his encouragement, motivation, patience and understanding. Thanks are also due to my loving sons Thenu and Kehan, for spending many many hours in child care and at after school care centres, allowing me to conduct my research. This would not have been possible without their unconditional love and sacrifice. I am deeply appreciative to my parents and parents in-law for flying thousands of miles to help with our family commitments at times when their support was most needed.

Dedication

To my family.....

Table of Contents

Abstract.....	iii
List of Abbreviations and Acronyms.....	vi
Acknowledgements.....	viii
Dedication.....	ix
Table of Contents.....	x
List of Figures.....	xvii
List of Tables.....	xxii
List of Publications.....	xxiv
Chapter 1 Introduction.....	1
1.1 Background.....	1
1.2 Research Question and Hypothesis.....	5
1.3 Objectives of the Study.....	7
1.4 Scope of the Study.....	8
1.5 Thesis Structure.....	9
Chapter 2 Literature Review.....	11
2.1 Introduction and Chapter Objectives.....	11
2.2 Properties and applications of gold.....	11
2.3 Double Refractory Gold Ores.....	12
2.4 Gold Hydrometallurgy.....	13
2.5 Thiosulfate Leaching of Gold.....	15
2.5.1 An Overview of Thiosulfate.....	15
2.5.2 Stability of Thiosulfate.....	16
2.5.2.1 Solution pH and Temperature.....	18
2.5.2.2 Availability of Copper.....	18
2.5.2.3 Availability of Oxygen/air and Sulfur Species.....	19
2.5.2.4 Presence of Impurities.....	19
2.5.3 Different Thiosulfate Leaching Systems.....	20
2.5.3.1 Copper Ammoniacal System.....	21
2.5.3.2 Calcium Thiosulfate - Air Leaching System.....	22
2.5.3.3 Ferric-EDTA System.....	25
2.5.3.4 Ferric-Oxalate System.....	25

2.5.3.5	Nickel-Ammonia System	26
2.6	Gold Recovery from Thiosulfate Leaching Solutions	26
2.6.1	Ion Exchange Resin	26
2.6.2	Activated Carbon	28
2.6.3	Mesoporous silica	29
2.6.4	Cementation	29
2.6.5	Chemical Reduction.....	30
2.6.6	Electrowinning.....	31
2.6.7	Solvent Extraction.....	31
2.6.8	Chemical Precipitation.....	32
2.7	Adsorption	33
2.7.1	Adsorption Mechanisms	33
2.7.2	Adsorption Isotherms.....	34
2.7.3	Adsorption Kinetics	35
2.7.4	Selectivity of Anions	36
2.8	Magnetic Nanomaterials	37
2.8.1	Magnetic Separation	38
2.8.1.1	Superparamagnetism.....	38
2.8.1.2	High Gradient Magnetic Separation.....	39
2.8.1.3	Magnetic separation of nanoscale magnetic particles	40
2.8.2	Iron Oxide Nanoparticles.....	42
2.8.2.1	Magnetite (Fe_3O_4)	42
2.8.2.2	Maghemite ($\gamma\text{-Fe}_2\text{O}_3$)	43
2.8.2.3	Hematite ($\alpha\text{-Fe}_2\text{O}_3$).....	44
2.8.3	Nanoparticle Synthesis	45
2.8.4	Surface Charge and Zeta Potential of Iron Oxide Nanoparticles.....	46
2.8.5	Nanoparticle Functionalisation	47
2.8.5.1	Citrate coating	47
2.8.5.2	Polyethylenimine coating.....	49
2.8.6	Metal and Metal Complexes Adsorption	52
2.8.7	Limitations Associated with Nanoparticles and Possible Remedies.....	54
2.8.7.1	Nanoparticle Aggregation and Agglomeration	54
2.8.7.2	Nanoparticle Dissolution.....	55
2.8.7.3	Magnetic Separation from a Solution	55
2.8.7.4	Environmental Concerns and Toxicity of MNPs.....	56

2.9	Gold and Copper Elution	56
2.9.1	Gold and Copper Elution from Ion Exchange Resins.....	56
2.9.2	Gold Elution from Nanoparticles.....	58
2.9.3	Copper Elution from Nanoparticles.....	60
2.10	Chapter Summary	60
Chapter 3	Materials and Experimental Methods	62
3.1	Introduction and Chapter Objectives	62
3.2	Materials and Chemicals.....	62
3.3	Functionalisation of MNPs	64
3.4	Characterisation of MNPs.....	64
3.4.1	Scanning Electron Microscope (SEM)	64
3.4.2	Transmission Electron Microscope (TEM)	64
3.4.3	Dynamic Light Scattering (DLS).....	65
3.4.4	Zeta Potential	65
3.4.5	X-ray Diffraction (XRD) and Quantitative X-ray Diffraction (QXRD).....	65
3.4.6	Raman Spectroscopy.....	66
3.4.7	X-ray Photoelectron Spectroscopy (XPS)	66
3.4.8	Fourier Transform Infrared Spectroscopy (FTIR)	66
3.4.9	X-ray Fluorescence Spectroscopy (XRF)	66
3.4.10	Atom Probe Tomography (APT)	67
3.4.11	SQUID Magnetisation Measurements	69
3.4.12	Thermogravimetric Analyses (TGA) and Differential Scanning Calorimetry (DSC).....	70
3.4.13	BET Surface Area.....	70
3.5	Solution Analysis.....	70
3.5.1	Atomic Absorption Spectroscopy (AAS)	70
3.5.2	Inductively Coupled Plasma Mass Spectroscopy and Optical Emission Spectroscopy (ICP-MS and ICP-OES)	71
3.5.3	High Performance Liquid Chromatography (HPLC).....	71
3.6	Nanoparticle Deagglomeration by Ultrasonic Dispersion	71
3.7	pH Dependent Dissolution of MNPs	72
3.8	Adsorption Experiments with Synthetic Leaching Solutions	73
3.8.1	Calcium Thiosulfate – Air Leaching System.....	73
3.8.1.1	Adsorbent dosage.....	73

3.8.1.2	Solution pH	73
3.8.1.3	Copper concentration	73
3.8.1.4	Thiosulfate Concentration	74
3.8.2	Other Thiosulfate Leaching Systems	74
3.8.2.1	Copper-Ammoniacal System	74
3.8.2.2	Nickel-Ammonia System	74
3.8.2.3	Ferric-Oxalate System.....	74
3.8.2.4	Ferric-EDTA System	75
3.9	Adsorption Kinetics Studies	75
3.10	Adsorption Isotherm Studies	76
3.11	Thermodynamic Studies	76
3.12	Gold and Copper Elution	76
3.13	Reuse of MNPs	77
3.14	Experiments with Gold Ore Samples.....	78
3.14.1	Leaching Tests	78
3.14.2	Adsorption Experiments with Gold Ore Leaching Solutions	78
3.14.3	Experimental Design.....	78
3.14.4	Metal Elution	80
Chapter 4	Nanoparticle Functionalisation and Characterisation	81
4.1	Introduction and Chapter Objectives	81
4.2	Functionalisation of MNPs	82
4.2.1	Citrate Coating.....	83
4.2.2	PEI Coating.....	83
4.3	Characterisation of MNPs.....	85
4.3.1	Size and Morphology	85
4.3.1.1	Scanning Electron Microscopy and Transmission Electron Microscopy.....	85
4.3.1.2	Dynamic Light Scattering	86
4.3.2	Zeta Potential	88
4.3.3	Crystal Structure Analysis	89
4.3.3.1	X-ray Diffraction.....	89
4.3.3.2	Raman Spectroscopy.....	92
4.3.4	Bulk and Surface Composition Analysis	94
4.3.4.1	X-ray Photoelectron Spectroscopy.....	94
4.3.4.2	FT-IR spectroscopy.....	99

4.3.4.3	X-ray Fluorescence Analysis of MNPs.....	102
4.3.5	Atom Probe Tomography Analysis of MNPs.....	102
4.3.6	Magnetic Properties	111
4.3.7	Thermogravimetric Analysis	113
4.4	Deagglomeration of MNPs by Ultrasonic Dispersion	115
4.4.1	Dispersion of Bare MNPs in DI Water	115
4.4.2	Dispersion of Bare MNPs in Citrate Solutions	116
4.4.3	Dispersion of PEI-MNPs in Surfactant Solution	116
4.4.4	Dispersion of PEI-MNPs in DI Water	117
4.5	pH Dependent Dissolution of MNPs	118
4.6	Chapter Summary	119
Chapter 5	Gold Adsorption by Polyethylenimine Coated Magnetic Nanoparticles	121
5.1	Introduction and Chapter Objectives	121
5.2	Gold Adsorption	121
5.2.1	Effect of Nanoparticle Dosage.....	122
5.2.2	Effect of Solution pH.....	123
5.2.3	Effect of Copper Concentration.....	123
5.2.4	Effect of Thiosulfate Concentration.....	125
5.3	Competitive Adsorption of Copper and Sulfur Species.....	127
5.3.1	Copper Adsorption.....	127
5.3.2	Sulfur Species Adsorption	127
5.3.3	Catalytic Degradation of Thiosulfate.....	129
5.3.4	Comparison of Gold, Copper and Sulfur Species Adsorption with IX Resin and Activated Carbon	131
5.4	Gold Adsorption Kinetics	132
5.4.1	Pure Gold Thiosulfate Solutions.....	132
5.4.2	Synthetic Leaching Solutions	133
5.4.3	Kinetics Model Fitting	134
5.5	Gold Adsorption Isotherms.....	137
5.6	Thermodynamic Studies	140
5.7	Gold Adsorption from Other Thiosulfate Leaching Systems	143
5.8	Chapter Summary	145

Chapter 6	Metal Elution and PEI-MNPs Reuse Studies.....	147
6.1	Introduction and Chapter Objectives	147
6.2	Parameters.....	147
6.2.1	Solid to Liquid Ratio.....	147
6.2.2	Elution Efficiency	147
6.3	Copper Pre-elution using EDTA.....	148
6.3.1	Effect of EDTA Concentration	148
6.3.2	Effect of Solution pH.....	149
6.3.3	Effect of Solution Temperature	150
6.3.4	Effect of Solid to Liquid Ratio	151
6.4	Gold Elution using NaOH.....	151
6.4.1	Effect of NaOH Concentration	151
6.4.2	Effect of Solution Temperature	152
6.4.3	Effect of Solid to Liquid Ratio	153
6.5	Elution Kinetics	154
6.5.1	Copper Elution Kinetics.....	154
6.5.2	Gold Elution Kinetics	154
6.6	Reuse of the Adsorbent.....	155
6.7	Chapter Summary	156
Chapter 7	Leaching, Metal Recovery and Elution Experiments with Gold Ore Samples.....	158
7.1	Introduction and Chapter Objectives	158
7.2	Leaching	158
7.3	Adsorption	159
7.4	Response Surface Methodology	161
7.4.1	Gold Adsorption	162
7.4.2	Copper Adsorption.....	165
7.4.3	Optimisation of Parameters for Maximum Gold Adsorption	166
7.4.4	Validation Experiments	168
7.5	Elution.....	168
7.5.1	Gold and Copper Elution	168
7.5.2	Elution of Other Elements	169
7.5.3	Comparison with Synthetic Leaching Solutions.....	170
7.6	Chapter Summary	170

Chapter 8	Conclusions and Recommendations	171
8.1	Functionalisation of Magnetic Nanoparticles	171
8.2	Characterisation of the Adsorbent	173
8.3	Evaluation of the Influence of Adsorption Process Parameters on Gold Adsorption Efficiency	174
8.3.1	Adsorption from Synthetic Leaching Solutions.....	174
8.3.2	Adsorption from Gold Ore Leaching Solutions.....	175
8.4	Determination of Adsorption Mechanism through Adsorption Kinetics, Adsorption Isotherms and Thermodynamic Analyses	175
8.5	Metal Elution and Reuse of PEI-MNPs	177
8.6	Schematic representation of the process	177
8.7	Recommendations for Future Investigations	179
	References.....	181
	Appendices.....	203
Appendix A	Other Adsorbents Attempted	203
Appendix B	Detailed Methods and Specifications of the Instruments used for Characterisation	206
B.1	XPS	206
B.2	XRD and QXRD	206
B.3	HPLC	207
Appendix C	Hydrodynamic Size Data by DLS.....	208
Appendix D	Different Metal Elution Systems	209
D.1	NaOH.....	209
D.2	HCl.....	210
D.3	Glycine.....	211
D.4	Thiosulfate, Sulfite and Chloride.....	212
Appendix E	Co-Author Attribution Statement	213
Appendix F	Permission Statements	214

List of Figures

Figure 1-1. Schematic representation of thesis chapter arrangement.....	10
Figure 2-1. Structure of gold thiosulfate complex derived from (Grosse et al. 2003) with permission.....	15
Figure 2-2. Stepwise stability constants of thiosulfate complexes (derived from (Grosse et al. 2003) with permission.	16
Figure 2-3. Oxidation states of sulfur species (derived from (O'Malley 2002)).....	17
Figure 2-4. Eh-pH diagram of Au-S-H ₂ O system at 25 °C derived from (Sitando 2017).....	22
Figure 2-5. Eh-pH diagram of Cu - S ₂ O ₃ ²⁻ - H ₂ O system at 25 °C, 0.2 M S ₂ O ₃ ²⁻ and 0.5 mM Cu(II) after (Zhang 2004).....	23
Figure 2-6. Magnetic matrices used in HGMS (Derived from HGMS brochure-Metso).....	40
Figure 2-7. Schematic illustration of crystal structure of magnetite (the black sphere is Fe ²⁺ , the green sphere is Fe ³⁺ and the red sphere is O ²⁻). Derived from (Wu et al. 2015).....	43
Figure 2-8. Schematic illustrations of crystal structure of maghemite derived from (Wu et al. 2015).....	44
Figure 2-9. Schematic illustrations of crystal structure of hematite Derived from (Wu et al. 2015).....	44
Figure 2-10. Schematic diagram of electrical double layer in particle-solution interface (reproduced from (Vidojkovic and Rakin 2016) with permission).....	47
Figure 2-11. Chemical structures of citric acid and trisodium citrate.....	48
Figure 2-12. Chemical structures of linear and branched Polyethylenimine.....	50
Figure 2-13. Simplified trithionate and sulfite elution process (reproduced from (Aylmore 2016c) with permission).....	58
Figure 3-1. Experimental set up of adsorption experiments in the orbital shaker (top) and magnetic separation (bottom). The beakers in the bottom image consist of 20 g/L PEI-MNPs concentration. An external magnetic field was applied to separate the PEI-MNPs.....	63
Figure 3-2. Schematic diagram of nanoparticle encapsulation in ZnO matrix (side view).....	67
Figure 3-3. APT specimen preparation process.	68
Figure 3-4. Cameca LEAP 4000X HR atom probe tomography at John de Laeter centre, Curtin University (image provided by Dr David Saxey).....	69
Figure 3-5. Instrument set up of ultrasonic dispersion of nanoparticles.....	72
Figure 4-1. Schematic illustration of surface functionalisation of bare MNPs with trisodium citrate and PEI.....	82

Figure 4-2. Nanopowder (bare MNPs) as received from the manufacturer.....	85
Figure 4-3. SEM images of bare MNPs (left) and PEI-MNPs (right)	85
Figure 4-4. TEM images bare MNPs (left) and PEI-MNPs (right).....	86
Figure 4-5. Thickness measurements of the surface coating layer	86
Figure 4-6. Hydrodynamic size distribution of 5 g/L bare MNPs before ultrasonic dispersion (A), after 600 s dispersion in a 10g/L trisodium citrate solution at pH 9.5 (B), PEI-MNPs (citrate coated and then PEI coated in 5% PEI solution at pH 9.5 and 90 °C and washed (C), and Au-PEI-MNPs (adsorption conducted in 10 mg/L gold, 0.1 M thiosulfate and 20 mg/L Cu solutions at 50°C and pH 8 (D)	87
Figure 4-7. Zeta potential measurements of MNPs	89
Figure 4-8. XRD patterns of bare MNPs and PEI coated MNPs	91
Figure 4-9. XRD diffractograms of bare MNPs	91
Figure 4-10. XRD diffractograms of PEI-MNPs	92
Figure 4-11. Peak 5 1 1 of bare MNPs and PEI-MNPs	92
Figure 4-12. Raman spectrum of bare MNPs (dotted lines) and PEI-MNPs (solid lines) at different laser powers in 60 s acquisition time.....	93
Figure 4-13. XPS survey spectra of bare MNPs, PEI-MNPs and Au-PEI-MNPs	94
Figure 4-14. Deconvoluted high resolution Fe 2p spectrum of PEI-MNPs (top) and bare MNPs (bottom)	96
Figure 4-15. Deconvoluted high resolution N 1s spectrum of PEI-MNPs.....	97
Figure 4-16. Deconvoluted high resolution C 1s spectrum of PEI-MNPs.....	97
Figure 4-17. Deconvoluted high resolution O 1s spectrum of PEI-MNPs.....	98
Figure 4-18. Deconvoluted high resolution Au 4f spectrum of Au-PEI-MNPs (adsorption was conducted in a pure gold thiosulfate solution (Sample 1) and in a synthetic leaching solution (Sample 2)).....	99
Figure 4-19. FTIR spectra of bare MNPs, Cit-MNPs, PEI-MNPs, pristine trisodium citrate and PEI.....	102
Figure 4-20. Schematic representation of APT. The diagram provided by Dr David Saxey, JDL Centre, Curtin University.	104
Figure 4-21. APT image of Au-PEI-MNPs arrangement in the needle specimen. The colours used are purple for Fe, turquoise for Zn, green for N, blue for C, golden yellow for Au and red for Cu.	104
Figure 4-22. APT mass spectrum of Au-PEI-MNPs. The major peaks are labelled without their charge.	105

Figure 4-23. APT images of bare MNPs (a), the atom maps of PEI-MNPs showing: carbon distribution (b), nitrogen distribution (c) and hydrogen distribution (d) and surface coating layer (e). The colours used are purple for Fe, green for N, blue for C and olive for H. the PEI coating was performed at pH 9.5 and 90 °C.....	107
Figure 4-24. APT images of metal adsorbed PEI-MNPs (a and b) and atom map of nitrogen (c), gold (d), copper (e) and sulfur (f). The colours used are purple for Fe, green for N, blue for C, golden yellow for Au, red for Cu and light blue for S.....	108
Figure 4-25. Composition profile of bare MNPs in the form of a proximity histogram	110
Figure 4-26. Composition profile of Au-PEI-MNPs in the form of a proximity histogram	110
Figure 4-27. Field dependent magnetisation measurements at a temperature of 300K	111
Figure 4-28. Temperature dependent magnetisation of bare MNPs and PEI-MNPs .	112
Figure 4-29. TGA and DSC curves of bare MNPs	114
Figure 4-30. TGA and DSC curves of PEI-MNPs.....	114
Figure 4-31. Hydrodynamic size distribution of nanoparticles dispersed in DI water at pH 9.5	115
Figure 4-32. Hydrodynamic size distribution of bare MNPs dispersed in trisodium citrate solutions at pH 9.5	116
Figure 4-33. Hydrodynamic size distribution of PEI-MNPs dispersed in commercial surfactant at pH 7.....	117
Figure 4-34. Hydrodynamic size distribution of PEI-MNPs dispersed in DI water at pH 7	117
Figure 5-1. Composition of Au, Cu, S and Ca as a percentage (weight basis) in synthetic leaching solution consists of 0.1 M calcium thiosulfate, 10 mg/L gold thiosulfate and 20 mg/L copper sulfate.	122
Figure 5-2. Effect of magnetic nanoparticle dosage on gold adsorption. The solution consists of 0.1 M thiosulfate, 20 mg/L copper, approximately 10 mg/L gold at pH 8, 50°C after one hour adsorption time.....	122
Figure 5-3. Effect of initial solution pH on gold adsorption after one hour in solutions consisted of 0.1 M thiosulfate, 20 mg/L copper, approximately 10 mg/L gold and 5 g/L PEI-MNPs at 50°C.....	123
Figure 5-4. Effect of initial Copper concentration on gold adsorption efficiency after one hour with 0.1 M thiosulfate, 0-120 mg/L Cu, 10 mg/L Au at pH 8 and 50 °C.....	125
Figure 5-5. Effect of initial copper concentration and time on gold adsorption	125

Figure 5-6. Effect of initial free thiosulfate concentration on gold adsorption in 20 mg/L copper, approximately 10 mg/L gold at pH 8 and 50°C temperature solutions at different adsorbent dosages.	126
Figure 5-7. Thiosulfate degradation (A) and the formation of tetrathionate (B), trithionate (C) and sulfate (D) in pure thiosulfate solutions without copper (Solution 1) and in thiosulfate, gold and copper solutions (Solution 2)	130
Figure 5-8. Comparison of metal adsorption efficiency of PEI-MNPs with IX resins and AC from a solution consisting of 0.1 M thiosulfate, 10 mg/L gold and 21 mg/L copper, pH 8, 50 °C, after 1 hour with an adsorbent dosage of 5 g/L (a) and 20 g/L (b).	132
Figure 5-9. Gold adsorption kinetics in pure gold thiosulfate solution at pH 8 and 50 °C.....	133
Figure 5-10. Comparison of gold adsorption kinetics in different solutions (Solution 1 = 0.09 M CaS ₂ O ₃ + 10 mg/L Au + 20 mg/L Cu; Solution 2 = 0.09 M CaS ₂ O ₃ + 10 mg/L Au) at pH 8 and 50 °C.....	133
Figure 5-11. Pseudo-first-order adsorption kinetics of Au adsorption onto PEI-MNPs	135
Figure 5-12. Pseudo-second-order adsorption kinetics of gold adsorption onto PEI-MNPs	135
Figure 5-13. Intra-particle diffusion model for the gold adsorption onto PEI-MNPs	137
Figure 5-14. Langmuir isotherm model fitting. Synthetic leaching solutions consist of 0.1 M thiosulfate, 20 mg/L copper and different initial gold concentrations ranging from 4 to 429 mg/L. Adsorption was conducted at temperatures of 25, 35 and 50°C and a pH of 8.	139
Figure 5-15. Freundlich isotherm model fitting. Synthetic leaching solutions consist of 0.1 M thiosulfate, 20 mg/L copper and different initial gold concentrations ranging from 4 to 429 mg/L. Adsorption was conducted at temperatures of 25, 35 and 50°C and a pH of 8.	140
Figure 5-16. ln Kc vs 1/T.....	143
Figure 5-17. Gold adsorption efficiency in different thiosulfate leaching systems at 5 g/L adsorbent dosage	144
Figure 5-18. Metal adsorption in different thiosulfate leaching systems at 5g/L adsorbent dosage. The solution preparation is according to Table 5-5.	144
Figure 6-1. Copper complexation with EDTA forming an octahedral complex (derived from (Tseng et al. 2009) with permission).....	148
Figure 6-2. Effect of EDTA concentration on metal elution at pH 6, 2.5 g/L of S/L ratio and 25 °C for 15 minutes.....	149
Figure 6-3. Effect of solution pH on metal elution at copper pre-elution stage with 0.02 M EDTA at 25 °C and 2.5 g/L S/L ratio for 15 minutes.....	150

Figure 6-4. Effect of solution temperature on gold and copper elution efficiency in 0.02 M EDTA solution at 15 minutes and 2.5 g/L of S/L ratio	150
Figure 6-5. Effect of solid to liquid ratio on metal elution with 0.02 M EDTA at pH 6 and 25 °C after 15 minutes	151
Figure 6-6. Effect of NaOH concentration on gold elution at 50 C and 2.5 g/L of S/L ratio	152
Figure 6-7. Effect of solution temperature on gold elution efficiency in 0.01 M NaOH solutions at 2.5 g/L of S/L ratio at 15 minutes.....	153
Figure 6-8. Effect of S/L ratio on gold elution efficiency in 0.01 M NaOH solutions at 50°C	153
Figure 6-9. Copper elution kinetics at different temperatures (25, 40 and 50 °C), at pH 8 and 2.5 g/L S/L ratio	154
Figure 6-10. Gold elution kinetics at different temperatures (25, 40 and 50 °C), at pH 12 and 2.5 g/L S/L ratio	155
Figure 6-11. Reuse of eluted PEI-MNPs up to six cycles. The adsorption solutions consist of 10 mg/L gold, 20 mg/L copper and 0.1 M free thiosulfate (Solution 1) at 5 and 20 g/L adsorbent dosages and 10 mg/L gold thiosulfate (Solution 2) at 5 g/L adsorbent dosage at a pH value of 8 and 50 °C	156
Figure 7-1. Response surfaces of interactive effect of adsorbent dosage and time on gold adsorption efficiency (left) and copper adsorption efficiency (right)	164
Figure 7-2. Response surfaces of interactive effect of adsorbent dosage and temperature on gold adsorption efficiency (left) and copper adsorption efficiency (right)	164
Figure 7-3. Response surfaces of interactive effects of temperature and time on gold adsorption efficiency (left) and copper adsorption efficiency (right) .	164
Figure 7-4. Predicted Vs actual values of gold adsorption (left) and copper adsorption (right)	165
Figure 7-5. Desirability of satisfying the selected optimisation criteria 2	167
Figure 7-6. Gold elution efficiency at different S/L ratio	169
Figure 8-1. Schematic representation of the adsorption-elution-reuse cycle	178
Figure App D.1 Gold elution efficiency at different temperatures by NaOH at pH 12	210
Figure App D.2 Copper elution efficiency at different temperatures by NaOH at pH 12	210

List of Tables

Table 2-1. Stability constants (β) of some Au (I) and Au (III) complexes	14
Table 2-2. Summary of different thiosulfate based leaching systems.....	20
Table 2-3. Process conditions of some nanoparticle synthesis methods and properties	45
Table 2-4. Some magnetic nanoadsorbents used for gold and copper adsorption from aqueous solutions.....	53
Table 2-5. Gold elution from different adsorbents.....	59
Table 2-6. Copper elution from different adsorbents.....	60
Table 3-1. Independent variables and their corresponding levels.....	80
Table 4-1. Intensity based Z-average, polydispersity index (PDI) and peak positions of nanoparticle size distribution	88
Table 4-2. XPS analysis data of main peaks.....	95
Table 4-3. Summary of functional group frequencies from FTIR analysis	101
Table 4-4. XRF analysis of as received bare MNPs and PEI-MNPs for bulk composition.....	102
Table 4-5. Summary of hydrodynamic sizes of PEI-MNPs in different media	118
Table 4-6. Nanoparticle dissolution in acidic and alkaline solutions before and after coating.....	119
Table 5-1. Sulfur species analysis results by HPLC and copper adsorption analysis results.....	128
Table 5-2. Kinetic parameters of pseudo-first-order and pseudo-second-order models.....	136
Table 5-3. Model parameters of Langmuir and Freundlich adsorption isotherms.....	138
Table 5-4. Summary of the thermodynamic parameters	142
Table 5-5. Conditions and content of leaching solutions of different thiosulfate systems.....	143
Table 7-1. Mineralogical composition of ore sample by QXRD analysis	159
Table 7-2. Elemental composition of the ore sample by XRF and LECO combustion analysis	159
Table 7-3. Concentration of elements in the filtered solution after 48 hours of leaching.....	159
Table 7-4. Experiment design matrix and corresponding gold and copper adsorption efficiencies.....	160
Table 7-5. Adsorption efficiency of other elements available in leaching solution based on particle analysis and (XRF) and solution analysis (ICP- MS)	161

Table 7-6. Analysis of variance (ANOVA) for the quadratic model of gold adsorption	162
Table 7-7. Coefficients of determination for the quadratic model of gold adsorption	163
Table 7-8. Analysis of variance (ANOVA) for the quadratic model of copper adsorption	165
Table 7-9. Coefficients of determination for the quadratic model of copper adsorption	166
Table 7-10. Optimisation criteria	167
Table 7-11. Actual vs predicted values of reconfirmation experiments	168
Table 7-12. Elution efficiency of gold, copper and other competitively adsorbed elements	169
Table 8-1. Hydrodynamic sizes of nanoparticles after ultrasonic dispersion	172
Table 8-2. Summary of the adsorption kinetics model parameters.....	176
Table 8-3. Summary of the adsorption isotherm model parameters	176
Table 8-4. Summary of thermodynamic parameters of gold adsorption.....	176
Table App A.1. Different magnetic nanoparticles attempted in the study	204
Table App C.1. DLS size measurements	208
Table App D.1. Metal elution with HCl as the eluant.....	211
Table App D.2. Gold elution efficiencies with 0.1 M glycine solutions.....	211
Table App D.3. Copper elution efficiencies with 0.1 M glycine solutions.....	212

List of Publications

- Ilankoon, N. D., Aldrich, C., Oraby, E. A. and Eksteen, J. J. 2020. Use of polyethylenimine functionalised magnetic nanoparticles for gold thiosulfate recovery. *Hydrometallurgy* 195.
- Ilankoon, N. D., Aldrich, C., Oraby, E. A. and Eksteen, J. J. 2019. Extraction of Gold and Copper from a Gold Ore Thiosulfate Leachate by Use of Functionalized Magnetic Nanoparticles. *Mineral Processing and Extractive Metallurgy Review* 1-12.
- Ilankoon, N. D., Oraby, E. A., Eksteen, J. J. and Aldrich, C. 2018. Gold adsorption and elution in thiosulfate leaching system using functionalised magnetic nanoparticles. IMPC 2018 - 29th International Mineral Processing Congress, Moscow, Russia.

Chapter 1 Introduction

1.1 Background

For more than a century, cyanidation has been the preferred method for leaching gold from different types of ores. Yet, cyanidation of complex double refractory gold ores, specifically carbonaceous and sulfidic ores, has proven to be ineffective as a result of the high affinity of gold cyanide complex to carbon. For example, a gold-cyanide complex will readily adsorb onto carbonaceous materials such as humic acid, graphite, bitumens and asphaltic compounds in the ore itself; a process known as preg-robbing. This leads to higher reagent consumption and gold losses to tailings (Aylmore and Muir 2001, Ji et al. 2013). Furthermore, there are restrictions on the use of cyanide for gold leaching in some areas of the world, owing to its adverse environmental impact (Oraby 2009). This has prompted the development of alternative lixivants to cyanide.

The use of thiosulfate as a lixiviant for leaching gold has been known since the late nineteenth century (Aylmore and Muir 2001). Sodium, ammonium or calcium salt of thiosulfate, with copper as the oxidant, with or without ammonia are the main reagents used in the thiosulfate leaching system. The gold-thiosulfate complex does not show a good affinity for carbon, which makes it a viable alternative lixiviant for the leaching of refractory carbonaceous ores (Gallagher et al. 1990). Moreover, from an environmental perspective, the use of thiosulfate as an alternative lixiviant to cyanide for gold leaching shows considerable promise.

However, the addition of both copper and ammonia introduced uninvited problems into the system making the solution chemistry more complex. The availability of numerous anionic and cationic complexes, and copper catalysed thiosulfate oxidation leads to the formation of thiosulfate degradation products such as polythionates, and these, along with volatility and the environmental impact of using ammonia in the system are just a few of the current problems faced. Thus, the development of a thiosulfate-based leaching system that has a lower impact on the environment has been investigated. To achieve this, the possibility of using lesser amounts of copper, the total or partial elimination of ammonia, and the use of a thiosulfate salt with the minimum impact on the environment has been considered (Feng and van Deventer 2010b, Ji et al. 2013).

As a result of this, a process was developed using calcium thiosulfate and moderate amount of air. This process consumes only a low amount of copper whilst no ammonia is required. Currently this system is industrially implemented at Barrick Gold's Goldstrike operation in

Nevada, USA to treat double refractory gold ores after pre-oxidation in autoclaves (Choi 2013). However, gold thiosulfate complex does not adsorb well onto activated carbon. This makes the well-established carbon in leach (CIL) and carbon in pulp (CIP) processes unsuitable for gold recovery in the thiosulfate leaching system (Gallagher et al. 1990). This leads to the finding of alternative gold recovery methods to adsorb gold thiosulfate complex. Ion exchange resins, modified AC and mesoporous silica were investigated for gold recovery from thiosulfate leaching solutions. Attempts were made to recover gold thiosulfate with Cupric ferrocyanide impregnated AC (Parker et al. 2008, Yu et al. 2015) and Silver ferrocyanide impregnated AC (Yu et al. 2018). However, these adsorbents added cyanide to the recovery solution. The maximum adsorption capacity of the latter adsorbent was only 3.55 kg/ton. Although the adsorption capacity of mesoporous silica was high, in the near neutral pH range (6.5 - 7.5), it reduced dramatically when the pH was above 8. It has been recommended to use this adsorbent in near neutral pH solutions (pH 7.5) for a longer life cycle. Furthermore, the fine size of the adsorbent made the separation from the pulp difficult (Fotoohi and Mercier 2014). Weak base ion exchange resins also suffer from poor loading capacities in alkaline pH solutions. Therefore, at present, a strong base anion exchange resin appears to be the most promising alternative for gold recovery from a thiosulfate leaching system (Choi and Chefai 2017).

The resin-in-leach (RIL) operating conditions used in the Goldstrikes plant consist of a calcium thiosulfate (CaS_2O_3) concentration of approximately 0.1M, with a low concentration of copper and a moderate addition of air at a temperature of 50°C (Choi 2016). Currently strong basic ion exchange resins are used for gold recovery from the leach. More detailed information on this system will be presented in the second chapter of this thesis. The majority of the experiments conducted in this research study used simulated leaching solutions of aforementioned calcium thiosulfate leaching system.

Although the amount of polythionate formation is less in this system compared to the conventional ammoniacal thiosulfate system, resin poisoning with polythionates remains one of the major challenges to overcome (Daenzer et al. 2016). Furthermore, the competitive adsorption of copper and the drop in loading capacity due to resin swelling at loading-stripping cycles are also drawbacks associated with the use of resins. The use of resin beads necessitates a filtration step where screens are used to separate solids and liquids for further processing. The metal elution from the strong base anion exchange resin was also found to be complicated and demanded high reagent concentrations (Jeffrey et al. 2010).

Mainly polythionate, thiocyanate, chloride and nitrate based elution systems have been proposed for gold elution from strong base IX resins. In addition, combinations of sulfite ions

with the aforementioned eluants also have been proposed (O'Malley 2002, Fleming et al. 2003, Jeffrey et al. 2010). The use of concentrated trithionate solutions for gold elution in polythionate systems makes the solution unstable, leading to the loss of trithionate. Furthermore, complete regeneration of the resin is required prior to gold adsorption in the next cycle, as all exchange sites are occupied by trithionate. Unfortunately, thiocyanate elution system suffers from high reagent costs, and the regeneration of the resin is rather complex. In the nitrate elution system, the resin returns to adsorption without regeneration. It can therefore accumulate nitrate in the process water, which ultimately affects gold loading. Gold elution was very poor, even with 2 M sodium chloride in the chloride elution system. All the systems consumed high amount of reagents (Jeffrey et al. 2010). The use of sulfite, together with eluant (NaCl) could solve this problem to some extent, but considerable time still would be needed to completely elute gold and copper from the resin (Braul 2013). Furthermore, trithionate accumulation and poisonous chlorine generation during electrowinning are probable with this system (Dong et al. 2017). An oxygenated ammonia system was proposed for copper pre-elution, but due to its complexity there was minimal interest in pursuing this option. Ammonium thiosulfate 0.5 M was proposed for copper elution as it was a simpler solution compared to the oxygenated ammonia system (Jeffrey et al. 2010).

Adsorption processes associated with magnetic separation have been studied widely for heavy metal and precious metal removal in environmental and biomedical applications. Nanosized magnetite and maghemite have often been used as core materials (Gómez-Pastora et al. 2014, Aghaei et al. 2017). When particle sizes are reduced to the nanoscale range, the properties of magnetite such as magnetism and specific surface area vary significantly and the nanoparticles become superparamagnetic (Blaney 2007). It is calculated that the specific surface area of 200 nm of magnetite is only 6 m²/g while for 50 nm magnetite it is around 100 m²/g (Cornell and Schwertmann 2006, Blaney 2007). Non-magnetic nanoparticles need to be attached onto a solid matrix such as carbon, zeolites, silica and membranes for effective solid-liquid separation (Easwaramoorthi and Natarajan 2009, Hu et al. 2017, Gholamali et al. 2018). However, these additional steps can be avoided by using magnetic nanoparticles which, by their very nature, can be separated magnetically. Furthermore, with magnetic separation, filtration and centrifugation steps become unnecessary.

Magnetic nanoparticles are often functionalised with specific surface functional groups which are suitable for the intended use. The functional group(s) determine the selectivity towards specific ions and molecules to be adsorbed. Furthermore, surface functionalisation prevents nanoparticle aggregation and protects the magnetic core from oxidation (Liu et al. 2017). Polyethylenimine (PEI) was often used as a functional group for magnetic nanoparticles

(MNPs) and other adsorbents in environmental and biomedical applications for anion separation (Xu et al. 2011, Zhang et al. 2014, Yang et al. 2017). Moreover, PEI coated magnetite NPs have been successfully employed for gold NPs adsorption at pH 7 (Goon et al. 2009, Wang et al. 2012).

The amine rich structure of PEI permits protonation even in alkaline pH solutions. It was reported that 42% and 50% of amine groups protonated in 0.1 M NaCl solutions at pH 7.5 and pH 6.5, respectively (Radeva and Petkanchin 1997). Similarly, protonation of 32% and 64% of amino groups was observed in pH 8 and pH 4 solutions, respectively (Hostetler and Swanson 1974). The point of zero charge (pH_{PZC}) of a PEI molecule is approximately pH 10.8-11.0 (Lindquist and Stratton 1976, Radeva and Petkanchin 1997). As a result, PEI coated MNPs demonstrated a high positive surface charge density (20 - 25 mEq/g) even in alkaline pH solutions (Guillem and Aliño 2004). In addition, PEI coating does not significantly influence the saturation magnetisation of the magnetic core. In some instances a slight decrease in saturation magnetisation was observed, but there was still enough for efficient magnetic separation (Xu et al. 2011, Lu et al. 2014).

Considering the previous usage for the anionic species adsorption, the PEI modified MNPs, as a potential adsorbent for gold recovery from thiosulfate leaching solutions was considered in this study. As gold exists as an anionic complex, the adsorbent surface should exhibit a cationic surface charge to adsorb gold from the leaching solution. Due to its higher cationic charge density together with a higher pH_{pzc} (pH at point of zero charge) value, PEI showed great potential, and was selected as the functional group for coating the magnetic core. Moreover the PEI coating is known to have an insignificant negative effect in the saturation magnetisation of the magnetic core. This facilitated the easy magnetic separation even after surface coating. Trisodium citrate was used as the intermediate coating layer to impart a highly negative surface charge to the already anionic MNPs surfaces which increase the charge density of the surface which will be augmented subsequent PEI molecule adsorption as the outer layer. The separation of gold loaded MNPs (Au-PEI-MNPs) was carried out by use of an external magnetic field. In contrast to the separation of larger particles (resin beads, activated carbon) by filtration using screens, this proposed method utilises a magnetic field to separate the nanosized adsorbent. The practical application of this technology is discussed in the succeeding chapters of this thesis. Furthermore, a comparatively simple and fast two-step selective metal elution process which consumes low amounts of eluants is also proposed. The reusability of the nanoadsorbent is also investigated. The chemicals and reagents were carefully chosen with the purpose of minimising the negative effect on environment. The iron oxide magnetic core was biocompatible and environmentally benign. Both of the

functionalising agents, sodium citrate and PEI, have been deemed safe to use and are also often used for the surface coating of MNPs in biomedical applications. In summary, this research covers the preliminary work of adsorbent preparation, characterisation, gold adsorption (effect of reagent concentrations and adsorption process conditions on gold adsorption, gold adsorption kinetics, gold adsorption isotherms), competitive adsorption of other molecules, selective metal elution from the adsorbent and reuse of the adsorbent in synthetic leaching solutions and in actual gold ore leachates.

1.2 Research Question and Hypothesis

Currently, thiosulfate is the main industrially implemented alternative lixiviant to cyanide for gold leaching from refractory ores. Although numerous studies have been conducted based on ammoniacal thiosulfate leaching system, the industrially established system is based on CaS_2O_3 with a low copper dosage and a mild air supply, operated in slightly alkaline pH conditions. Resin-in-leach is used to recover gold from the leaching solution using strong basic anion exchange resins. However, gold elution from IX resins can be challenging. Furthermore, the use of resin beads necessitates a filtration process to separate from solutions. Activated carbon cannot be used due to the poor affinity of the gold thiosulfate complex to carbon. Other conventional recovery methods such as precipitation, cementation, electrowinning and solvent extraction show little promise due to major drawbacks associated with these techniques, as discussed in Section 2.6.

Considering the limitations associated with existing/current recovery methods, the exploration of alternative adsorbents for gold recovery from thiosulfate solutions is obviously worthwhile. An ideal adsorbent would; be selective for anionic gold complex in alkaline pH solutions, stable in alkaline pH solutions, have high adsorption capacity, be easy to separate from the solution, be easy to selectively elute gold and be reusable.

In this study the main research questions were defined as;

- Can a polyethylenimine functionalised magnetic nanoadsorbent be used to recover gold from thiosulfate leaching solutions, taking advantage of magnetic separation?
- Would polyethylenimine coated magnetic nanoadsorbents produce effective gold adsorption capacity along with selectivity?
- Would the metal elution process from this particular adsorbent be effective?
- Can polyethylenimine coated magnetic nanoadsorbents be reused?

The use of magnetic nanoadsorbents for biomedical applications and environmental applications has been extensively studied and reasonably well understood. This is not the case in metallurgical applications for precious metal recovery where a great deal more development is needed. Some work has been carried out regarding gold adsorption from aqueous gold-chloride solutions in acidic solutions (Zhang et al. 2013c, Roto et al. 2016, Abd Razak et al. 2018). Gold exists in +3 oxidation state in these solutions. Adsorption of Au (I) anionic complexes from alkaline leaching solutions using functionalised magnetic nanoadsorbents has not yet gained much attention except for a very recent study (Betancur et al. 2019).

Based on the literature review, it is hypothesised that polyethylenimine coated MNPs can be effectively used for gold recovery from thiosulfate leaching solutions, followed by selective elution of gold and possible reuse of the MNPs for further cycles. Gold loaded MNPs can presumably be separated from the solutions by applying an external magnetic field.

In order to further develop and support the aforementioned hypothesis, several assumptions were made:

- Surface functionalised magnetic nanoadsorbents can be effectively used for anionic gold complex adsorption from thiosulfate leaching solutions
- Bare iron oxide MNPs alone are insufficient to recover anionic gold thiosulfate ($Au(S_2O_3)_2^{3-}$) complex from alkaline solutions, as the surface charge of bare iron oxide MNPs is also anionic above pH_{PZC} . A suitable surface coating which introduces a cationic surface charge is necessary to promote the electrostatic attraction between the adsorbate and the adsorbent
- Polyethylenimine (PEI) will be a suitable surface coating agent to impart a positive surface charge to a MNP surface even in highly alkaline solutions, as a result of its high cationic charge density and high pH_{PZC} value
- Trisodium citrate can be used as the intermediate coating layer to impart a highly negative surface charge to the already anionic MNPs surfaces which increase the charge density of the surface which will be augmented subsequent PEI molecule adsorption as the outer layer
- Citrate and PEI coated nanoparticles can recover gold from the thiosulfate leaching solutions. Copper thiosulfate complex and any other anionic complex too can adsorb on to the same adsorbent

- Gold loaded MNPs can be simply separated from the solutions by applying an external magnetic field.
- The loaded gold and copper can be selectively eluted from the nanosorbent using appropriate eluants. The preliminary elution of copper followed by gold elution would ensure the purity of the final gold product whilst the eluted copper can be reused for subsequent leaching circuits.
- The metal eluted MNPs can be reused for several more cycles for gold adsorption.

1.3 Objectives of the Study

In this study, the recovery of gold from thiosulfate leaching solutions was attempted using functionalised MNPs. Polyethylenimine coated iron oxide nanoparticles were used as the adsorbent to recover gold from the solution. Electrostatic attraction was favoured in this instance, as the leaching system operated at an alkaline pH range and the PEI coating provided a positive surface charge to the nanoparticles of up to pH 11, which is the pH_{PZC} of coated nanoparticles. It was assumed that the electrostatic attraction/physical adsorption would facilitate easy metal elution at subsequent metal elution stage. The adsorption behaviour of functionalised nanoparticles towards gold was investigated and the maximum gold adsorption capacity, gold adsorption kinetics and adsorption isotherms were determined. Gold adsorption mechanism was explored via a thermodynamic approach. The systematic metal elution from loaded nanoparticles was conducted and the reuse of nanoparticles for several cycles was evaluated. Solid-liquid separation was accomplished via magnetic separation.

The main objectives of this study were;

- 1) To functionalise the magnetic nanoparticles with polyethylenimine in order to adsorb anionic gold complex from thiosulfate leaching solutions in alkaline pH conditions.
- 2) To characterise the nanoparticles before and after surface functionalisation and after the adsorption process.
- 3) To evaluate the influence of different reagent concentrations and adsorption process conditions on gold adsorption efficiency from thiosulfate leaching solutions onto functionalised MNPs.
- 4) To determine the gold adsorption mechanism onto functionalised MNPs.
- 5) To selectively elute adsorbed gold from MNPs and to reuse the regenerated MNPs.

1.4 Scope of the Study

This research focuses on the adsorption of gold from synthetic thiosulfate leaching solutions. In addition, gold and copper adsorption from a leachate of mild refractory gold ore that does not yield high gold recoveries in conventional cyanidation, was also investigated. Citrate and PEI functionalised iron oxide MNPs (PEI-MNPs) were used as the adsorbent. Rather than evaluating many adsorbents, only the aforementioned adsorbent was used and a comprehensive particle characterisation was undertaken. Amongst the numerous particle characterisation techniques used, X-ray photoelectron spectroscopy (XPS) and atom probe tomography (APT) methods were employed to comprehensively visualise the effectiveness of surface functionalisation and gold adsorption process. Other characterisation methods were used to support the conclusions.

The industrially established calcium thiosulfate-air (CaS_2O_3 -air) leaching system was mainly considered for all the adsorption experiments. Other thiosulfate leaching systems such as the ammoniacal thiosulfate system, the ferric-EDTA system, the ferric-oxalate system and the nickel-ammonia system were studied for the purpose of comparison only, and therefore not in detail. Gold adsorption kinetics, isotherms and thermodynamics were investigated and the adsorption mechanism was determined. Adsorption from clarified leaching solutions was considered and pulp application is suggested as a future research interest. Competitive adsorption of the copper and sulfur species was considered briefly. However, a detailed investigation was not carried out, as gold was the target adsorbate in this study.

During the elution stage, copper and gold elution was attempted whereas the sulfur species elution was not considered.

1.5 Thesis Structure

This thesis comprises eight chapters as outlined below.

- **Chapter 1** introduces the background and the research question, problems associated with the current system and the main objectives and scope of the study. The hypothesis and the organisation of thesis chapters are also included
- **Chapter 2** presents the literature review on the thiosulfate leaching system, existing methods for gold recovery from the system, magnetic nanoparticle synthesis, functionalisation, characterisation and practical application on metal adsorption from aqueous solutions. A brief introduction to key concepts of essential theories and methods is also included
- **Chapter 3** explains the experimental methods, reagents and procedures used for nanoparticle surface functionalisation, characterisation, metal adsorption and metal elution studies
- **Chapter 4** discusses the results of nanoparticle functionalisation, along with characterisation and deagglomeration studies
- **Chapter 5** describes the results of the adsorption experiments conducted with synthetic leaching solutions
- **Chapter 6** discusses the attempts made towards metal elution from the adsorbent used in synthetic leaching solutions, and reuse of the adsorbent
- **Chapter 7** includes the results of processing an actual gold ore sample, from leaching through to metal elution
- **Chapter 8** summarises the results and major conclusions derived from this study and discusses gaps in knowledge and some recommendations for further investigations in future

A schematic representation thesis chapter arrangement is shown in Figure 1-1.

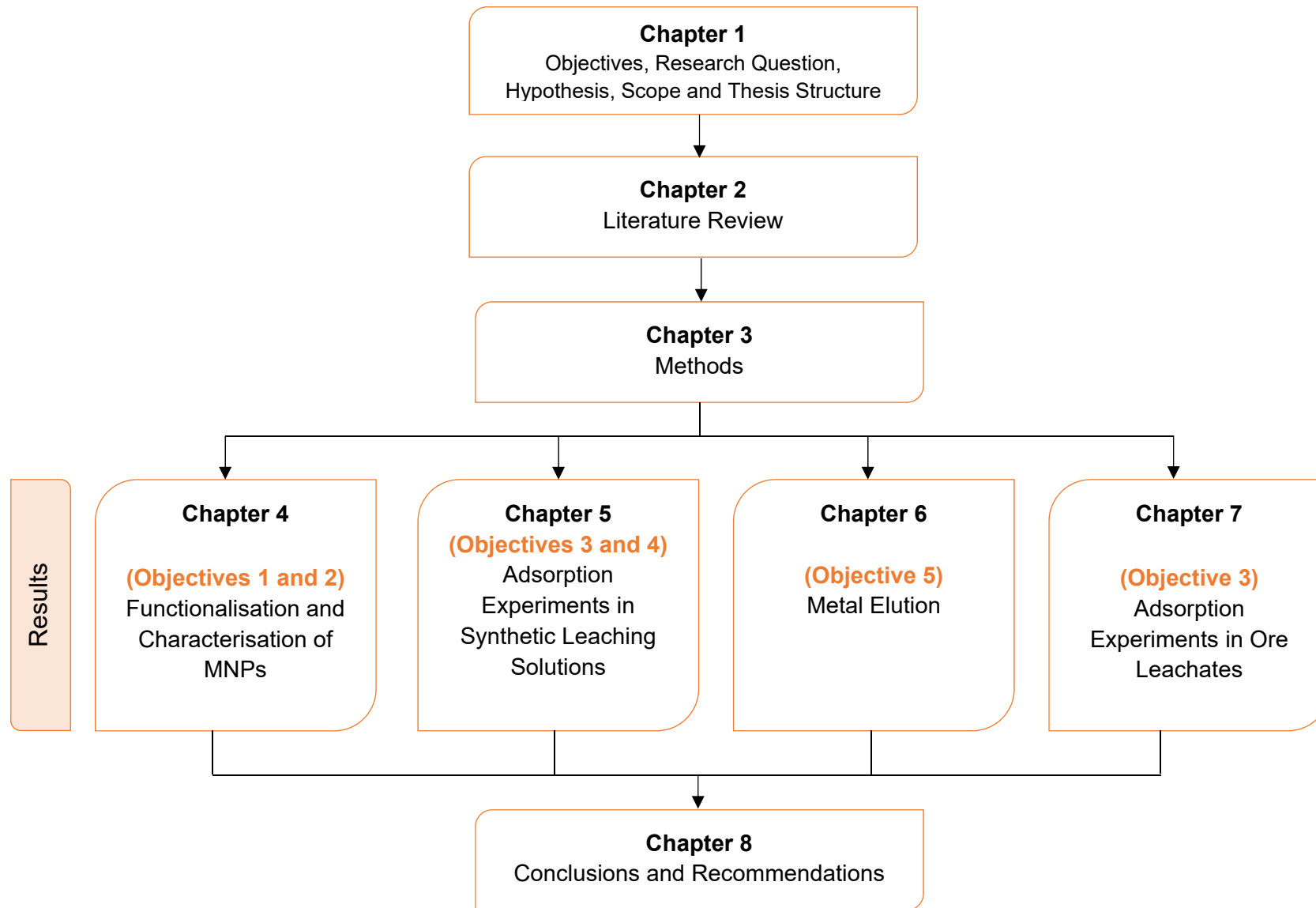


Figure 1-1. Schematic representation of thesis chapter arrangement

Chapter 2 Literature Review

2.1 Introduction and Chapter Objectives

In this chapter, some of the existing literature on the subject under study is reviewed. The literature review mainly consists of two main segments: one exploring the gold hydrometallurgy and thiosulfate leaching systems (heading number 2.2-2.7) and the other segment is dedicated for magnetic nanomaterials (heading number 2.8-2.9). In former segment, some background information is briefly given on the chemistry of gold in aqueous media, gold hydrometallurgy and different thiosulfate based leaching systems. An introduction to double refractory gold ores is also included. Current practices of gold recovery from thiosulfate leaching systems and the problems and challenges associated with the current methods are also highlighted. This is followed by brief explanations of adsorption process, theoretical backgrounds of essential mechanisms such as isotherm models, adsorption kinetics, and adsorption mechanisms. In the latter segment, the use of magnetic nanoparticles for metal adsorption, magnetic separation, nanoparticle functionalisation, limitations associated with nanoparticles and metal elution techniques are covered.

The information included in this chapter supports and influences selection of particular functional groups, eluants and setting up of experimental conditions in surface functionalisation and metal elution processes. Some important characterisation results reported in other studies are also included to compare and verify the accuracy of the results obtained in this study.

2.2 Properties and applications of gold

Gold is a precious metal that humans have used since ancient times, owing to its malleable and ductile properties and the occurrence in its native state. It was traditionally used primarily for jewellery and for monetary payment purposes. Methods of using gold in jewellery have not changed to this day and in addition, in the modern world, it is used in variety of electronic devices and biomedical applications (Choudhary et al. 2018, Zhang et al. 2018).

Gold is inert at ambient temperature and pressure. Pure gold is an excellent thermal and electrical conductor. The density of pure gold is $19\,300\text{ kg/m}^3$, although this value drops to around $15\,000\text{ kg/m}^3$ for native gold, due to being alloyed with impurities, mainly silver. In addition, gold can be alloyed with tellurium, selenium, bismuth, mercury, copper, iron, rhodium and platinum (Marsden and House 1960). The nature of the ore determines the optimum method to extract gold from the ore. Based on treatment and recovery techniques,

gold ores can mainly be divided into two categories; free milling ores and refractory ores. The free milling ore gives above 90% gold with conventional cyanide leaching but refractory ores require higher amounts of reagents or more complex pre-treatment processes to recover a considerable amount of gold (Zhou and Cabri 2004).

2.3 Double Refractory Gold Ores

Gold ore minerals that are not amenable to leaching with conventional cyanide processes are known as refractory gold ores. These refractory gold ores can be, sulfidic and/or carbonaceous ores. In sulfidic ores, fine gold is encapsulated in sulfide minerals, mainly inside an iron sulfide matrix such as pyrite, marcasite or arsenopyrite. This inhibits the interaction of cyanide with gold in forming a soluble gold cyanide complex. Sulfide content can vary from 0.5% to 3.5% in this type of ore, which locks approximately < 0.2 to 132 ppm of gold inside a sulfide matrix (pyrite). In this case, the gold is known to be invisible and sealed inside a solid solution of a sulfide matrix. The presence of carbonaceous materials such as hydrocarbons, humic acid, activated elemental carbon graphite, bitumens and asphaltic compounds are also known to be a cause of refractoriness in gold ore. These carbonaceous materials adsorb dissolved gold from cyanide leach solutions in a process termed preg-robbing, and the adsorbed gold ends up in tailings. The deleterious carbon content in the ore can vary from 0.1% to approximately 4%, and even content as low as 0.1% carbon can trigger preg-robbing action (Marsden and House 1960, Baron et al. 2016).

Gold ores, which consists of both sulfidic and carbonaceous matter are known as double refractory gold ores. These ores demand special process flows to get rid of the deleterious actions of sulfidic and carbonaceous matter. Barrick gold's Goldstrike mine in Nevada, Carlin Mill 6 and Twin Creeks Gold Mine – both in Newmont are some examples of double refractory gold ores in the USA. To liberate gold, ultrafine grinding and/or strong oxidising conditions are required. The oxidative pretreatment is achieved through roasting, pressure oxidation or bio-oxidation. In roasting at 500-600 °C, sulfide oxidises to sulfur dioxide, and iron in the sulfides oxidises to iron oxides (hematite), while carbonaceous content ultimately oxidises to carbon dioxide, exposing gold values for the subsequent leaching process. Although pressure oxidation (either acidic or alkaline) can effectively oxidise almost all the sulfidic matter, the complete elimination of carbonaceous matter is difficult. This remains one of the problems associated with preg-robbing to some extent. Bio-oxidation that uses bacteria to oxidise the ore also suffers from similar limitations observed in pressure oxidation in that this method is ineffective in totally eliminating the preg-robbing effect (Marsden and House 1960, Baron et al. 2016).

To overcome the aforementioned limitations, the use of thiosulfate has been proposed as a lixiviant to treat the double refractory gold ore, preferably after oxidative pretreatment. The sulfides in the ore are oxidised by oxidative pretreatment, whilst thiosulfate leaching can be effectively used for the treatment of already oxidised ore, which still contains carbonaceous matter (Choi 2016). Unlike the gold cyanide complex, the gold thiosulfate complex is known to be only poorly attracted towards carbonaceous matter (Aylmore and Muir 2001).

2.4 Gold Hydrometallurgy

Due to the availability in its native form as metallic gold, gravity concentration was the earliest technology used for gold recovery from alluvial deposits. Amalgamation with mercury was also practiced (although it is harmful to the environment) and it is still sparingly used in some areas in the world for artisanal gold mining (Esdale and Chalker 2018). Chlorination was used in the 19th century, with this method being replaced by cyanidation. The modern cyanidation process was patented by MacArthur and the Forrest brothers in 1888. The first commercial application was in the Crown mine in New Zealand (Marsden and House 1960).

Gold sits with copper and silver in group IB in the periodic table, and its atomic weight is 196.96 g/mol. Despite the similarities of gold, copper and silver in their electron structure and ionisation potential, their redox chemistry shows important differences (Marsden and House 1960).

Typically gold exist in aqueous solutions in +1(aurous) and +3 (auric) oxidation states with standard reduction potentials being 1.83 V and 1.52 V, respectively. Being categorised as a soft Lewis acid, gold can make stable complexes with some soft electron donor ligands such as cyanide (CN^-), thiosulfate ($S_2O_3^{2-}$), thiourea ($(NH_2)_2C = S$) and thiocyanate (SCN^-) ; all of which can be used as lixiviants for gold leaching. Accordingly, gold can form stable complexes with the above-mentioned ligands to varying degrees of stability. Gold presents as Au (I) in complexes with the above-mentioned ligands. Hard electron donor atoms such as halides prefer to form complexes with Au (III). In such complexes, the preferred coordination numbers are 2 and 4 for Au(I) and Au(III), respectively, resulting in linear and square planar structures (Marsden and House 1960, Martell and Hancock 1996).

The reaction between a metal (M) and a ligand (L) can be expressed as;



The overall stability constant (β) is a measure of the stability of a complex formed by a metal (M) with a particular ligand (L) and can be expressed as seen in equation (2-2) (Marsden and House 1960).

$$\beta = \frac{[ML_x]^{(y-nx)+}}{[M^{y+}][L^{n-}]^x} \quad (2-2)$$

A high beta value is an indicative of a stronger complex with the ligand. Stability constants of some ligands, which form stable complexes with either Au (I) or Au (III), are summarised in Table 2-1.

Table 2-1. Stability constants (β) of some Au (I) and Au (III) complexes

Ligand	Complexes	Au(I)	Au (III)
Cyanide	$Au(CN)_2^-$	2×10^{38}	10^{56}
Thiosulfate	$Au(S_2O_3)_2^{3-}$	5×10^{28}	-
Glycine	$Au(NH_2CH_2COO)_2^-$	10^{18}	-
Thiocyanate	$Au(SCN)_2^-, Au(SCN)_4^- *$	1.3×10^{17}	10^{42}
Thiourea	$Au(SC(NH_2)_2)_2^+$	2×10^{23}	-
Chloride	$AuCl_2^-, AuCl_4^- *$	10^9	10^{26}
Bromide	$AuBr_2^-, AuBr_4^- *$	10^{12}	10^{32}
Iodide	$AuI_2^-, AuI_4^- *$	10^{19}	10^{47}
Ammonia	$Au(NH_3)_2^+, Au(NH_3)_4^{+*}$	$10^{18}-10^{26}$	$10^{30}-10^{46}$

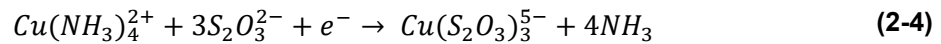
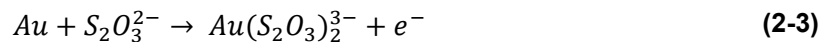
(data from (Marsden and House 1960) and (Senanayake 2004))

*- Au(III) complexes

Each gold leaching system requires a ligand to form a complex with gold (lixiviant) and an oxidant to oxidise the gold. A commercially well-established and the most widely used method for over 100 years is cyanide leaching. Several lixivants other than cyanide have been reviewed by different authors (Swaminathan et al. 1993, Sparrow and Woodcock 1995). Compared to different cyanide alternatives, such as halides (Qi and Hiskey 1991), ammonia (Han and Meng 1994), thiourea (Murthy et al. 2003), thiocyanate (Kholmogorov et al. 2002) and glycine (Eksteen and Oraby 2015, Oraby and Eksteen 2015a, Oraby and Eksteen 2015b), the thiosulfate system is the most widely studied cyanide alternative. Furthermore, mixed cyanide and another lixiviant which minimises cyanide usage have also been proposed (Muir 2011, Oraby et al. 2017).

2.5 Thiosulfate Leaching of Gold

The efficacy of thiosulfate in gold leaching has been recognised for more than a century. In the Von Patera process, gold and silver ores were first subjected to a chloridising roast, followed by thiosulfate leaching (Aylmore and Muir 2001). However, Genik-Sas-Berezowsky et al. (1978) and Kerley (1981, 1983) separately patented the use of thiosulfate leaching to recover precious metals from refractory ores. Leaching gold with thiosulfate is an electrochemical reaction with gold oxidation from zero state to Au (I) thiosulfate and reduction of Cu (II) to Cu (I) thiosulfate. The half-cell reactions are given in equations (2-3) and (2-4).



Ammonium thiosulfate, sodium thiosulfate or calcium thiosulfate is mainly used in conventional thiosulfate leaching systems as a lixiviant. Copper is often used as the oxidant, while ammonia acts as a stabiliser by keeping Cu(II) in the solution. Furthermore, ammonia helps to prevent gold passivation. One of the major drawbacks associated with thiosulfate leaching of gold is the formation of polythionates by oxidation of thiosulfate. These polythionate species have proven to be detrimental to the gold recovery process by competitively adsorbing on to ion exchange resins.

2.5.1 An Overview of Thiosulfate

A thiosulfate anion ($S_2O_3^{2-}$), formerly known as hyposulfite, has a tetrahedral arrangement, which is similar to a sulfate ion where one oxygen atom is replaced by a sulfur atom. This structure is responsible for its strong complexing and reducing properties (Hiskey and Atluri 2007). Gold thiosulfate is a linear complex as illustrated in Figure 2-1.

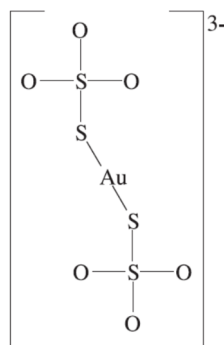


Figure 2-1. Structure of gold thiosulfate complex derived from (Grosse et al. 2003) with permission

Commercially, thiosulfate is mainly available in its sodium and ammonium form as a solid at room temperature, whereas calcium thiosulfate is in the form of a clear solution. Thiosulfate is used in the paper-making industry, leather goods production industry, in textile dyes and in photography. Significantly, sodium thiosulfate is used as a medication to treat cyanide poisoning and calcium accumulation in some parts of the body, a condition known as *calciophylaxis* (Generali and Cada 2015, Zakharov et al. 2015). Calcium thiosulfate is a well-known liquid plant fertiliser and it is used to treat calcium and sulfur deficiency in plants (Gan et al. 2000).

Thiosulfate can form complexes with various metal ions to a varying degree of stability. The stepwise stability constants of some metal thiosulfate complexes are represented in Figure 2-2. M and L denote the metal and ligand, respectively. Thiosulfate predominately forms stable complexes with Au(I), Hg(II), Pb(II), Fe(II) and Ag(I) (Grosse et al. 2003).

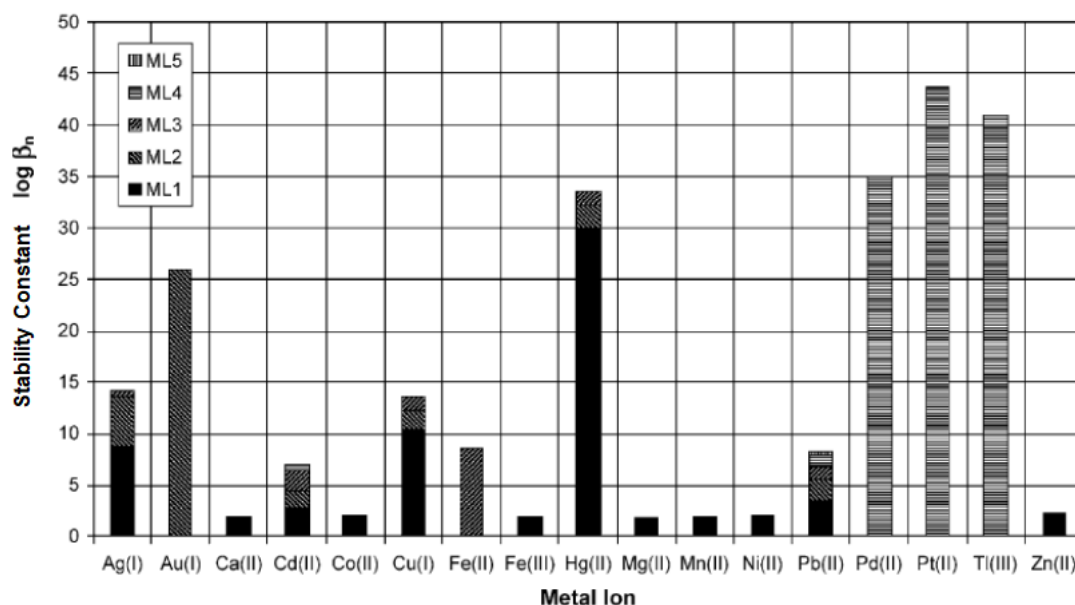


Figure 2-2. Stepwise stability constants of thiosulfate complexes (derived from (Grosse et al. 2003) with permission.

2.5.2 Stability of Thiosulfate

Thiosulfate is known to be metastable which means it chemically decomposes in aqueous media depending on the Eh and pH values of the solution. The oxidation of thiosulfate by oxygen in aqueous solution is reported to be very slow in ambient temperature and pressure (Marsden and House 1960). In alkaline conditions, available copper catalyses this phenomenon by oxidising thiosulfate to polythionates, such as trithionate ($S_3O_6^{2-}$), tetrathionate ($S_4O_6^{2-}$), pentathionate ($S_5O_6^{2-}$) and ultimately to a most stable sulfate (SO_4^{2-}) form. The oxidation states of different sulfur species are illustrated in Figure 2-3.

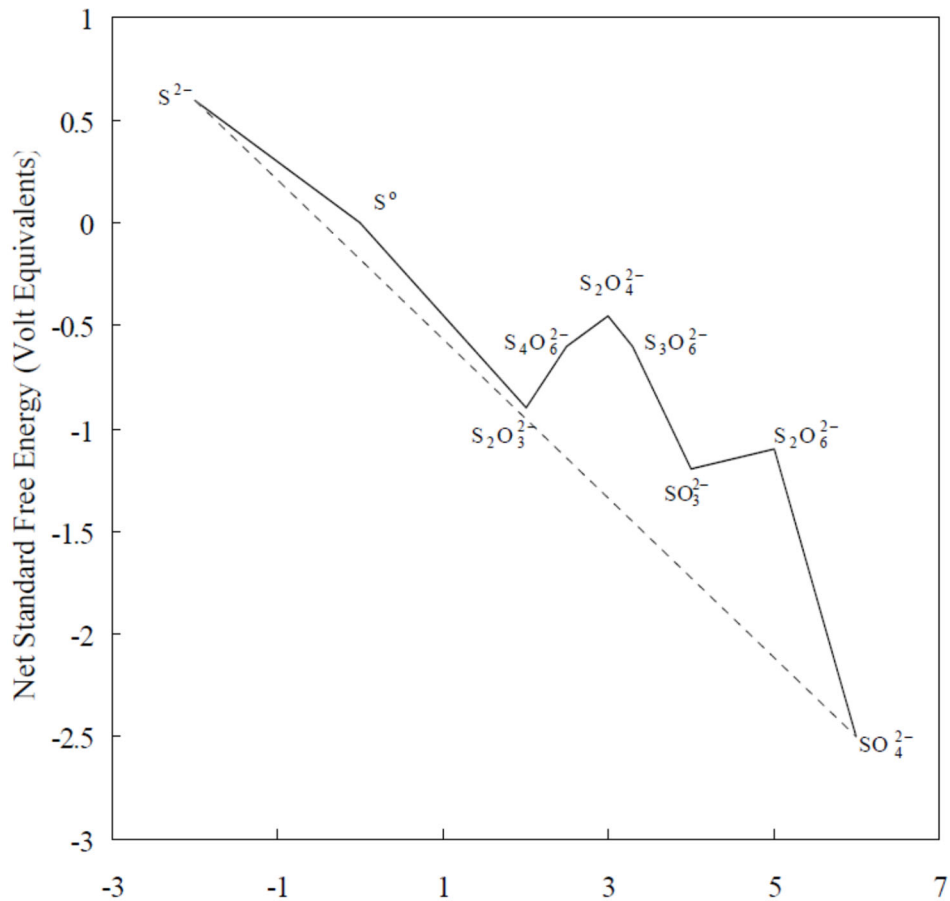
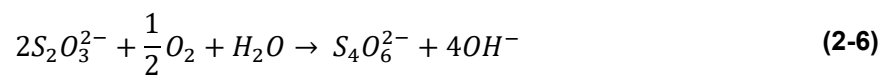
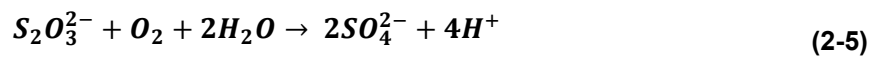
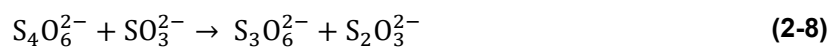
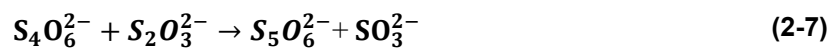


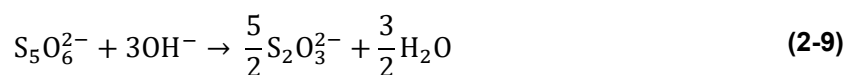
Figure 2-3. Oxidation states of sulfur species (derived from (O'Malley 2002))

The oxidation of thiosulfate with the available O₂ or Cu is represented in equations (2-5) and (2-6).



The generated tetrathionate (S₄O₆²⁻) undergoes further oxidation as represented below in equations (2-7) to (2-9).





The stability of thiosulfate in aqueous solutions mainly depends on several parameters as listed below.

2.5.2.1 Solution pH and Temperature

Jeffrey and Brunt (2007) investigated the chemical speciation of leach solutions which consist of ammonium thiosulfate, ammonium sulfate and copper (I) thiocyanate. It was concluded that tetrathionate and pentathionate are dominant at pH 8.5 and 9, whilst trithionate and sulfate are present in the solution at pH 10.4. According to Aylmore (2016b), the stability region of thiosulfate is limited to a narrow Eh range in neutral to basic pH solutions. Furthermore, Cu (II) oxidises thiosulfate to trithionate in the pH 4-10 range with catalytic oxidation. It is worth noting that trithionate is unstable above pH 10.

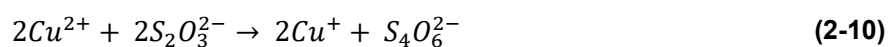
In general, thiosulfate and polythionates are stable at temperatures below 4 °C and with pH values above 2. At a pH of 2, even at such a low temperature as 4 °C, thiosulfate decomposes in to trithionate, tetrathionate, sulfate and elemental sulfur. At 15 °C and above thiosulfate is relatively stable in alkaline pH solutions, however it decomposes in acidic pH solutions. At 30 °C or above, thiosulfate and polythionates are reactive for the entire pH range from 2-9 (Range and Hawboldt 2018).

Zhang and Dreisinger (2003b) found that by adjusting the solution pH and the temperature, the tetrathionate degradation rate could be increased. It has been reported that in order to achieve 99% tetrathionate degradation, when the pH is above 10.5 in the leaching solution, it takes 6.8, 3.6 and 1.9 hours at temperatures of 30, 35 and 40 °C respectively. With a pH of 11, at 35 °C, degradation took only 1.2 hours. Some experiments have been conducted where the tetrathionate added leach solution was kept at a pH of 12 and set aside for 6 hours until the tetrathionate degraded. This was followed by adding the IX resin to adsorb the gold.

2.5.2.2 Availability of Copper

Copper (II) catalyses thiosulfate oxidation in solutions to tetrathionate as represented in equation (2-10). Xia et al. (2003) suggested reducing the copper sulfate addition to a minimum possible value (0.75 mM to 1 mM) or replacing copper sulfate with nickel sulfate to reduce thiosulfate consumption, in the specific leach solution tested. This study highlighted the adverse effect of excess copper in the solution on rapid thiosulfate decomposition and retarded

gold dissolution. The decrease in copper concentration by fivefold was able to reduce the rate of thiosulfate oxidation by a factor of two (Breuer and Jeffrey 2003).



Furthermore it is reported that the absence of ammonia in the solution leads to rapid oxidation of thiosulfate by Cu(II) as ammonia can stabilise copper (Senanayake 2005c, Senanayake 2005a).

2.5.2.3 Availability of Oxygen/air and Sulfur Species

Dissolved oxygen is one of the main reasons for thiosulfate decomposition, which is catalysed by copper species. Breuer and Jeffrey (2003) tested the effect of oxygen concentration on the thiosulfate oxidation rate. The rate of thiosulfate oxidation was clearly higher when pure oxygen was sparged rather than using air where all the thiosulfate was consumed in less than 25 minutes. A gas consisting of 1.9% oxygen in nitrogen was able to preserve the thiosulfate whereas only 10% of thiosulfate oxidation was observed even after 2 hours. The addition of sulfite, sulfide or hydroxide ions to the leach liquor has been proposed in order to suppress the effect of thiosulfate oxidation products, mainly trithionate and tetrathionate. Sulfite can reduce tetrathionate back to thiosulfate by oxidising itself to sulfate form. The addition of sulfide can reduce both tri- and tetrathionate back to thiosulfate, but can precipitate gold and copper in their sulfide form. The treatment of thiosulfate leach liquor with sodium hydrogen sulfide (NaHS) resulted in partial or complete precipitation of gold and copper in the solution prior to reducing polythionates to a considerable level (Fleming et al. 2003).

2.5.2.4 Presence of Impurities

The presence of different species such as hematite and iron contaminants, was investigated (Feng and van Deventer 2002, Feng and van Deventer 2007, Feng and van Deventer 2010a). Hematite, elemental iron and ferric ions catalysed the oxidative decomposition of thiosulfate in the presence of oxygen. Xu and Schoonen (1995) investigated the effects of pyrite on the thiosulfate decomposition rate and on respective partial decomposition products like sulfite (SO_3^{2-}), sulfate (SO_4^{2-}) and tetrathionate ($S_4O_6^{2-}$) formation rates in aqueous solutions of pH 2.9 - 8.6 at a temperature of 20 °C. In addition, the effect of elemental sulfur, galena (PbS), sphalerite ((Zn,Fe)S), and hematite (α -Fe₂O₃) was also examined in pH 2.9 solutions. A significant increase in the thiosulfate oxidation rate was observed in the presence of pyrite for the whole pH range tested and the rate was directly proportional to the pyrite surface concentration. It was concluded that pyrite surface catalysed oxidation of thiosulfate to

tetrathionate by dissolved oxygen was the main mechanism under the tested conditions. The contribution of elemental sulfur to the decomposition of thiosulfate was insignificant and no tetrathionate was observed in the decomposition products. However the presence of galena, sphalerite, and hematite enhanced the thiosulfate decomposition rate considerably where 243, 112 and 204 μM tetrathionate was available after 8 days of reaction from 500 μM of initial thiosulfate concentration, respectively.

2.5.3 Different Thiosulfate Leaching Systems

An ammoniacal thiosulfate leaching system with a copper-ammonia oxidant-ligand pair is the most extensively studied system. In addition to this, a few other oxidant and stabiliser pairs have also been reported. These include nickel (III) with ammonia (Arima et al. 2004), iron (III) with EDTA (Zhang et al. 2005) and ferric oxalate with thiourea as the catalyst (Chandra and Jeffrey 2005). All of these alternative systems highlighted a lower thiosulfate consumption compared to the copper ammonia system. Those systems are briefly discussed below, together with the calcium thiosulfate – air system which is industrially implemented. The reagents used and the general operating conditions of the different thiosulfate leaching systems investigated are summarised in Table 2-2.

Table 2-2. Summary of different thiosulfate based leaching systems

Lixiviant	Oxidant	Complexing agent	Other additives	Solution pH	Temperature	Reference
$(\text{NH}_4)_2\text{S}_2\text{O}_3$	Cu(II)	NH_4^+	-	9.5 to 11.5	Ambient temperature	(Aylmore and Muir 2001, Grosse et al. 2003)
$\text{Na}_2\text{S}_2\text{O}_3$	Cu(II)	NH_4^+	-	8.5 to 10.5	25 to 60 °C	(Abbruzzese et al. 1995)
$\text{Na}_2\text{S}_2\text{O}_3$	Fe(III)	EDTA	Thiourea as a catalyst	6-7	Ambient temperature	(Heath et al. 2008)
$\text{Na}_2\text{S}_2\text{O}_3$	Fe(III)	oxalate	Thiourea as a catalyst	4.5 to 6	Ambient temperature 20-22 °C	(Chandra and Jeffrey 2005, Heath et al. 2008)
$(\text{NH}_4)_2\text{S}_2\text{O}_3$	Ni(II)	EDTA	-	9.5	Ambient temperature	(Arima et al. 2004)
CaS_2O_3	Cu(II)/air	-	-	8	50 °C	(Choi 2013)

2.5.3.1 Copper Ammoniacal System

Thiosulfate leaching systems that contain ammonium thiosulfate or sodium thiosulfate together with copper and ammonia have received the most attention over the last two decades (Zhao et al. 1998, Breuer and Jeffrey 2002, Feng and van Deventer 2011, Ji et al. 2013). Copper acts as a catalyst and oxidant for gold oxidation, and ammonia stabilises the copper by forming a cupric amine complex and additionally, prevents gold passivation (Aylmore and Muir 2001). The activation energy required to oxidise metallic gold to the Au(I) state, in the presence of copper and ammonia, is reported as 15.54 kJ/mol whereas it increases to 27.99 kJ/mol in the absence of this pair (Grosse et al. 2003). Although the addition of copper and ammonia to the solution facilitates the rate of gold oxidation significantly, the process is known to be associated with some adverse effects.

In the presence of reducing sulfide minerals, copper can precipitate as copper sulfide passivating gold, or cause rapid decomposition of thiosulfate to form polythionates in solution and this can dramatically reduce gold recovery. In addition, ammonia can be lost by volatilisation in most open vessels or heap leach systems at a pH > 9.2. Higher temperatures can further exacerbate ammonia consumption (Grosse et al. 2003). The co-existence of different cations and anions in solution makes the solution chemistry more complex. In order to achieve an acceptable level of gold leaching and recovery, this system should be operated in a narrow pH and Eh range. In addition, both cationic copper and ammonia are hazardous to the environment and toxic to aquatic life (Ji et al. 2013).

The influence of thiosulfate salt on gold leaching in pure gold and pyrite concentrates has been investigated. The gold extraction rate decreases in the order of calcium thiosulfate > ammonium thiosulfate > sodium thiosulfate in pure gold, while thiosulfate consumption was highest with ammonium salt and least with sodium salt. The difference in the leaching rate was attributed to the ability of ion pair formation. For pyrite concentrates, it was concluded that ammonium thiosulfate is suitable for high sulfide ores, whilst calcium thiosulfate is preferred for treating low-sulfide ores (Feng and van Deventer 2010b).

The use of ammoniacal thiosulfate leaching systems as an environmental friendly alternative to cyanidation is therefore questionable. Ideally, there is a need for a system that eliminates or minimises the use of either copper or ammonia, or both if possible.

2.5.3.2 Calcium Thiosulfate - Air Leaching System

The calcium thiosulfate – air leaching system can be simply represented in equation (2-11). The corresponding Eh-pH diagrams of Au-S-H₂O system and Cu-S₂O₃²⁻-H₂O system are represented in Figure 2-4 and Figure 2-5, respectively.

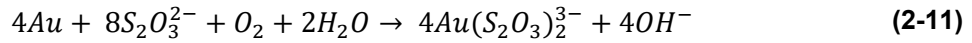


Figure 2-4 shows that $Au(S_2O_3)_2^{3-}$ is stable at a higher Eh and lower pH whilst AuS^- is stable at a lower Eh and higher pH. It is apparent that $Cu(S_2O_3)_3^{5-}$ is the most predominant species in typical thiosulfate leaching conditions as illustrated in Figure 2-5. However, this further depends on the Cu to thiosulfate ratio in the solution. Moreover sulfide, oxide and hydroxide derivatives of copper are possible, depending on the Eh and pH conditions of the solution. These precipitates can passivate gold, ultimately obstructing the leaching process (Sitando et al. 2018). The precise control of solution pH and Eh is crucial to efficient gold leaching.

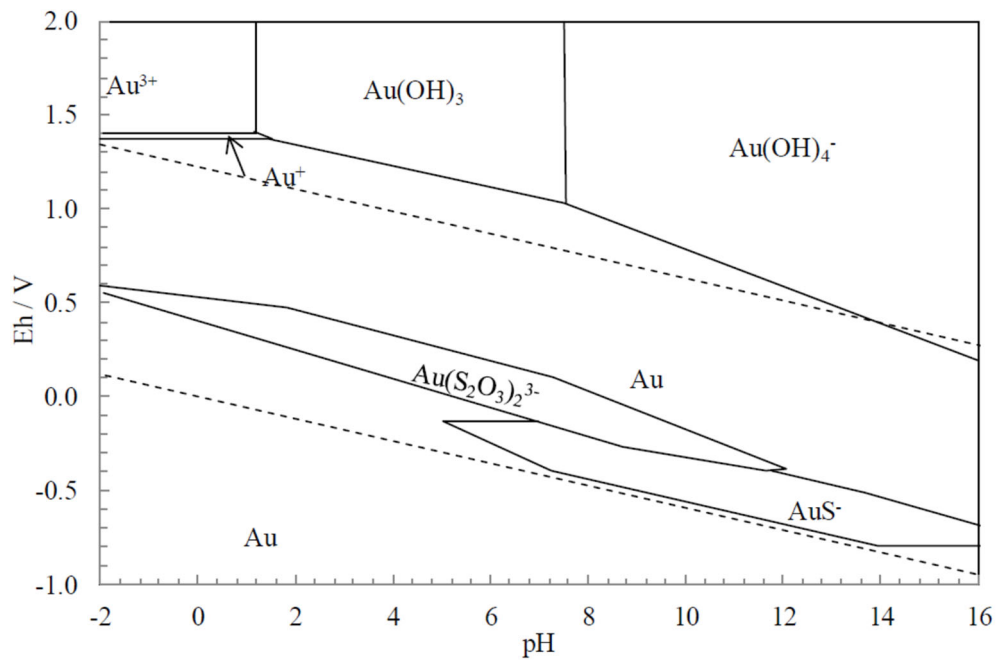


Figure 2-4. Eh-pH diagram of Au-S-H₂O system at 25 °C derived from (Sitando 2017)

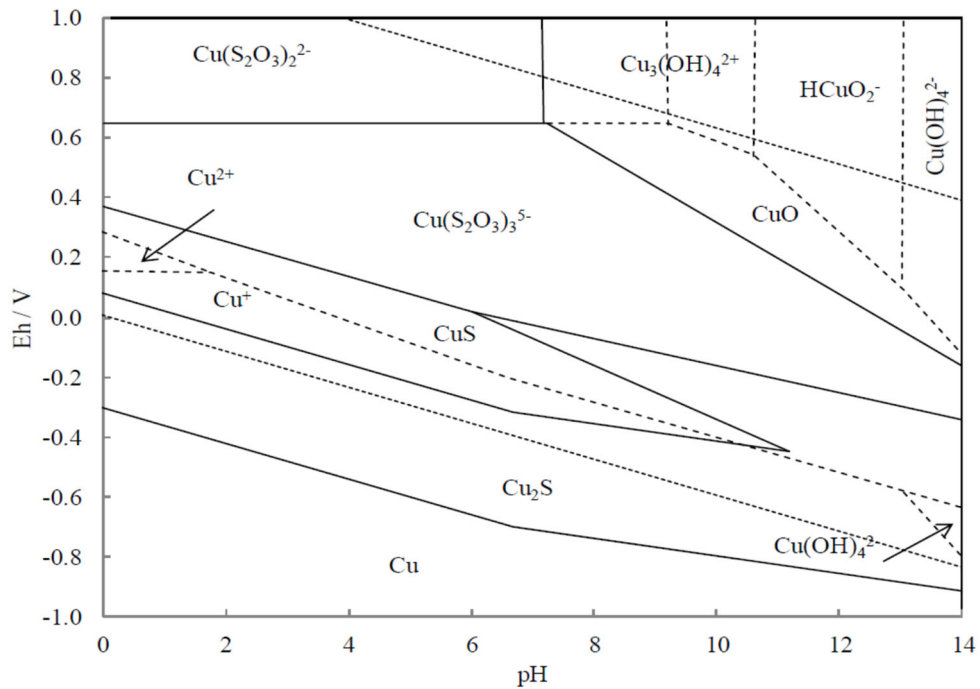


Figure 2-5. Eh-pH diagram of Cu - S₂O₃²⁻ - H₂O system at 25 °C, 0.2 M S₂O₃²⁻ and 0.5 mM Cu(II) after (Zhang 2004)

The role of copper in the absence of a strong ligand like ammonia is not very clear yet (Zhang and Nicol 2005). However, the addition of copper has been shown to have beneficial effects on the initial gold leaching rate in thiosulfate leaching solutions (Senanayake 2005b). At the same time, copper decreases free thiosulfate concentration in the solution by complexation with thiosulfate and oxidation to polythionates and sulfate. According to Rabai and Epstein (1992), Zhang and Nicol (2005), Senanayake (2005b) and Sitando (2017), in the absence of ammonia, it is suggested that copper:

- forms intermediate/metastable complexes with thiosulfate - $[(S_2O_3)_3Cu.O_2]^{5-}$, $[Cu(S_2O_3)_3]^{5-}$, $[Cu(S_2O_3)_2]^{2-}$
- forms a mixed complex- $[(Au, Cu)(S_2O_3)_2]^{3-}$
- prevent gold passivation by sulfur/sulfide enhancing gold oxidation
- assists in the removal of polythionate from the gold-thiosulfate interface.

Until recently, at the Goldstrikes mine in Nevada, pressure oxidation in autoclaves followed by cyanidation was the common practice for the treatment of single refractory sulfide ores. Oxidation is required to dissolve some or all of the sulfide components to expose the surfaces of trapped gold values. Double refractory ores which contain high carbonaceous matter were put through a roasting process prior to cyanidation in order to oxidise the carbon and sulfides.

The two circuits, one with a roaster and the other with autoclaves, were used to process carbonaceous and sulfidic ores, respectively, until recently. With the depletion of single refractory ores and the ineffectiveness of the autoclave unit in treating remaining double refractory ores, the pressure oxidation circuit with autoclaves was slowed. As a result of many years of research, the circuit with autoclaves was converted to a thiosulfate leaching facility to treat double refractory ores (Braul 2013).

This patented process (Choi and Chefai 2012) uses calcium thiosulfate with a lower concentration of copper and a moderate amount of air (at Barrick Gold's Goldstrike operation in Nevada), and has become an industrially proven alternative process for treating double refractory gold ores after pre-oxidation (e.g. by pressure oxidation in an autoclave). The first gold bar using this process was poured at the Goldstrike mine, Nevada in 2014 (Choi 2016). Calcium thiosulfate was selected over sodium or ammonium thiosulfate due to its more environmental friendly nature.

The resin-in-leach (RIL) operating conditions include a CaS_2O_3 concentration of approximately 0.1M, with low levels of copper and moderate air addition at a temperature of 50 °C and pH 8 (Choi 2016). This system provides a number of benefits over conventional thiosulfate leaching systems by using less copper and completely eliminating the use of harmful ammonia in the system. The reduced reagent cost, reduction of the environmental impact and increased solution stability as a result of operating at a pH in the region of 8 are all major benefits. In addition, there are indications that the formation of polythionates is reduced (Choi 2013). Mild thiosulfate concentrations are recommended to suppress the adverse effects of thiosulfate degradation products on gold loading.

The effect of different additives on thiosulfate degradation and gold oxidation has been investigated by Daenzer et al. (2016). The selected additives were pyrite (FeS_2), hematite ($\alpha\text{-Fe}_2\text{O}_3$), copper and gypsum in a calcium thiosulfate - air leaching system. Pyrite was added to 0.1M initial CaS_2O_3 solutions (pH 10) and the decomposition of thiosulfate was observed over time. Thiosulfate degradation was insignificant with a blank solution while considerable loss of thiosulfate was observed along with the formation of tetrathionate and trithionate in the pyrite and pyrite + copper added solutions. Thiosulfate degradation and polythionate formation increased over time. In summary, the addition of hematite did not reveal any gold stability issue in synthetic leach solutions, while pyrite, gypsum and the addition of activated carbon produced some gold stability issues. The longevity of these additives precipitated gold in the solution. However, the mechanism behind gold precipitation remains unknown yet (Daenzer et al. 2016). In addition, tri- and tetrathionate can also contribute to gold precipitation which can be avoided by adding a resin to the leach solution (RIL).

Although solution chemistry is not fully understood for this system, some findings have been reported on the effect of polythionates and some other species on the recovery of gold. Daenzer et al. (2016) reported the results of a study on the effect of polythionates on gold loading onto Purolite A500 anion exchange resin. It was observed that at equal molarities, tetrathionate was less favourable to gold loading than trithionate. The increase in initial polythionate (either trithionate or tetrathionate) concentration in the synthetic leaching solutions significantly reduced the gold loading. In a solution containing 0.1 M CaS_2O_3 , 8 mg/L gold and 4 mM tetrathionate, 61% of the resin capacity was taken up by tetrathionate that replaced the previously adsorbed thiosulfate. Further it was stated that even a small amount (4 mM) of tetrathionate could severely impact upon the gold loading onto IX resin.

2.5.3.3 Ferric-EDTA System

A ferric-EDTA complex was able to dissolve gold, with pure oxygen as the oxidant, although the reaction was very slow. The addition of small amount of thiourea catalysed the reaction and a significant increase in gold oxidation was observed. In addition, the reaction of Fe-EDTA with thiosulfate was less significant and as a result thiosulfate oxidation was considerably less with this system than with the copper-ammonia system (Zhang et al. 2005, Heath et al. 2008). This system operates at nearly neutral pH solutions (pH 6-7) and at 22 - 25 °C. However, no commercial applications have yet been reported.

2.5.3.4 Ferric-Oxalate System

Gold dissolution in thiosulfate leaching solutions with the presence of ferric oxalate as the oxidant has been reported (Chandra and Jeffrey 2005). The thiosulfate consumption was negligible compared to the ammoniacal thiosulfate system. Similar to the Fe-EDTA system, the gold dissolution rate was significantly improved in the presence of thiourea as a catalyst. Thiourea supposed to be accelerate the old oxidation half reaction under favourable conditions. According to literature no evidence of the formation of gold-thiourea complex. Unfortunately the mechanism behind gold oxidation by thiourea in thiosulfate solutions is not clear yet (Chandra and Jeffrey 2004).

This leaching system operates at slightly acidic pH range (4.5 to 6) which is the natural pH of the solution. The pH values less than 4 cannot be used as thiosulfate decomposes to sulfur. However, at pH values above 6.2, Fe(III) can precipitate as $\text{Fe}(\text{OH})_3$.

Thermodynamically, to dissolve gold in a 1 M and 0.1 M thiosulfate solution, an oxidant with a reduction potential greater than 0.15 V and 0.1 V, respectively is needed (Chandra and Jeffrey 2005). Ferric ions were used in the study owing to the low cost and sufficient potential

to oxidise gold in thiosulfate solutions. Oxalate was selected as the ligand to bind with ferric ions. Oxalate forms strong complexes with ferric where the stability constant ($\log \beta$) of $\text{Fe}(\text{C}_2\text{O}_4)_2^-$ and $\text{Fe}(\text{C}_2\text{O}_4)_3^{3-}$ would be 13.81 and 18.6, respectively (Smith et al. 1985).

2.5.3.5 Nickel-Ammonia System

Nickel can be used as a catalyst in gold oxidation in thiosulfate leaching solutions consisting of thiosulfate and ammonia (Arima et al. 2004). This system operates at a pH of 9.5 and at ambient temperatures. Nickelous oxide [Ni_3O_4] formed from nickel amine complex [$\text{Ni}(\text{NH}_3)_6^{2+}$] acts as an oxidant for gold. Gold is oxidised by forming a gold-amine complex [$\text{Au}(\text{NH}_3)^+$] which is not stable and this then immediately converts to a gold-thiosulfate complex. As little as 0.1 mM of nickel is sufficient for 95% gold recovery in 24 hours from a silicate type ore with a gold ore grade of 16.26 g/t. Thiosulfate consumption was 1.2 kg/t (ore) which is approximately 1-5 kg/t less than that needed in a copper-ammonia catalysed leaching system.

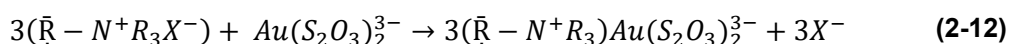
2.6 Gold Recovery from Thiosulfate Leaching Solutions

Gold recovery from pregnant thiosulfate leaching solutions and pulps has mainly been attempted with IX resins and activated carbon. Both pristine activated carbon and chemically modified AC have been reported upon. In addition, a few other adsorbents like mesoporous silica have been investigated. Conventional recovery techniques other than adsorption, such as cementation, chemical reduction, solvent extraction, precipitation and electrowinning have also been examined.

2.6.1 Ion Exchange Resin

The use of IX resins for gold recovery from thiosulfate leaching solutions has been widely studied (Nicol and O'Malley 2002, Zhang and Dreisinger 2002). Strong base anion exchange resins are found to superior to weakly basic varieties with regard to a higher exchange capacity. Weak base resins consist of either primary, secondary or tertiary amine groups and are protonated at acidic pH solutions. These protonated resins attract anions within the protonated pH range and most commonly desorb the anions at alkaline pH solutions. Strong basic resins are based on quaternary amine complexes and can be used within a wide range of pH values as they are inherently protonated (permanently positively charged).

The adsorption of gold thiosulfate complex onto a strong base anion exchange resin can be represented as in equation (2-12). The counter ions are denoted by X (O'Malley 2002).



Resin strength and durability are of the utmost importance for the application in the recovery process. The resins can physically degrade and break as a result of continuous abrasion with particles in the pulp, with adjacent resin particles and screens. Osmotic shock during successive loading and stripping cycles can detrimentally affect the resin's lifespan (O'Malley 2002).

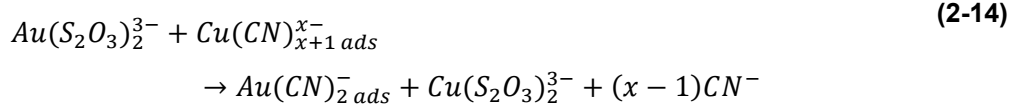
The competitive adsorption of copper and polythionates onto IX resins and the detrimental effect on gold loading in ammoniacal thiosulfate system has been reported (Zhang and Dreisinger 2002). Furthermore, the increase in copper concentration has been promoted thiosulfate degradation. Tetrathionate was the most deleterious compound for gold adsorption. For instance, a 0.01 M tetrathionate addition was able to drop gold loading onto IX resins by approximately 90%. Most of the active sites of the resin were occupied by tetrathionate poisoning the resin. The adsorption of polythionates (tri, tetra and penta) and thiosulfate adsorption onto strong base anion exchange resins were investigated by Muslim et al. (2009). Based on the rate constants and equilibrium constants it was concluded that tetrathionate adsorbs more strongly than trithionate, whilst pentathionate has a higher affinity for the resin over tetrathionate. Similar types of relative affinities were reported elsewhere (Choi and Chefai 2017). A co-current and counter-current RIL approach is discussed in this study which consists of six RIL tanks.

In a calcium thiosulfate – air leaching system, the increase in trithionate and tetrathionate concentration adversely affected gold loading onto Purolite A500 resin, while tetrathionate showed the most deleterious effect at equal molarities (Daenzer et al. 2016). As an example, in a solution consisting of 0.1 M CaS_2O_3 , 50 mg/L Cu, 8 mg/L Au and 4 mM tetrathionate, almost 61% of resin capacity was occupied by tetrathionate, while a further 22% of capacity was occupied by trithionate and thiosulfate.

In the published work, the resin to slurry ratio used for gold recovery from a $CaS_2O_3 - O_2$ based leaching systems is in the range of 1:60 to 1:50 which is approximately equivalent to 18 g/L to 21.6 g/L resin concentration in the case of Purolite A500 (a strong basic anion exchange resin) (Breuer et al. 2012, Choi and Olvera 2017) and 10-25 g/L range in co- and counter current resin applications (Choi and Chefai 2017). In the same study, it was recommended to use higher concentrations of resins at the beginning of the RIL process (in the first few tanks) in order to provide ample adsorption sites for gold, before being preg-robbed or occupied by other competitive species.

2.6.2 Activated Carbon

It is known that well established carbon in leach (CIL) or carbon-in-pulp (CIP) systems used in cyanidation cannot be effectively applicable to the thiosulfate leaching system due to the poor loading of gold thiosulfate complexes onto activated carbon (AC). The affinity of AC towards some gold (I) complexes has been investigated. The order of gold complex adsorption was in the order of $SCN^- > SC(NH_2)_2^- > CN^- \gg S_2O_3^{2-} > S_2O_3^{2-}$. For $Au(S_2O_3)_2^-$, bed saturation was achieved in less than five minutes and the gold adsorption onto AC was less than 1% (Gallagher et al. 1990). The ineffectiveness of AC for gold thiosulfate recovery was verified by Navarro et al. (2007) too. The maximum gold recovery by different types of carbon adsorbents was reported to be 17.9% in the 6-11 pH range. The leach solution did not contain copper, but only thiosulfate and ammonia (Kononova et al. 2001). Abbruzzese et al. (1995) investigated the effect of AC dosage and time on gold thiosulfate adsorption and achieved 21.59% and 42.77% gold recovery after one hour at 5 g/L and 60 g/L AC concentrations, respectively. Furthermore, gold recovery increased to 95% after six hours at 60 g/L AC dosage. An attempt was made to use copper-cyanide loaded AC to recover gold from thiosulfate solutions by using the affinity of gold for cyanide. Gold in the solution binds with cyanide loaded onto carbon, while copper was released to the solution to complex with thiosulfate, as presented in equations (2-13) and (2-14). The adsorbed gold-cyanide can then be processed via normal processing techniques to produce gold bullion (Parker et al. 2008).



The reason for the poor loading is not still well understood; the size or the charge of gold thiosulfate complex may be the reason (Grosse et al. 2003). As a result of poor gold loading onto pristine AC, the use of chemically modified AC was also attempted in gold recovery. Yu et al. (2018) used silver ferrocyanide impregnated AC to recover gold thiosulfate. The maximum adsorption capacity of the adsorbent was only 3.55 kg/ton. Cupric ferrocyanide impregnated AC also has been investigated (Parker et al. 2008, Yu et al. 2015). However, these adsorbents added cyanide to the recovery solution deviating from one of the main purposes for considering alternative lixivants; the environmental concern.

2.6.3 Mesoporous silica

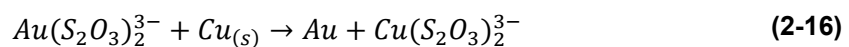
Amine and thiol groups functionalised mesoporous silica were used for gold recovery from ammoniacal thiosulfate solutions (Fotoohi and Mercier 2014). An average of 80% gold recovery was noticed in both neutral and alkaline pH solutions. The mesoporous adsorbent with a high specific surface area (441 m²/g) exhibited approximately 600 mg/g adsorption capacity. The highest gold loading was achieved with the lowest copper amount (2.5 mM) and at the lowest thiosulfate concentrations (0.05 M) at 0.1 M ammonia dosage. The presence of chloride ions in the simulated leach solutions were found to be detrimental to the gold loading onto mesoporous silica. Importantly, sodium and potassium ions concentration should not exceed 0.1M. Initially, the adsorption kinetics were slow and the system only reached equilibrium after 18-20 hours. The competitive adsorption of free thiosulfate and polythionates was reported while copper was not stated as a significant competitor. Furthermore, only near neutral pH values are preferred to ensure the long life cycle of the mesoporous silica framework (Fotoohi and Mercier 2014).

2.6.4 Cementation

Cementation is simply the electrochemical precipitation of the desired metal using a zerovalent base metal powder (Guerra and Dreisinger 1999). The carefully selected base metal, based on the galvanic series, replaces the precious metal (gold) by reducing it to metallic form. This is one of the oldest methods of metal recovery (O'Malley 2002). Commonly used metals are copper and zinc whilst aluminium and iron powders are also considered in some instances (Arima et al. 2002, Navarro et al. 2004). The well-known Merille-Crowe process uses zinc cementation. The base metal (M) supplies necessary electrons for the gold thiosulfate complex to reduce to metallic gold as illustrated in equation (2-15).



Copper is the preferred choice of metal due to few reasons. Copper is relatively inexpensive and since it is already used as an additive in the thiosulfate leach liquors it can simply be recycled for leaching (Grosse et al. 2003, Choo and Jeffrey 2004). Zinc, aluminium and iron can precipitate both gold and copper in the solution resulting in lower gold grades (Arima et al. 2002, O'Malley 2002). The reaction is expressed in equation (2-16).



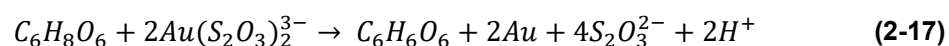
A detailed study on gold cementation with copper in ammoniacal thiosulfate leaching solutions was conducted by Guerra and Dreisinger (1999). The cementation process was controlled by mass transfer. Higher temperature, higher pH and higher ammonia concentrations enhanced cementation performance while the availability of sulfite and copper had a negative effect.

The use of copper, zinc, iron and aluminium to precipitate gold from ammonium thiosulfate solutions in similar conditions was investigated (Karavasteva 2010). The gold cementation rate decreased in the order of $Cu > Zn > Mg > Fe > Al$. However, zinc is undesirable as it precipitates all the gold and copper in the solution and negatively influences gold leaching in thiosulfate solutions (Kerley 1983). The use of iron also causes co-cementation of copper with gold. The unavailability of any soluble aluminium complexes in thiosulfate solutions makes the use of this metal ineffective. Moreover, the formation of oxide layers on these metals in the presence of air or oxygen prevents the cementation process and consumes excess metal (O'Malley 2002).

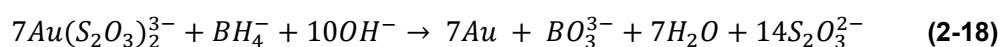
2.6.5 Chemical Reduction

Ascorbic acid, sodium borohydride, and sodium sulfite have been used as reducing agents for gold thiosulfate. This chemical reduction method is also known as electroless plating. Some limited work has been reported with hydrogen as well. The higher reduction potential of the gold thiosulfate complex allows the selection of a number of reducing agents over gold cyanide (O'Malley 2002).

Sodium L-ascorbic acid was used as a reducing agent together with hydrogen peroxide as an additive to minimise thiosulfate accumulation in the chemical bath; which would otherwise decrease the gold deposition rates (Sullivan and Kohl 1995). Hydrogen peroxide breaks down thiosulfate into trithionate and sulfate. However, this ultimately increases the ascorbic acid use as it reacts with hydrogen peroxide as shown in equation (2-17).



In slightly acidic solutions and at ambient temperatures, borohydride can reduce gold thiosulfate complex to very fine crystals of metallic gold, according to equation (2-18) (Awadalla and Ritcey 1991).



The major problem associated with this method is the excessive consumption of borohydride by other impurities mainly iron, copper and nickel in the solution; these impurities contaminate the gold precipitate. Furthermore, borohydride is expensive and poisonous which poses environmental concerns.

The sodium sulfite-sulfate pair is known to be simple and mild reducing agent for gold thiosulfate reduction. Several other additives, together with sulfite-sulfate have been proposed as solutions to increase the deposition rates, along with extending the longevity of the bath process (O'Malley 2002). Electroless plating is not really an optimum method for gold leaching plants. It is an expensive and complex process. Moreover, it cannot be applied for pulps to recover gold.

2.6.6 Electrowinning

The application of direct current to recover metal ions in a solution is known as electrowinning. In general, this applies to the recovery of gold from eluates. Gold thiosulfate complex migrates to cathode to form a metallic gold deposition. The co-deposition of other metals such as silver also can occur. The presence of excess amounts of metallic cations (Cu(I), Cu(II)) can also contaminate the gold product. The electrochemical reaction which occurs at the cathode surface is given in equation (2-19).



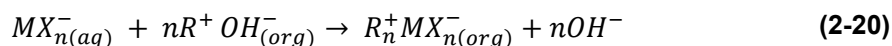
In addition, two parasitic reactions occur at the cathode, involving the reduction of water and dissolved oxygen and consuming electricity (Abbruzzese et al. 1995). Thiosulfate can also reduce to sulfide causing gold precipitation as gold sulfide at the cathode if the potential is too negative. It is reported that a constant cathode potential (-400 mV versus SHE) should be maintained (Dai et al. 2013).

At the anode, the evolution of oxygen takes place by oxidation of water. Moreover, the presence of free thiosulfate in the solution can lead to the generation of polythionates which necessitate the periodical treatment of eluate to convert polythionates back to thiosulfate (Aylmore 2016a). The unavoidable existence of various copper and thiosulfate based products in these solutions makes the electrowinning process challenging (Grosse et al. 2003).

2.6.7 Solvent Extraction

In solvent extraction, clarified leach liquor is contacted with an organic solvent containing a gold selective extractant. The gold complex is transferred to the organic phase, ideally leaving

other metal ions in the aqueous phase. The organic phase is separated and gold is stripped. Usually kerosene is used to dissolve the organic reagent which contains a suitable functional group (R^+) to exchange with anionic metal complex (MX_n^-) as given in equation (2-20).

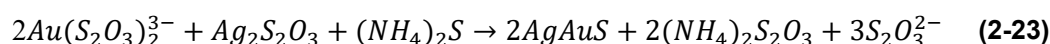
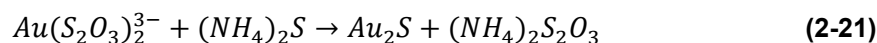


Few studies have been reported on the finding of suitable solvents for gold thiosulfate in alkaline pH values. Primary, secondary and tertiary amines have been tested for gold thiosulfate recovery with aromatic and aliphatic hydrocarbons as diluents (Zhao et al. 1998). The degree of gold extraction decreased in the order of primary > secondary > tertiary. Moreover, alkyl phosphorous ester and primary amine mixed with tributyl phosphate (TBP) and trialkyl amine oxide (TRAO) were also considered (Zhao et al. 1997, Zhao et al. 1999). The use of trioctylmethylammonium chloride (TOMAC) has been investigated at a wide pH range (3-11.5) with different diluents (n-octane, kerosene and benzene) (Kejun et al. 2004).

Higher capacity, better selectivity and fast kinetics are the main advantages associated with this method (Zhao et al. 1999). However this method needs a clarified solution which necessitates solid-liquid separation steps. It requires additional processing steps and equipment which can considerably improve the capital cost. The loss of the organic phase by dissolution in the aqueous phase through chemical degradation and evaporation also need to be evaluated (Grosse et al. 2003).

2.6.8 Chemical Precipitation

The use of ammonium sulfide to precipitate gold and silver from clarified leaching solutions has been reported. Sulfide can precipitate gold (and silver) as their respective sulfides. If the solution contains both silver and gold, gold will coprecipitate with silver, which contaminates gold, as shown in equations (2-21) to (2-23). The major limitation of this process is the need for excess sulfide to prevent redissolving of the gold by thiosulfate which is formed (Kerley 1983, O'Malley 2002).



Lead acetate and sodium borohydride have also been used to precipitate gold from clarified thiosulfate leaching solutions which consist of gold, silver and some platinum group metals (PGM) (Groves and Blackman 1995). The formed lead-precious metal sponge is further treated to recover precious metals by de-leading. The high process cost, safety and the need of filtration to get clear solutions make the process impractical for application on a large scale.

2.7 Adsorption

The adsorption process involves the separation of a substance (adsorbate) from one phase by accumulation of the substance onto the surface of another substance (adsorbent). The two phases can be liquid - gas, liquid - liquid, solid - liquid and solid - gas. The adsorption is purely a surface phenomenon where only the surface of the adsorbent is involved. In porous adsorbents, the pore surfaces (walls) also act as adsorption sites.

2.7.1 Adsorption Mechanisms

Primarily two types of adsorption mechanisms are defined, physical adsorption (physisorption) and chemical adsorption (chemisorption). In addition, ion exchange is indeed a kind of adsorption where the simultaneous desorption of equivalent amount of the same charge ionic species occurs (Dąbrowski 2001).

Physical adsorption, which is also known as physisorption, nonspecific adsorption, outer sphere adsorption or ion pair formation occurs by electrostatic attraction and hence is influenced by the ionic strength of the solution. In a pure physisorption system, anion adsorption is only possible below the pH_{PZC} value. This mechanism is sometimes non-selective, meaning that most of the ions with same type of surface charge in the bulk phase can adsorb to the adsorbent surface bearing the opposite charge. In this case, the degree of anion adsorption is proportional to their concentration in the solution (to a certain extent). Physisorption is known to be a multilayer process although the binding could get weaker when the number of layers increased (Artioli 2008).

In the occurrence of chemical adsorption, the adsorbate bonds chemically to the adsorbent surface predominantly by covalent bonds. Chemical adsorption is also known as chemisorption, specific adsorption or inner sphere adsorption and in the case of ligands, ligand exchange. This phenomenon occurs when the chemical component of the adsorption free energy predominates, irrespective of the surface charge of the adsorbent (Cornell and Schwertmann 2006). The chemically adsorbed ions mainly display a covalent bonding nature and may change the surface charge of the iron oxide core resulting in a change in the pH_{PZC}

value. In contrast to physisorption, chemisorption is a monolayer process. Under favourable conditions, both mechanisms can operate simultaneously or alternatively (Dąbrowski 2001).

2.7.2 Adsorption Isotherms

For any novel adsorbent-adsorbate system, it is utmost important to understand the equilibrium correlation between the adsorbate and the adsorbent. A proper understanding of this relationship is crucial for the effective design and optimisation of an adsorption system (Tauetsile et al. 2018). Adsorption isotherms related to solid-liquid systems describe the interaction between the amount of adsorbate on the adsorbent and in the solution phase. In more general use, adsorption isotherm models are often used for the determination of adsorption mechanisms and for the calculation of the maximum adsorption capacity of the adsorbent. Many adsorption isotherm models have been defined. However, Langmuir, Freundlich, Dubinin-Radushkevich and BET isotherm models are predominantly used for the understanding of different species adsorption onto magnetic nanoparticles. The latter two models are mainly used for porous adsorbents. Apart from these models, Gibbs, Temkin and Elovich's isotherm models are also worth mentioning.

The Langmuir theory is based on few assumptions as mentioned below (Langmuir 1918, Do 1998).

1. Monolayer adsorption onto a homogenous surface, which means adsorption energy is constant at all sites on the surface.
2. The adsorption onto the surface is localised, that is the adsorption occurs at definite localised sites only.
3. Each site can accommodate only one molecule of adsorbate.

The Freundlich isotherm describes adsorption onto a heterogeneous surface which is not restricted to monolayer adsorption. Given that, this model does not correspond to the saturation of the surface. This is frequently used for systems, which use activated carbon as the adsorbent. Although this was originally proposed as an empirical equation, it can be theoretically derived by assuming the adsorption energy in the heterogeneous surface is distributed patch-wise, and then applying the Langmuir equation for each patch (Do 1998).

The Dubinin-Radushkevich isotherm model is also an empirical model and often used to distinguish between chemical and physical adsorption mechanisms in porous adsorbents (Dubinin and Radushkevich 1947). This equation is temperature dependent (Foo and Hameed 2010).

The BET isotherm model (1938) is a theoretical equation and assumes multilayer adsorption from flat surfaces. All the other assumptions are the same as the Langmuir model, except the multilayer adsorption. This was first developed for adsorption onto flat surfaces and was an important milestone in the consideration of multilayer adsorption of gases (Do 1998).

2.7.3 Adsorption Kinetics

Understanding of adsorption kinetics is of the utmost importance with regard to any adsorption system. In many circumstances, adsorption kinetics are dependent upon initial adsorbate concentration, particle size, temperature and film thickness (Ho and McKay 1998). Adsorption kinetics data provides valuable insights into the determination of adsorption mechanism. However kinetics data alone are not sufficient for the purpose of determining the adsorption mechanism (Tran et al. 2017).

Mainly few models, such as pseudo-first-order (Lagergren 1898), pseudo-second-order (Blanchard et al. 1984), the Elovich model and the intra-particle diffusion model (Weber and Morris 1963, Crank 1975) are often used to model adsorption kinetics in solid-liquid phase sorption systems. Hao et al. (2010) used pseudo-first-order, pseudo-second-order, Elovich and intra-particles diffusion models to explain the Cu(II) adsorption kinetics onto amine coated MNPs. The pseudo-second-order model best fitted the data. According to Choudhary et al. (2018), gold adsorption kinetics from acidic solutions on to PEI functionalised bio mass was in accordance with the pseudo-second-order model.

The role of diffusional mass transport models like the intra-particle diffusion model is important when ion exchange and ionic bonding are not prevailing in the adsorption process (Ho and McKay 1998). The diffusion models are usually based on one or more of the following steps.

- External mass transfer from bulk solution across the hydrodynamic layer surrounding the particle
- Diffusional mass transfer within the internal structure of particles (by a pore, branched pore or a surface). This can be one process or combination of processes.
- Adsorption at a surface site

Although these diffusion models have been originally developed for the removal of dyes and organic matters from waste water using AC or similar porous adsorbents, the current use has

extended to other different adsorbents (Hua et al. 2012, Kumar and Chawla 2013, Choudhary et al. 2018).

2.7.4 Selectivity of Anions

Selective adsorption is paramount in a multicomponent solution. Grosse et al. (2003) explains the major factors of selective adsorption of gold thiosulfate onto IX resins as the size, shape and charge density of the anionic complex. Gold thiosulfate complex is known to be linear whereas copper thiosulfate complex is trigonal. The former complex bears a (3-) charge while the latter complex bears a (5-) charge. In addition, the size of divalent trithionate and tetrathionate anions are reported to be much smaller which is advantageous in order to the designing of a gold thiosulfate selective adsorbent.

The selectivity ratio (S/R) of a resin is defined as;

$$\frac{S}{R}\{Au, M\} = \frac{[Au]_{Resin}}{[M]_{Resin}} \quad (2-24)$$

where, M is a metal ion and $[M]_{Resin}$ is the molar concentration of metal on the resin and $[Au]_{Resin}$ is the concentration of gold on the resin. However this can strongly depend on the initial concentrations of the metal ions. The selectivity ratio of Purolite 500C resin in ammoniacal thiosulfate leaching solutions for gold over copper is reported as 0.034 - 0.038. This was 2.39 for Amberjet 4200 resin. Both resins were strong base anion exchangers consisting of quaternary ammonium moieties (Grosse et al. 2003).

The surface functional groups of the adsorbent play a vital role in selective adsorption (Kononova et al. 2001). According to Riveros (1993), the hydrophilic nature, ionic density and functional groups of the resin significantly affect the selective adsorption of the gold cyanide complex. Furthermore, the length of alkyl groups attached to the nitrogen atom also contribute to the selectivity.

The total ionic strength of the solution, polarisation and size of the adsorbate also affects the selectivity of gold in cyanide solution to IX resins (Lukey et al. 1999). It was shown that the selectivity of gold over copper was increased in saline solutions as a result of the formation of a tetrahedral $[Cu(CN)_4]^{3-}$ complex which demands at least three active sites in correct size. Linear $[Au(CN)_2]^-$ complex is smaller in size and can be easily adsorbed onto the functional groups of resin (Lukey et al. 1999, Lukey and van Deventer 2004).

Recently, Li et al. (2014) proposed taking advantage of ionic potential to decide the potential adsorbents for arsenic removal. Ionic potential (ϕ) is defined as the ion's charge divide by its radius in Å. In other words, ionic potential is a measure of charge density. Ionic potential indirectly represents the ability of an adsorbate to replace the surface hydroxyl groups and is helpful in determining potential metal oxides to adsorb specific ions.

In the case of MNPs, selectivity is often achieved through surface modification. Many researchers have used Pearson's hard soft acid base (HSAB) theory (Pearson 1963) to determine the potential functional groups for specific adsorbates (Tahmasebi and Yamini 2013, Zhang et al. 2013c). According to HSAB theory, precious metals such as Au, Ag, Pd and Pt are classified as soft acids. These soft acids tend to coordinate with functional groups containing soft bases such as nitrogen and sulfur atoms (Aghaei et al. 2017). Immobilisation of amine and thiol groups to mesoporous MCM-41 adsorbent for selective gold adsorption from a solution consisting of Au(III), Cu(II) and Ni(II) was attempted by Lam et al. (2008). The same two adsorbents were tested in gold mining solutions consisting of Au, Cu, Pd, Pt and Fe as their respective chloride salts. Amine coated MCM-41 was superior in its selective adsorption of Au and Pd whilst thiol modified MCM-41 attracted all types of metals in greater or lesser amounts.

The use of different pH values for selective adsorption is yet another option. Lotfi Zadeh Zhad et al. (2013) selectively recovered Au(III) and Ag(I) at pH 2-3 and 8-9, respectively by using Tris(2-Aminoethyl) amine functionalised Fe₃O₄ NPs. Au(III) adsorption was dominated by electrostatic attraction whilst Ag(I) coordinated with amine groups at alkaline pH solution. However this method is not very promising for complex solutions consisting of numerous anionic complexes. Yet, in some solutions, such as thiosulfate leaching solutions, selective adsorption of preferred anions is challenging and in those cases, selective elution was considered (Jeffrey et al. 2010).

2.8 Magnetic Nanomaterials

Nanoscale magnetic materials are continually attracting research attention in different disciplines all over the world. Nanoparticles (NPs) are ultrafine particles in the order of nanometre size. Generally the particles, from 1 to 100 nm in size (at least one dimension), are termed nanoparticles, although few hundred nanometre sized particles are also considered in the same category in some instances (Wu et al. 2008, Yokoyama 2012). Magnetic nanoparticles commonly consist of magnetic elements such as iron, nickel, cobalt or their chemical compounds which can be manipulated by means of an external magnetic field. These MNPs show many novel properties, especially, magnetisation behaviour different to that of

the corresponding bulk material (Ambashta and Sillanpaa 2010, Gupta and Nayak 2012). Under some critical dimensions, the nanosized magnetic materials become superparamagnetic exhibiting no magnetism once the external magnetic field is detached (Gómez-Pastora et al. 2014). Recently, the use of nanosized magnetic materials as adsorbents has attracted increasing interest due to their high surface area and unique superparamagnetism (Pang et al. 2011a, Hanif and Shahzad 2014). These properties lead to high adsorption efficiency, a high removal rate of contaminants and the simple and rapid separation of adsorbent from solution using a magnetic field. In many instances magnetic nanoparticles are reusable after desorption and regeneration (Shen et al. 2009).

The application of nanoparticles (NPs) in different sectors is often being investigated. Currently, magnetic nanoparticles are used in a wide range of applications (Ilankoon 2014). Magnetic nanomaterials in biotechnology and biomedicine have great potential in many applications such as cell labelling and separation (Wilhelm and Gazeau 2008), magnetic resonance imaging (MRI) (Schleich et al. 2013), enzyme and protein separation (Chang et al. 2010), targeted drug delivery (Sahu et al. 2012) and magnetic ferrous fluids hyperthermia (Laurent et al. 2011). Furthermore MNPs have been experimented for shape-selective catalysis (Garro et al. 2005), chromatographic separations (Hou et al. 2004) and enzyme encapsulation. A number of reviews have been published on using NPs for environmental applications, heavy metal removal and dye removal from water (Shan et al. 2009, Hua et al. 2012, Giakisikli and Anthemidis 2013, Kumar and Chawla 2013, Tang and Lo 2013b, Sivashankar et al. 2014). The use of nano- and micro-sized magnetic particles for precious metal adsorption, mainly Au(III), Ag(I), Pd(II) and Pt(II), from leach solutions and wastewater has also been reviewed (Aghaei et al. 2017).

2.8.1 Magnetic Separation

2.8.1.1 Superparamagnetism

Superparamagnetism becomes important when the ferromagnetic and ferrimagnetic substances scale down to nanometre size. The critical size of the nanoparticles (NPs) to demonstrate superparamagnetic behaviour varies from a few nanometres to a few tenths of a nanometres (O'Handley 2000, RuizMoreno et al. 2012, Patsula et al. 2016). These NPs are single domain and in the absence of any applied magnetic field, the net moment is zero. Ideally the coercivity and hysteresis is zero for superparamagnetic NPs (Xie et al. 2015). Once a magnetic field is applied, the particles attracted to the magnetic field behave similarly to paramagnetic substances, but with a much higher magnetic susceptibility. In contrast to ferromagnetic and ferrimagnetic substances that display a paramagnetic nature only above the

Curie temperature (T_c), superparamagnetic materials exhibit this behaviour below T_c . Nanosized magnetic materials typically have anisotropy which means often their magnetisation aligns in a certain direction. MNPs randomly flip this direction and this can be induced by thermal energy. The average time between two flips is known as *Neel relaxation time*. In the absence of an applied field, when the measurement time taken is longer than the Neel relaxation time, the value of magnetisation appears to be zero, which is a characteristic of superparamagnetism (Marghussian 2015).

2.8.1.2 High Gradient Magnetic Separation

With the introduction of high gradient magnetic separation (HGMS) during the 1950s, expansion in the field of magnetic separation accelerated. Typically, a high gradient magnetic separator consists of an electromagnet which is designed to produce a strong adjustable magnetic field gradient inside a column. This column volume is loosely packed with filamentary wires of ferromagnetic materials which can attract even weakly magnetic materials, due to the strong magnetic field gradients generated around the wires. The dimensions of these wires are chosen in order to match the size of the magnetic particles to be captured in the feed material. The feed solution/slurry is passed downwards through the column where magnetic materials in the slurry are captured by the magnetised wire matrix, separating magnetic particles from non-magnetic species and the solution.

The arrangement of wires inside the column is designed in order to pass through the other nonmagnetic solids and solution easily. To ensure effective separation of magnetic particles by HGMS, the magnetic force of the wires must dominate the fluid drag, gravitational forces, inertial, and diffusion forces as the slurry flows through the magnetic separator. The attached magnetic particles can be detached easily by adjusting the magnetic field to zero and flushing with water (Oberteuffer 1974, Ambashta and Sillanpaa 2010).

In the modern world, HGMS operation mostly automated with the use of modern technology and available in different sizes and customized designs to optimise the separation process based on the feed material (Metso 2015). Commonly, woven wire mesh, steel wool (shown in Figure 2-6), grooved plates, steel rods, steel balls and expanded metal are used as magnetic matrices in HGMS. Amongst them, steel wool has the highest magnetic field gradient reaching 2.5×10^4 T/m. The proper selection of magnetic matrix and optimisation of the magnetic matrix significantly improves separation efficiency cost effectively. This is preferable to an increase in magnetic field intensity and magnetic field gradient which results in high energy consumption and ultimately, high processing costs (Ge et al. 2017).

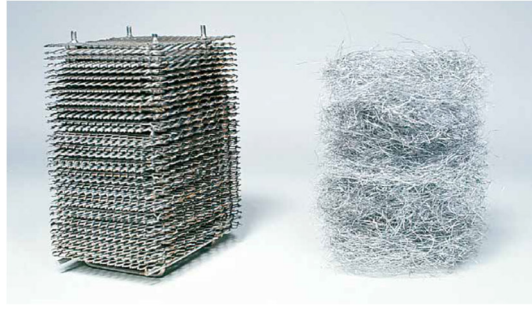


Figure 2-6. Magnetic matrices used in HGMS (Derived from HGMS brochure-Metso)

2.8.1.3 Magnetic separation of nanoscale magnetic particles

The separation of particles with the aid of an external magnetic field is more efficient, selective and often much faster than conventional filtration and centrifugation (Yavuz et al. 2006). Moreover, magnetic separation is much less sensitive to the solution pH, surface charge, temperature and ionic strength of the solution (Pamme 2006).

However when ferromagnetic iron oxides reach a certain nanometre size, their magnetic behaviour becomes superparamagnetic in nature. These nanosized particles can still be separated using HGMS as reported (Chantrapornchai et al. 2009). Kelland (1985, 1993) estimated the smallest size of particle that could be separated magnetically is 3 nm. In similar agreement with this, Takayasu et al. (1983) estimated the critical particle radius for magnetite to be 2.2 nm. Further, it was concluded that critical particle size is independent of the size of the HGMS collector. Gerber et al. (1983) attempted to generalise the HGMS theory for ultrafine particle capturing using HGMS. The limiting particle size was calculated as 40 nm and 200 nm for magnetite and hematite particles, respectively dispersed in water for capturing in dynamic mode. The magnetisation of the wire (50 μm diameter) was 135 emu/g at an applied magnetic field of 1 T. Critical particle size for efficient magnetic separation by extrapolation from bulk material behaviour was suggested as 50 nm (Fletcher 1991). Extrapolation from bulk material properties to a nanoscale level has been seen as problematic (Yavuz et al. 2006). In another study, an increase in the volume of the wire matrix and the use of superconducting magnets to generate high magnetic field strengths was proposed to capture nanometre size particles (Tsukamoto et al. 1995). Later, Kelland (1998) attempted nanometre size magnetic particle separation from aqueous dispersion using two HGMS approaches; matrix and continuous modes. The mean diameter of the feed of ferrofluid was 68 nm.

Bench scale HGMS experiments have been conducted for polymer coated and phospholipid coated nanosized Fe_3O_4 magnetic particles, using a 22.6 cm long glass column loosely and randomly packed with stainless steel wool. Variable strength magnetic fields (1.3 T)

perpendicular to the solution flow were produced by an electromagnet. It was observed that particle size is a major factor and the formation of small aggregates is beneficial for high separation efficiency in HGMS. The minimum size of aggregates was calculated to be 40 nm and 70 nm to permanently capture phospholipid coated and polymer coated nanoparticles, respectively. The saturation magnetisation of Fe₃O₄ core was reported as 63 ± 5 emu/g, although values after surface coating have not been reported (Moeser et al. 2004).

Ditsch et al. (2005) investigated the magnetic separation of polymer coated Fe₃O₄ nanoparticles. Nanoclusters in the range of 50 nm or above were able to separate by using the HGMS column efficiently. Longer columns and lower velocities enhanced the separation efficiency. In another study, decanoic acid coated 8 nm Fe₃O₄ nanoparticles were separated efficiently (Bucak et al. 2003). Furthermore, the analytical methods of separating and isolating magnetic nanoparticles has been comprehensively reviewed (Stephens et al. 2012).

Nevertheless, the minimum critical size of the particle depends on the applied magnetic field, the magnetic field gradient of the wire matrix and the magnetic properties of the particles to be separated, as given in equations (2-25) and (2-26) (Moeser et al. 2004).

$$F_m = \mu_0 V_p M_p \cdot \nabla H \quad (2-25)$$

$$M_p = \chi H \quad (2-26)$$

where F_m is magnetic force acting on the particles, μ_0 is the permeability constant of the vacuum (H/m), V_p is the volume of the particle, M_p is the magnetisation of the particle (A/m), ∇H is the gradient of magnetic field at the position of the particle, χ is magnetic volume susceptibility and H is magnetic field strength (A/m) (Bucak et al. 2003).

Recently, nanocrystals 16 nm in diameter were separated from a homogeneous dispersion with a low gradient (23 T/m) external magnetic field within minutes (Yavuz et al. 2006). The time for the separation depends on particle size and the solution concentration. For complete nanoparticle separation from a dispersion, the field should be increased as the particle size decreases. A 0.2 T field was able to separate 12 nm and 20 nm particles, but was unable to separate 8 nm Fe₃O₄ particles effectively. In order to separate effectively, particles must overcome the Brownian motion (F_B) as given in equation (2-27) (Yavuz et al. 2006).

$$F_B = \frac{K_B T}{d} \quad (2-27)$$

Where, K_B is the Boltzman constant, d is particle diameter and T is temperature.

According to the aforementioned studies, the minimum particle size that can be magnetically separated lies within a quite wide range. The size of single particles and small aggregates varies from 3 nm to 70 nm. Formation of small aggregates/ nanoclusters were beneficial for effective magnetic separation. In addition to the particle size, the properties of HGMS collector such as wire thickness, magnetic field strength, and type of magnet used also play an important role in efficient magnetic separation.

2.8.2 Iron Oxide Nanoparticles

Iron is one of the most abundant materials in the earth. The widespread availability, biocompatibility and ease of synthesis makes iron oxide based nanomaterial a relatively low cost nanosorbent for use in different applications (Hua et al. 2012). The ability to manipulate the nanoparticles in solution using an external magnetic field is the driving force for the use of this type of NPs for several applications. The saturation magnetisation of nanosized iron oxides is relatively lower than the respective bulk material. For instance, bulk magnetite exhibits 92-100 emu/g while this drops to approximately 60 emu/g when the particles reach nanoscale sizes, but the size is still sufficient to be separated by an external magnetic field.

All iron oxides consist of closed packed oxygen anion lattice, with ferric and ferrous cations occupying octahedral and/or tetrahedral lattice sites. Nano-sized magnetite (Fe_3O_4), maghemite ($\gamma\text{-Fe}_2\text{O}_3$), hematite ($\alpha\text{-Fe}_2\text{O}_3$) and goethite ($\alpha\text{-FeO(OH)}$) are well known iron oxides. An overview of magnetite and maghemite NPs is included in the following sections, as these two iron oxides are the main components in the adsorbent used in this study. The lattice structure of hematite is also briefly discussed.

2.8.2.1 Magnetite (Fe_3O_4)

Magnetite in its bulk form is an opaque jet black colour, non-porous mineral found in the earth with a density of 5.18 g/cm^3 (Cornell and Schwertmann 2006). Magnetite NPs are one of the most frequently studied iron oxide NPs in different areas. They are also assumed to be non-porous (Blaney 2007). Magnetite has an inverse spinel structure and the unit cell is face centred cubic (fcc). It consists of both Fe^{2+} and Fe^{3+} ions in a 1:2 ratio which can be rewritten as $\text{FeO}\cdot\text{Fe}_2\text{O}_3$. All the oxide ions are arranged in a close-packed cubic array in the spinel structure and Fe^{2+} occupies half of the octahedral sites whilst Fe^{3+} occupies the remaining octahedral and all the tetrahedral sites. A schematic representation of crystal structure can be found in Figure 2-7. The lattice parameter of magnetite is 8.397 \AA . Bulk magnetite is ferromagnetic and demonstrates superparamagnetic behaviour when it reaches the nanoscale size range. In

general, magnetisation varies around 92-100 emu/g for bulk magnetite whilst this drops to 30-60 emu/g range for nanosized particles (Harris et al. 2003).

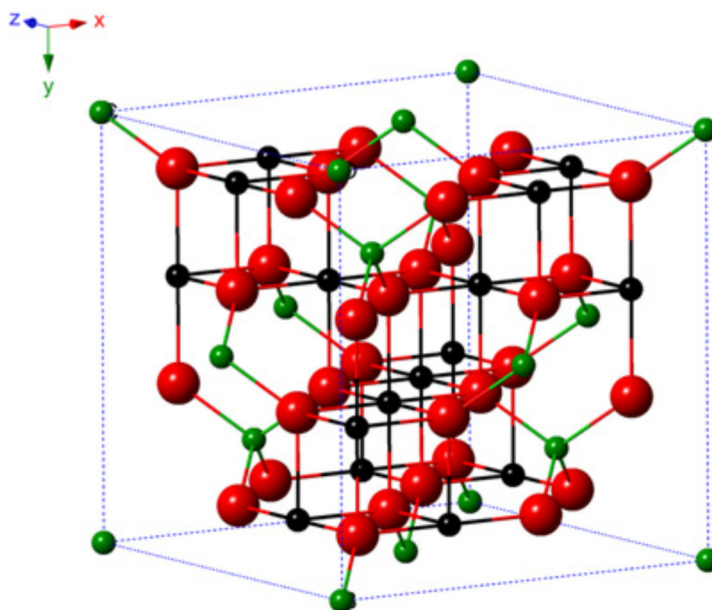


Figure 2-7. Schematic illustration of crystal structure of magnetite (the black sphere is Fe^{2+} , the green sphere is Fe^{3+} and the red sphere is O^{2-}). Derived from (Wu et al. 2015)

2.8.2.2 Maghemite ($\gamma\text{-Fe}_2\text{O}_3$)

Maghemite contains only Fe^{3+} cations in the spinel structure and is more often formed by oxidation of magnetite. Maghemite is reddish brown in colour and the density is 4.87 g/cm^3 (Teja and Koh 2009). The crystal structure of maghemite is schematically represented in Figure 2-8. The unit cell is cubic and oxygen anions are arranged in cubic close-packed manner while Fe^{3+} occupies tetrahedral and octahedral sub lattices. In contrast to the bulk material where Fe vacancies occur only in the octahedral sites (Armstrong et al. 1966, Haneda and Morrish 1977), some studies report the occurrence of vacancies in both octahedral and tetrahedral sub-lattices in the case of nanoscale maghemite (Petkov et al. 2009, Cervellino et al. 2014). In different reports, the lattice parameters for maghemite were found to be spread across quite a wide range ranging from approximately 8.34 to 8.4 (Kim et al. 2012, Cervellino et al. 2014). Similar to magnetite, bulk maghemite is also ferromagnetic, whilst nanoscale maghemite shows superparamagnetic characteristics. Anyway magnetisation is somewhat lower than that of magnetite where bulk magnetite shows 92-100 emu/g whilst maghemite is in the 60-80 emu/g range (Cornell and Schwertmann 2006, Yogo et al. 2011).

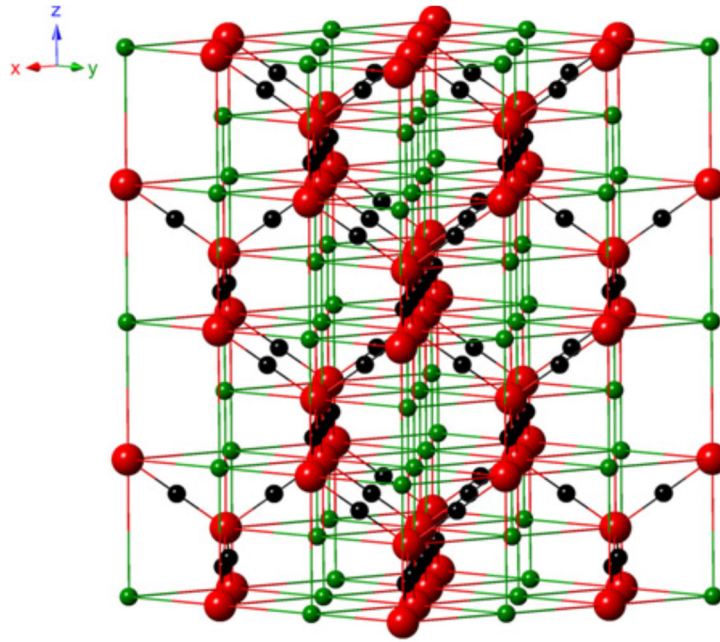


Figure 2-8. Schematic illustrations of crystal structure of maghemite derived from (Wu et al. 2015)

2.8.2.3 Hematite ($\alpha\text{-Fe}_2\text{O}_3$)

Hematite, with characteristic red to reddish brown colour, is the most stable iron oxide at ambient conditions under oxidising conditions (Wu et al. 2015). The unit cell is hexagonal with the lattice parameters $a=5.0356 \text{ \AA}$ and $c=13.749 \text{ \AA}$ (PDF-00-033-0664) and Fe^{3+} ions occupy the octahedral sites (shown in Figure 2-9). Hematite is antiferromagnetic with 5.26 g/m^3 of density, slightly greater than that of magnetite (Cornell and Schwertmann 2006).

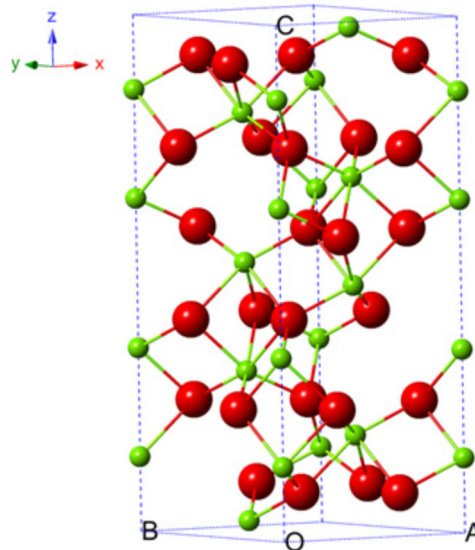


Figure 2-9. Schematic illustrations of crystal structure of hematite Derived from (Wu et al. 2015)

2.8.3 Nanoparticle Synthesis

To date, many technologies, mainly co-precipitation (Mahdavian and Mirrahimi 2010, Ge et al. 2012), microemulsion (Drmota et al. 2012), thermal decomposition (Sharma and Jeevanandam 2012), hydrothermal synthesis (Xin et al. 2012), microwave assisted methods (Ahmed et al. 2013), sol-gel synthesis (Huang and Hu 2008) and sonochemical synthesis (Vijayakumar et al. 2000) have been employed for the synthesis of magnetic nanoparticles.

The precise control of nanoparticle size and the size distribution is challenging. In the co-precipitation technique, these parameters depend on reagent concentrations and synthesising conditions mainly on the type of salts used (e.g. chlorides, sulfates, nitrates), the $Fe^{2+}: Fe^{3+}$ ratio, the pH value, the reaction temperature, and the ionic strength of the media. Short bursts of nucleation followed by slow controlled growth produces monodisperse nanoparticles. The addition of organic anions (e.g. PVA, oleic acid) during synthesis could also help to stabilise nanoparticles. (Lu et al. 2007). The process parameters and main characteristics of the nanomaterials synthesised with few major synthesis methods are summarised in Table 2-3.

Table 2-3. Process conditions of some nanoparticle synthesis methods and properties

Synthesis method	Process conditions and properties	Reference
Co-precipitation	Synthesis is simple and fast (minutes), 20-90 °C temperature, pH 11-12 Relatively narrow size distribution Shape control is hard	(Lu et al. 2007)
Hydrothermal	Simple, needs high pressure and temperature above 200°C Very narrow size distribution	(Teja and Koh 2009)
Thermal decomposition	Synthesis process is fairly complicated, inter atmosphere, 100-320 °C Very narrow size distribution Excellent shape control	(Lu et al. 2007)
Microemulsion	Complicated process Relatively wide range of size and shape, but can be controlled Ambient conditions, temperature 20-50°C Short time duration for synthesis (hours)	(Lu et al. 2007)
Sol-gel	Suitable wet route for metal oxide NP synthesis Results 3D metal oxide nanostructure network (gel) Starts with room temperature, then high temperature treatment Monodisperse particles	(Laurent et al. 2008)

2.8.4 Surface Charge and Zeta Potential of Iron Oxide Nanoparticles

In aqueous media, a magnetite nanoparticle surface holds a pH dependent surface charge by undergoing changes to $FeOH$ surface hydroxyl groups and hence changing the agglomeration behaviour. At pH values below pH_{PZC} , nanoparticle surface is positively charged due to the formation of $FeOH_2^+$ by adding protons and when the solution pH is above pH_{PZC} , the surface charge becomes negative as a result of FeO^- formation arises from the acidic dissociation and the loss of protons according to equations (2-28) and (2-29). At the pH_{PZC} , the number of $FeOH_2^+$ and the number of FeO^- are equal (Cornell and Schwertmann 2006, Vidojkovic and Rakin 2016). (\equiv denotes surface groups)



An ionic cloud of counter ions with opposite charge to the colloidal particle surface is generated in the solution phase to compensate the surface charge. The charged surface together with counter ions in the solution phase is known as the electric double layer. The components of electric double layer is presented in Figure 2-10. The closely compacted layer of counter ions closest to the particle surface is known as the *Stern layer* whilst the surrounding layer in the solution phase next to the Stern layer is known as the *diffuse layer*. The boundary between these two layers is called the *shear plane*. The difference of electric potential between bulk solution and shear plane is known as zeta potential. Once the pH is similar to the pH_{PZC} value, the amount of negatively charged and positively charged particles are the same, thus making the zeta potential value zero. At this point, the colloidal suspension is in its most unstable state and the nanoparticles tend to agglomerate and can form agglomerates up to few micrometres in size (Illés and Tombácz 2006, Tóth et al. 2017). The sign and the magnitude of the zeta potential typically depends on the solution pH, ionic strength and temperature (Vidojkovic and Rakin 2016).

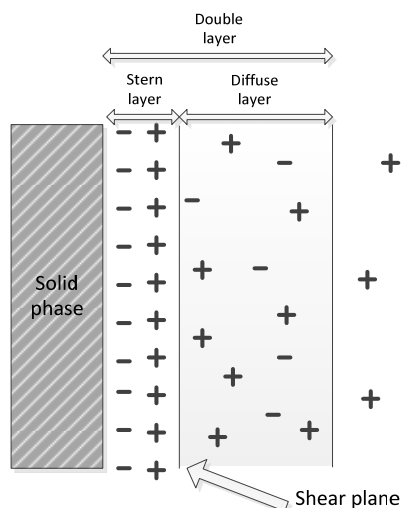


Figure 2-10. Schematic diagram of electrical double layer in particle-solution interface (reproduced from (Vidojkovic and Rakin 2016) with permission)

2.8.5 Nanoparticle Functionalisation

The stability of magnetic nanoparticles is vital to their application. Stability can be greatly improved by preventing oxidation and agglomeration through surface modification. Modification of the surface of magnetic nanoparticles by attaching organic and/or inorganic materials is proven to greatly enhance stability and prevent agglomeration. Further, these attached groups provide specific functionalities that can be selective for ion uptake and reach optimal particle surface charge appropriate for the intended end use (Girginova et al. 2010). Surface functionalisation can be performed with organic materials such as amino groups, silane groups, carboxyl acids such as citric acid, oleic acid and lauric acid, natural polymers such as dextran, starch and chitosan, synthetic polymers such as PVA, PAA, PEI and alginate. In addition, inorganic materials such as silica, gold, silver, platinum, palladium, iron, carbon and metal oxides/metal sulfides are also often used (Wu et al. 2008). Surface functionalisation using citrate/citric acid and PEI will be discussed in detail in the following sections.

2.8.5.1 Citrate coating

Trisodium citrate ($\text{Na}_3\text{C}_6\text{H}_5\text{O}_7$, $M_w = 258.06$ g/mol) is the sodium salt of citric acid ($\text{C}_6\text{H}_8\text{O}_7$, $M_w = 192.12$ g/mol). Citric acid is a well-known carboxylic acid. The structures are illustrated in Figure 2-11.

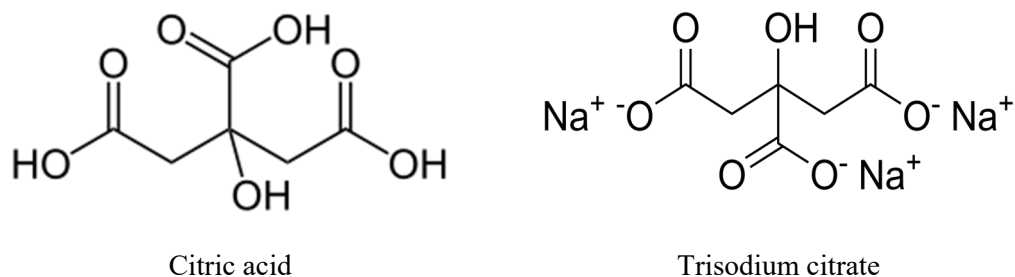


Figure 2-11. Chemical structures of citric acid and trisodium citrate

Citric acid is known to be chemisorbed to an iron oxide particle surface by coordinating one or two carboxylate group(s) with the hydroxyl groups in the particle surface leaving at least one carboxylate group exposed for further functionalisation or adsorption, making the surface hydrophilic and suppressing particle agglomeration (de Sousa et al. 2013, Li et al. 2013). Citric acid coated MNPs tend to be water dispersible and the colloidal stability retained for extended period (Nigam et al. 2011). Highly stable colloidal suspensions which were stable over six months have been reported (Saraswathy et al. 2014).

The smaller size of citrate molecule attracted research attention as a versatile functional group for nanoparticles. The ease of preparation, simple conjugation chemistry, and preservation of the binding affinity of the nanoparticles, which could have been lost due to the steric hindrance of using long chain polymers or larger molecules, have favoured the use of citrate as the primary functional group for many nanocomposites (Sahoo et al. 2005, Nigam et al. 2011).

A comparison of the synthesis conditions of citrate coating of MNPs has been undertaken. Citric acid coating was applied onto Fe_3O_4 MNPs in three different approaches, (1) simultaneous synthesis and citrate coating, (2) MNP synthesis followed by citrate coating and (3) coating synthesised/commercially available Fe_3O_4 MNPs as two-step process (Li et al. 2013). The influence on NP size of adding citric acid at different stages was insignificant. Increased temperatures were beneficial to higher citric acid adsorption on NP surfaces and lower hydrodynamic sizes.

The preservation of saturation magnetisation in citrate coated nanoparticles has been frequently reported. This property is indispensable as it facilitates efficient magnetic separation in subsequent processes. It is reported that the use of a silica layer prior to PEI coating has considerably reduced the magnetisation of nanocomposite and it takes a longer time to reach the adsorption equilibrium (Pang et al. 2011b). The ability to maintain the same saturation magnetisation similar to uncoated Fe_3O_4 NPs, even after citrate coating, is reported. Fe_3O_4 NPs of 9 nm and 25 nm exhibited 50 emu/g and 46 emu/g M_s value, respectively, almost the same as the corresponding uncoated NPs M_s value; 51 and 46 emu/g, respectively (Li et

al. 2013). However, a slight decrease in magnetisation is possible due to the coating (Saraswathy et al. 2014). In contrary, a considerable drop in saturation magnetisation after trisodium citrate coating was also reported, with 49 and 35 emu/g for uncoated and trisodium citrate coated NPs, respectively (Misra et al. 2015).

Citrate coated MNPs hold a highly negative surface charge reaching approximately -45 mV to -47 mV range for a wide pH range (Wang et al. 2009, Zhang et al. 2014). This facilitates particle deagglomeration in aqueous suspensions and provide an excellent platform for the subsequent attachment of cationic species.

The use of elevated temperatures for citrate coating has been highlighted in many studies. Stirring Fe₃O₄ NPs in a trisodium citrate solution, at 80 °C for 6 hours resulted a nanosorbent with optimum coating thickness and magnetic properties (Saraswathy et al. 2014). Cheraghipour et al. (2012) obtained well-dispersed iron oxide NPs having 74 emu/g saturation magnetisation after citrate coating at 90 °C for one hour. The magnetic core used was spherical and the average diameter was 10 nm. The same coating temperature and duration was reported elsewhere as well for the same size magnetic core which resulted in coated NPs with 57 emu/g of M_s (Nigam et al. 2011). Li et al. (2013) observed a considerable decrease in hydrodynamic particle size and an increase in the efficiency of citrate adsorption onto MNPs when increasing the coating temperature from 30 °C to 90 °C. A citrate coating at 90 °C for 1 hour gave the maximum surface coverage and lowest hydrodynamic size. In other published work, the optimum coating temperature and reaction time for citrate coating varied from 80 - 95 °C and 60 - 90 minutes, respectively (Racuciu et al. 2006, de Sousa et al. 2013, Na et al. 2014). However, lower (30-50 °C) and much higher temperatures (170-180 °C) outside this range have been reported occasionally (Srivastava et al. 2011, Andreas et al. 2012).

2.8.5.2 Polyethylenimine coating

Polyethylenimine (PEI) is a water soluble amine rich polycation which exists in either linear or branched form and in a wide range of molecular weights. The linear polymer consists of only secondary amines, whilst branched polymer is a combination of primary, secondary and tertiary amine groups. Linear PEI is a solid and the branched polymer is a viscous liquid at room temperature regardless of molecular weight (Lungu et al. 2016). Branched PEI consists of primary, secondary and tertiary amine groups in 1:2:1 ratios, respectively (Pandey and Sawant 2016). However, a ratio of approximately 1:1:1 has also been identified in commercial PEI which demonstrates its highly branched nature (von Harpe et al. 2000). Branched PEI is known to more strongly binds with metal ions than linear products. Most interestingly, PEI

doses not retain alkali or alkaline earth metal ions at any pH (Ghoul et al. 2003, Lindén et al. 2015).

PEI is a biocompatible polymer produced on an industrial scale for various applications as water treatment agents, detergents and adhesives (Ge et al. 2015). The molar mass of commercially available PEI ranges broadly from 800 g/mol to 750000 g/mol. Amongst them 25000 g/mol branched PEI has often been reported in biomedical applications like gene transfer (Bus et al. 2018). Furthermore PEI coated MNPs have been used in different areas mainly for biological applications such as cancer cell separation (Lu et al. 2014), DNA transfection, gene delivery (Arsianti et al. 2010), and in environmental applications as a functional coating to adsorb heavy metals from water (Larraza et al. 2012, Sui et al. 2015). Furthermore, PEI is known to be the organic macromolecule with the highest cationic charge density due to its amine rich structure and hence availability of higher number of nitrogen molecules which can be protonated (Goon et al. 2010, Xu et al. 2011). Its high buffering capacity over a wide pH range has also been reported (Boussif et al. 1995). The structures of linear and branched PEI are given in Figure 2-12.

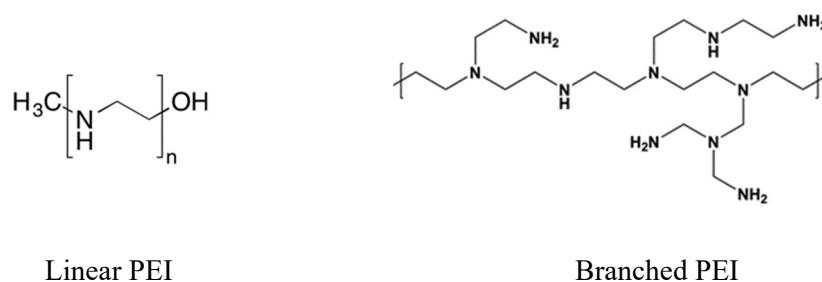


Figure 2-12. Chemical structures of linear and branched Polyethylenimine

The point of zero charge of PEI is at pH 10.8 – 11.0 and the average PEI molecule diameter is known to be approximately 10 nm in 0.2 M NaCl at pH 10 (Radeva and Petkanchin 1997). Similarly, the diameter of a 20 000 g/mol PEI molecule is reported as 7 nm (Hostetler and Swanson 1974). The shape of the PEI molecule is known to be spherical. The pK_a values of PEI were known to be above a pH of 8; the same as most polyamines. pK_a values increase when increasing the molecular weight (von Harpe et al. 2000). However the pK_a values reported for 25 000 Mw branched PEI varied from 7.11 to 8.4 (von Harpe et al. 2000, Mady et al. 2011). The amine groups present in PEI show different pK_a values making PEI versatile compared to conventional weak anion exchangers (Bakerbond 2012, Lu et al. 2014).

The positive zeta potential values of PEI modified adsorbents in alkaline solutions has been often reported. This characteristic is beneficial for anion adsorption from alkaline solutions. Xu et al. (2011) used PEI coated MNPs to immobilise *Pannonibacter phragmitetus* LSSE-09

cells to reduce Cr(VI) to Cr(III). PEI coated MNPs exhibited a pH_{PZC} value of 11.5 and 62.3 emu/g of M_s value. Below pH 11.5 the nanosorbent is positively charged due to the protonation of amine groups. Cuboidal shaped 50 nm size Fe_3O_4 NPs were functionalised with PEI (50 mg/L) shifting isoelectric point to approximately pH 9.5 from pH 7.5 for uncoated NPs (Goon et al. 2010). Those particles were used for copper detection and remediation. PEI coated magnetite nanoparticles demonstrated good adsorption of gold nanoparticles in aqueous media at pH 7. An increase in PEI concentration clearly increased the amount of PEI on the NP surface which ultimately increased the amount of Au adsorption and reduced particle agglomeration. Interestingly, it was further found that PEI having an average 25 000 g/mol of molecular weight (M_w) provided greater stability against particle agglomeration (50 nm particles) over PEI with 800 g/mol and 60 000 g/mol of molecular weights. These NPs were resistant to agglomeration over 30 days, which demonstrates the stability of PEI coated MNPs (Goon et al. 2009). However, a higher particle agglomeration tendency after PEI modification than the citrate coated particles is reported (Wang et al. 2009, Zhang et al. 2014). The instant switching of the surface charge from highly negative to highly positive may be the reason for this. PEI grafted Fe_3O_4 magnetic porous powder displayed an isoelectric point as high as 11.8 (Pang et al. 2011b). Wang et al. (2009) found that both zeta potential and aggregate size of PEI coated magnetite NPs directly depend on PEI:MNPs weight ratio. Higher ratios lead to more positive surface charges and smaller aggregate sizes. Similar observations were reported elsewhere (Steitz et al. 2007, Goon et al. 2010, Ge et al. 2015). In summary, the pH_{PZC} /isoelectric point of PEI coated magnetic nanomaterials were within the 9.5 to 11.5 range.

Polymers, like PEI provide nanoparticle colloidal stability through steric stabilisation (Boyer et al. 2010). The adsorbed polymer effectively increases the interparticle distance by steric repulsion. Furthermore, the dissociation of the polymer increases electrostatic repulsion (Kamiya 2012). The reduced tendency to agglomeration was observed in γ - Fe_2O_3 -Au nanocomposites coated with branched PEI (Seino et al. 2009). Some common approaches are prominent for nanoparticle surface modification using PEI. In-situ synthesis of PEI conjugated MNPs and surface coating of already synthesised MNPs in a PEI solution through electrostatic attraction are frequently reported (Zhang et al. 2014, Liu et al. 2017, Yang et al. 2018).

The adsorption of branched PEI to hematite has been investigated. The molecule arrangement on hematite surfaces was determined by PEI concentration. With low PEI concentrations, unfolding of the molecules was observed, whereas molecule flattening sufficient to cover the particle surfaces was observed at higher PEI concentrations. The hydrodynamic thickness of the polymer coating was determined to be 3 nm although the PEI molecule diameter was 10 nm. This claim is also supported by others (Radeva and Petkanchin 1997), where a flattening

of the molecules was observed once adsorbed onto silica nanoparticles (Lindquist and Stratton 1976).

PEI coated Fe_3O_4 NPs were able to successfully adsorb gold NPs, ultimately resulting in $\text{Fe}_3\text{O}_4/\text{Au}$ nanocomposite (Wang et al. 2012). In another study, synthesis of composite Fe_3O_4 -Au core-shell nanoparticles was attempted with PEI as the intermediate layer which binds two composites to each other (Goon et al. 2009). PEI modified magnetic graphene oxide nanocomposite and PEI grafted magnetic porous powder showed high adsorption capacities for Cu(II) reaching 157 mg/g at pH 6 - 7.5 in aqueous solutions (Pang et al. 2011b, Sui et al. 2015).

In many instances, saturation magnetisation of PEI coated MNPs drops only slightly which is advantageous for subsequent magnetic separation (Lu et al. 2014). PEI modified magnetite NPs exhibited 62.3 emu/g of saturation magnetisation. Citrate was used as the intermediate coating layer (Xu et al. 2011).

2.8.6 Metal and Metal Complexes Adsorption

Iron oxides can adsorb both anions and cations chemically or physically based on the surface, solution and adsorbate characteristics. Citrate, silicate, phosphate, arsenate, selenite, chloride, fluoride and oxalate are popular anions that chemically adsorb to iron oxide surfaces. In contrast, nitrate and perchlorate are some examples for nonspecific (physical) adsorption (Kalaruban 2017).

Gold recovery from different aqueous solutions with nanosized iron oxide magnetic adsorbents was attempted, where in the majority of instances gold was in the +3 oxidation state as AuCl_4^- at acidic pH solution. Thiol modified Fe_3O_4 MNPs, with intermediate silica coating, were able to adsorb gold from dilute AuCl_4^- solutions (Zhang et al. 2013c, Roto et al. 2016, Abd Razak et al. 2018). The maximum adsorption capacities calculated from the Langmuir adsorption isotherm were within the 84.75 mg/g to 222.22 mg/g range. The adsorption mechanism was concluded to be chemisorption through kinetic model fitting and thermodynamic approaches. The most favourable solution pH was in the range of 3-5. The decline of adsorption efficiency in alkaline pH values was noteworthy in all the circumstances.

Gold recovery from copper anode slime by means of silica coated magnetite NPs was reported with thiourea used as the lixiviant for leaching (Ranjbar et al. 2014). Thiourea dissolved all the gold from copper anode slime, forming a $\text{Au}(\text{CS}(\text{NH}_2)_2)_2^{2+}$ cationic complex, subsequently adsorbed on to silica coated magnetite surface at pH 1.2-1.4. Another attempt

was made to recover gold from chloride solutions using nano sized magnetite powder and 4.4 $\mu\text{mol/g}$ loading was achieved at a pH value of 6-7 (Alorro et al. 2010).

Chitosan-magnetite composite was able to recover Au(III) and Ag(I) in water successfully. The maximum uptake values were 3.6 and 2.1 mmol/g for Au(III) and Ag(I), respectively (Donia et al. 2007). Gallic acid modified magnetite particles were used for Au(III) recovery and maximum adsorption was observed at pH 3 (Rahmayanti et al. 2016). Polythiophene coated magnetite NPs were capable of adsorbing Au(III) at pH 2 (Tahmasebi and Yamini 2013). Moreover, cobalt-ferrite (CoFe_2O_4) MNPs, manganese-ferrite MNPs with and without surface functional groups have been attempted for use in Au(III) recovery from aqueous solutions at acidic pH range (Kraus et al. 2009, Jainae et al. 2010, Neyestani et al. 2017).

It is worth noting that the $\text{Au}(\text{S}_2\text{O}_3)_2^{3-}$ complex is less prone towards adsorption onto goethite surfaces than AuCl_4^- due to its resistance to hydrolysis. Steric factors such as size and shape of the anionic complexes also play a major role. Au (III) chloride is a square planar complex and the size matches perfectly with the distance between hydroxyl groups on goethite surfaces. In contrast, Au (I) thiosulfate complex is a large linear complex which hinders effective adsorption onto goethite (Machesky et al. 1991).

Few magnetic nanoadsorbents used for gold and copper adsorption in aqueous solutions are listed in Table 2-4. It should be noted that this is not a comprehensive list but only a list of commonly investigated nanoadsorbents.

Table 2-4. Some magnetic nanoadsorbents used for gold and copper adsorption from aqueous solutions

Adsorbent	Adsorbate	pH	Adsorption capacity (mg/g)	Reference
PEI coated magnetic graphene oxide nanocomposite	Cu (II)		157	(Sui et al. 2015)
PEI grafted magnetic porous powder	Cu (II)	6-7.5	157.8	(Pang et al. 2011b)
Amino functionalised Fe_3O_4 MNPs	Cu (II)	6	25.8	(Hao et al. 2010)
Thiol modified Fe_3O_4 MNPs, with intermediate silica coating	AuCl_4^-	5		(Abd Razak et al. 2018)
		3		(Roto et al. 2016)
		5		(Zhang et al. 2013c)
Polythiophene coated magnetite NPs	Au(III)	2		(Tahmasebi and Yamini 2013)
Novel magnetic ion imprinted polymer	Au(III)	3-5		(Ebrahimzadeh et al. 2012)

2.8.7 Limitations Associated with Nanoparticles and Possible Remedies

2.8.7.1 Nanoparticle Aggregation and Agglomeration

Nanoparticles in dry powder form can exist either as agglomerates (loosely bound to each other by weak physical interactions) or aggregates (strongly bonded particles which are hard to break by mechanical means). These can largely be controlled during the synthesising stage. Once NPs are dispersed in a solution, they can exist either as single particles, agglomerates or aggregates, surrounded by an electric double layer (EDL). The form of the particles depends on the solution characteristics and the particle characteristics like the zeta potential and the thickness of the electric double layer. While the thickness of the electric double layer is a function of ionic strength (inversely proportional relationship), an increase in EDL thickness or zeta potential facilitates an electrostatic repulsive interaction favouring a decrease in the hydrodynamic size of particles (Jiang et al. 2008).

The colloidal stability of MNPs in aqueous solutions can be attained either with steric stabilisation or with electrostatic stabilisation (Boyer et al. 2010). According to Wang et al. (2009), lower pH values are favoured for NP deagglomeration as a result of increased protonation of amino groups thus increasing steric repulsion between particles. PEI coated Fe₃O₄ nanoparticles were de-aggregated through acidification (at pH 2 for 10 minutes) before being washed and neutralised. The particle neutralisation did not lead to re-aggregation of nanoparticles, demonstrating that de-aggregation by acidification is an irreversible process. However, the risk associated with this approach is the possibility of NP dissolution in strongly acidic solutions.

High shear milling has also been reported for the deagglomeration of particles. Unfortunately milling efficiency is drastically reduced for particle sizes of less than 500 nm (Cho et al. 1996). Longer milling times and higher collision speeds may help, but with this comes the risk of unwanted phase transition and contamination. Some chemical methods of de-agglomeration involve the selective dissolution of inter-particle bridges (necks) (Laarz et al. 2000). Extreme care is necessary to dissolve only the aforementioned necks while keeping the particles intact.

In general, the maintenance of solution pH well above or below the isoelectric point/pH_{PZC} supports the increase of the repulsive forces between particles and subsequently suppresses the agglomeration. In circumstances where the pH needs to be constant or to only vary within a narrow range, the introduction of a dispersing salt and ultrasonic dispersion is performed

(Faure et al. 2013, Vikram et al. 2016). The ionic strength of the solution also impacts upon the dispersibility (Kamiya 2012).

Ultrasonic dispersion is one of the easiest, fastest and most straightforward methods for effective nanoparticle deagglomeration, whilst probe ultrasonication surpassed bath ultrasonication in many instances (Jiang et al. 2008, Nguyen et al. 2011, Yeap et al. 2017). Acoustic cavitation, that is the formation, growth and implosive collapse of bubbles in a liquid, generates intense local heating (≈ 5000 K) and high pressure (≈ 1000 atm) spots, extreme heating and cooling rates and liquid jet streams (≈ 400 km/h) in the liquid which help to break the agglomerates (Suslick 1998). Furthermore, it is stated that ultrasound is reproducible which enables the linear scale up to bulk scale (Hielscher 2005).

2.8.7.2 Nanoparticle Dissolution

pH dependent NP dissolution is crucial for different applications. Wang et al. (2009) confirmed that PEI coated Fe_3O_4 NPs are stable at pH 2 and PEI dissolution or Fe leaching does not occur. However this was tested for only 10 minutes and long term exposure could be problematic.

In another study, the pH stability of PEI-MNPs was evaluated by exposing the particles to solutions at acidic and alkaline pH values for 3 hours. Fe leaching was insignificant in 0.2 to 1 M HCl and NaOH solutions and the treated PEI-MNPs were able to retain their adsorption capacity in the same way as the untreated particles. In contrast, uncoated MNPs were completely dissolved in 1 M HCl solution. However, 100% Fe leaching from PEI-MNPs was observed in a 4 M HCl solution (Pang et al. 2011b). The high stability of silica and amine groups coated Fe_3O_4 MNPs in acidic solutions (0.01 to 1 M HCl) has been reported. Fe leaching efficiency has been tested for up to 120 hours which resulted in 3.6% and 99.2% of Fe leaching in coated and uncoated NPs, respectively (Wang et al. 2010). Therefore, it is apparent that the surface functional groups can provide protection to the magnetic core against dissolution in extreme pH solutions.

2.8.7.3 Magnetic Separation from a Solution

Typically, the separation of MNPs in a solution is attained by applying an external magnetic field. The response of magnetic nanoparticles in a low field gradient is particle size dependent (Yavuz et al. 2006). However some surface coatings can negatively affect the effective magnetic separation as a result of reduced magnetisation of the nanocomposite. Silica coating is likely to reduce the magnetisation of the adsorbent and ultimately longer durations would be required for magnetic separation (Larumbe et al. 2012, Thangaraj et al. 2019). The thickness

of the silica layer is directly related to the saturation magnetisation of the surface coated nanomaterial as is the solvent used to suspend the particles (Yuan et al. 2012). PEI and silica coated Fe₃O₄ magnetic porous powder (0.05 g in 20 mL solution) required 5 minutes to separate (Pang et al. 2011b). The preservation of magnetisation of the magnetic core in PEI coated MNPs has been frequently reported (Xu et al. 2011, Lu et al. 2014). An optimisation of surface coating thickness and the composition and size of the magnetic core is necessary to improve the magnetic separation while maintaining the intended functionality of the nanomaterial. Nevertheless, the need for full recovery (separation) of MNPs from the solution could not be ignored to prevent any potential hazard to the environment by accumulating nanomaterials in natural waters (Mandel and Hutter 2012).

2.8.7.4 Environmental Concerns and Toxicity of MNPs

Toxicity to living beings and the release of magnetic nanomaterials into the environment are the main concerns associated with the use of MNPs. However, iron oxide MNPs are known to be biocompatible and they are often used in a wide range of biomedical applications (O'Grady 2002, Tran and Webster 2010, Mohammed et al. 2017). Due to their more stable chemical state than nanosized zero valent iron (NZVI), magnetite and maghemite show a minimal toxic effect on living cells. However, the release of Fe²⁺ by any means can cause cytotoxicity. A surface coating can depress the possible toxic effects substantially by reducing the direct exposure of the magnetic core to cells or bacteria (Tang and Lo 2013a). The environmental impact and the enzyme immobilisation efficiency of PEI coated MNPs was evaluated which demonstrate satisfactory levels in both the indicators (Feijoo et al. 2018). To this end, PEI coated magnetite and maghemite NPs can be considered to have minimal to no adverse effects on the environment.

2.9 Gold and Copper Elution

2.9.1 Gold and Copper Elution from Ion Exchange Resins

Different elution systems have been proposed for gold thiosulfate elution from ion exchange resins. Thiocyanate, polythionates, nitrate, mixed chloride + sulfite and mixed trithionate + sulfite based elution systems have mainly been suggested (O'Malley 2002, Fleming et al. 2003, Jeffrey et al. 2010). Each system has its advantages and disadvantages. Highly concentrated solutions are required for most of the elution processes (Fleming et al. 2002, Zhang and Dreisinger 2003a). A mixture of trithionate and sulfite is used in the Barrick gold Goldstrike plant to elute gold from the resin (Choi et al. 2015, Aylmore 2016b).

A two-step elution process was developed for the Goldstrike mine, which uses concentrated ammonium thiosulfate (100-200 g/L) for copper elution. This is followed by gold elution with a strong thiocyanate (50-100 g/L) solution for elution of copper and gold from Purolite A500C anion exchange resin (Fleming et al. 2003). Although gold elution with thiocyanate is rapid, this process is relatively costly and requires complex regeneration methods to recover thiocyanate for reuse. Furthermore, the presence of thiocyanate in tailings is unacceptable from the environmental perspective. The rapid pH change in between the gold elution (pH 6-8) and regenerations steps (strongly acidic) exacerbates the resin damage due to osmotic shock.

Considering the complications associated with thiocyanate regeneration process, the use of polythionates (200g/L trithionate alone and a mixture of trithionate (~40 g/l) and tetrathionate (~80 g/l)) was considered in the same study. The use of polythionates for gold elution is an effective method due to the higher affinity of these species onto anion exchange resins. However, this strong adsorption necessitates a regeneration step for the eluted resin. Treatment of the metal eluted resin with sulfide ions (NaHS) was attempted. In addition, the instability of the concentrated trithionate solution leads to a rapid loss of trithionate by ultimately increasing the total process cost. As a solution, in-site polythionates synthesis process is proposed. However, gold elution efficiency was almost 100% with both thiocyanate and polythionates eluants, despite their complex regeneration.

For the nitrate elution process, it has been reported that concentrated ammonium nitrate solutions (2M) are required for gold elution but a resin regeneration step is unnecessary. Yet this can accumulate nitrate ions in the process water that can adversely impact gold loading and create environmental problems. Copper elution was accomplished by 2M ammonia solution in 40 bed volumes in column application. Elution kinetics are comparatively slow, for instance, it took 4 hours and 30 hours to elute approximately 100% gold from the resin in column and batch elution methods, respectively (O'Malley 2002).

The addition of sulfite ions to some eluants could lead to a reduction in the eluant concentration and more efficient elution of gold from strong base ion exchange resins. Mixed chloride-sulfite, nitrate-sulfite and mixed trithionate-sulfite systems have been reported (Jeffrey et al. 2010, Jeffrey 2011). In the presence of sulfite, $Au(S_2O_3)_2^{3-}$ is converted to $Au(S_2O_3)(SO_3)^{3-}$ where the latter complex shows only a weak affinity to IX resins. Consequently, gold elution could be achieved with relatively weak eluants like chlorides, which considerably reduce the process costs.

The use of 0.5 M sodium thiosulfate for copper pre-elution from Purolite A500 resin has been reported (Choi et al. 2015). Hydrogen peroxide is added to the same solution which generates

some amount of trithionate by thiosulfate oxidation which is loaded onto the copper eluted resin. Subsequently, a mixture of trithionate (0.2 M) and sulfite (0.2 M) is used for gold elution. Ultimately, the resin now loaded with trithionate is regenerated with sulfide which results in a thiosulfate loaded resin which can be directly sent for gold loading. The in-situ generation of most of the required reagents and ability to reuse the solutions for subsequent leaching and elution cycles makes this process interesting. However, the addition of H_2O_2 should be conducted with great care to control the amount of trithionate generation, otherwise this could also strip the gold during the copper pre-elution stage. A simplified version of the process flow sheet is illustrated in Figure 2-13.

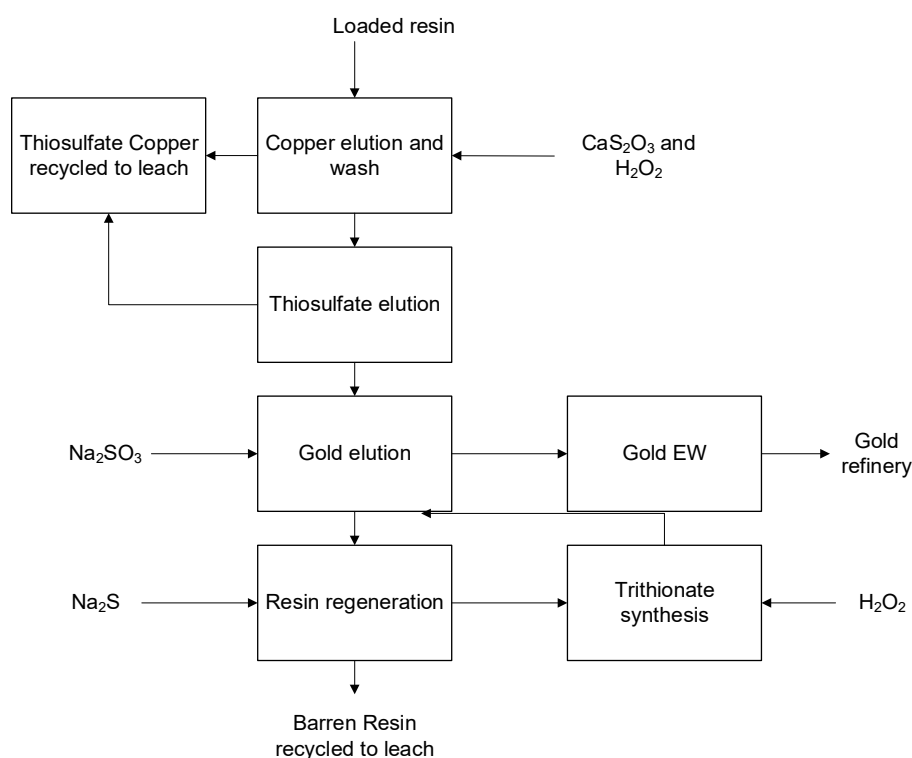


Figure 2-13. Simplified trithionate and sulfite elution process (reproduced from (Aylmore 2016c) with permission)

2.9.2 Gold Elution from Nanoparticles

The desorption of Au(I) complexes from different adsorbents was successfully accomplished using diluted NaOH solutions. The anionic Au(I) complex was resistant to adsorb onto an eggshell membrane in alkaline pH solutions, which had been advantageously used for desorption. Approximately 95% of gold was eluted by a 0.1 M NaOH solution (Ishikawa et al. 2002). Aurocyanide adsorption onto activated carbon is an exothermic process, which indicates that the increased temperatures would favour gold desorption from AC (van Deventer and van der Merwe 1994).

Thiourea has often been reported in gold elution from different magnetic nanosorbents. The ability to form stable complexes with gold makes this useful as an eluant for gold desorption. Au (III) elution from polythiophene coated Fe₃O₄ MNPs was attempted by using a 1M thiourea solution. The elution process was carried out at acidic pH solutions to facilitate the protonation of the adsorbent, so that it would desorb the loaded cationic metals easily as a result of weakening of the complexation between adsorbent and metal (Tahmasebi and Yamini 2013). In addition, thiourea mixed with an acid is frequently discussed. Thiourea (0.5 M) acidified with 0.2 M H₂SO₄ was able to elute gold from magnetite-chitosan resin. The elution was conducted in a column application (Donia et al. 2007). In another study, 0.1M of thiourea, together with 0.1 to 1 M H₂SO₄ was able to elute gold (III) from tris(2-aminoethyl)amine-functionalised Fe₃O₄ nanoparticles. Different concentrations of HCl (0.1 to 2 M) and H₂SO₄ (0.1 to 1 M) acid solution were tested, but the elution efficiencies were lower in the absence of thiourea in the solution (Lotfi Zadeh Zhad et al. 2013). A summary of the different eluants used for gold elution from different nanosorbents and a few other adsorbents is illustrated in Table 2-5 below.

Table 2-5. Gold elution from different adsorbents

Adsorbent	Adsorbate	Eluant	Reference
Thiourea modified Fe ₃ O ₄ nanoparticles	Au(III)	0.7 M thiourea with 2% HCl	(Lin and Lien 2013)
Polythiophene modified Fe ₃ O ₄ nanoparticles	Au(III)	1 M thiourea	(Tahmasebi and Yamini 2013)
Fe ₃ O ₄ @SiO ₂ core-shell nanoparticles modified with thiol group	Au(III)	Thiourea with 1 M HCl	(Roto et al. 2016)
Chitosan-Fe ₃ O ₄ resin modified with thiourea/glutaraldehyde	Au(III)	0.5 M thiourea with 0.2 M H ₂ SO ₄	(Donia et al. 2007)
Polystyrene-coated CoFe ₂ O ₄ functionalised with 2-(3-(2-aminoethylthio)propylthio)ethanamine	Au(III)	1 M thiourea with 2% HCl	(Jainae et al. 2010)
tris(2-aminoethyl)amine-functionalised Fe ₃ O ₄ nanoparticles	Au(III)	0.1M thiourea with 0.1 to 1 M H ₂ SO ₄	(Lotfi Zadeh Zhad et al. 2013)
Fe ₃ O ₄ @SiO ₂ microspheres functionalised with 4'-aminobenzo-15-crown-5-ether	Au(III)	2% thiourea with 0.1 M HCl	(Ye et al. 2014)
Decarboxylated <i>C. glutamicum</i> biomass	Au(I)	0.1 M NaOH in DI water	(Kwak and Yun 2010)
Eggshell membrane	Au(I)	0.1 M NaOH	(Ishikawa et al. 2002)

2.9.3 Copper Elution from Nanoparticles

EDTA is well known for use in copper elution from different adsorbents. Vilar et al. (2007) used 2 mM EDTA for copper desorption from *Gelidium* algal biomass and 78% to 91% elution efficiency was achieved in less than 30 minutes. An enhanced elution efficiency was observed with the increase of EDTA concentration, and metal complexation with EDTA was at a 1:1 molar ratio. In another study, 5 mM of EDTA was able to desorb Cu (II) from a magnetic polymer adsorbent at pH 5.5 and desorption kinetics, isotherms and desorption mechanisms were investigated (Tseng et al. 2009). Copper adsorbed onto magnetic chitosan nanoparticles was desorbed with 0.02 M EDTA and 90% elution efficiency was achieved. The efficiency increased to 96% by using 0.1 M EDTA (Yuwei and Jianlong 2011). Some selected eluants used for copper elution are summarised in Table 2-6.

The change of solution pH to reverse the adsorption process is another approach for metal elution from magnetic nanomaterials. This is applicable in systems where the physical adsorption mechanism is predominant. In accordance with the above technique, in some studies, diluted HCl acid has been used for copper elution (Hao et al. 2010, Sui et al. 2015). However, magnetic core dissolution is a possibility with this technique at low pH solutions. The stability of MNPs in acidic media should be considered prior to using this method.

Table 2-6. Copper elution from different adsorbents

Adsorbent	Adsorbate	pH	Eluant	Reference
Carboxymethyl- β -cyclodextrin conjugated Fe ₃ O ₄ NPs	Cu (II)	-	0.1 M citric acid, 0.1 M Na ₂ EDTA and 0.1 M acetic acid	(Badruddoza et al. 2011)
PEI functionalised mesoporous diatomite	Cu (II)	1	Water/diluted H ₂ SO ₄ solution	(Nosrati et al. 2017)
Rice Straw/Fe ₃ O ₄ Nanocomposite	Cu (II)	-	0.1 M HNO ₃ acid	(Khandanlou et al. 2015)
Amino-functionalised Fe ₃ O ₄ nanoparticles	Cu (II)	-	0.1 M HCl acid	(Hao et al. 2010)
Magnetic polymer adsorbent	Cu (II)	5.5	5mM EDTA	(Tseng et al. 2009)

2.10 Chapter Summary

It would seem from most of the literature consulted, that the thiosulfate leaching system is a viable alternative to cyanidation for the leaching of double refractory gold ores. Despite their

effectiveness, however, thiosulfate leaching solutions bring difficulties and complexities as a result of the availability of oxidant-ligand pairs. Many complications associated with conventional ammoniacal thiosulfate leaching systems can be minimised by employing a calcium thiosulfate - air leaching system. Yet the recovery of gold from such a system is challenging, due to resin poisoning with polythionates, difficulty in gold elution from the resin, and other inherent limitations associated with IX resins. The use of magnetic nanoadsorbents for precious metal and heavy metal recovery is a fast developing research area. There is a vast potential for magnetic nanoadsorbents to be used in the metallurgical industry for the recovery of precious metals. High gradient magnetic separation can be used on nanosized magnetic materials which would be a huge step forward in the use of nanomaterials on an industrial scale. A suitable surface coating can be used to adsorb gold onto the magnetic nanoadsorbents, which can be then separated magnetically. Polyethylenimine is a versatile functionalising agent, which can be implemented for different end uses. The unique properties of branched PEI demonstrate considerable promise for use in anion separation from aqueous solutions. A composite of magnetic nanoparticles and PEI seems to be a good candidate for gold adsorption from alkaline leaching solutions. Gold elution from such an adsorbent seems to be simpler than that from IX resins.

Chapter 3 Materials and Experimental Methods

3.1 Introduction and Chapter Objectives

All the chemicals used within this study are detailed in this chapter, along with the methods used for nanoparticle functionalisation, leaching (wherever applicable), metal adsorption, metal elution and reuse of the adsorbent. Nanoparticle characterisation technologies and solution analysis methods along with the sample preparation, instrument settings and procedures are also included. Conventional experiments and experiment design techniques are also described wherever applicable.

To fulfil the objectives as set out in Chapter 1, the preparation and comprehensive characterisation of the adsorbent was accomplished based on the literature review. The selection of characterisation technologies was subject to the relevance and availability of instruments. The majority of test work was conducted using synthetic leaching solutions. In addition to this, gold adsorption from a gold ore leachate was also conducted in order to evaluate the performance of the adsorbent under those conditions. The main leaching system used was the calcium thiosulfate - air system while other thiosulfate leaching systems consisting of different oxidant-ligand pairs were also tested just for comparison purposes.

3.2 Materials and Chemicals

All the chemicals used were of analytical reagent grade. Deionised water was used to prepare all the solutions. Sodium aurothiosulfate (I) from Surepure chemicals (USA) was used as the gold source. Polyethylenimine (PEI), branched (average $M_w \sim 25,000$) and ammonium thiosulfate, were bought from Sigma Aldrich, Australia. Magnetite and maghemite nanopowders were sourced from US Research Nanomaterials, Inc, USA. In addition, calcium thiosulfate was obtained from Acros organics, Belgium; sodium thiosulfate and trisodium citrate from Rowe Scientific, Australia; and copper sulfate pentahydrate, EDTA and sodium sulfite from Univar were used. Ammonia solution (28%) and nickel nitrate were sourced from Sigma Aldrich, Australia. 0.1 M H_2SO_4 and 0.1 M NaOH solutions were used for the pH adjustments, unless otherwise stated.

The adsorption experiments and metal elution experiments were conducted in an Orbital shaker (Ratek OM11) at 250 rpm unless otherwise stated. A small neodymium magnet (50mm

x 50 mm x 12 mm) was used for solid-liquid separation during this study as shown in Figure 3-1.

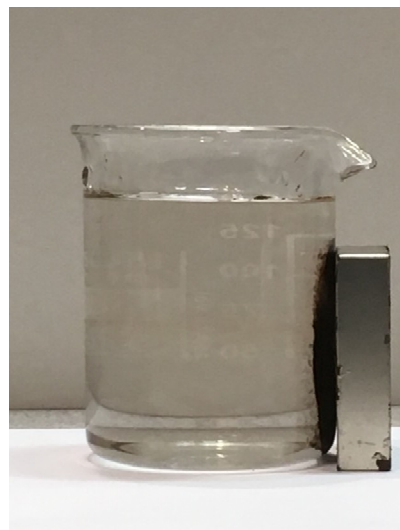


Figure 3-1. Experimental set up of adsorption experiments in the orbital shaker (top) and magnetic separation (bottom). The beakers in the bottom image consist of 20 g/L PEI-MNPs concentration. An external magnetic field was applied to separate the PEI-MNPs.

3.3 Functionalisation of MNPs

Iron oxide nanoparticles were first coated with trisodium citrate as the intermediate layer followed by the PEI coating as the outer layer. A method followed by Zhang et al. (2014) was used in this study after substantive modifications. Firstly, a 10 g/L trisodium citrate solution was prepared by dissolving trisodium citrate in DI water and the pH was adjusted to 9.5 using NaOH. Secondly, 0.5 g of magnetite nanopowder was dispersed in 50 mL of 10 g/L trisodium citrate solution for a specified time to disperse them evenly using an ultrasonic probe (Heilscher UP200Ht). The nanoparticle dispersion was then added to a 250 mL Erlenmeyer flask and the solution was made up to 100 mL by adding more 10 g/L trisodium citrate solution. The pH was adjusted to 6 using 0.1 M H₂SO₄ and kept under mechanical stirring for one hour at 90 °C. After one hour, a measured amount of 5% PEI solution was slowly added to the aforementioned solution and stirred for two hours at 90°C and at a pH of 9.5. Finally the PEI coated MNPs were washed thoroughly five times with DI water and dried in an oven at 40°C. The dried nanopowder was gently ground with the aid of an agate mortar and pestle before being used for characterisation or adsorption studies. The final product is hereinafter denoted as **PEI-MNPs**.

3.4 Characterisation of MNPs

3.4.1 Scanning Electron Microscope (SEM)

A ZEISS NEON 40EsB dual-beam Field Emission Scanning Electron Microscope (FESEM) was used for SEM imaging of nanoparticles at a lower voltage electron beam. The purpose was to get a topographical image of nanoparticle surface, size measurement and to observe the effect of ultrasonic dispersion on particle deagglomeration. The samples were prepared in a manner that first, nanoparticles being dispersed in a preferred solution using ultrasonic dispersion. One to two drops of nanoparticle dispersion were then drop-cast onto a silicon wafer attached to a SEM stub, using a pipette. The sample was either allowed to air dry at room temperature or placed under a heat lamp for two minutes. The dried specimens were coated with a thin platinum layer before being analysed under the SEM. In some occasions, dry nanoparticles were directly deposited on a carbon tape attached to a SEM stub.

3.4.2 Transmission Electron Microscope (TEM)

An FEI Talos F200X TEM was used at 200 kV, spot size 3 with a condenser aperture of 100 for morphology evaluations. The dry powder samples were dispersed in DI water with the aid of ultrasonication and a drop of the dispersion was put onto a carbon coated copper grid and

left for air-drying overnight. A TEM provides topographical information on the internal structure and phases of the substance. In addition, information on particle deagglomeration can also be acquired.

3.4.3 Dynamic Light Scattering (DLS)

Size measurements were performed using the dynamic light scattering (DLS) function on a Malvern Zetasizer Nano-ZS (Malvern Instruments, Malvern, UK). Firstly, the nanopowder was ultrasonically dispersed in a preferred solution using an ultrasonic probe for the desired time. The samples were irradiated with HeNe laser red light at a wavelength of 632.8 nm to analyse the intensity fluctuation of scattered light. The samples were measured at a temperature of 25 °C in disposable fluorescent cuvettes. Each sample was measured in triplicate and the average value determined. The obtained data was analysed with proprietary software using the cumulative and distribution fits for the autocorrelation function within the proprietary software and it was assumed that the solutions refractive index (n) and viscosity (η) would be equivalent to that of water, where $n=1.33$ and $\eta=0.888$. The intensity size distributions were originally obtained and converted to volume and number based distributions using the proprietary software, wherever required.

3.4.4 Zeta Potential

The zeta potential measurements were carried out using a Malvern Zetasizer Nano-ZS (Malvern Instruments, Malvern, UK). In brief, a 0.314 g of nanopowder sample was dispersed in 30ml of DI water before adjusting the pH to the desired value using HCl or NaOH. The sample was left to equilibrate for 24 hours before the pH was measured again before determining the zeta potential utilising a disposable folded capillary style cell. The pH range varied from 5-12 and the ionic strength was maintained by using 0.01M NaCl. Three values were measured for each sample and the average value determined.

3.4.5 X-ray Diffraction (XRD) and Quantitative X-ray Diffraction (QXRD)

XRD analysis of the crystalline phase of nanopowder samples was performed with a Bruker D8 Advance Powder Diffractometer (Bruker AXS, Germany) with a Co $K\alpha$ radiation source ($\lambda=1.79\text{\AA}$). A nanopowder sample was suspended in few drops of absolute ethanol and the suspension was pipetted onto low background sample holders and allowed to air dry before the XRD measurements were taken. Crystalline phases were identified by matching with standard powder diffraction data (PDF). DIFFRAC. EVA. 3.2 software was used to find the

matching PDF files. QXRD analyses were performed in a PANalytical X'Pert Pro PW3040 diffractometer under Co K α radiation ($\lambda=1.79\text{\AA}$). This technique is helpful for a quantitative analysis of the mineral phase. Further information on instrument settings is included in Appendix B.2.

3.4.6 Raman Spectroscopy

Raman spectra were collected on a Labram 1B dispersive Raman spectrometer with 632.8 nm excitation, 0.02 to 0.5 mW of laser power at the sample, a 150 μm slit, 50x objective, 1800 lines per mm diffraction grating, and a Peltier-cooled CCD detector at -40°C . Collection times varied from 4 to 60 seconds. Information on iron oxide phases and surface functionalisation can be extracted from Raman spectra.

3.4.7 X-ray Photoelectron Spectroscopy (XPS)

XPS measurements were performed on a Kratos Axis Ultra DLD spectrometer. A thin layer of powder sample was put directly onto a small carbon tape attached to a specimen holder. Samples were measured with a neutraliser to compensate for charging effects. CasaXPS software was used for data analysis. XPS analysis provides valuable information on the quantitative surface elemental composition to a depth of 5-10 nm. Moreover, deconvolution of the main peaks can give information on oxidation state of each element along with possible bonds. Detailed information on instrument settings is mentioned in appendix B.1.

3.4.8 Fourier Transform Infrared Spectroscopy (FTIR)

In order to identify the surface functional groups, the infrared spectra were collected using a Nicolet iS50 FTIR fitted with a dedicated single-bounce diamond ATR purged with dry nitrogen. Sixty-four background scans and 64 sample scans were co-averaged and ratioed to produce a transmission spectrum. The absorbance spectrum was ATR corrected for the effect of the wavelength on the depth of penetration. Any sample preparation was not required and a small amount of powder or liquid sample was placed onto the diamond as it is, just before the analysis.

3.4.9 X-ray Fluorescence Spectroscopy (XRF)

Elemental composition of the nanoparticles and ore samples was determined based on XRF analysis. The principle behind this technique is that when individual atoms are excited by an external energy source, X-ray photons are emitted with characteristics pertaining to the energy

or wave length. The identification and quantification of each element is conducted by counting the number of photons relevant to each energy level. All the XRF analyses were conducted by Bureau Veritas analytical laboratory in Perth, Western Australia.

3.4.10 Atom Probe Tomography (APT)

Atom probe tomography analysis was carried out to explore the atomic arrangement of PEI-MNPs before and after metal adsorption in near atomic scale using Cameca LEAP 4000X HR (France). The specimen preparation was conducted by embedding nanoparticles within a ZnO matrix on a Si substrate, as reported previously (Friedrich et al. 2019).

Nanoparticle encapsulation within ZnO matrix: Firstly, small silicon wafers were sputter coated (PVD) with a 500 ± 50 nm of ZnO layer at Melbourne Centre for Nanofabrication (MCN, Australia). Following this, a 100 ± 10 nm ZnO coating layer was deposited via atomic layer deposition (ALD) at 250°C . A dilute solution of bare MNPs (approximately 1 mg/mL) was then drop-cast on to ZnO surfaces using a pipette and allowed to air dry overnight. The nanoparticles were ultrasonically dispersed in DI water and allowed to settle for five minutes prior to being drop-cast. This procedure eliminates the presence of large agglomerates on the specimens. The same procedure was followed for PEI-MNPs and Au-PEI-MNPs. A 25 ± 2.5 nm thick ZnO ALD layer was then deposited at 200°C to encapsulate the nanoparticles between the two ALD coating layers. This thin ALD layer minimises any voids that may otherwise occur during PVD coating. Finally, a 600 ± 50 nm ZnO film was sputter coated on top of the film. The schematic representation of the deposition process is shown in Figure 3-2. As shown in Figure 3-3a, the raised features on the ZnO layers are prominent which assisted in deciding the Region of Interest (ROI).

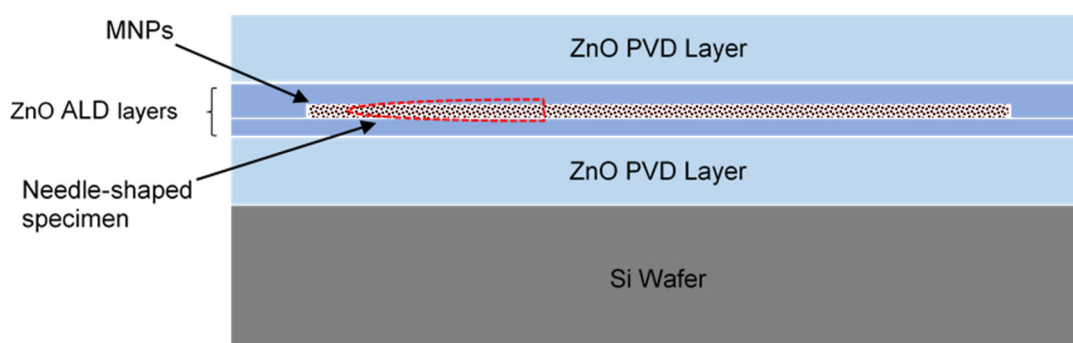


Figure 3-2. Schematic diagram of nanoparticle encapsulation in ZnO matrix (side view)

Needle-shaped specimen preparation for APT analysis: The needle-shaped specimen preparation was conducted using Tescan LYRA focused ion beam scanning electron microscopy (FIB-SEM). A site-selective standard lift out - nanotip mounting - nanotip

sharpening method was employed to prepare the needles on silica posts. The APT specimens were prepared in a way that the encapsulated nanoparticles were positioned parallel to the needle axis (cross-section orientation). SEM images of step-wise specimen preparation process are illustrated in Figure 3-3.

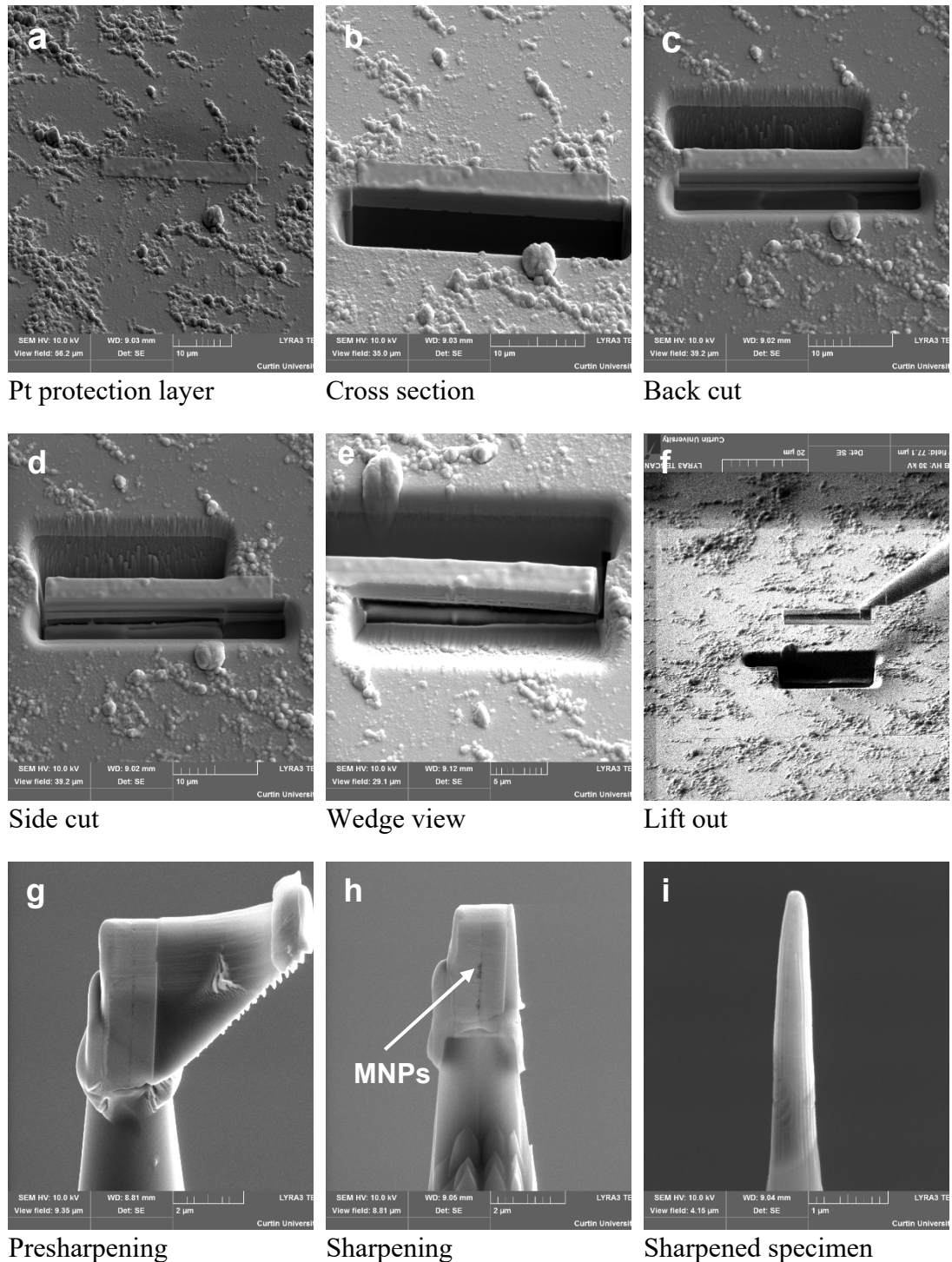


Figure 3-3. APT specimen preparation process.

Smooth tapered circular cross-sectioned needle-shaped specimens are preferred for APT analysis. The circular cross-section is of paramount importance to ensure proper data reconstruction. Firstly a thin layer of platinum is deposited onto the ROI to protect the specimen during the milling process and to mark the region to be extracted (image a). The dimensions of the platinum strip are approximately 2-3 μm wide, 25 μm long and 100 nm thick. Trenches are then milled on three sides of the ROI, and this is followed by tilting the specimen and cutting the underside before being lifted out (images b-f). This wedge (approximately 20 μm long) is then mounted onto a suitable specimen mount (pre-fabricated Si posts) using Pt deposition. Finally the wedge-shaped specimen is sharpened to a needle shape with annular milling patterns (images g-i). The darker strip in the image h is the layer of nanoparticles to be analysed.

An image of the APT instrument used is shown in Figure 3-4.



Figure 3-4. Cameca LEAP 4000X HR atom probe tomography at John de Laeter centre, Curtin University (image provided by Dr David Saxey)

3.4.11 SQUID Magnetisation Measurements

Field dependent and temperature dependent magnetisation measurements of nanopowder samples were conducted using a Quantum Design MPMS 5XL superconducting quantum interference device (SQUID) Magnetometer. Magnetic nanoparticles were packed inside plastic capsules for the measurements. Field dependence was performed at a temperature of 300K, in an applied magnetic field of up to 20 kOe.

For zero field cooled and field cooled (ZFC and FC) measurements, the powder samples were mounted at room temperature followed by cooling down to 5 K without any applied magnetic field. The sample was then warmed up to 300 K in an applied field of 100 Oe. The data was collected during warming. For FC measurements, the powder sample was cooled to 5K again with an applied magnetic field of 100 Oe and data was collected during cooling.

3.4.12 Thermogravimetric Analyses (TGA) and Differential Scanning Calorimetry (DSC)

Thermogravimetric analyses were performed on a TA Instruments SDT Q600 simultaneous DTA-TGA. Approximately 30 mg of nanopowder sample was weighed into a 110 μ L platinum crucible with a matched empty crucible as a control reference. The sample was heated from ambient temperature to 850°C at 10°C per minute in a nitrogen atmosphere flowing at 100 ml per minute. TA instruments, Universal V4.5A software was used for the data analysis. The thermal decomposition of the sample provides information on the mass percentage of organic coating and magnetic core. DSC measurement indicates the heat induced phase changes of the material.

3.4.13 BET Surface Area

The specific surface area of nanoparticles was determined by the Brunauer-Emmett-Teller method (BET, Micromeritics TriStar 3000) with nitrogen gas as the adsorbate at a temperature of 77.3 K (-195.85 °C).

3.5 Solution Analysis

3.5.1 Atomic Absorption Spectroscopy (AAS)

An Agilent 55B AAS was employed for solution analysis for gold and copper concentrations. The flame source was a mixture of acetylene (1.5 dm³/h) and air (3 dm³/h) which was ignited for the analysis. The respective lamp which contains the cathode is of the element being analysed, emits the light beam which goes through the spectroscope where the wavelength slit is adjusted per particular element. The intensity of the monochromatic light passing through the flame is recorded by a photomultiplier. The amount of radiation absorbed by the sample is compared to that of the standard solutions of the element under similar conditions and concentration of the element under examination is calculated. The solutions were diluted with DI water wherever required, prior to analysis. The dilution ratio was varied from 10 times to 100 times depending on the concentration of the element to be analysed. Two readings were taken for each solution to obtain an accurate value.

3.5.2 Inductively Coupled Plasma Mass Spectroscopy and Optical Emission Spectroscopy (ICP-MS and ICP-OES)

ICP-OES 735-ES from Agilent (CSIRO, Waterford, Australia) and ICP-MS (Bureau Veritas, Canning Vale, Australia) instruments were used for metal analysis in solutions where high accuracy was required. An ICP-MS was also used for analysis of the total dissolved sulfur in the solution.

3.5.3 High Performance Liquid Chromatography (HPLC)

To analyse sulfur species (thiosulfate, polythionates, sulfite and sulfate) in the solution, a Waters 2695 HPLC separation module was used. The technique separates, purifies, identifies and quantifies species in a complex mixture. Sulfur species analysis was conducted in *before* and *after* adsorption solutions to determine the stability of thiosulfate and the competitive adsorption of the species to the adsorbent. The Empower™ software package (Waters Corporation) was used to control the HPLC and calculate the peak areas. Detailed information on the analysis procedure and the columns used can be found in Appendix B.3.

3.6 Nanoparticle Deagglomeration by Ultrasonic Dispersion

Magnetic nanoparticles were dispersed in preferred solutions using a Hielscher UP200Ht (200W, 26kHz) handheld ultrasonic homogeniser by immersing approximately half of the probe into the solution. Firstly, a measured weight of dry nanoparticles was dispensed in to a small container and a 50 ml of preferred solution was added. The preferred solutions are listed below.

1. DI water, pH 9.5 for bare MNPs and pH 7 for PEI-MNPs
2. 10 g/L trisodium citrate solutions, pH 9.5 for bare MNPs
3. Commercially available nanoparticle surfactants, pH 9.5 for bare MNPs and pH 7 for PEI-MNPs.

Commercially available nanoparticle surfactants were sourced from US research nanomaterials. It is a clear viscous liquid with a 45% of solid content. According to manufacturer, it possesses the hydrogen bonding of its hydrophilic polyethylene oxide parts.

Nanoparticle concentrations were varied from 1 to 10 g/L in a constant solution volume of 50 mL. Ultrasonic time was set from 30s to 600s. Based on the literature review of the ultrasonic dispersion of nanoparticles and a few preliminary tests, the sonication power was set to 100 W and amplitude to 60% (approximately equivalent to 54 μm) in continuous mode (Hielscher 2005, Taurozzi et al. 2011). The ultrasonic probe used had a tip diameter of 14mm. The suspension container was immersed in an ice-water bath to minimise the overheating of the suspension at extended duration of ultrasonication, as illustrated in Figure 3-5. In addition to this, one minute of idle time was maintained after every three minutes of ultrasonication. Hydrodynamic size measurements were conducted using DLS analysis. pH adjustments were performed using NaOH.

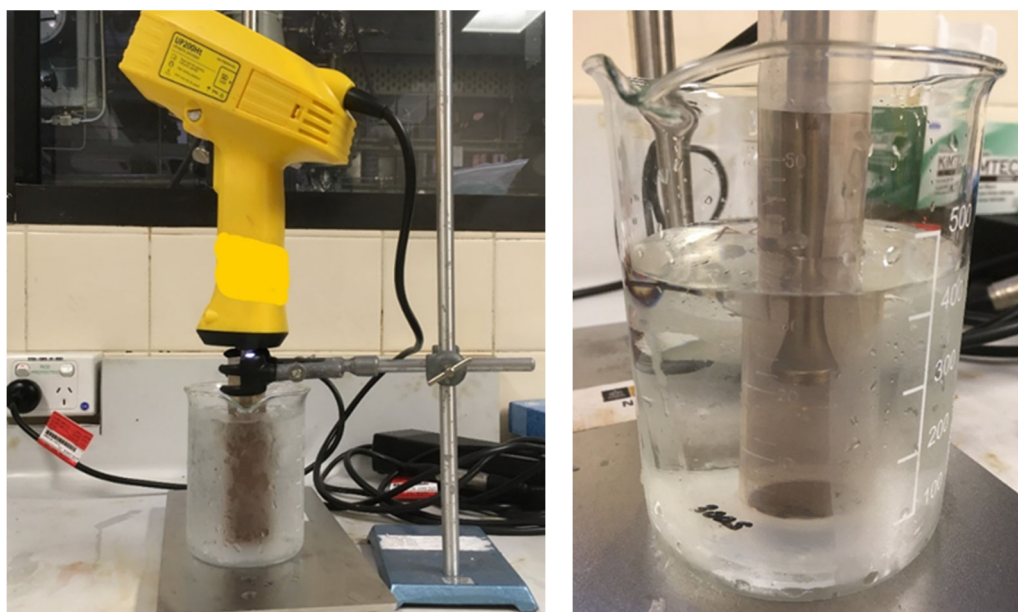


Figure 3-5. Instrument set up of ultrasonic dispersion of nanoparticles

3.7 pH Dependent Dissolution of MNPs

Nanoparticle dissolution in acidic and alkaline solutions were evaluated by exposing bare MNPs and PEI-MNPs to HCl and NaOH solutions for up to 3 hours within the range of pH 2-12. Nanoparticles were added to the solution and agitated for up to 3 hours at 25 °C in an orbital shaker. Finally, the nanoparticles were separated and the supernatant solutions were analysed for Fe concentration. Moreover PEI-MNPs used in pH 2 and pH 12 solutions were used for adsorption studies to ensure they maintained a similar adsorption performance.

3.8 Adsorption Experiments with Synthetic Leaching Solutions

3.8.1 Calcium Thiosulfate – Air Leaching System

Gold stock solution was prepared by dissolving the required amount of sodium aurothiosulfate ($Na_3Au(S_2O_3)_2$) powder in deionised water. Approximately 10 mg/L of gold stock solution was used throughout the research for adsorption experiments, with the exception of the isotherm studies. Measured amounts of calcium thiosulfate (CaS_2O_3) and copper sulfate ($CuSO_4$) were added to the prepared gold stock solution to prepare the synthetic leaching solutions. After adjusting the pH, the solution was added to the Erlenmeyer flask with the desired amount of nanoparticles. The closed flasks were stirred in an orbital shaker at 250 rpm and at the desired temperature for the desired time. Diluted sodium hydroxide and sulfuric acid were used for pH adjustments. Once the adsorption process was finished, the solid-liquid separation was accomplished with the aid of an external magnet. Supernatant solution was analysed with Atomic Absorption Spectroscopy (AAS) or inductively coupled plasma optical emission spectrometry (ICP-OES) for residual gold and copper concentrations. Metal-loaded MNPs were used for metal elution studies. The effects of reagent concentrations and process parameters on gold adsorption in $CaS_2O_3-O_2$ system were investigated as follows.

3.8.1.1 Adsorbent dosage

Synthetic leach solutions were prepared and once the pH was adjusted to 8 and the solutions reached a temperature of 50 °C, nanoparticles were added, equivalent to 5, 10, 20, 50 and 75 g/L. The samples were run for one hour before the sample aliquots were collected and analysed for residual metal concentrations.

3.8.1.2 Solution pH

The initial pH value of the solutions was adjusted to 5, 6, 7 and to 8.8 for the adsorption studies. The solutions consisted of 0.1 M CaS_2O_3 , 20 mg/L copper and approximately 10 mg/L gold. The natural pH values of the solutions were in between 6.5-7 and adjusted to the desired value either with 0.1 M NaOH or 0.1 M H_2SO_4 solutions.

3.8.1.3 Copper concentration

The influence of copper concentration in the solution on gold loading was tested by changing the copper concentration from 0 to 120 mg/L, keeping the other parameters constant at 0.1 M CaS_2O_3 and approximately 10 mg/L gold as gold thiosulfate.

3.8.1.4 Thiosulfate Concentration

Synthetic leaching solutions were prepared by changing the calcium thiosulfate concentration from 0 to 0.2 mM. The initial solution pH and the temperature were set to 8 and 50 °C, respectively.

3.8.2 Other Thiosulfate Leaching Systems

3.8.2.1 Copper-Ammoniacal System

The gold stock solution was prepared by dissolving the required amount of gold as sodium aurothiosulfate (I) complex in deionised water. For the adsorption experiments, sodium thiosulfate was dissolved in the required volume of gold solution in an Erlenmeyer flask. Copper sulfate and ammonia were mixed together and added to the gold and thiosulfate solution while adjusting the pH to the desired value using 0.1M sodium hydroxide and 0.1M sulfuric acid solutions. A sample aliquot was collected for analysis and finally the adsorbent (PEI- MNPs) was added to the solution and the flasks were kept stirring in an orbital shaker for the desired time period at room temperature. The metal-loaded MNPs were then separated using an external magnet with the supernatant solution used for the analysis and the MNPs used for the elution and reuse studies.

3.8.2.2 Nickel-Ammonia System

Sample preparation was almost similar to that for copper-ammoniacal system. In brief, nickel nitrate was dissolved in the desired amount of ammonia solution and added to the gold thiosulfate and ammonium thiosulfate mixture. The solution was stirred vigorously and the pH was adjusted. The required amount of functionalised MNPs were weighed and added to the Erlenmeyer flask. This was followed by the addition of the prepared synthetic leach solution. Adsorption was conducted at room temperature and pH 10.

3.8.2.3 Ferric-Oxalate System

In this particular leaching system, the order of mixing the chemicals is important during the solution preparation in order to prevent thiosulfate oxidation by Fe(III). Firstly, ferric chloride ($FeCl_3$) and sodium oxalate ($Na_2C_2O_4$) were mixed together and the desired mass of sodium thiosulfate and gold stock solution was then added to the solution. In this way, thiosulfate oxidation by Fe is avoided as Fe already coupled with oxalate. The pH was then adjusted using 0.1 M $NaOH$ and 0.1 M H_2SO_4 solutions. A measured amount of PEI-MNPs equivalent to 5 g/L was added to the above mixture and stirred in an incubating shaker at room temperature.

3.8.2.4 Ferric-EDTA System

Firstly, the required amounts of ferric chloride and EDTA were mixed in DI water and the pH was adjusted to pH 7 before adding sodium thiosulfate dissolved in gold stock solution into the mixture. The natural pH of the Fe-EDTA mixture was on the acidic side (pH 2.5). The direct addition of thiosulfate at this pH decomposes it and makes the solution cloudy. PEI-MNPs were then added and the sample was stirred at room temperature.

3.9 Adsorption Kinetics Studies

Kinetic tests were performed with approximately 10 mg/L initial gold concentration at a pH of 8 and 50°C. Three different solutions were prepared as follows.

1. Solution 1- approximately 0.1M calcium thiosulfate, 10 mg/L gold and 20 mg/L copper.
2. Solution 2 - approximately 0.1M calcium thiosulfate and 10 mg/L gold
3. Solution 3 - approximately 10 mg/L gold as gold thiosulfate in DI water.

Sample aliquots were collected after 5, 10, 20, 30, 40, 60 and 180 minutes and analysed using an AAS for remaining gold concentrations. In addition to this, sample aliquots were collected from Solution 1 more frequently (after 1, 2, 3, 4, 8 and 12 minutes), in order to get sufficient data points for kinetics modelling. The metal adsorption efficiency (R as a %) and adsorption capacity (q in mg/g) were calculated based on equations (3-1) and (3-2).

$$R = \left(\frac{C_e - C_i}{C_i} \right) 100 \quad (3-1)$$

$$q = \frac{V}{m} (C_e - C_i) \quad (3-2)$$

where, C_i and C_e are the metal ion concentration at initial and equilibrium stages respectively, in mg/L. V is the sample volume in L and m is the weight of the adsorbent used in g. The data obtained from Solution 1 was used for adsorption kinetic model fitting.

3.10 Adsorption Isotherm Studies

Isotherm studies were carried out using synthetic CaS_2O_3 – air leaching solutions. Synthetic leaching solutions consisting of different initial gold concentrations ranging from 4 to 429 mg/L were prepared. Adsorption was conducted at temperatures of 25, 35 and 50°C and a pH of 8 for 24 hours. The gold-loaded MNPs were then separated using an external magnet and sample aliquots were collected from the clear supernatant solutions. The isotherm data fitted with the Langmuir and Freundlich isotherm models.

3.11 Thermodynamic Studies

Adsorption isotherm experiment results at different temperatures were used to calculate thermodynamic parameters. The change in Gibbs free energy (ΔG°), enthalpy (ΔH°) and entropy (ΔS°) were calculated according to equations (3-3), (3-4), (3-5) and (3-6) in order to reveal the adsorption mechanism.

The value of ΔG° can be obtained by,

$$\Delta G^\circ = -RT \ln K_C \quad (3-3)$$

The relationship between ΔG° , ΔH° and ΔS° is given as

$$\Delta G^\circ = \Delta H^\circ - T \Delta S^\circ \quad (3-4)$$

From equations (3-3) and (3-4);

$$\ln K_C = -\frac{\Delta H^\circ}{RT} + \frac{\Delta S^\circ}{R} \quad (3-5)$$

The relationship between K and K_L ,

$$K_C = K_L M_{adsorbate} \times 10^3 \times 55.5 \quad (3-6)$$

where, R is the universal gas constant (8.3144 J/mol.K), T is the absolute temperature in Kelvin and K_C is a dimensionless equilibrium constant. The value of K_C can be derived from the Langmuir constant, K_L using equation (3-6) (Zhou and Zhou 2014, Tran et al. 2016).

3.12 Gold and Copper Elution

PEI-MNPs used in synthetic CaS_2O_3 – air leaching system were used for the elution studies. A two-step batch elution process was conducted; copper pre-elution followed by gold elution.

For copper pre elution, a 0.02 M EDTA solution was used. Gold and copper loaded magnetic nanoparticles were added to the above-mentioned solution and stirred continuously at room temperature (25°C) for 15 minutes. Sample aliquots were collected for gold and copper concentration analysis using an AAS. The copper eluted MNPs were washed with DI water to neutrality and added to a 0.01M NaOH solution for subsequent gold elution for 15 minutes. The influence of different process parameters such as eluant concentration, solid to liquid ratio, solution pH and temperature on metal elution efficiency was evaluated by changing the relevant parameter in a given range while keeping the other parameters constant.

The elution kinetics experiments were performed in duplicate by adding metal-loaded PEI-MNPs and eluant solution to a 125 mL Erlenmeyer flask, followed by mixing the solution at 250 rpm for the desired time at the desired temperature. Sample aliquots were collected at predetermined time intervals of up to one hour. Magnetic separation was used for solid-liquid separation. The solution was further filtered using syringe membrane filters (0.22 µm pore size). The S/L ratio was maintained at 2.5 g/L, unless otherwise stated, for all elution kinetics experiments. Copper eluted adsorbent was used for gold elution studies. In this case the copper elution process was conducted at 0.02 M EDTA, at 25 °C and at a pH level of 6 for 15 minutes.

Elution efficiency was calculated according to equation (3-7), where M_{eluted} is the amount of metal eluted and $M_{adsorbed}$ is the amount of metal adsorbed.

$$\text{Elution efficiency (\%)} = \left(\frac{M_{eluted}}{M_{adsorbed}} \right) * 100 \quad (3-7)$$

Several other eluants such as diluted NaOH, diluted HCl acid, glycine and the eluant systems used for gold elution from IX resin were also evaluated. The methods used are included in Appendix D.

3.13 Reuse of MNPs

Six consecutive adsorption-elution cycles were conducted in duplicate to examine the reusability of nanoparticles. Each single cycle included metal adsorption, copper pre-elution, and finally, gold elution. Intermediate washing with DI water was carried out after each step, until the solution pH reached neutrality. Sample aliquots were collected from the supernatant solution for analysis after magnetic separation at the end of each adsorption and elution step. During the adsorption studies, the adsorbent dosage was set to 5 g/L -20 g/L and during elution the S/L ratio was maintained at 2.5 g/L.

3.14 Experiments with Gold Ore Samples

3.14.1 Leaching Tests

Ore samples received from Cortez ore in the Nevada region (USA) were used for these experiments. The required amount of calcium thiosulfate and copper sulfate was dissolved in DI water and the pH was adjusted to 8-8.5 with hydrated lime. The ore samples used were ground to 80% passing 75 μm . The desired weight (400g) of ore was added into a 2L high density polyethylene bottle and the prepared solution was added maintaining a solid to liquid ratio of 40:60. The closed bottle was rotated in an incubator bottle roller at a temperature of 50 $^{\circ}\text{C}$ for 48 hours. The bottle lid had a small hole made in it to ensure an adequate air supply. Sample aliquots were collected at different time intervals to analyse the gold concentration in the solution. The solid-liquid separation was performed using a vacuum filter and the clear solution was used for adsorption studies. The solution aliquots used for metal analysis were further filtered with syringe membrane filters with a 0.22 μm pore size.

The ore sample was characterised using X-ray fluorescence spectroscopy (XRF), LECO combustion analysis and quantitative X-ray diffraction (QXRD) methods for the mineral phase identification and elemental composition determination.

3.14.2 Adsorption Experiments with Gold Ore Leaching Solutions

The filtered leaching solution was used for the metal adsorption process. Adsorption studies were conducted using 125 mL Erlenmeyer flasks. Firstly, the solution pH was adjusted to 8.1 ± 0.1 using hydrated lime and diluted H_2SO_4 wherever required. Once the desired temperature was reached in the solution, a measured amount of PEI-MNPs and the solution was mixed in the flask and set in an incubator orbital shaker (Ratek OM11), from which point onwards the reaction time was measured. The flasks were covered with two layers of aluminium foil to prevent any temperature or solution loss. The shaker speed was set to 250 rpm for all the tests. Gold and copper concentrations of the solutions, before and after adsorption, were analysed by an AAS. Other elements were analysed by ICP-MS.

3.14.3 Experimental Design

All the adsorption experiments were designed based on the central composite design (CCD). Central composite experiment design offers several advantages over conventional experiments. In the conventional approach, one variable is changed while keeping the other variables constant. The repeating of same for every single variable can be tedious, especially

when the number of variables are high. Moreover, this conventional approach does not consider the combined effect of variables on the response variable (Hamzaoui et al. 2008, Ha et al. 2014). The optimisation of the parameters by response surface methodology (RSM), a statistical based practice, is a popular and a reliable method. This creates a second order response surface and considers the effect of individual variables as well as the interaction of those variables. The optimisation of the parameters for the purpose of maximisation or minimisation of response variables is often reported using RSM. Vargas et al. (2012) used RSM to analyse the adsorption behaviour of acid dyes onto activated carbon. The optimisation of arsenic adsorption from aqueous solutions using chitosan and lead, and cadmium adsorption by ZnO nanoflowers is also reported (Dehghani et al. 2018, Kataria and Garg 2018). Moreover the use of RSM for the optimisation of thiosulfate leaching of gold from spent circuit boards has also been attempted (Ha et al. 2014).

The adsorption tests were conducted in random order to prevent any systematic error. The independent variables were chosen as adsorbent dosage (X_1) in g/L, adsorption time (X_2) in minutes and the solution temperature (X_3) in °C, while the response variables were set as adsorption efficiencies (%) of gold (Y_{Au}) and copper (Y_{Cu}). The respective coded and actual values of independent variables are listed in Table 3-1. The design comprised a full three factor factorial at two levels (8 runs), 6 runs at the axial points of the design based on $\alpha = 1.682$ and 6 centre runs (20 runs in total) in order to generate a second order response surface. The α value denotes the distance from the centre (zero) point to the axial point, also known as star point. The axial points represents extreme values for each factor in the design space. The α value was calculated according to equation (3-8). The number of factors is denoted by k .

$$\alpha = [2^k]^{\frac{1}{4}} \quad (3-8)$$

Response surface methodology (RSM) was used to determine the optimum adsorption conditions to find the most appropriate combination of three independent variables to achieve maximum gold adsorption efficiency. The response surface models (one for each of the two response variables) had the general structure of;

$$Y = \beta_0 + \sum_{i=1}^3 \beta_i X_i + \sum_{i=1}^3 \beta_{ii} X_i^2 + \sum_{i=1}^3 \sum_{(j>i)}^3 \beta_{ij} X_i X_j \quad (3-9)$$

where, Y is the response, β_0 is the intercept, and β_i , β_{ii} and β_{ij} are the linear, quadratic and interaction coefficients respectively.

The relationship between the coded values and the actual values of the independent variables are represented as;

$$X_i = \frac{x_i - x_0}{\Delta x_i} \quad (3-10)$$

where, X_i is the dimensionless coded value for each factor, x_i is the corresponding actual value for each factor, x_0 is the actual value at the centre point and Δx_i is the step change value.

Table 3-1. Independent variables and their corresponding levels

Independent variables	Coded values and actual values				
	-1.682	-1	0	+1	1.682
X ₁ Adsorbent dosage (g/L)	3.18	10	20	30	36.82
X ₂ Adsorption time (min)	4.77	15	30	45	55.23
X ₃ Solution temperature (°C)	23.18	30	40	50	56.82

The data obtained from CCD experiments was statistically analysed using Design-Expert 11 software. Analysis of variance (ANOVA) was used to check the significance of the model and the p-values associated with the linear, quadratic and interaction terms were used to assess the significance of each term. Variables associated with p-values > 0.05 were considered insignificant and eliminated from the model (Vargas et al. 2012).

3.14.4 Metal Elution

Metal elution was conducted as reported previously in Section 3.12. Briefly, metal loaded MNPs were magnetically separated and then washed with deionised water. Copper pre-elution was conducted using 0.02 M EDTA solutions at a pH of 6 and at 25°C for 15 minutes. The MNPs were washed with deionised water again prior to the gold elution. Gold elution was accomplished by 0.01 M NaOH solutions at pH 12.0 and at a temperature of 25-50°C. The elution time was adjusted from 15 minutes to 3 hours. Elution efficiency was calculated according to equation (3-7).

Chapter 4 Nanoparticle Functionalisation and Characterisation

4.1 Introduction and Chapter Objectives

The preparation of a suitable magnetic nanoadsorbent for anionic gold complex adsorption was aimed in this study. To accomplish this, the surface functionalisation of nanosized magnetic cores with different functional groups was attempted. Branched polyethylenimine was seen to be the most promising functionalisation agent possibly due to its amine rich structure. Trisodium citrate was used as the intermediate coating layer. The preparation of the trisodium citrate and polyethylenimine coated MNPs (PEI-MNPs) is described in this chapter.

A better understanding of the characteristics of the prepared adsorbent is indispensable for its subsequent use in effective gold recovery from alkaline pH solutions. Therefore, the main objective of this chapter is to illustrate the results of the characterisation work, verification of the successful surface coating and metal adsorption, and to predict behaviour in subsequent processes. A comprehensive characterisation of the adsorbent at different stages of the process; before surface coating, after surface coating and after metal adsorption is illustrated and discussed. Zeta potential, being one of the most important parameters of physical adsorption systems, is explained. The identification of the crystalline structure and surface elements and functional groups in every stage are discussed. Quantitative results are included wherever possible. The topographical analysis of the surface, and the internal phases of MNPs are represented. Size measurement with two different techniques, SEM and DLS, is included. Saturation magnetisation and temperature dependent magnetic properties of the adsorbent, which are of the utmost importance for magnetic separation, are also discussed. Outcomes of the thermogravimetric analysis and nanoparticle dissolution studies are also included. Mainly FTIR, XRD, Raman spectroscopy, and TGA were used to characterise bare MNPs and surface functionalised MNPs while the use of XPS and APT analysis methods extended to Au-PEI-MNPs.

Nanoparticles have an inherent tendency to agglomerate to reduce their surface energy. This tends to occur more prominently when nanoparticles are magnetic. Although the surface coating can suppress this to a satisfactory level, deagglomeration prior to surface functionalisation is vital, in order to coat individual particles, or at least to coat small unbreakable aggregates made up of several particles. The outcome of nanoparticle

deagglomeration trials conducted using ultrasonic dispersion is elaborated upon in this chapter. In summary, the content of this chapter supports and validates the effectiveness of the surface functionalisation process, particle deagglomeration process and metal adsorption process, and helps to predict the performance of the adsorbent in the adsorption system.

4.2 Functionalisation of MNPs

A few different magnetic nanoadsorbents were attempted to adsorb anionic gold thiosulfate from simulated leaching solutions and from pure gold thiosulfate solutions (in some occasions only). The optimisation of the functionalisation process parameters such as PEI concentration, MNP/PEI ratio (weight basis), pH, temperature and reaction time was evaluated to assess maximum adsorption efficiency (the results are not included in this thesis). The comparison of the different adsorbents was based on the gold adsorption efficiency using a simulated calcium thiosulfate leaching solution, all conducted under identical conditions, and results are listed in Appendix A. However, a detailed characterisation was not conducted on other adsorbents, which showed little promise. Only size measurements and SEM imaging were conducted.

Trisodium citrate and PEI coated iron oxide magnetic nanoparticles (PEI-MNPs) were the most promising adsorbent and will be discussed in the following sections. The proposed surface functionalisation of MNPs is schematically illustrated in Figure 4-1. Citrate groups coordinate to MNPs by forming a bridging complex involving two oxygen atoms in carboxylate group. It is assumed that, primary amine groups in PEI reacts with the available carboxylate groups.

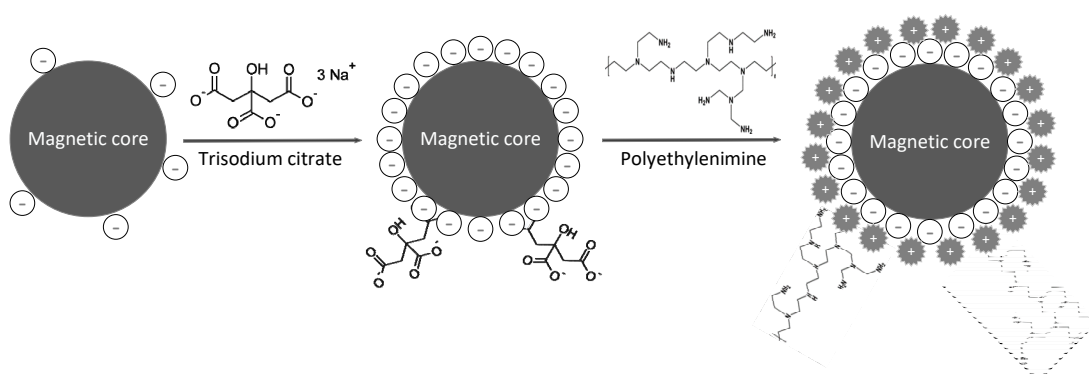


Figure 4-1. Schematic illustration of surface functionalisation of bare MNPs with trisodium citrate and PEI

4.2.1 Citrate Coating

The purpose of the intermediate citrate coating was to impart a higher negative surface charge to the nanoparticle surface. Bare iron oxide MNPs, both magnetite and maghemite, hold a negative surface charge above pH_{PZC} . However, citrate groups can dramatically increase the charge density (amount of anionic groups in a specific surface area) of MNP surfaces. Citric acid is known to be chemisorbed onto an iron oxide particle surface by forming a carboxylate group with the hydroxyl groups on the particle surface (de Sousa et al. 2013). It is reported that the highest surface coverage on the iron oxide NPs was achieved at a 90°C of coating temperature (Li et al. 2013). The efficacy of citrate coating at elevated temperatures, around 90 °C, has often been reported (Cheraghipour et al. 2012, Saraswathy et al. 2014). Therefore, a temperature of 90 °C was used for citrate coating in this study. A significant improvement in particle dispersion was perceived after citrate coating, which was later verified by DLS size measurements. The high negative surface charge on the NP surfaces normally tend to repel each other preventing particle agglomeration.

As will be illustrated in Section 4.3.2, the pH_{PZC} value of bare MNPs was measured at pH 5.7. The negativity of MNPs increased with the increase in solution pH reaching -30 mV at pH 9.5. Therefore, nanoparticle deagglomeration was accomplished in citrate solutions at or slightly above pH 9.5. It is known that where absolute value of zeta is above 30 mV, or at least several pH units away from pH_{PZC} , nanoparticle agglomeration is minimal (Ding and Pacek 2008). In this research, once deagglomeration by ultrasonic dispersion was completed, the solution pH was adjusted to pH 6 by adding diluted sulfuric acid. The zeta potential of citrate coated MNPs (Cit-MNPs) was -37.6 eV at a pH of 8. The success of the citrate coating was verified by FTIR analysis as will be discussed in Section 4.3.4.2. According to FTIR analysis it is most likely citrate forms a bridging complex with bare MNPs.

4.2.2 PEI Coating

Given that thiosulfate leaching systems are operated at alkaline pH values, and as the gold-thiosulfate complex is anionic, the adsorbent should be positively charged in alkaline solutions to facilitate the electrostatic attraction between the adsorbent and the adsorbate. The selected functionalising agent predominantly should be able to show a good affinity for anionic gold thiosulfate. It should also be stable at alkaline pH conditions, and impart a positive surface charge to nanoparticle surfaces in alkaline pH solutions. Based on the reported studies, PEI is the most convenient and appropriate functional group for nanoparticle coating to achieve a higher pH_{PZC} value. Other potential coating agents such as amine, thiol (Singh et al. 2011) and silica (Ferreira et al. 2010) shows comparatively low pH_{PZC} values which may not be effective

for gold adsorption through electrostatic attraction in alkaline pH solutions. In summary, highest cationic charge density, high point of zero charge, and preservation of magnetisation properties were the main reasons for selecting PEI as the functional group.

Branched polyethylenimine ($M_w = 25\ 000\ \text{g/mol}$) was used as the final coating to impart a positive surface charge to the citrate coated NP surface. Primary, secondary and tertiary amine groups are arranged in such a way that there is a branching site at every 3-3.5 nitrogen atoms, ready to be protonated (Jia et al. 2014). This is the reason for the high cationic charge density. As will be discussed in Section 4.3.2, the NP surface is highly cationic after PEI coating. The aforementioned advantages compensate for the high affinity of PEI coated adsorbents towards copper.

Higher nanoparticle to PEI ratios (weight basis) are known to produce well covered nanoparticles i.e., improved PEI adsorption. Therefore, the initial NP to PEI weight ratio was maintained at 1:4. The ratios above and below these values were also considered and 1:4 gave the best results, that means the gold adsorption efficiency started to level-off at 1:4 ratio. It was an indication of a saturation of nanoparticle surfaces with PEI at 1:4 ratio. The efficacy of NP surface coverage by PEI will be discussed under particle characterisation using APT.

The PEI coating process is often performed at high temperatures, which allows for shorter coating times. Surface coating at room temperature is also possible, but demands longer durations up to 24 hours. As the citrate coating process was most effective at 90 °C, and the overall coating process is supposed to be carried out in one pot, the same temperature used for citrate coating was also used for the PEI coating process.

In another study, based on PEI adsorption onto silica gel, it was reported that at pH values around 10, the molecule size of the PEI is reduced and hence it is easy for it to diffuse onto a silica surface (Hostetler and Swanson 1974). When the pH moves into a more acidic region, protonation increases, resulting in a high cationic charge and a larger hydrodynamic size. Although the increase in cationic charge is useful for subsequent anion adsorption, the repulsion of PEI molecules approaching the silica surface by already adsorbed PEI molecules is detrimental to the binding of more PEI molecules onto the silica surface. On the other hand, the cationic surface charge of PEI reaches zero around pH 11. Therefore, it was suggested that pH values not lower than 9 and not higher than 11.5 would be ideal for this particular system. A similar kind of behaviour could also be expected for PEI adsorption onto iron oxide NP surfaces. Hence the PEI coating process was performed at a pH of 9.5 in this study.

4.3 Characterisation of MNPs

4.3.1 Size and Morphology

An image of ‘as received’ iron oxide nanopowder is shown in Figure 4-2. The nanopowder is brown-black in colour.



Figure 4-2. Nanopowder (bare MNPs) as received from the manufacturer

4.3.1.1 Scanning Electron Microscopy and Transmission Electron Microscopy

The size and morphology of bare MNPs and functionalised MNPs were analysed using scanning electron microscopy (SEM) and transmission electron microscopy (TEM). Both techniques were attempted as SEM gives topographical information about the surface of the sample whereas TEM can provide topographical information on the internal structure/phases. As depicted in Figure 4-3, according to the SEM images, the nanoparticles seemed to have a bimodal size distribution. The approximate size of the smaller particles varied from 13-20 nm and the larger particles were in the range of 36-84 nm. TEM images showed in Figure 4-4 indicated that the shape of the larger particles was cuboidal and/or pyramidal, while the smaller particles were spheroidal. The BET surface area of the nanoparticles was approximately 99.04 m²/g.

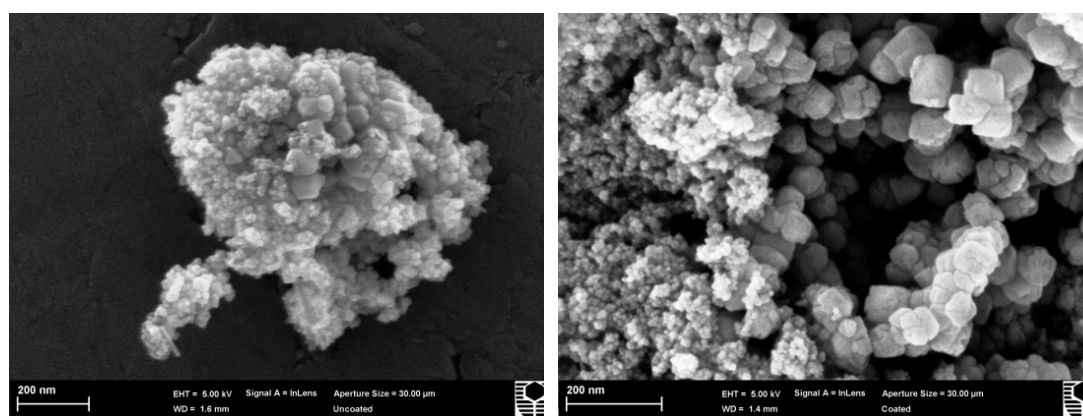


Figure 4-3. SEM images of bare MNPs (left) and PEI-MNPs (right)

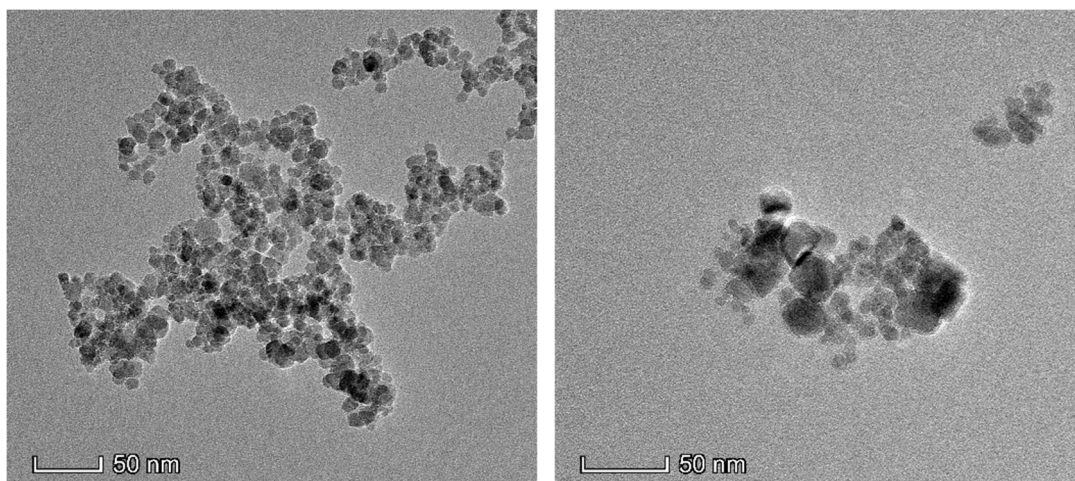


Figure 4-4. TEM images bare MNPs (left) and PEI-MNPs (right)

The thickness of the surface coating layer was measured during TEM analysis, as illustrated in Figure 4-5. A well-defined coating layer was observed, while the measured thickness varied from approximately 1.3-2.3 nm. The observed thickness lies within the values reported elsewhere (Radeva and Petkanchin 1997, Li et al. 2013). There are instances of single particle coating as well as coating of a cluster of NPs.

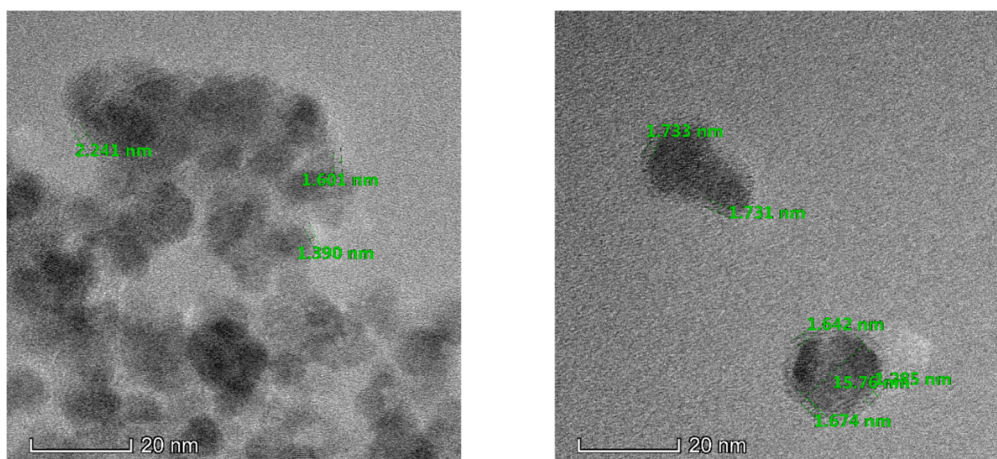


Figure 4-5. Thickness measurements of the surface coating layer

4.3.1.2 Dynamic Light Scattering

DLS was employed to measure the hydrodynamic size distribution of MNPs at different stages of the functionalisation and adsorption process. The number based size distributions of bare MNPs just before surface coating process, after PEI coating, and after metal adsorption are represented in Figure 4-6.

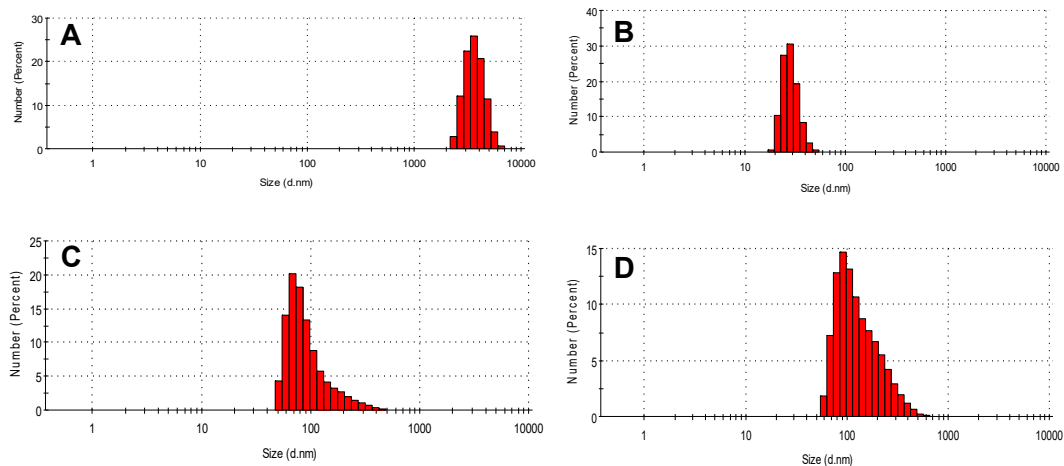


Figure 4-6. Hydrodynamic size distribution of 5 g/L bare MNPs before ultrasonic dispersion (A), after 600 s dispersion in a 10g/L trisodium citrate solution at pH 9.5 (B), PEI-MNPs (citrate coated and then PEI coated in 5% PEI solution at pH 9.5 and 90 °C and washed (C), and Au-PEI-MNPs (adsorption conducted in 10 mg/L gold, 0.1 M thiosulfate and 20 mg/L Cu solutions at 50°C and pH 8 (D)

Ultrasonic dispersion was carried out only for bare MNPs prior to the coating process. The well dispersed bare MNPs that ultrasonically dispersed in 10 g/L trisodium citrate solutions for 600 s, were used for subsequent surface functionalisation using trisodium citrate and PEI. The resultant PEI-MNPs were used for gold adsorption from a synthetic leaching solution. Hydrodynamic size distributions of aforementioned PEI-MNPs and Au-PEI-MNPs were illustrated in image C and D in Figure 4-6. These MNPs did not undergo any ultrasonic dispersion later in the process.

The intensity weighted mean diameter derived from cumulant analysis is known as Z-average and this is the primary result of the DLS technique. It can be converted to number and volume-based distributions for comparison using the Mie theory (Nobmann and Morfesis 2009). Intensity-based size distribution is very sensitive to the presence of aggregates or large contaminants. The respective z-average values (intensity based) and polydispersity index values (PdI) are summarised in Table 4-1. PdI gives an idea of the broadness of the size distribution. In general, PdI values greater than one indicate that the size distribution is highly polydispersed and unsuitable for size measurement using the DLS technique (Shaw 2014).

An increase in hydrodynamic size after PEI coating is obvious, as a consequence of the attachment of surface functional groups to the MNP surface. A slight increase in hydrodynamic size of MNPs was also observed after metal adsorption, which could be attributed to the adsorbed species. It may possibly also be due to particle agglomeration to a certain degree, as a result of the drop in absolute value of zeta potential. As will be discussed in Section 4.3.2, the zeta potential value of Au-PEI-MNPs is +19.2 mV. The corresponding

PdI values, ranging from 0.231 to 0.389, are lying in the mid-range of PdI. This mid-range is the range over which the distribution algorithms operate best (Shaw 2014).

Table 4-1. Intensity based Z-average, polydispersity index (PdI) and peak positions of nanoparticle size distribution

Sample description	Intensity weighted Z-Ave (nm)	PdI	Peak intensity		
			Peak 1	Peak 2	Peak 3
Bare MNPs, after 600 s sonication	120.6	0.368	168.5	4640	0
	112.1	0.367	153.1	4733	0
	112.3	0.389	164.7	4463	0
PEI-MNPs	181.2	0.231	195.9	4937	0
	174.3	0.254	192.9	4534	36.61
	171.7	0.237	202.8	4901	0
Metal adsorbed MNPs	221.1	0.272	275.1	4735	0
	208.5	0.264	231.3	4301	0
	206	0.272	235.7	2732	0

4.3.2 Zeta Potential

The Zeta potential of a particular colloid is sensitive to solution pH. Every colloid has a pH value where the net surface charge becomes zero, and this is known as the point of zero charge (PZC). The colloid is at its most unstable state at PZC. The pH_{PZC} of magnetite can vary considerably with background electrolytes (Illés and Tombác 2006).

The intermediate citrate coating introduced a high negative charge density to the NP surface. According to previous studies, it was observed that citric acid coated magnetite NPs have a negative zeta potential over a wide pH range starting from pH 2 (Wang et al. 2009). This intermediate coating helps to prevent or minimise particle aggregation by facilitating electrostatic repulsion. Furthermore, the negatively charged particles are able to adsorb cationic PEI easily. Due to the increased number of anionic binding sites per unit area, compared to bare MNPs, the amount of PEI adsorbed also increases (Wang et al. 2009).

The zeta potential measurements are illustrated in Figure 4-7. In this study no electrolyte was used and the analysis was performed in a DI water matrix. However the presence of NaCl is possible due to pH adjustments with NaOH and HCl. It is evident that the pH at point of zero charge (pH_{PZC}) increased significantly following the PEI coating. Based on the results, the pH_{PZC} value was around 5.7 and 11 for bare MNPs and PEI-MNPs, respectively. The isoelectric point or pH_{PZC} value reported for bare magnetite varies from 3.2 to 6.9 at 25°C in

different background electrolyte solutions (Hristovski et al. 2007, Vidojkovic and Rakin 2016). The pH_{PZC} for PEI coated MNPs is in accordance with the results reported elsewhere (Goon et al. 2010, Pang et al. 2011b).

Calcium thiosulfate – air leaching system operates in mild alkaline conditions, at around pH 8. Zeta potential analysis data revealed that at pH 8, a bare MNP surface is negatively charged, which may not encourage electrostatic attraction. This had been verified by adsorption studies conducted using bare nanoparticles as the adsorbent for gold adsorption, where no gold adsorption was observed. The Zeta potential of citrate-coated MNPs (Cit-MNPs) and Au-PEI-MNPs was (-37.6) mV and 19.2 mV at pH 8, respectively. Further functionalisation of MNPs with PEI resulted in a positively charged particle surface supporting electrostatic attraction. The reduction of the surface charge following the metal loading is due to the adsorption of anionic complexes, thus reducing the net positive charge.

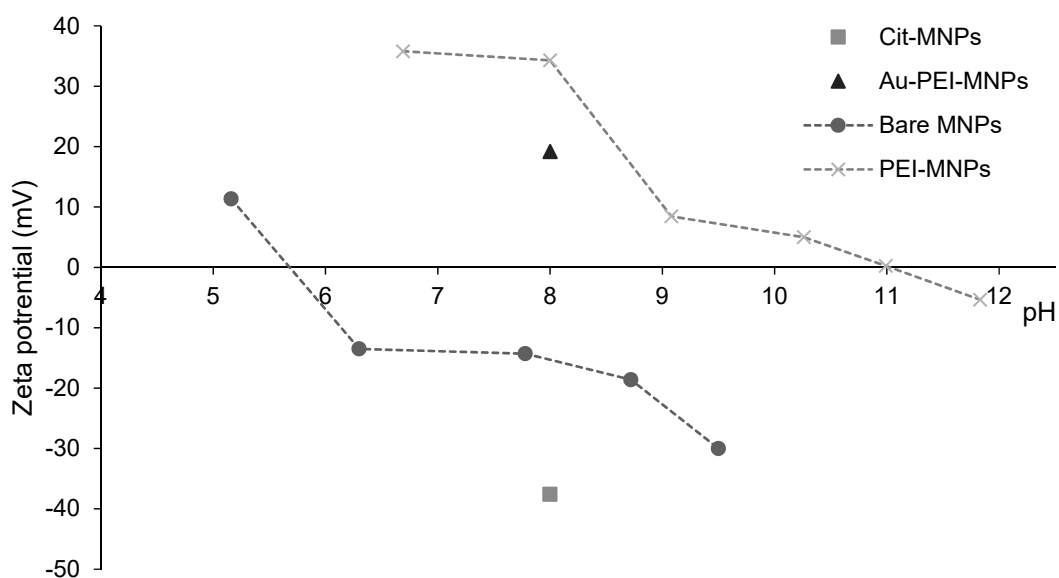


Figure 4-7. Zeta potential measurements of MNPs

4.3.3 Crystal Structure Analysis

4.3.3.1 X-ray Diffraction

For powder diffraction, the use of cobalt radiation over copper radiation for iron-containing sample analysis is recommended due to its lower noise generation and thus more accurate phase identification. This is of particular importance in the case of magnetite and maghemite mixture analysis as the diffractograms are distinguishable only by a few low intensity peaks (Mos et al. 2018). Thus, cobalt radiation was used for XRD analysis in this study. XRD

patterns of nanoparticles before and after PEI coating are illustrated in Figure 4-8 to Figure 4-10. The broad diffraction peaks observed are due to the small crystallite size (Rudolph et al. 2012). Almost the same XRD patterns were evident for uncoated and coated MNPs, revealing that any phase change was not resulted by coating. The peaks at 2θ values, 21.33, 35.28, 41.62, 50.67, 63.43, 67.66, 74.67 and 88.77 were assigned to miller indices 1 1 1, 2 2 0, 3 1 1, 4 0 0, 4 2 2, 5 1 1, 4 4 0 and 5 3 3, respectively. The pattern displays a cubic structure which could be related to either magnetite and/or maghemite. It is known that differentiation of magnetite and maghemite patterns is difficult, owing to their almost identical lattice parameters, 8.396 Å for magnetite and 8.3515 Å for maghemite. A very low intensity peak observed at approximately 38.8° was assigned to (1 0 4) peak of hematite, which indicates a slight amount of hematite in the nanopowder mixture. No characteristics peaks for any impurities were observed in the pattern, confirming that nanopowder is a high pure iron oxide mixture.

Some maghemite and magnetite peaks overlapped which made proper identification difficult. Based on the PDF data for pure maghemite, two low intensity peaks (5%) were visible at 27.67 and 30.41 2θ (Co K α radiation) indexed to (2 1 0) and (2 1 1), respectively, which can be used to distinguish it from the magnetite phase. The availability of these two peaks however, does not guarantee that the nanopowder is single phase maghemite, or a composition of the mixture. Therefore, the step scan of the peak (5 1 1) approach, as taken by (Kim et al. 2012) can be used to quantitatively estimate the two phases in the nanopowder mixture.

In this study, the peaks related to (2 1 0) and (2 1 1) of maghemite are hardly visible in the two diffractograms, but, in addition to all the high intensity peaks, three low intensity peaks indexed to (6 4 2), (7 3 1) and (8 0 0) related to maghemite are clearly identified in both patterns. 2θ values indexed to the (5 1 1) peak lie at 67.23° (30% intensity) and 67.63° (24% intensity) for pure magnetite and pure maghemite, respectively. As shown in Figure 4-11, two distinct peaks were not identified in this nanopowder, but one broad peak lay in between 67.2° and 67.9° which is indicative of almost the same percentages of magnetite and maghemite in the mixture. This was later confirmed by QXRD results. The QXRD analysis revealed that the crystalline phases of bare iron oxide nanopowder consisted of approximately 52% γ -Fe₂O₃, 47% Fe₃O₄ and <1% α -Fe₂O₃.

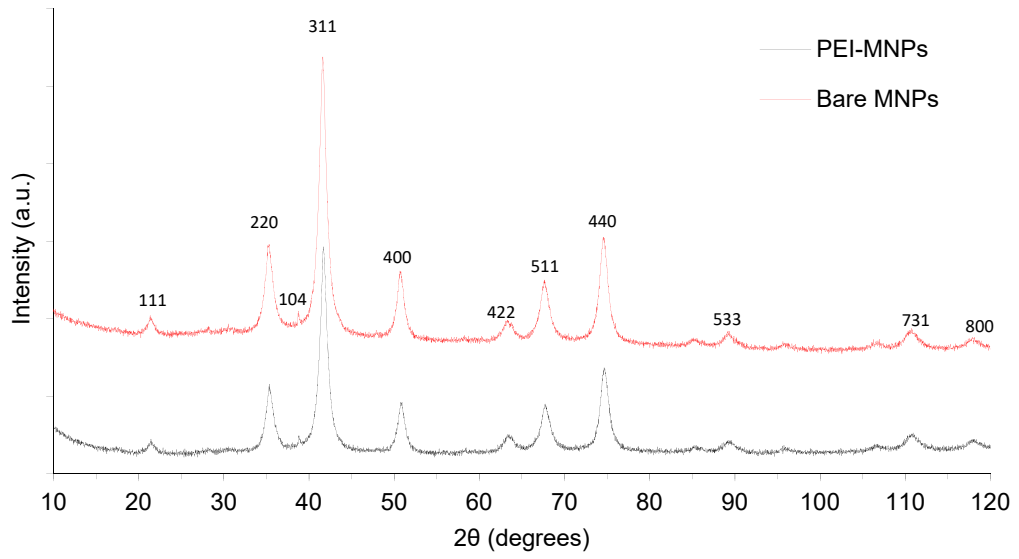


Figure 4-8. XRD patterns of bare MNPs and PEI coated MNPs

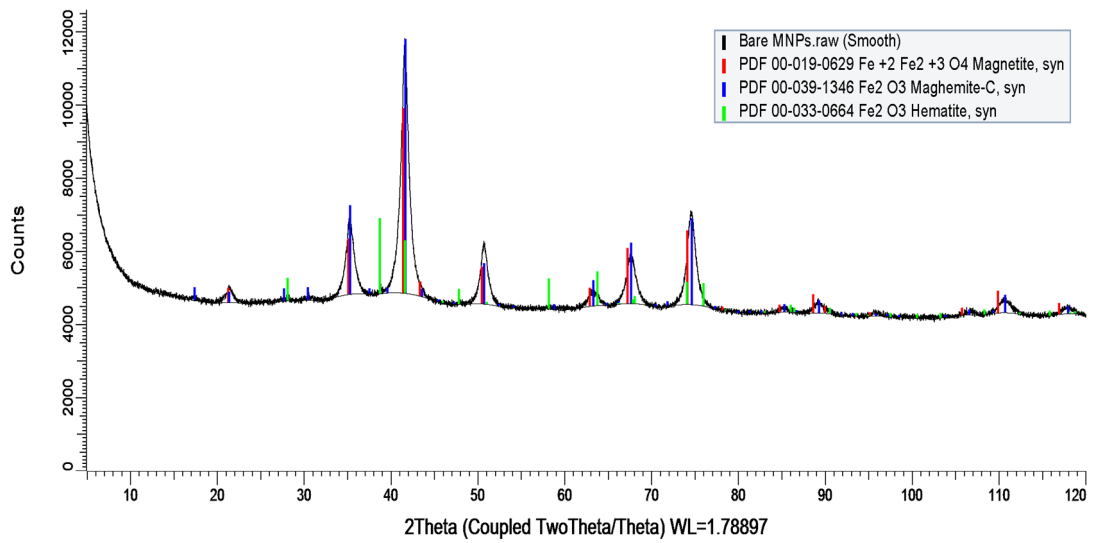


Figure 4-9. XRD diffractograms of bare MNPs

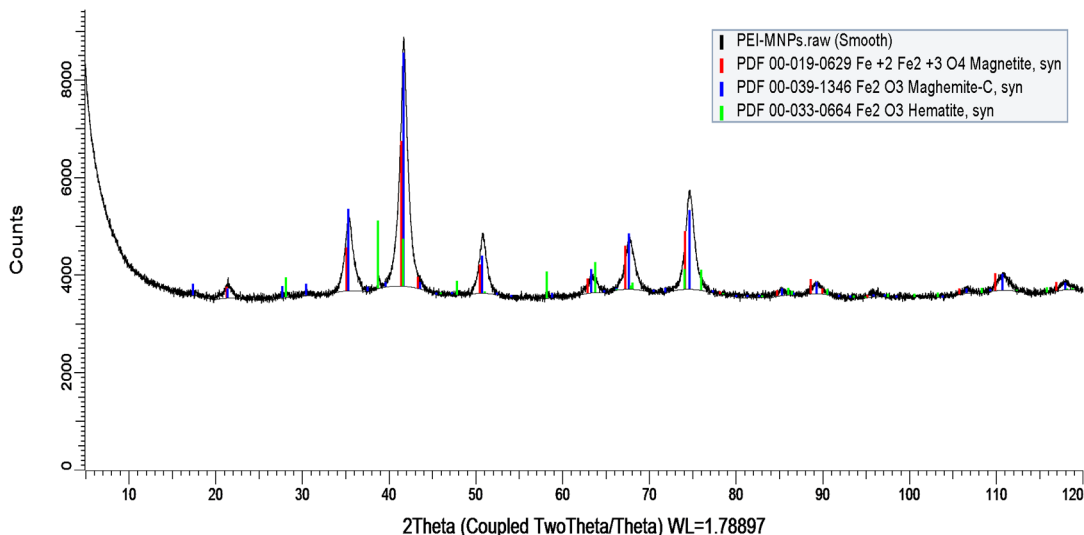


Figure 4-10. XRD diffractograms of PEI-MNPs

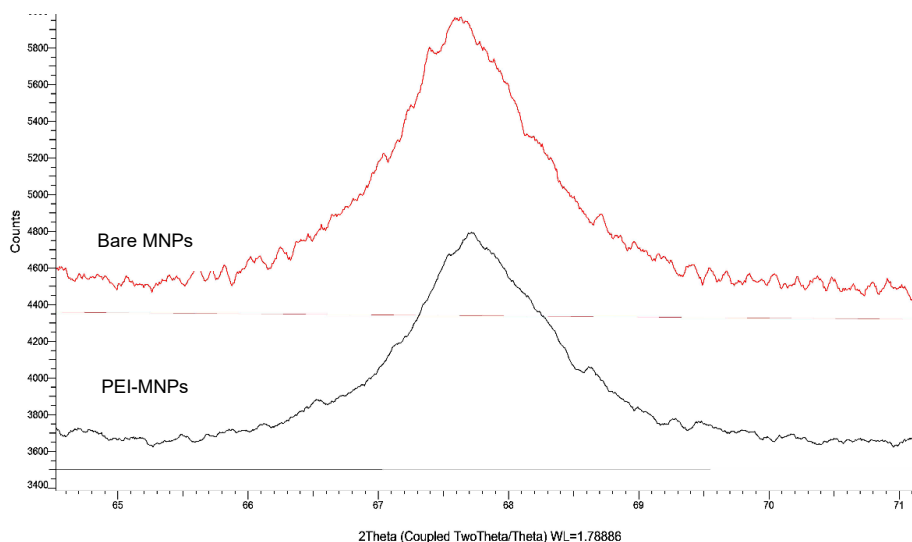


Figure 4-11. Peak 5 1 1 of bare MNPs and PEI-MNPs

4.3.3.2 Raman Spectroscopy

Raman spectra for bare MNPs and PEI-MNPs were obtained at different laser powers to identify the iron oxide phases. Any special sample preparation was unnecessary in this analysis. Powder samples were thinly spread onto a glass strip and placed under the laser beam. The acquisition time for all the samples was 60s, unless otherwise stated, and all the measurements were carried out at atmospheric pressure and room temperature at different laser powers ranging from 0.02 mW to 1 mW. It is known that at lower laser power, magnetite has a weak Raman scattering. On the other hand, high laser powers can trigger the laser-induced phase transformation by ultimately converting magnetite to hematite (Shebanova and Lazor 2003, Slavov et al. 2010). This degradation phenomenon is directly related to particle size and

the form. The degradation of iron oxide is fast and prominent, even with a slight increase in laser power, in nanosized powder samples (Shebanova and Lazor 2003).

The Raman spectra of bare MNPs and PEI-MNPs at different levels of laser power are illustrated in Figure 4-12. A prominent strong peak of around 670 cm^{-1} is characteristic to magnetite, and this is visible even at the lowest laser power used (0.02 mW). However, this peak is broad which can be resulted by overlapping the maghemite peak at 712 cm^{-1} . When the laser power was set to 0.2 mW , two additional peaks at 360 and 500 cm^{-1} appeared and these were assigned to maghemite (Slavov et al. 2010). Once the laser power was further increased to 0.5 mW , some extra peaks appeared at approximately 216 , 279 and 1297 cm^{-1} together with the previously mentioned maghemite peaks, which indicate the further oxidation of magnetite to hematite. The presence of a magnetite peak at 670 cm^{-1} , together with these peaks, is indicative of either partial oxidation of magnetite and/or a mixture of iron oxides (magnetite, maghemite and hematite). Slavov et al. (2010) observed a total disappearance of the peak at 670 cm^{-1} after exposing the powder to 1.95 mW of laser power due to the phase transition. A new peak formed at 1297 cm^{-1} was assigned to the magnon scattering in hematite (de Faria et al. 1997, Soler and Qu 2012).

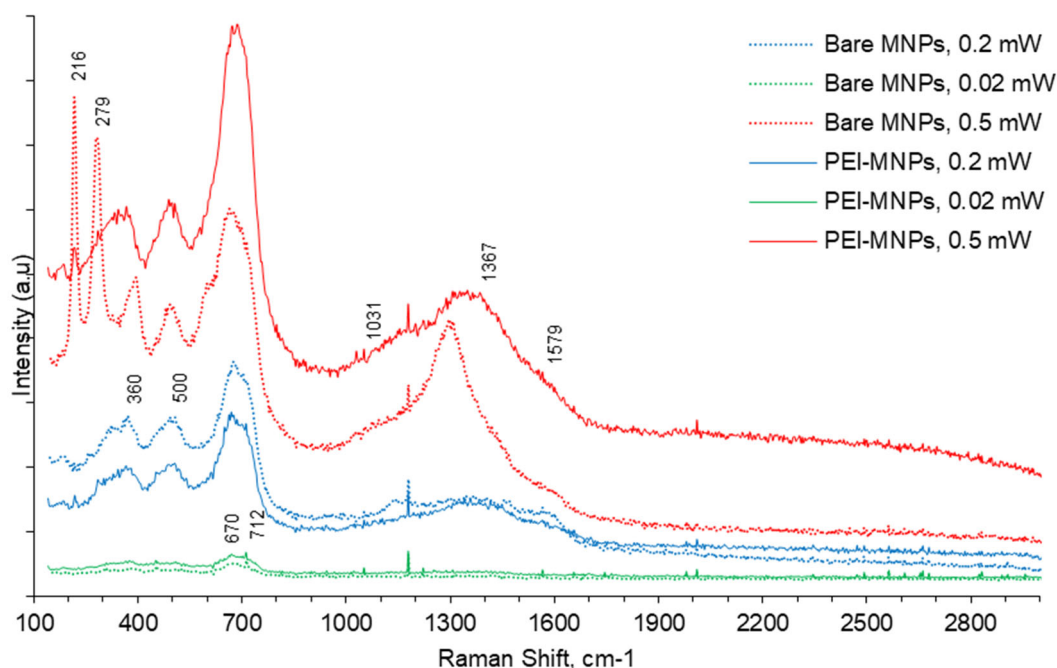


Figure 4-12. Raman spectrum of bare MNPs (dotted lines) and PEI-MNPs (solid lines) at different laser powers in 60 s acquisition time

The Raman spectra of PEI-MNPs are almost identical to the bare MNPs at lower laser powers. At 0.5 mW , the hematite peaks in the PEI-MNPs spectrum are not as prominent as in bare MNPs, which may be due to the delay in internal core oxidation as a result of the surface

coating. In conclusion, the nanopowder used was mainly magnetite, although the possibility of the presence of some maghemite cannot be ruled out.

4.3.4 Bulk and Surface Composition Analysis

4.3.4.1 X-ray Photoelectron Spectroscopy

XPS analysis was used to determine the surface elemental composition and chemical states of the material. XPS survey spectra of bare MNPs, PEI-MNPs and metal loaded MNPs (Au-PEI-MNPs) are presented in Figure 4-13. The corresponding peak positions (binding energy in eV), full width half maximum (FWHM) values and area percentages are listed in Table 4-2.

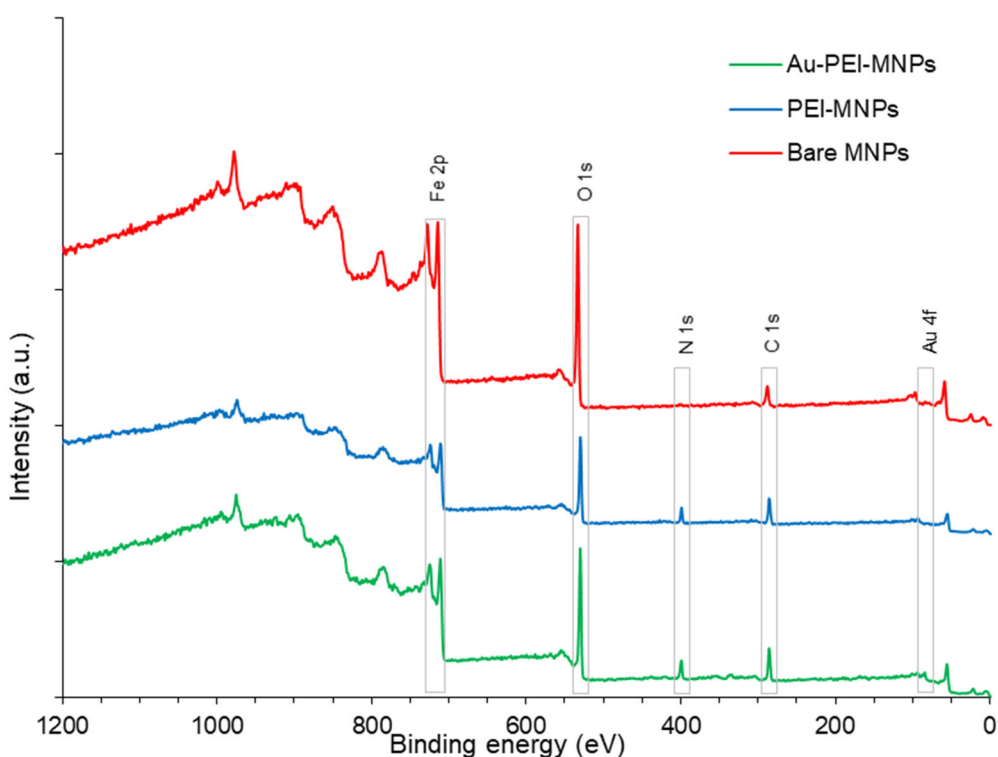


Figure 4-13. XPS survey spectra of bare MNPs, PEI-MNPs and Au-PEI-MNPs

Two major peaks at binding energies of approximately 284.8 eV and 529.5 eV, in the spectrum of bare MNPs, were designated for C 1s and O 1s, respectively. Fe_3O_4 can be expressed as $\text{FeO}\cdot\text{Fe}_2\text{O}_3$, with a $\text{Fe}^{2+}:\text{Fe}^{3+}$ ratio of 1:2. Moreover $\gamma\text{-Fe}_2\text{O}_3$ contains iron in the Fe^{3+} state only. The peak positions of Fe $2p_{1/2}$ and Fe $2p_{3/2}$ are found at 724.2 eV and 710.5 eV, respectively. A satellite peak of Fe $2p_{3/2}$ can be observed at around 719.2 eV, positioned approximately 8 eV higher than the main Fe $2p_{3/2}$ peak, in accordance with the literature. This satellite peak is characteristic of $\gamma\text{-Fe}_2\text{O}_3$ (Yamashita and Hayes 2008). The main peaks and satellite peak positions mentioned above are associated with the Fe^{3+} state, while the presence of a quantity of Fe^{2+} is also possible (Preisinger et al. 2005). Therefore, this magnetic nanopowder could be

a mixture of magnetite (Fe_3O_4) and maghemite ($\gamma\text{-Fe}_2\text{O}_3$). The detection of magnetite-maghemite mixture in commercially available magnetite nanopowder is also reported elsewhere (Chowdhury et al. 2010).

Table 4-2. XPS analysis data of main peaks

Sample	Element	Position	FWHM	% Area
Bare MNPs	O 1s	529.5	3.19	49.82
	C 1s	284.8	3.82	19.54
	Fe 2p	710.5	4.88	30.64
PEI-MNPs	O 1s	530.4	3.02	37.33
	C 1s	286.4	3.04	33.35
	Fe 2p	710.4	4.52	19.28
	N 1s	399.4	2.59	10.03
Au-PEI-MNPs	O 1s	530.6	3.05	38.91
	C 1s	285.6	2.95	31.39
	Fe 2p	710.6	4.22	19.38
	N 1s	399.6	2.7	8.78
	Au 4f	85.2	1.61	0.14
	S 2p	167.6	4.95	1.4

The method followed by Grosvenor et al. (2004) and Biesinger et al. (2011) for Fe 2p peak fitting was employed in this study. Although XPS is a powerful method used to analyse surface composition, it does not provide information on the bulk composition of the nanocomposite. Only a few nanometre thick surface layer is analysed by this method. High resolution Fe 2p spectra of bare MNPs and PEI-MNPs are illustrated in Figure 4-14. The multiplet splitting of Fe 2p spectra of bare MNPs revealed that the surface composition was 87.6 % maghemite and 12.4 % magnetite. This could be due either to the oxidation of the surface layer to maghemite during synthesis and with the storage of NPs, or it could be the actual local composition of the nanopowder sample. However the composition of magnetite and maghemite is considerably different to the composition given by QXRD. The reason is that QXRD provides evidence of bulk composition whereas XPS measures only the surface composition to a depth of a few nanometres. Interestingly, no peaks corresponding to magnetite were visible in the Fe 2p spectra of both PEI-MNPs (results shown) and Au-PEI-MNPs (results not shown). This can be attributed to the surface coating and surface adsorbed species which further reduces the x-ray penetration depth.

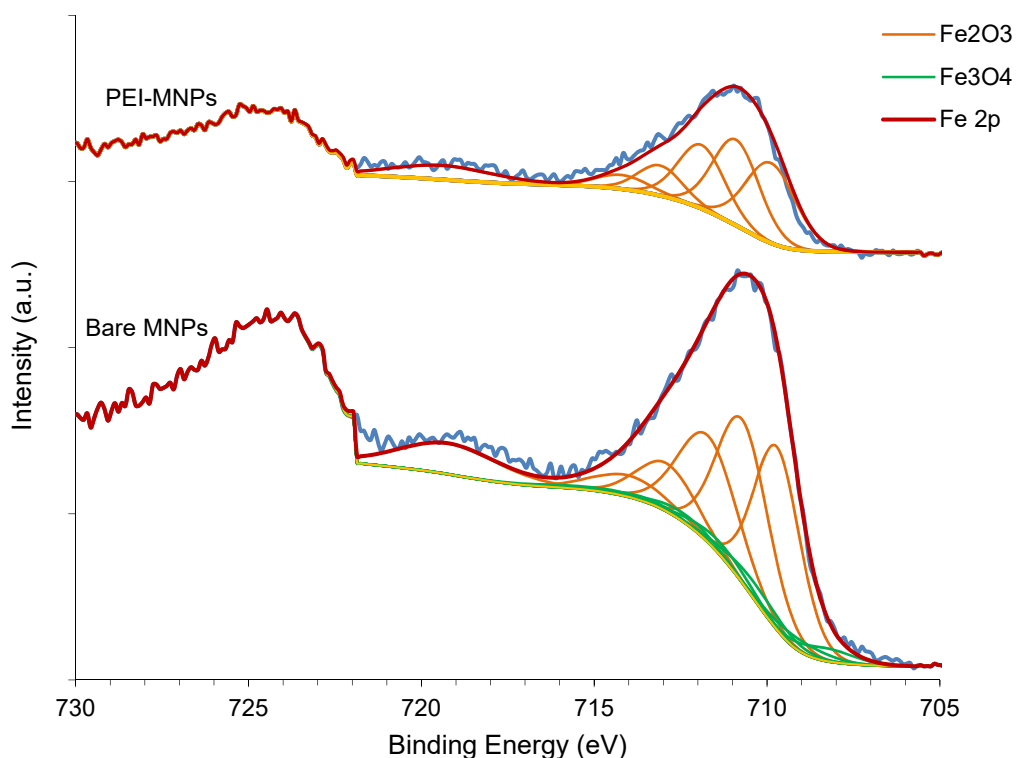


Figure 4-14. Deconvoluted high resolution Fe 2p spectrum of PEI-MNPs (top) and bare MNPs (bottom)

The clear N1s peak observed for PEI-MNPs at 399.8 eV indicates the coordination of nitrogen from amine groups in PEI with nanoparticles, which confirmed the success of the PEI coating. The surface nitrogen composition was 10% after PEI coating. The N 1s high-resolution spectrum was deconvoluted into two main peaks, as depicted in Figure 4-15. The peak at 399.8 eV was assigned to C-N and N-H bond in amines, whilst the peak at 401.3 eV was attributed to protonated amine groups of PEI. These observations are compatible with the values observed elsewhere (Adenier et al. 2004, Kim et al. 2016, Ravi et al. 2018). Any considerable deviation in N 1s peak positions have not been identified in Au-PEI-MNPs (not shown). An enhancement of the area of the shoulder peak (401.3 eV) was observed, but any deviation in the peak position was not detected. This would be a strong indication of the absence of any N-Metal covalent bonds in the analysed powder sample.

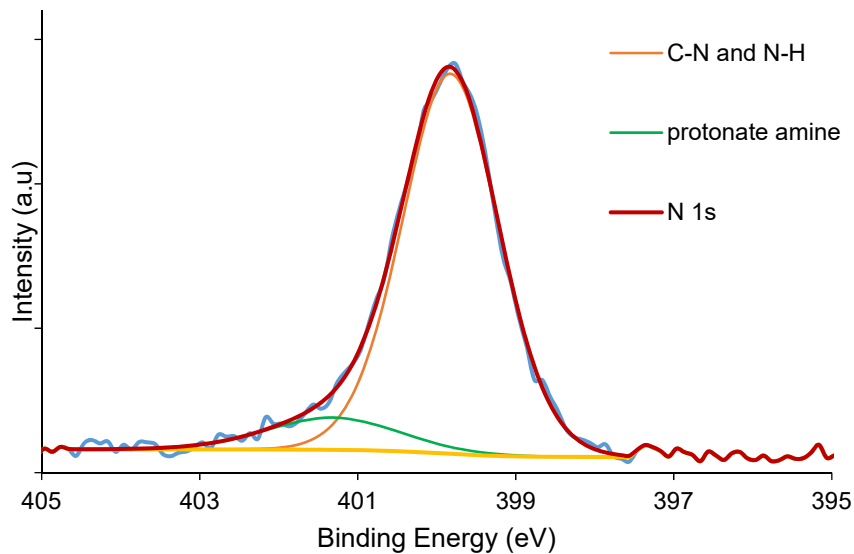


Figure 4-15. Deconvoluted high resolution N 1s spectrum of PEI-MNPs

Carbon peak in the XPS spectrum can arise from adventitious carbon and from the organic carbon resulting from citrate and PEI coating. Almost all samples exposed to the atmosphere were known to be contaminated with adventitious carbon, typically with a 1-2 nm thick layer (XPSsimplified web site). As listed in Table 4-2, the carbon percentage is considerably higher in PEI-MNPs than in that of bare MNPs. The shoulder peak at 284.8 is assignable to C-C bond, which would be resulted from adventitious carbon and C-C bonds in citrate groups and PEI chains. The most intense peak at 286.3 eV in C 1s spectrum shown in Figure 4-16 can be attributed to the C-O and C-N bonds. The small peak at 288.8 eV is considered to arise from the O-C=O bond of carboxylate group (Wilson and Langell 2014). These three peaks verify the attachment of citrate and PEI on to MNPs.

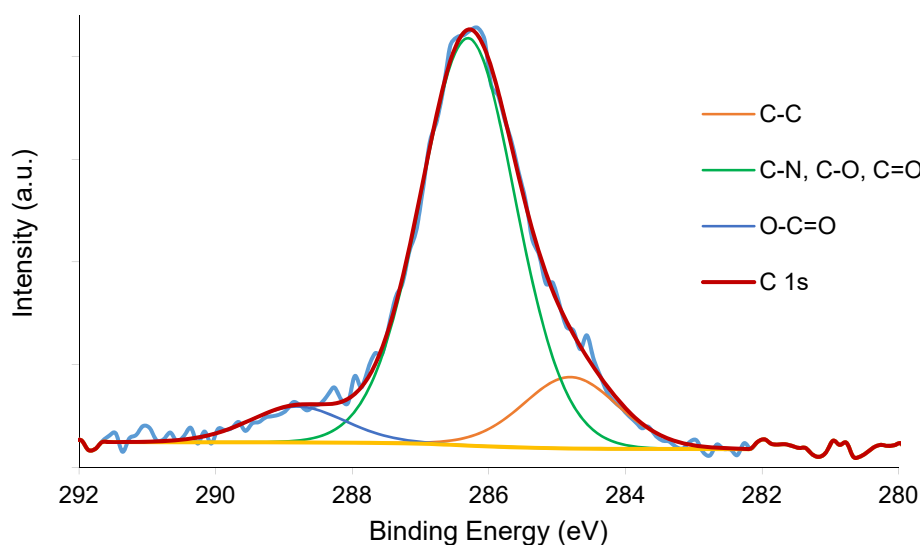


Figure 4-16. Deconvoluted high resolution C 1s spectrum of PEI-MNPs

O 1s spectrum of PEI-MNPs is illustrated in Figure 4-17. The peak shows slight asymmetry towards the higher binding energy side. The main peak can be deconvoluted into three separate peaks at approximately 530.1 eV, 531.1 eV and 533.8 eV. The most intense peak at 530.1 eV is corresponding to lattice oxygen (Fe-O) in the iron oxide mixture. The wide peak at 531.1 eV was assigned to the combined effect of OH groups, organic oxygen (C=O) and C-O groups. The small peak at 533.8 eV is attributed to the carboxylate group (Wilson and Langell 2014, Hiura et al. 2015).

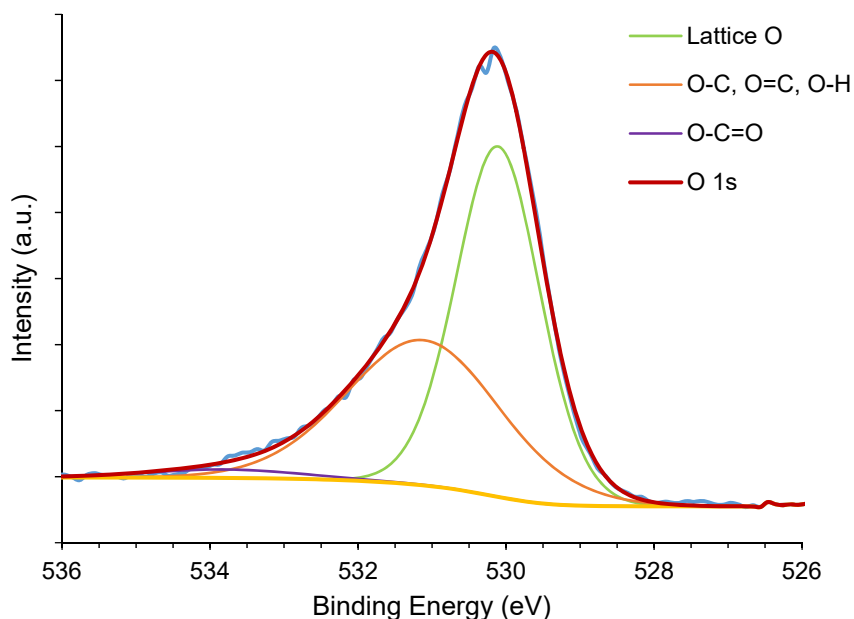


Figure 4-17. Deconvoluted high resolution O 1s spectrum of PEI-MNPs

The high resolution Au 4f spectrum of Au-PEI-MNPs is illustrated in Figure 4-18. The Au 4f_{7/2} peak is located at binding energy (BE) values of 85.4 to 85.6 eV, while Au 4f_{5/2} is located at 89.1 to 89.3 eV which is consistent with the values reported elsewhere (Casaletto et al. 2006, Makhova et al. 2007). The appearance of doublets is due to the spin-orbit coupling (Odio et al. 2014). Sample 1 represents the gold adsorption from a pure gold thiosulfate solution, whilst Sample 2 was used to adsorb gold from a synthetic leaching solution. The Au 4f_{7/2} spectrum of Sample 1 was deconvoluted into two components. The major peak corresponded to the Au (I) state which accounted for 98.3% of gold on the PEI-MNPs surface. Moreover, an insignificant amount of metallic gold can also be present which caused by reduction of Au(I) by amine groups after adsorption. A reduction of Au (III) to Au(0) by amine groups in PEI has been reported elsewhere (Sun et al. 2005, Mohammed et al. 2013). The Au 4f_{7/2} spectrum of Sample 2 can be fitted with only one peak attributed to Au(I) state which indicates the gold adsorption process is physical adsorption only and no redox reaction has occurred. The peaks at 84.9 eV in Sample 1 and 85.1 eV in sample 2 are consistent with Au-S interaction (Odio et al. 2014). This confirms the adsorption of gold thiosulfate complex onto PEI-MNPs.

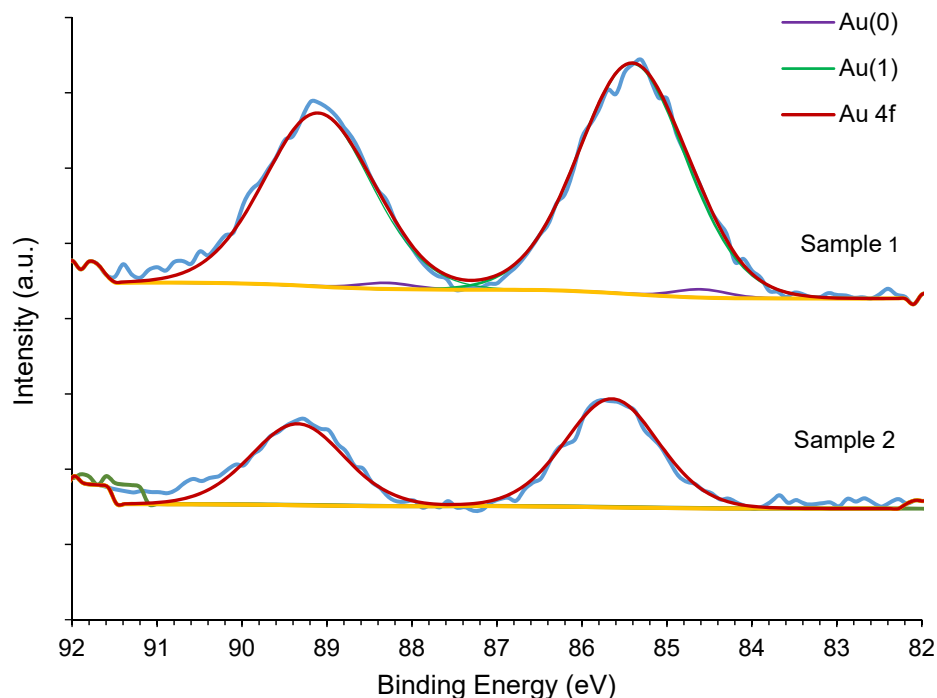


Figure 4-18. Deconvoluted high resolution Au 4f spectrum of Au-PEI-MNPs (adsorption was conducted in a pure gold thiosulfate solution (Sample 1) and in a synthetic leaching solution (Sample 2))

The adsorption of sulfur species is confirmed by S 2p peak in Au-PEI-MNPs. However, the peak is associated with high background noise and a proper deconvolution was not performed. Instead, a tentative deconvolution was performed and clear maximums at 162 - 163 eV and 163.9 eV confirmed the Au-S interactions (not shown). Likewise, the copper peak was also hardly detected, which may be due to the localised low concentration on the nanoparticle surface in the used powder sample.

4.3.4.2 FT-IR spectroscopy

To confirm the success of the surface functionalisation, the FTIR spectra of bare MNPs, Cit-MNPs and PEI-MNPs were investigated. Furthermore, pristine sodium citrate and PEI was also analysed and the respective FTIR spectra are illustrated in Figure 4-19. Some important peaks were well diagnosed for pure trisodium citrate. The wide peak around 3400 cm^{-1} and 1064 cm^{-1} are assignable to OH groups. The strong peaks at 1580 cm^{-1} and 1388 cm^{-1} corresponded to the carboxylate group of citrate. In pristine PEI, bands at 2811 cm^{-1} and 2932 cm^{-1} corresponded to aliphatic C-H stretching vibrations. The peak at 1594 cm^{-1} and 1455 cm^{-1} assigned to N-H vibrations of primary and secondary amine groups, respectively. Furthermore, the peak at 1455 cm^{-1} corresponded to CH_2 moiety as well. The wide peak at 1288 cm^{-1} and peaks at 1113 cm^{-1} and 1045 cm^{-1} corresponded to the C-N stretching vibration (Kasprzak et

al. 2015). A strong peak at 760 cm^{-1} was assigned to out-of-plane bend of NH_2 group (Smith 1999).

In the FTIR spectra of bare MNPs, Cit-MNPs and PEI-MNPs, the peaks at approximately 428 cm^{-1} and 544 cm^{-1} correspond to the vibration bands of Fe-O bonds at octahedral and tetrahedral sites, respectively (Cornell and Schwertmann 2006). This confirms the magnetic core as iron oxides. Although Cit-MNPs is only an intermediate product, the verification of successful citrate group attachment is crucial. The well-resolved peaks related to the stretching of the carboxylate group (CO_2^-) at 1612 cm^{-1} and 1390 cm^{-1} reveals successful interaction of carboxylate groups with the iron oxide surface. The difference between the asymmetric and symmetric C-O stretch bands (Δ) provides information on the binding mechanism of carboxylate ligand to a metal (Nakamoto 2009, Odio et al. 2014). A Δ value much higher than the respective of ionic value implies a unidentate complex while a Δ value much less than ionic value corresponds to a chelating (bidentate) complexation. A close value of Δ to the ionic value is an indication of bridging complex formation. In this case both O atoms in carboxylate group bind to two metal ions, separately. The magnitudes of Δ are 192 and 222 cm^{-1} , for ionic form (pristine citrate) and for Cit-MNPs, respectively. The fairly close values indicate the formation of bridging complex with iron in bare MNPs and carboxylate groups in trisodium citrate.

In the spectrum of PEI-MNPs, the bands around 3354 cm^{-1} and around 1632 cm^{-1} correspond to the N-H stretching vibration of primary/secondary amine and the N-H bending vibration of secondary amine groups of PEI, respectively (Coates 2000, Xu et al. 2011). The peaks at 1059 cm^{-1} and 1470 cm^{-1} can be assigned to the C-N stretching vibration of tertiary amine groups and C-H bending vibrations, respectively. The peaks in between 3000 and 2800 cm^{-1} corresponded to the asymmetric and symmetric C-H stretching vibrations. This confirms the availability of amine groups on the adsorbent surface. In brief, FTIR analysis confirms the successful surface functionalisation of iron oxide surfaces with citrate and amine functional groups. A summary of peak positions and their assignments is listed in Table 4-3.

Table 4-3. Summary of functional group frequencies from FTIR analysis

Spectrum	Wavenumber (cm ⁻¹)	Assignment	Reference
Bare MNPs	428	Fe-O vibration at octahedral sites	(Cornell and Schwertmann 2006)
	544	Fe-O vibration at tetrahedral sites	(Cornell and Schwertmann 2006)
Trisodium citrate	3400	O-H stretch	(Na et al. 2014)
	1580 and 1388	Asymmetric and symmetric stretch of carboxylate (COO ⁻)	(Coates 2000), (Smith 1999)
	1064	OH groups	
Pristine PEI	3286	N-H stretching vibration of secondary amine	(Smith 1999)
	2811 and 2932	Asymmetric and symmetric C-H stretching vibrations	(Kasprzak et al. 2015)
	1594	N-H scissoring vibration of primary amine groups	(Smith 1999, Coates 2000, Kasprzak et al. 2015)
	1455	N-H vibrations of secondary amine groups / CH ₂ moiety	(Kasprzak et al. 2015)
	1288 and 1113-1045	C-N stretching vibration	(Kasprzak et al. 2015)
	760	Out of plane bend (wag) of NH ₂	(Smith 1999)
Cit-MNPs	3392	Structural OH groups	(Na et al. 2014)
	1612 and 1390	Asymmetric and symmetric stretch of carboxylate (COO ⁻)	(Coates 2000), (Smith 1999)
	1253	Symmetric stretching of C-O	(Na et al. 2014)
	1068	OH groups of citrate	(Na et al. 2014)
PEI-MNPs	3354	N-H stretching vibration of primary/secondary amine	(Coates 2000, Xu et al. 2011)
	3000-2800	asymmetric and symmetric C-H stretching vibrations	(Karimzadeh et al. 2017)
	1632	N-H bending vibration of secondary amine groups	(Coates 2000, Xu et al. 2011)
	1560	NH ₂ scissoring vibration	(Smith 1999)
	1470	C-H bending vibrations	(Khoobi et al. 2015)
	1059	C-N stretching vibration	(Smith 1999)

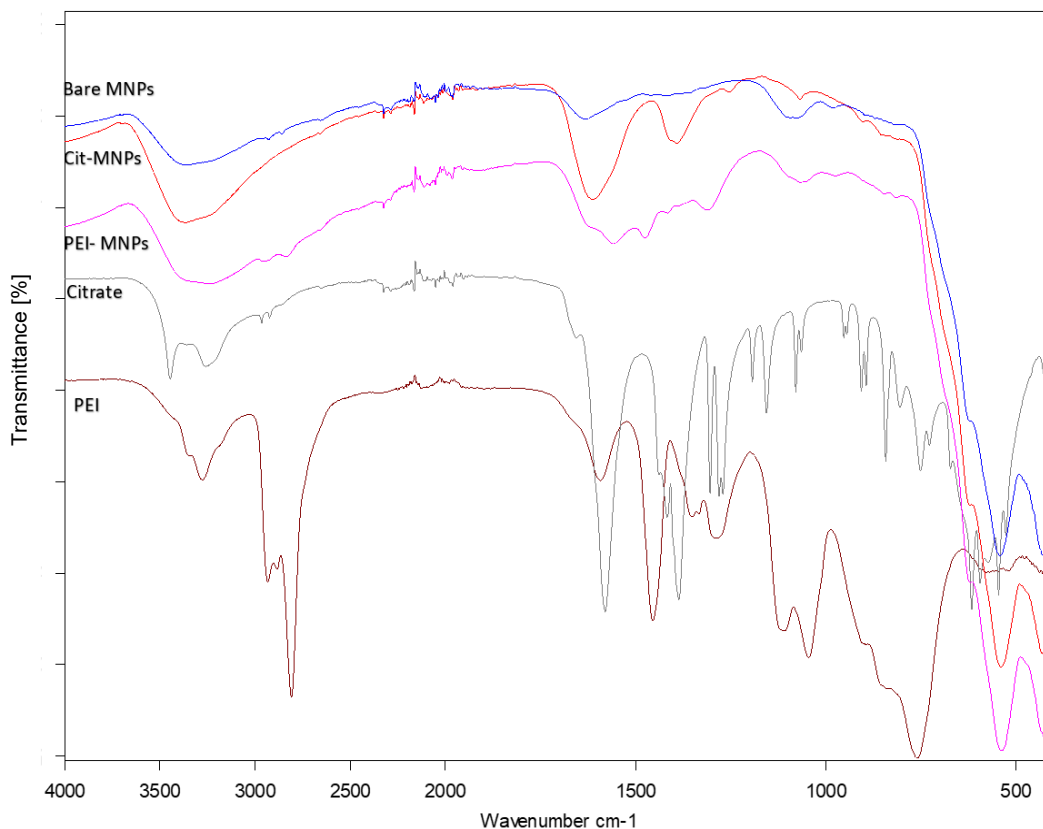


Figure 4-19. FTIR spectra of bare MNPs, Cit-MNPs, PEI-MNPs, pristine trisodium citrate and PEI

4.3.4.3 X-ray Fluorescence Analysis of MNPs

Bare MNPs and PEI-MNPs were analysed by XRF to check the bulk elemental composition. Bare MNPs were bought as a 99.5%, high purity product and the powder analysis results are represented in Table 4-4. Some contaminants were identified, and the values are given as a weight percentage. However, almost all the contaminants present in trace levels only.

Table 4-4. XRF analysis of as received bare MNPs and PEI-MNPs for bulk composition

Element	Cu	Fe	Si	Al	Ca	Cr	Mg	S	Mn	Co	Ni	Na ₂ O
Bare MNPs	0.015	65.45	0.03	0.02	0.03	0.13	0.1	0.017	0.33	0.005	0.041	0.05
PEI-MNPs	0.007	61.20	0.14	0.03	0.03	-	-	0.018	0.32	-	0.033	0.05

The values are given as a percentage.

4.3.5 Atom Probe Tomography Analysis of MNPs

Atom probe tomography (APT) was employed for the visualisation of the chemical arrangement of the adsorbent, in near atomic scale. APT is the chemically most sensitive and highest resolving probing technique used to characterise micro- and nanoscale materials down to a near atomic scale (Rusitzka et al. 2018). However, this technique does not seem popular

for the analysis of the surface coating and adsorption processes. There is a huge potential of using APT for the visualisation of surface functional groups and adsorbed metal complexes.

In APT, individual atoms, as ions, are progressively removed from a needle-shaped specimen by using pulsed field evaporation (Larson 2006). Thermal energy generated from the laser pulse initiates the removing (evaporation) of individual atoms from the tip of the specimen. Each atom is spatially, chemically and isotopically identified by a position-sensitive detector and precisely reconstructed three dimensionally.

Spatial reconstruction usually separates in to X and Y coordinates (lateral) and Z coordinate (depth). A reverse projection model is used to identify the original position of each ion on the specimen for each detector impact location in order to reconstruct the lateral coordinates. Depth location is primarily identified by the sequence of evaporation. Such analysis is possible over regions of interest (ROI) over 100s nm in size (Saxey et al. 2018). This type of information is indispensable for nanoscale materials.

For the chemical identification of each ion, the time-of-flight is converted in to mass-to-charge ratio during data processing. The results are usually displayed in a histogram, known as mass spectrum (Gault and Larson 2018). APT provides chemical identification of the evaporated atom by calculating the mass-to-charge ratio as given in equation (4-1).

$$\frac{m}{n} \approx 2eV \left(\frac{t_{flight}}{L} \right)^2 \quad (4-1)$$

where, m is the mass, n is the charge state, e is the elementary charge, V is the voltage at the time of evaporation, L is the distance from the tip to detector and t_{flight} is the time consumed to travel the distance L (McCarroll 2018).

The schematic representation of the basic arrangement of APT is shown in Figure 4-20. The specimen is progressively destroyed as the atoms leave the surface. The specimen temperature is usually maintained at 20-100K to reduce thermal diffusion of surface atoms prior to evaporation.

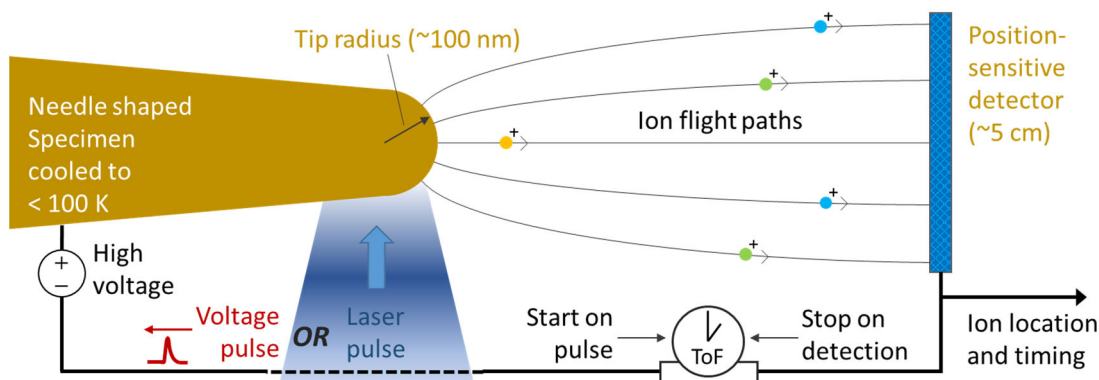


Figure 4-20. Schematic representation of APT. The diagram provided by Dr David Saxey, JDL Centre, Curtin University.

In this research, nanoparticles were embedded in a ZnO matrix to facilitate more controlled evaporation of individual atoms. This capping layer can protect nanoparticles from any potential damage during the FIB specimen preparation (Larson 2006). The overall atom map of the specimen is illustrated in Figure 4-21. In an atom map, the atomic positions of each element (mainly Fe, Zn, Au, Cu, S, C, N and H in this case) in the original needle specimen is represented as a point. The needle shaped specimen consist of a good layer of nanoparticles (shown in purple) which denotes the preciseness of the specimen preparation process. The ZnO matrix (shown in aqua colour) surrounds the nanoparticles.

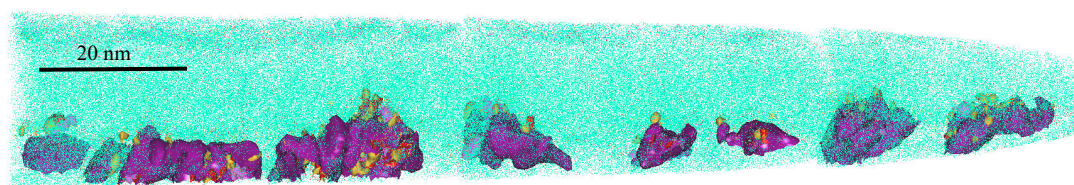


Figure 4-21. APT image of Au-PEI-MNPs arrangement in the needle specimen. The colours used are purple for Fe, turquoise for Zn, green for N, blue for C, golden yellow for Au and red for Cu.

The mass spectrum of the specimen is shown in Figure 4-22. A mass spectrum shows the mass-to-charge ratio of elements and is used to identify ions in the analysed specimen. Gold has a single isotope and is uniquely placed away from the other elements in the mass spectrum. Therefore, gold does not have any risk of overlapping with any other element considered in this study. In contrast, zinc, sulfur and oxygen peaks can overlap in the mass spectrum. Zinc has five isotopes in total (^{64}Zn , ^{66}Zn , ^{67}Zn , ^{68}Zn , ^{70}Zn), sulfur has four isotopes (^{32}S , ^{33}S , ^{34}S , ^{36}S) and oxygen has three isotopes (^{16}O , ^{17}O , ^{18}O), which demonstrate a good chance of overlapping.

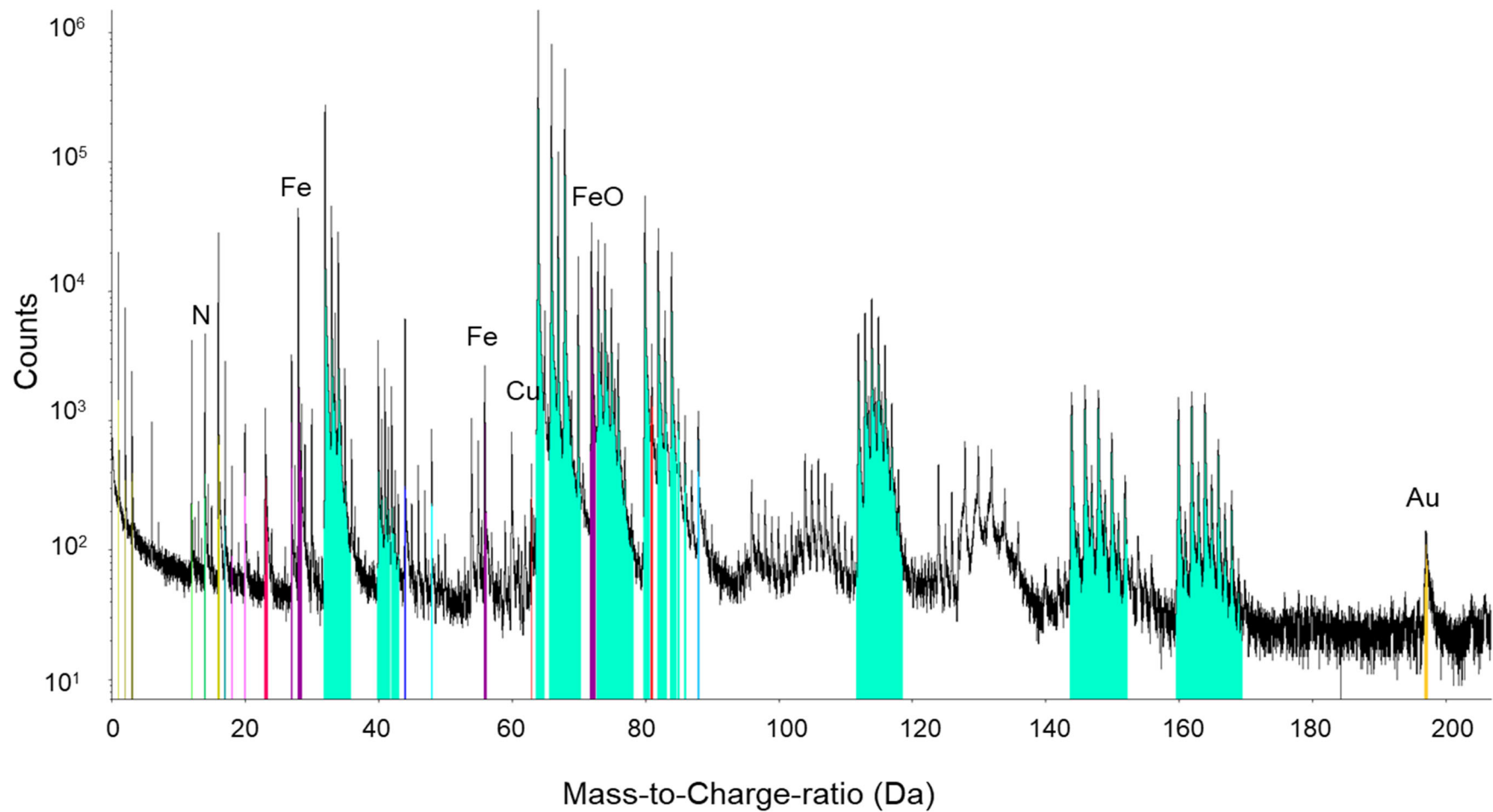


Figure 4-22. APT mass spectrum of Au-PEI-MNPs. The major peaks are labelled without their charge.

APT analyses were performed using three samples; before surface coating (bare MNPs), after surface coating (PEI-MNPs) and metal loaded MNPs (Au-PEI-MNPs). Surface coating was conducted in two steps; trisodium citrate coating using 10 g/L citrate coating at pH 6 and 90 °C followed by a PEI coating in 5 % PEI solution at pH 9.5 and 90 °C.

To investigate the success of the surface coating, bare MNPs and PEI-MNPs were analysed for their carbon and nitrogen atom arrangement on the iron oxide surfaces. The respective APT images are shown in Figure 4-23. The atoms related to the ZnO matrix were disregarded for clarity. The enhanced concentration of carbon (blue spots) and nitrogen (green spots) on the PEI-MNPs surface is apparent, compared to bare MNPs which are associated with the PEI coating on nanoparticle surfaces. Carbon and hydrogen could have been resulted from both primary citrate coating and secondary PEI coating. The individual atom maps of C, N and H are also included for a better understanding of the arrangement of surface coating layers.

The surface coverage of NPs by functional groups is illustrated in Figure 4-23e. According to the images, the full coverage of the MNP surface was achieved to a satisfactory level. The purple surface is the MNP surface and the blue surface is the coating layer. The generation of the surface coating layer was by considering the C, N and H atom distribution around the MNPs surface. The gap appears because there is a slight offset between the Fe distribution and the C, N and H distribution, which can be interpreted as being due to the PEI coating. However, the exact location of the two visualised surfaces depends on the concentration threshold level chosen to define each surface. For this visualisation, threshold values were chosen that tend to emphasise this difference, so that the layers might appear more separated for the purpose of ‘visualising’ the presence of the PEI coating. This is really a qualitative result and does not necessarily indicate the thickness of the coating. The proxigrams or 1D chemical profiles contain more quantitative information and are more appropriate for trying to gauge the size of a chemical distribution.

In contrast, there are some particles that were not fully covered with the surface coating, as shown in image c of Figure 4-24. There may be a few reasons for this. The presence of NP agglomerates and aggregates during the surface functionalisation can prevent individual particle coating. On the other hand, the PEI coating can be damaged or migrate at subsequent ultrasonic dispersion processes or during the encapsulation process (in a ZnO matrix) at high temperatures. Unfortunately, the exact reason cannot be ascertained with the existing data. Considering a lower temperature during the ZnO ALD layer coating would be worthwhile. However, the risk of formation of voids is higher at lower temperatures.

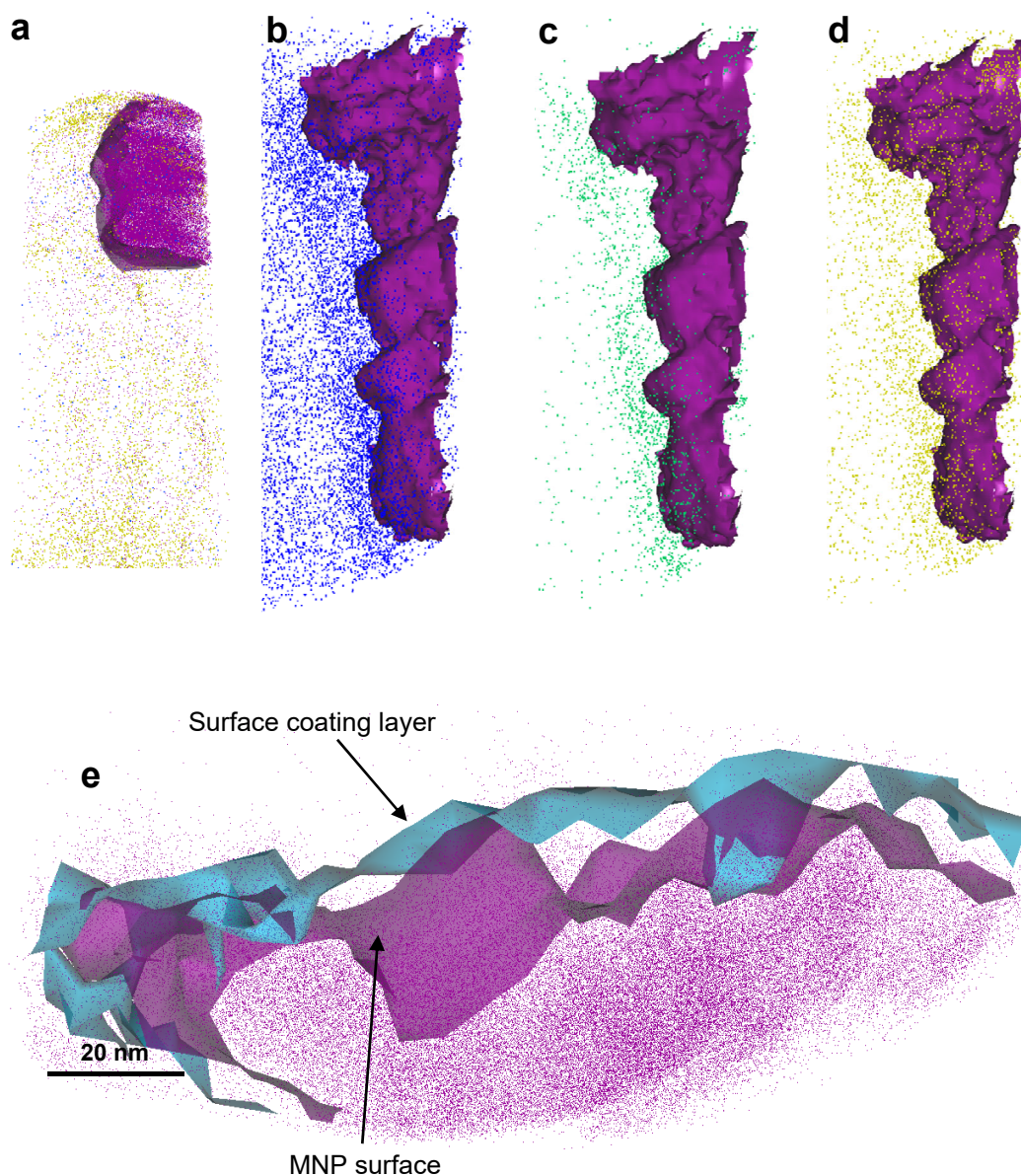


Figure 4-23. APT images of bare MNPs (a), the atom maps of PEI-MNPs showing: carbon distribution (b), nitrogen distribution (c) and hydrogen distribution (d) and surface coating layer (e). The colours used are purple for Fe, green for N, blue for C and olive for H. the PEI coating was performed at pH 9.5 and 90 °C.

The APT images of Au-PEI-MNPs are illustrated in Figure 4-24. All the images are from the same sample. Images a and b show the same cluster of nanoparticles from two different angles. The individual atom maps of N, Au, Cu and S are represented in images c, d, e and f, respectively. Successful gold adsorption is well demonstrated (as represented by golden yellow colour spots in the images a, b and d). Both monolayer and multilayer gold adsorption were observed in some areas in Figure 4-24d. Moreover, the copper and sulfur adsorption was also verified.

The atoms shown at a distance away from the nanoparticle surfaces appear as isolated atoms in the reconstruction. These isolated atoms are an expected result from the background noise in the mass spectrum. During the sample preparation, a ZnO ALD layer was coated at a temperature of 200 °C. As mentioned before, a migration of PEI coating or adsorbed metal ions is possible, but cannot be confirmed with the available data. A sulfur peak can easily overlap with zinc and oxygen signals in mass spectrum and can lead to misinterpretations.

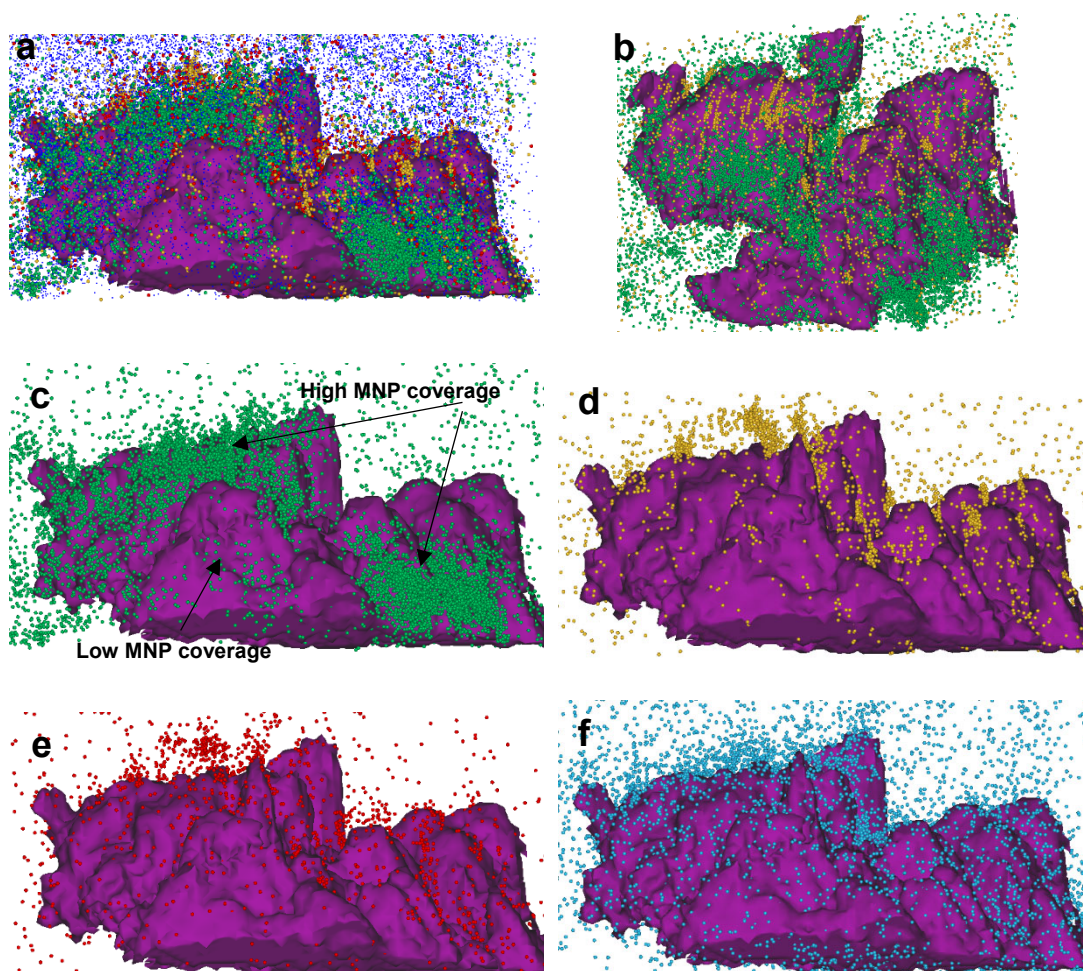


Figure 4-24. APT images of metal adsorbed PEI-MNPs (a and b) and atom map of nitrogen (c), gold (d), copper (e) and sulfur (f). The colours used are purple for Fe, green for N, blue for C, golden yellow for Au, red for Cu and light blue for S.

A chemical proximity histogram (also known as a proxygram) provides valuable information about atom distribution across an interface. The atomic concentration (as a percentage) of each element on either side of the interface can be calculated, as a function of distance from the interface. The proxygrams of bare MNPs and Au-PEI-MNPs are depicted in Figure 4-25 and Figure 4-26, respectively. The regions used to generate the proxygrams are shown in the insets.

In the proxygram of bare MNPs (Figure 4-25), the ‘zero’ distance location in the profile data corresponds to the NP surface boundary. Negative distances are outside the particle and the

distance increases positively as the profile moves in toward the centre of the particle. These bare MNPs were dispersed in trisodium citrate solution prior to being deposited on ZnO coated silicon wafers. Consequently, traces of dispersant media are also expected in the composition profiles. As shown in the proxygram, the particles mainly consisted of Fe and O. A high concentration of O outside the particle is possibly a result of the ZnO matrix. A small amount of Na and H was also found, probably from sodium citrate. The Na concentration inside the particle was due to particle contamination, as confirmed by the manufacturer and later confirmed by XRF analysis. A negligible amount of Mn, Ca and Mg was also detected (not shown in the proxygram).

Assuming that the bare MNPs consisting of both Fe_3O_4 and $\gamma\text{-Fe}_2\text{O}_3$, the O composition should be around 57% to 60%. However, as per the proxygram, the maximum value reached only up to 38.5% which is considerably lower than the calculated value. It is known that the oxygen counts in atom probe analysis of oxides do tend to be lower than the expected stoichiometry (Kinno et al. 2014, Santhanagopalan et al. 2015, Maier et al. 2016). It is also reported that the oxygen composition reduces when the magnetite is reduced to a smaller size. However, the crystal structure remains unchanged (Blaney 2007).

In Figure 4-26, the 'zero' location in the chemical profile is somewhere within the nanoparticles (not the particle surface interface as was on bare MNPs) and the distance increased from left-to-right in the selected interface. As displayed in the proxygram of Au-PEI-MNPs, the high concentration of C, N and H is obvious on the surface of iron oxide. At the same position, the Fe concentration starts to decline, as it is the iron oxide and PEI coating interface. Similarly Au and Cu concentrations are also higher at the NP surface in accordance with the N layer. The S signal inside the MNPs is questionable. It is assumed that this is due to the overlap with O in mass spectrum.

From the APT analysis results illustrated in Figure 4-23 to Figure 4-26, the surface functional group attachment and successful gold adsorption were confirmed. The reconstructed images provided a better understanding of the atomic arrangement of different elements. The conclusions derived from this technique are compatible with the other characterisation techniques. Despite the possible overlaps in mass spectrum, the APT technique provided valuable information on the surface coating and gold adsorption onto MNPs.

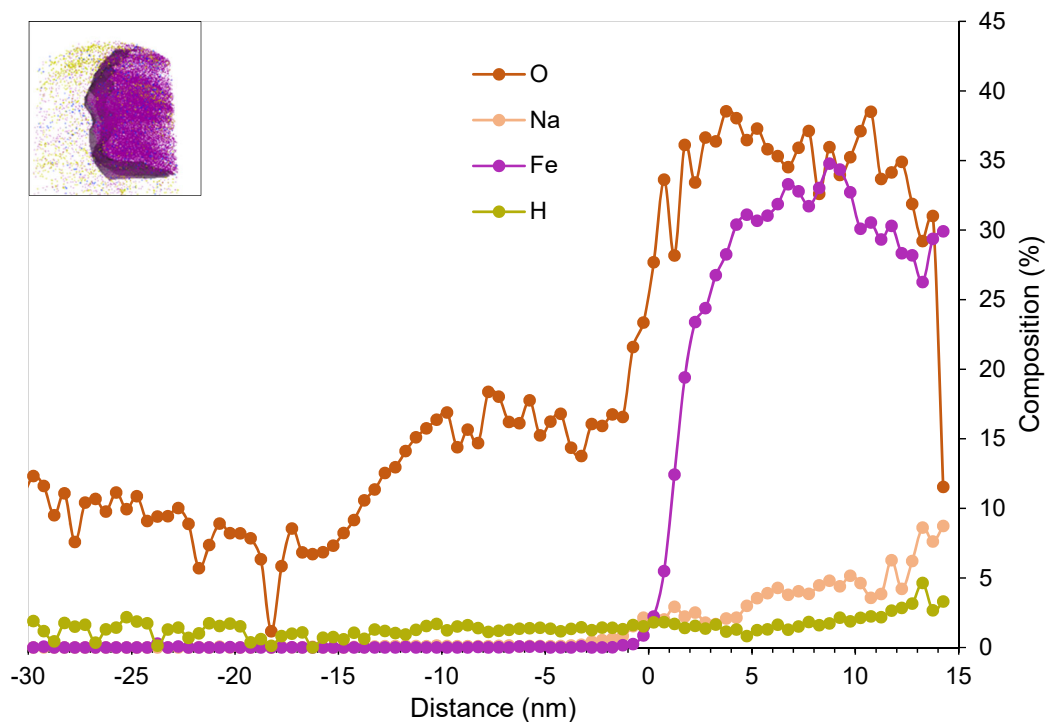


Figure 4-25. Composition profile of bare MNPs in the form of a proximity histogram

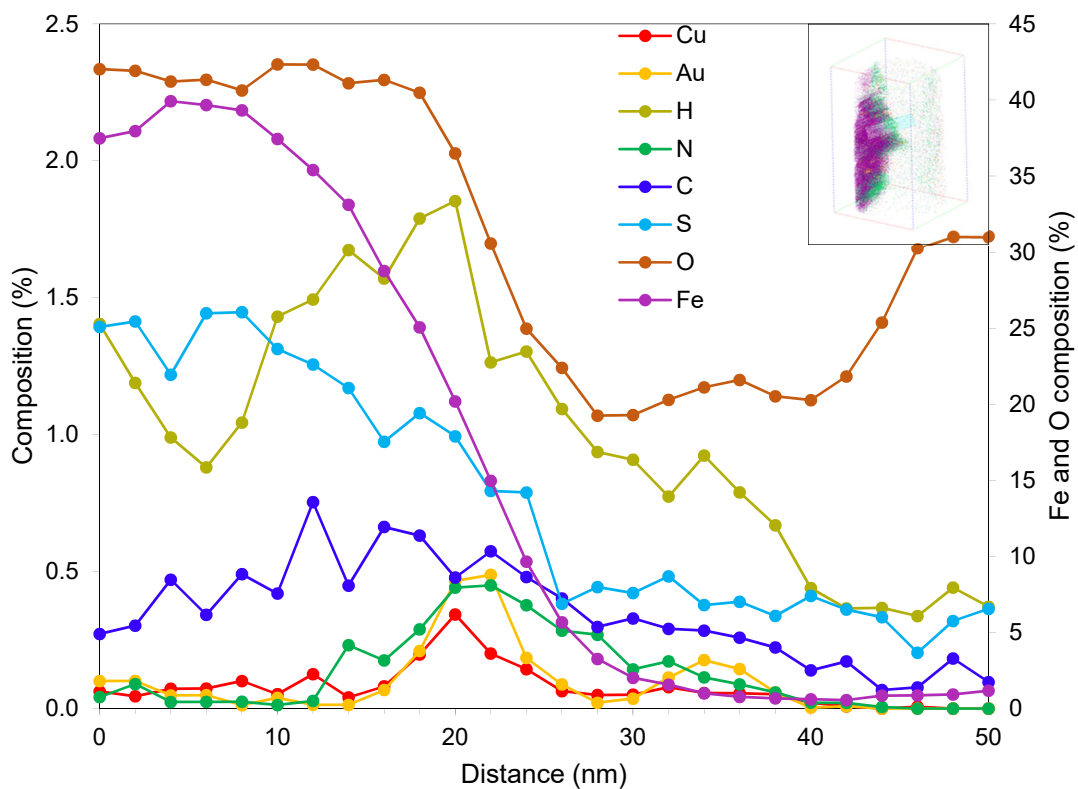


Figure 4-26. Composition profile of Au-PEI-MNPs in the form of a proximity histogram

4.3.6 Magnetic Properties

Saturation magnetisation and zero field cool and field cool (ZFC/FC) measurements were conducted for bare MNPs, PEI-MNPs and Au-PEI-MNPs using SQUID. Saturation magnetisation measurements provide variation in magnetisation at different applied fields (M in emu/g vs H in kOe). The measurements were taken at a temperature of 300K and the results are illustrated in Figure 4-27. The hysteresis loops of both samples show zero coercivity which confirms the superparamagnetic nature of the nanopowder. A slight drop in saturation magnetisation was observed after surface coating, which is expected. The saturation magnetisation was 60.5 emu/g and 52.3 emu/g for bare MNPs and PEI-MNPs respectively. As reported in the literature, a slight drop is typical for PEI coated MNPs. The Au-PEI-MNPs show a saturation magnetisation value of 50.5 emu/g, which still enables successful magnetic separation. A further drop could be due to the adsorption of different adsorbate species to the MNP surface.

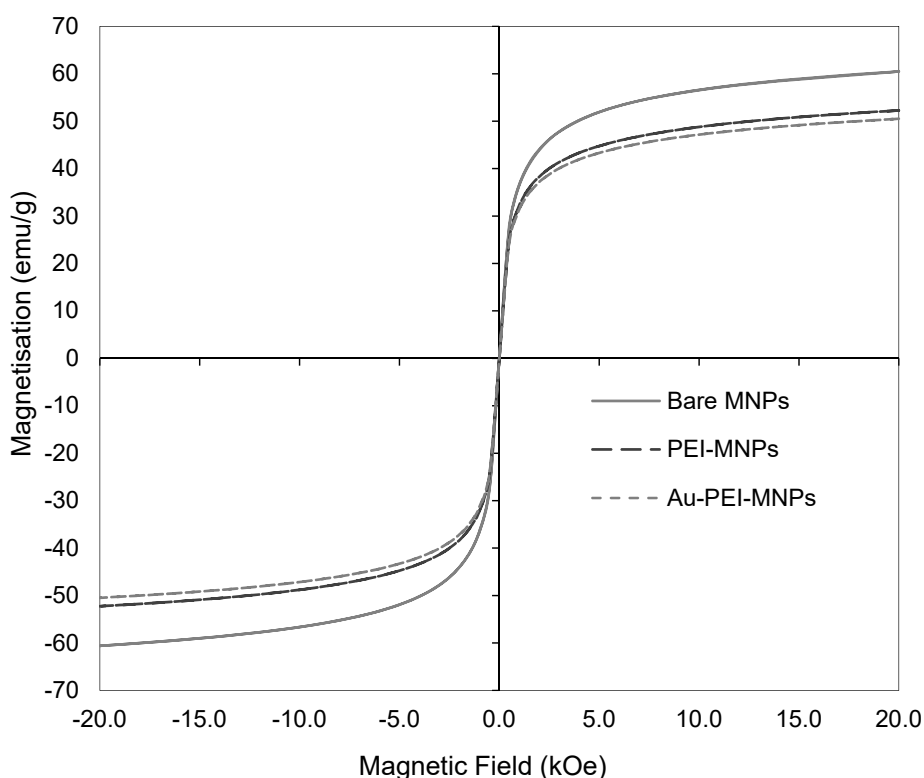


Figure 4-27. Field dependent magnetisation measurements at a temperature of 300K

The temperature dependence of the nanoparticles (before and after PEI coating) was also analysed and the results are shown in Figure 4-28. The ZFC measurements were carried out by first cooling down the sample to 5 K without any applied field. Once stabilised, the sample was heated to 300 K in the presence of an applied field of 100 Oe where the measurements

were recorded. For FC measurements, the sample was cooled down to 5 K with an applied magnetic field of 100 Oe and warmed back to 300K. These measurements are important for the determination of blocking temperatures (T_B) of the particles. Below the blocking temperature, anisotropy energy dominates over thermal energy (Upadhyay et al. 2016). Once the temperature reaches blocking temperature, the spin alignment is disrupted by thermal energy (Boyer et al. 2010). Above T_B the particles demonstrate superparamagnetic behaviour (Tanwar et al. 2012). Normally the blocking temperature is determined by the temperature at the inflection point of the curve or the temperature at maximum magnetisation in the ZFC curve. Above T_B the magnetisation decreases as the temperature increases following the Curie-Weiss behaviour. However the accurate determination of T_B in polydispersed nanoparticle samples is not straightforward, due to the broad peak (Bruvera et al. 2015).

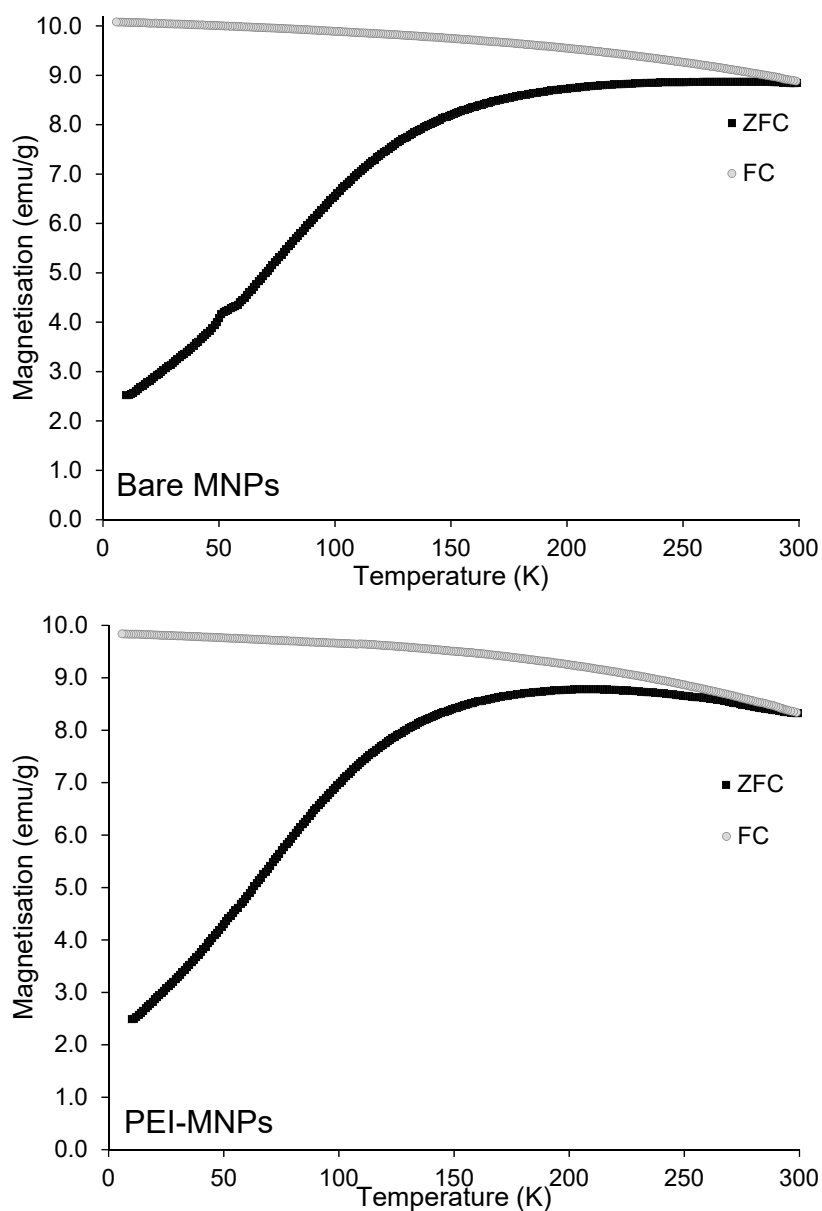


Figure 4-28. Temperature dependent magnetisation of bare MNPs and PEI-MNPs

It was observed that both samples exhibit blocking temperatures above 200K. For bare MNPs the broad peak of the ZFC curve lies at approximately 240-293 K. Above 293 K, magnetisation starts to drop slightly until the maximum temperature of 300K. The broad peak and flattened shape of the peak of bare MNPs may be due to the strong interaction of iron oxide MNPs and anisotropic distribution which is a result of broad size distribution. In the case of PEI-MNPs, maximum magnetisation was observed at 202-214 K which designates the blocking temperature within this region. The reduced T_B value after PEI coating is more of an indicator of the less agglomerated behaviour of the particles than that of bare MNPs (Arsalani et al. 2019).

4.3.7 Thermogravimetric Analysis

Bare MNPs and PEI-MNPs were exposed to heat (up to 850 °C) under a nitrogen gas atmosphere to estimate the composition of functional moieties in the nanosorbent through weight reduction with increasing temperature. The weight loss (TGA analysis) and temperature difference (DSC analysis) results of bare MNPs and PEI-MNPs are presented in Figure 4-29 and Figure 4-30, respectively. A typical three step weight loss was observed in PEI-MNPs. Approximately a 3% of weight reduction at around 57 °C may be due to the loss of water molecules bound to NP surfaces while the weight losses at 200 - 400 °C and again 475 - 625 °C were assigned to decomposition of PEI and citrate. It is reported that low molecular weight PEI starts to decompose at 250 °C in air and at 300 °C in an inert atmosphere. Ammonia, ethylamine and pyrrole and C-substituted ethylpyrroles were the thermal degradation products (Nedel'ko et al. 1975). The total weight loss of bare MNPs and PEI-MNPs at 850 °C was 9% and 19%, respectively, which endorsed the composition of attached functional groups in the adsorbent as approximately 10%.

The final product was a black powder which may have been wustite ($Fe_{1-x}O$, where x ranging from 0.83 to 0.95), which forms under most reducing conditions. Bearing in mind that the nanopowder used in this study is a mixture of magnetite and maghemite (with <1% of hematite), under reducing conditions, maghemite and hematite may first reduce to magnetite with the increase in the temperature and ultimately to wustite and ferrite (Parkinson 2016).

In the DSC curves, strong endothermic peaks observed at approximately 45-52 °C can be assigned to the elimination of water molecules attached to the particle surfaces. The exothermic peak observed at 284.8 C was due to the phase transformation from Fe_2O_3 to Fe_3O_4

(Zhang et al. 2013b). Extra peaks attained in the DSC curve of the PEI-MNPs may be attributed to the changes in the functional groups.

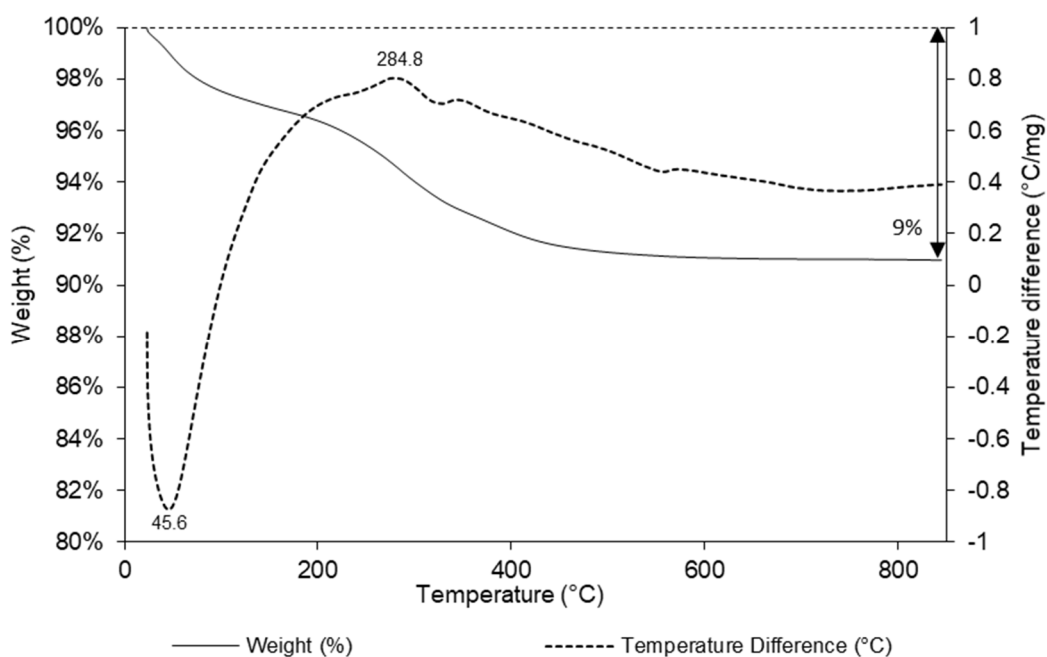


Figure 4-29. TGA and DSC curves of bare MNPs

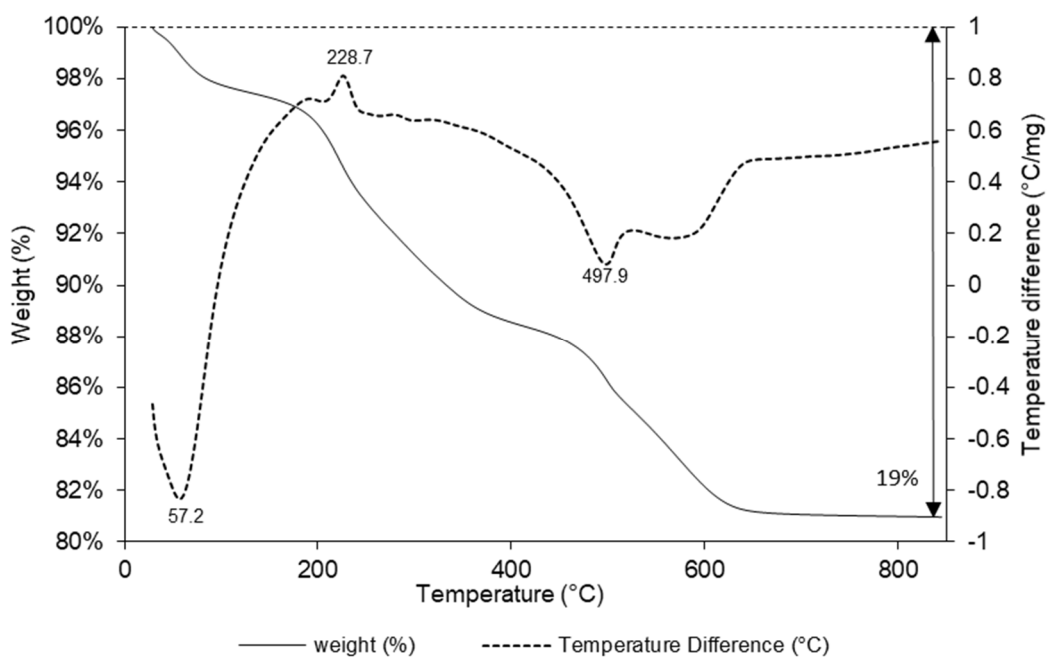


Figure 4-30. TGA and DSC curves of PEI-MNPs

4.4 Deagglomeration of MNPs by Ultrasonic Dispersion

Ultrasonic dispersion of MNPs was carried out using an ultrasonic probe. Nearly half of the ultrasonic probe was immersed in the solution. DI water and 10 g/L trisodium citrate solutions were used as the dispersants for bare MNPs, where the pH of the both solutions were adjusted to pH 9.5. In general, at zeta potential values above 30 mV, the suspensions are known to be most stable (Ding and Pacek 2008). According to zeta potential measurements, bare MNPs hold a -30 mV surface charge at pH 9.5 and hence the same pH was chosen for the dispersion. Likewise DI water and commercially available surfactant solutions at pH 7 were used as dispersion media for PEI-MNPs as the zeta potential was well above 30 mV. The ultrasonication settings were 100W power, 60% amplitude (approximately equivalent to 54 μm) and “continuous” operating mode. The NP concentration and sonication time were varied from 1-10 g/L and 30-600 S, respectively.

4.4.1 Dispersion of Bare MNPs in DI Water

The size distribution data revealed that in DI water, nanoparticles do not reach their single particle diameter even after 600 s ultrasonication. All the size measurements were in micrometre size range, as illustrated in Figure 4-31. According to Shaw (2014), the hydrodynamic size depends not only on the size of the particle core, but also the type and surface structure of the particle, and ionic strength of the solution. Furthermore, it is mentioned that to introduce a sufficient surface electric potential, the pH adjustment of the medium alone is insufficient and the addition of an electrolyte with dissociation properties is essential (Kamiya 2012).

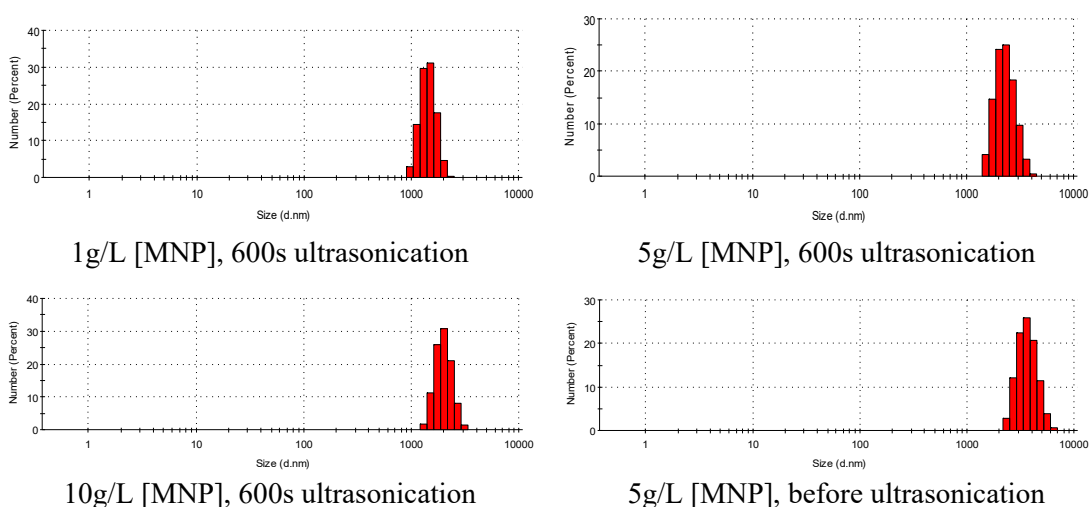


Figure 4-31. Hydrodynamic size distribution of nanoparticles dispersed in DI water at pH 9.5

4.4.2 Dispersion of Bare MNPs in Citrate Solutions

The duration of ultrasonication apparently influenced the hydrodynamic size of the NPs. Irrespective of the concentration of NPs, lower hydrodynamic sizes were observed at longer ultrasonication durations. For the same duration of ultrasonication, a 5g/L NP concentration yielded slightly smaller hydrodynamic size (Z-average) than 1 g/L NP concentration, which implies that better deagglomeration was probably due to increased interparticle collision (Taurozzi et al. 2011). As it stands, the concentration of NPs in the dispersion did not seem to be a major factor for the tested range. The number based hydrodynamic size distribution of NPs for different concentrations and durations are illustrated in Figure 4-32.

The variation of hydrodynamic sizes in two media (DI water and citrate solution) is attributed to the ionic strength difference and the surface charge of NPs. The higher ionic strength in the citrate solutions may compress the electric double layer, and hence the measured hydrodynamic size is lower. Moreover, in citrate solutions the citrate molecules bind to the NP surface under ultrasonication and this imparts a strong negative charge to the particle surfaces which prevents their agglomeration.

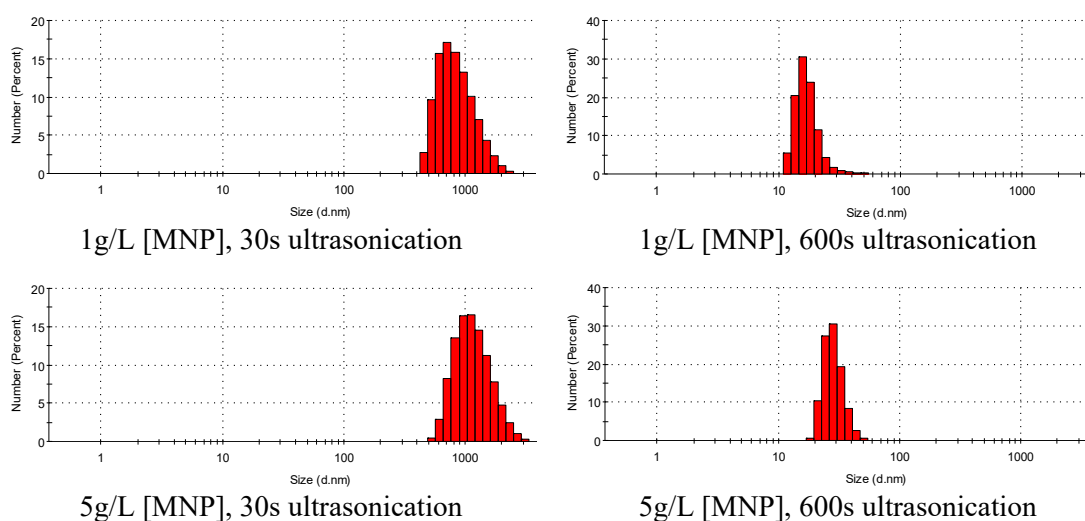


Figure 4-32. Hydrodynamic size distribution of bare MNPs dispersed in trisodium citrate solutions at pH 9.5

4.4.3 Dispersion of PEI-MNPs in Surfactant Solution

The hydrodynamic size distribution of PEI coated MNPs was also measured. First, PEI-MNPs in dry powder form were ultrasonically dispersed in commercially available surfactant solutions at a pH of 7.5 for different durations of ultrasonication. According to the size

distributions represented in Figure 4-33, a longer exposure to ultrasonic dispersion resulted in a smaller hydrodynamic size and a narrower size distribution.

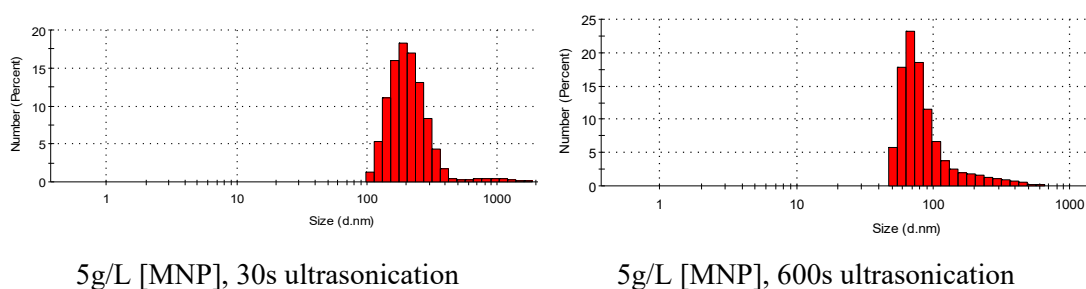


Figure 4-33. Hydrodynamic size distribution of PEI-MNPs dispersed in commercial surfactant at pH 7

4.4.4 Dispersion of PEI-MNPs in DI Water

Ultrasonic dispersion of PEI-MNPs in a DI water matrix was also attempted in order to compare with other media. The size distributions are represented in Figure 4-34. The size reduced to a certain extent when increasing the ultrasonic time. However, the resultant average hydrodynamic sizes were lower than the comparative sizes in surfactant solutions in shorter ultrasonic durations (30 S and 300 S) and almost identical after 600 S. The dispersion media does not seem to be a major factor for PEI-MNPs, as surface functional groups and mechanical forces predominate more so than the solution properties for deagglomeration. The size distributions after 300 s were not shown here.

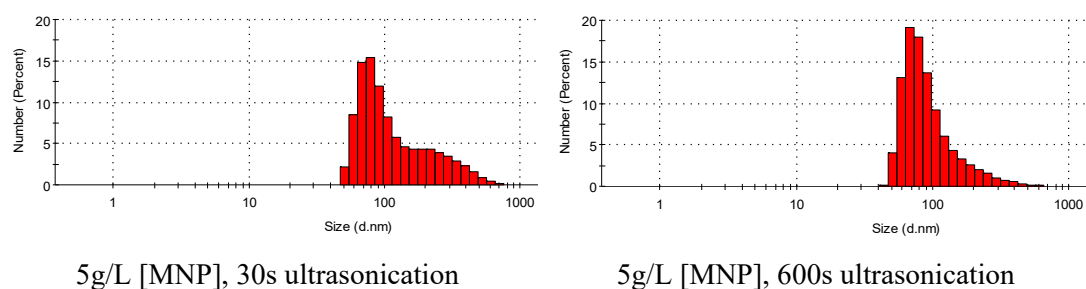


Figure 4-34. Hydrodynamic size distribution of PEI-MNPs dispersed in DI water at pH 7

The summary of the measurements in both media is listed in Table 4-5. Longer ultrasonication times resulted in a considerable reduction of hydrodynamic size in PEI-MNPs. This trend was applicable for both DI water and surfactant solutions.

It is worth discussing the discrepancy in the hydrodynamic sizes of PEI-MNPs mentioned in Section 4.3.1.2, where the particles were not subjected to a drying process and throughout the

process they were in aqueous suspension form. On the contrary, for ultrasonic dispersion trials in Section 4.4, all the nanoparticle samples came initially in dry powder form which was then added to the solutions for dispersion. For instance, the hydrodynamic size of dry PEI-MNPs ultrasonically dispersed in DI water for 600s and wet NPs just after surface functionalisation and washing (before drying) were 203.7 nm and 174.3 nm, respectively. This indicates the advantage of using wet NPs for adsorption. However, due to practical difficulties in precise sample weight measurements, PEI-MNPs were oven dried in this study.

Table 4-5. Summary of hydrodynamic sizes of PEI-MNPs in different media

Sample description	Intensity weighted Z-Ave (nm)	PdI	Mean diameter (nm)		
			peak 1	Peak 2	Peak 3
PEI-MNPs, surfactant, 30S	554.8	0.813	1194	234.7	5150
PEI-MNPs, surfactant, 300S	263.1	0.409	254.4	2956	0
PEI-MNPs, surfactant, 600S	209.7	0.335	290.1	4904	0
PEI-MNPs, DI water, 30S	325.5	0.432	356.4	4586	0
PEI-MNPs, DI water, 300S	295.5	0.473	319.8	3004	0
PEI-MNPs, DI water, 600S	203.7	0.361	406.5	4515	0

4.5 pH Dependent Dissolution of MNPs

The dissolution behaviour of MNPs before and after coating was examined by exposing the particles to aqueous solutions across a wide range of pH levels (pH 2 to 12) for 3 hours followed by solution analysis for Fe ion concentrations. As illustrated in Table 4-6, approximately 21.4 % of Fe leaching was observed as a result of dissolving bare MNPs in a pH 2 solution. When iron oxide is exposed to strong acidic conditions, it reacts to form Fe^{2+} and Fe^{3+} ions. These reactions are effective only at low pH levels. However, the corresponding Fe leaching from PEI-MNPs was only 5.4%, which exhibited the protection of the magnetic core by the surface coating. A slight amount of Fe leaching was observed in pH 3, 10, 11 and 12 solutions from bare MNPs, while PEI coated MNPs were resistant to dissolution within this range. Therefore, it is apparent that the surface coating was able to provide a protection for the magnetic core in terms of covering it.

Table 4-6. Nanoparticle dissolution in acidic and alkaline solutions before and after coating

pH	2	3	5	7	9	10	11	12
Fe leaching (PEI-MNPs), %	5.4	0.0	0.0	0.0	0.0	0.0	0.0	0.1
Fe leaching (Bare MNPs), %	21.4	0.3	0.0	0.0	0.0	0.9	1.9	0.4

The evaluation of the dissolution behaviour of PEI-MNPs in highly alkaline solutions is important, as gold elution is conducted in pH 12 solutions, as will be discussed in Section 6.4. Interestingly, Fe leaching is insignificant in PEI-MNPs at pH 12. To verify that the extreme pH does not impair the surface coating, PEI-MNPs used in the pH 2 and pH 12 solutions above were used for metal adsorption afterwards. Any change in the adsorption efficiency was not perceived, which indicates the excellent resistance of PEI-MNPs to highly acidic and alkaline conditions.

4.6 Chapter Summary

The surface functionalisation of iron oxide MNPs using citrate groups and PEI proved to be successful. The simple and relatively fast one-pot coating method resulted in well-dispersed PEI-MNPs. Nanoparticle deagglomeration prior to surface coating is an important aspect to consider. The ultrasonic dispersion method was able to produce an adequately deagglomerated nanoparticle suspension. The characterisation of bare MNPs revealed that the nanopowder is a mixture of iron oxide, predominantly containing magnetite and maghemite. Successful surface functionalisation with citrate groups and PEI was verified by various characterisation technologies. XPS and APT analysis revealed the adsorption of gold and some other species, such as copper and sulfur, onto PEI-MNPs.

The characterisation data provided indispensable information in deriving the mechanism of gold adsorption. According to the XPS analysis, gold predominantly exists in the Au(I) state on the surfaces of PEI-MNPs. This confirms that the gold exists as its thiosulfate complex rather than being reduced to metallic form. Any evidence of a redox reaction occurring could not be found. APT analysis results demonstrated the successful adsorption of gold, both monolayer and multilayer. In the reconstructed APT images, on the majority of occasions, gold atoms held together with sulfur atoms, which is indicative of gold adsorption as its respective thiosulfate complex. However, the existence of gold as gold clusters in some areas also cannot be ruled out.

It is evident that the characterisation of nanoparticles is challenging and complicated due to their size, agglomeration behaviour and magnetic properties. Thus, trying several characterisation methods and linking the results from each method is essential for obtaining a self-consistent picture of the material. Nanoparticles can undergo severe structural or phase changes instantly, during the characterisation stage or even during the sample preparation stage. As an example, the Raman spectrum of nanopowder samples dramatically changed at different laser powers as a result of laser-induced in-situ oxidation. This hinders the obtaining of actual information on the original material. Likewise, particle agglomeration can occur during the TEM sample preparation, especially during the drying stage, which can easily lead to misinterpretation. In the APT sample preparation, the encapsulation of MNPs in ZnO matrix was performed at a temperature of 200 °C, and this can change the original state of the surface coating and the adsorbed species.

The use of an electron beam in SEM and TEM analysis can also influence the shape and structure of nanoparticles. Obtaining a clear image with a TEM was harder due to the charge build up on the specimen. In a similar manner, x-rays also can cause damage to the original sample specimen. During the XPS analysis, longer times of exposure to x-rays were needed to obtain high resolution spectra of the elements of interest. This can alter evidence of the specimen's history and the properties of the surface coating.

Chapter 5 Gold Adsorption by Polyethylenimine Coated Magnetic Nanoparticles

5.1 Introduction and Chapter Objectives

This chapter consists of the results and the discussion of the adsorption experiments conducted using synthetic leaching solutions and pure gold thiosulfate solutions. The effects of different parameters and conditions are discussed with regard to gold adsorption efficiency in synthetic leaching solutions. Examples of some of these are: concentrations of lixiviant and other reagents, adsorbent dosage, solution pH, solution temperature and adsorption time. Most importantly, adsorption isotherms and adsorption kinetics modelling parameters are also presented. The adsorption mechanism was revealed through a thermodynamic approach.

The adsorption experiments were mainly conducted using the solutions simulating calcium thiosulfate - air leaching system. The adsorption efficiency of this adsorbent in different thiosulfate leaching systems other than calcium thiosulfate – air system is briefly mentioned, but not investigated in depth.

5.2 Gold Adsorption

Gold adsorption from synthetic leaching solutions of calcium thiosulfate – air system was carried out. These solutions consisted of calcium thiosulfate and gold thiosulfate with and without copper. In addition, gold adsorption efficiency in pure gold thiosulfate solutions, in the absence of competitive adsorbates, was also investigated. The solutions were prepared by dissolving sodium aurothiosulfate (I) powder in deionised water. pH adjustments were carried out using diluted NaOH and H₂SO₄ acid solutions, wherever required.

The composition of 0.1 M calcium thiosulfate, 10 mg/L gold thiosulfate and 20 mg/L copper sulfate solution is schematically represented in Figure 5-1. Only the elements of interest were considered and sodium was omitted, although approximately 6 mg/L could be available as a result of pH adjustment using NaOH and the balance amount from the sodium aurothiosulfate ($Na_3Au(S_2O_3)_2$) complex. Almost 99.7% was held by calcium and sulfur while the gold concentration was only as small as 0.1% (weight basis) and 0.2 % of copper. Therefore the competitive adsorption of these species is expected. The sulfur contribution from

$Na_3Au(S_2O_3)_2$ and $CuSO_4$ was negligible. However, it was added to the total sulfur in the graph. Selective adsorption of gold in such a trace level is expected to be challenging.

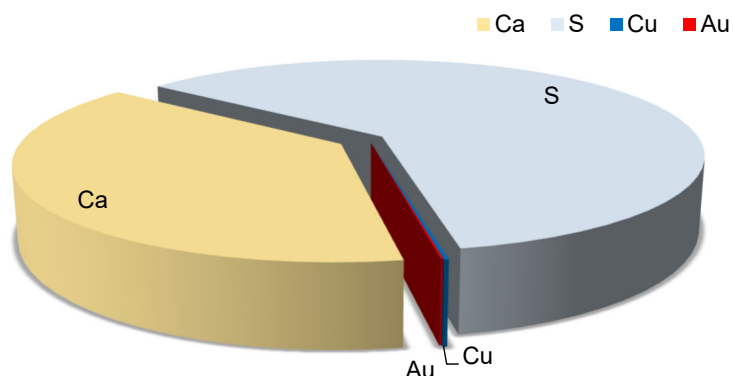


Figure 5-1. Composition of Au, Cu, S and Ca as a percentage (weight basis) in synthetic leaching solution consists of 0.1 M calcium thiosulfate, 10 mg/L gold thiosulfate and 20 mg/L copper sulfate.

5.2.1 Effect of Nanoparticle Dosage

The influence of adsorbent concentration on gold adsorption was evaluated and the results are presented in Figure 5-2. The test solution consisted of approximately 0.1 M thiosulfate, 10 mg/L gold and 20 mg/L copper. Once the pH was adjusted to 8 and the solutions reached a temperature of 50 °C, nanoparticles were added, equivalent to 5, 10, 20, 50 and 75 g/L. An increase in adsorbent dosage led to a significant increase in gold adsorption. The availability of more adsorption sites and hence less competitiveness may be the reason for higher gold adsorption. The next experiments were conducted at 5 g/L and 20 g/L PEI-MNPs dosages to compare the performance at two different PEI-MNPs concentrations.

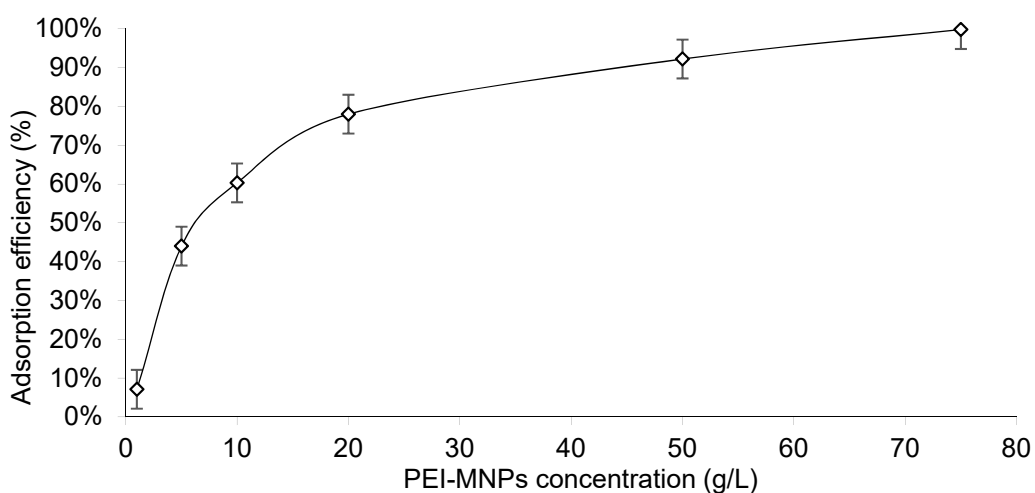


Figure 5-2. Effect of magnetic nanoparticle dosage on gold adsorption. The solution consists of 0.1 M thiosulfate, 20 mg/L copper, approximately 10 mg/L gold at pH 8, 50°C after one hour adsorption time.

5.2.2 Effect of Solution pH

The influence of the initial solution pH was evaluated in solutions consisting of 0.1 M thiosulfate, 10 mg/L gold, 20 mg/L copper, and 5 g/L adsorbent dosage at 50 °C. The pH of the solution did not show a considerable effect on the final metal loading onto PEI-MNPs in the tested pH range, as indicated in Figure 5-3. An initial solution pH range of 5 to 8.8 was selected. The adsorption efficiency would have been different outside this range, but was not practical to check, as pH values greater than 8.8 rendered the solution unstable and precipitation was evident due to the instability of copper (I) thiosulfate at a high pH, and copper precipitates as copper hydroxide at a high pH. On the other hand, thiosulfate is unstable in acidic pH solutions.

Gold adsorption efficiency at different pH solutions can depend on two aspects; the behaviour of the adsorbent and the adsorbate. With respect to the adsorbent, the zeta potential analysis results showed that the adsorbent surface charge is positive throughout the tested pH range (5 to 8.8) and this may be the reason for a similar degree of adsorption at every pH value tested. With regard to the adsorbate, gold speciation can vary with the solution pH. According to published data on gold speciation, gold (I) thiosulfate complex is the most stable form within the tested pH range (Aylmore and Muir 2001) which also supports the observed outcome.

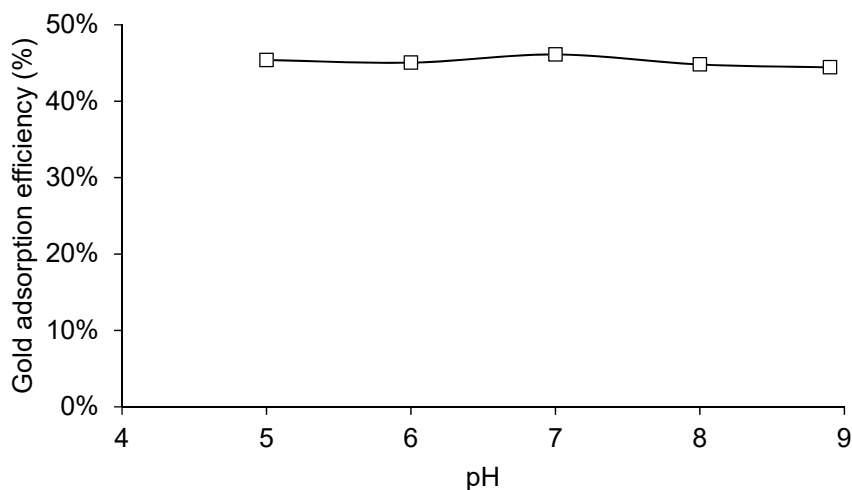
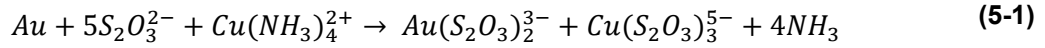


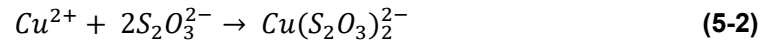
Figure 5-3. Effect of initial solution pH on gold adsorption after one hour in solutions consisted of 0.1 M thiosulfate, 20 mg/L copper, approximately 10 mg/L gold and 5 g/L PEI-MNPs at 50°C

5.2.3 Effect of Copper Concentration

In an ammoniacal thiosulfate system, copper acts as an oxidant and as a catalyst in the gold oxidation half reaction, as indicated in equation (5-1).



In a non-ammoniacal CaS_2O_3 –air leaching system, in the absence of ammonia, the role of copper is not yet well understood (Zhang and Nicol 2005, Zhang et al. 2013a). It is suggested that copper (in cuprous and cupric states) can exist as various copper-thiosulfate complexes, depending on the copper and thiosulfate concentrations and other solution parameters like the pH and which additives are available. $Cu(S_2O_3)_3^{5-}$ and $Cu(S_2O_3)_2^{2-}$ have been identified as the predominant species at pH 8 and at a 0.1 M thiosulfate concentration. Copper exists as Cu(I) and Cu(II) in the former and latter complexes mentioned above, respectively. In thiosulfate deficient solutions, copper can precipitate as CuS or Cu_2S (Senanayake 2005b). $Cu(S_2O_3)_2^{2-}$ complex is assumed to be the main contributor to thiosulfate degradation, as presented in equations (5-2) and (5-3).



To this end, gold adsorption behaviour was investigated at different initial copper concentrations ranging from 0 to 120 mg/L and the results are illustrated in Figure 5-4. The solution consisted of 0.1 M free thiosulfate as CaS_2O_3 and approximately 10 mg/L gold. Adsorption was conducted for one hour at 5 and 20 g/L PEI-MNPs dosages in pH 8 solutions.

When a 5 g/L PEI-MNPs dosage was used, the increase in copper concentration in the solution resulted in a slightly lower gold loading. At a copper concentration greater than 42 mg/L, gold adsorption efficiency started to drop slightly for the tested range. PEI shows a good affinity towards copper (Xu et al. 2015). Therefore copper can competitively adsorb onto PEI-MNPs reducing the gold adsorption. However, at a 20 g/L adsorbent dosage, the copper concentration did not seem to be a significant factor influencing the gold adsorption. An increase in copper concentration did not show any considerable effect on gold adsorption efficiency. The availability of ample adsorption sites may be the reason.

A linear regression model fitted to the data with the initial copper concentration and the time as a binary indicator or dummy variable indicated that neither the initial copper concentration, nor the time had a significant effect on gold adsorption at a 95% confidence level as illustrated in Figure 5-5.

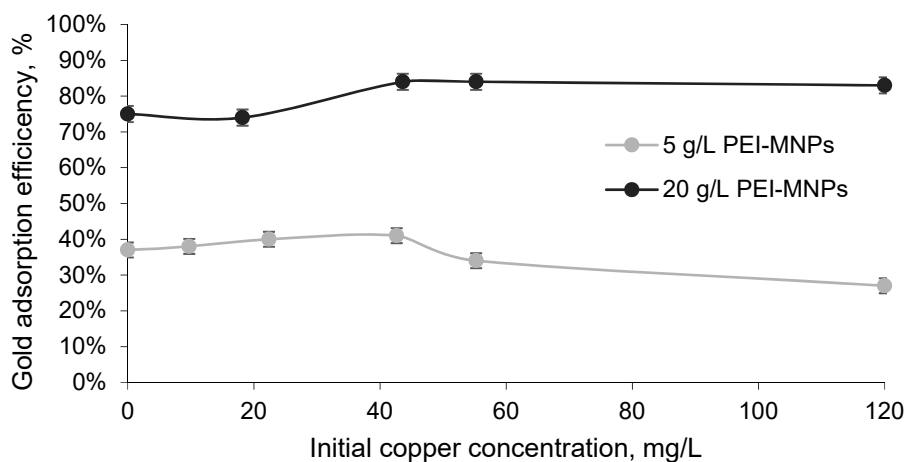


Figure 5-4. Effect of initial Copper concentration on gold adsorption efficiency after one hour with 0.1 M thiosulfate, 0-120 mg/L Cu, 10 mg/L Au at pH 8 and 50 °C

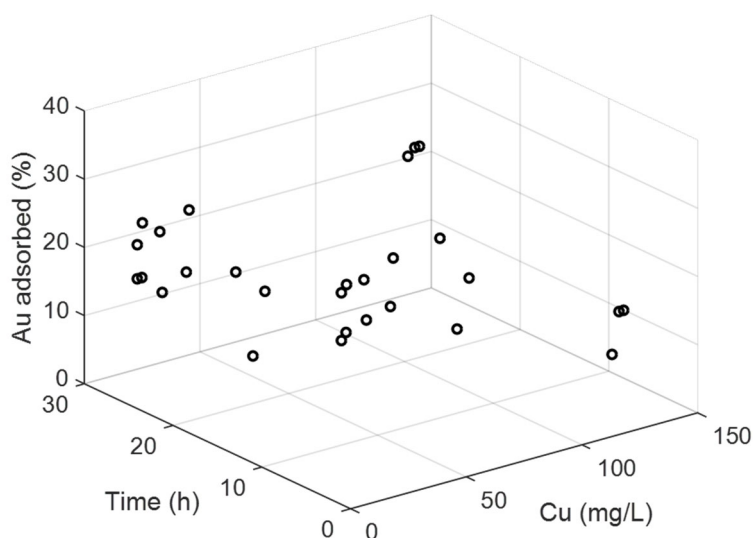


Figure 5-5. Effect of initial copper concentration and time on gold adsorption

5.2.4 Effect of Thiosulfate Concentration

Gold loading on to PEI-MNPs was investigated by varying the initial free thiosulfate concentration from 0 to 0.2 M. Gold was added as gold thiosulfate complex and thiosulfate as calcium thiosulfate liquid. It is evident from the results given in Figure 5-6 that the thiosulfate concentration is a significant factor which influences gold loading. The gold loading onto PEI-MNPs is significantly reduced by increasing the free thiosulfate concentration in the system. The reduced gold loading can possibly be due to competitive adsorption of thiosulfate onto the MNPs. This would obstruct the available adsorption sites for gold. Moreover, increased polythionate concentrations formed by oxidising thiosulfate would also compete for

adsorption sites on the MNPs, similar to the behaviour observed with IX resins (Daenzer et al. 2016) and activated carbon (Sitando et al. 2019). The adsorption of sulfur species were confirmed by atom probe tomography analysis discussed in Section 4.3.5. The use of a higher adsorbent dosage was beneficial to the adsorption of gold. Further insights gained into the system based on ion speciation analysis are discussed in Section 5.3.1.

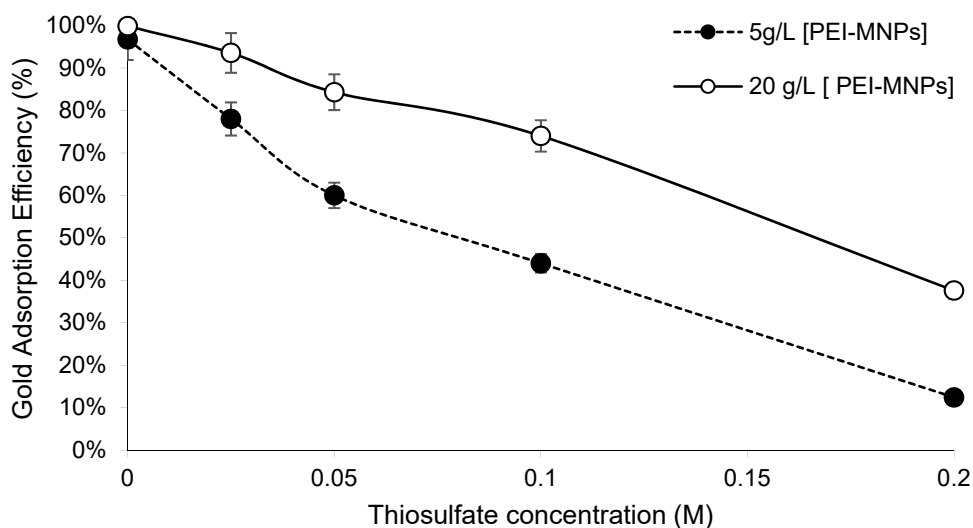


Figure 5-6. Effect of initial free thiosulfate concentration on gold adsorption in 20 mg/L copper, approximately 10 mg/L gold at pH 8 and 50°C temperature solutions at different adsorbent dosages.

In many reported works and commercial applications, the initial thiosulfate concentration is typically maintained at 0.1 M. A further increase of thiosulfate concentration to 0.2 M did not show any increase in gold leaching (Senanayake 2005b). Furthermore, free thiosulfate concentration in leachate after a few hours may be much less due to complexation with gold, copper and any other possible metals and by oxidation to polythionates and sulfate.

Although the solution chemistry is not fully understood for this system, some findings are reported on the effect of polythionates and some other species on the recovery of gold. Daenzer et al. (2016) reported the results of a study on the effect of polythionates on gold loading onto Purolite A500 anion exchange resin. It was observed that at equal molarities, tetrathionate was less favourable to gold loading than trithionate. The increase in initial polythionate (either trithionate or tetrathionate) concentration in the synthetic leaching solutions significantly reduced the gold loading onto the IX resin. In a solution containing 0.1 M CaS_2O_3 , 8 mg/L gold and 4 mM tetrathionate, 61% of the resin capacity was taken up by the tetrathionate that replaced the previously adsorbed thiosulfate.

A comparable scenario can occur with nanoparticles as well, replacing the already adsorbed gold thiosulfate by polythionates or sulfate. Another possible explanation is that free

thiosulfate itself in the solution can be adsorbed onto PEI-MNPs by obstructing the available adsorption sites for gold. The competitive adsorption of sulfur species will be discussed in the following section.

5.3 Competitive Adsorption of Copper and Sulfur Species

5.3.1 Copper Adsorption

PEI shows a good affinity towards copper (Xu et al. 2015). A competitive adsorption of copper was verified by solution analysis and particle analysis as shown in Table 5-1. The copper content found on the nanoparticles (by particle analysis) matched the calculated adsorption capacity by solution analysis. The reduction in adsorption efficiency over the time is assumed to be due to the sulfur species adsorption, replacing the already adsorbed copper. Cu(II) can form stable complexes with amine groups of PEI, having an approximate coordination number of 4. The formation constant was known to be in the order of $10^{16.6}$ (Kislenko and Oliynyk 2002, Xu et al. 2015). The preferential adsorption of copper onto PEI functionalised adsorbents has often been reported (Pang et al. 2011b, Lindén et al. 2015, Xu et al. 2015). As mentioned in Section 5.2.3, under the conditions given, copper can predominantly exist as Cu(I) in $Cu(S_2O_3)_3^{5-}$ and/or as Cu(II) in $Cu(S_2O_3)_2^{2-}$ complexes. Accordingly, electrostatic attraction of anionic copper species and complexation of Cu(II) with PEI by coordination are the possible adsorption mechanisms. However, a further exploration into the mechanism of copper adsorption was not conducted at this stage as it is beyond the scope of this study.

5.3.2 Sulfur Species Adsorption

The competitive adsorption of sulfur species was verified by XPS and APT analyses, as discussed in Section 4.3. Further solution analysis by HPLC was carried out to determine the sulfur speciation in the test solution. The particle analysis by XRF and LECO techniques revealed the net sulfur value adsorbed on to PEI-MNPs. This gives the actual sulfur adsorption onto the adsorbent, excluding the possible sulfur loss in the solution by precipitation.

As mentioned before, thiosulfate is metastable. Consequently, thiosulfate leaching solutions are unstable and the formation of polythionates and ultimately sulfates are inevitable in the presence of an oxidant. Therefore, sulfur speciation analysis was conducted to understand the solution chemistry and competitive loading of thiosulfate and its oxidation products onto PEI-MNPs, using a high performance liquid chromatography (HPLC) technique. The concentration of sulfur species at two different initial thiosulfate concentrations (0.1 M and

0.025 M) was investigated at two different adsorbent dosages (5 and 20 g/L). Sample aliquots were collected after 1 hour and 24 hours to observe the time-dependent thiosulfate decomposition. All the experiments were conducted using synthetic leaching solutions at a pH of 8 and at 50 °C. The results are listed in Table 5-1.

Table 5-1. Sulfur species analysis results by HPLC and copper adsorption analysis results

Sample description	Concentration (mM)						"S" mass loss, %	Cu adsorption, %	
	SO_4^{2-}	$S_2O_3^{2-}$	$S_3O_6^{2-}$	$S_4O_6^{2-}$	$S_5O_6^{2-}$	$S_6O_6^{2-}$			
Solution 1	Before adsorption	0.22	24.5	0.19	0.13	0.08	0.01		
	5g/L [NP], 1 hr	0.55	24.5	0.21	0.1	0.03	BDL	0%	84%
	5g/L [NP], 24 hrs	0.81	21.2	0.33	0.06	0.01	BDL	12%	78%
Solution 2	Before adsorption	0.26	99.8	0.21	0.1	0.05	BDL		
	5g/L [NP], 1 hr	0.31	99.8	0.56	0.08	0.11	0.01	0%	79%
	5g/L [NP], 24 hrs	0.66	91.8	0.8	0.37	0.18	0.01	6%	75%
Solution 3	Before adsorption	0.26	99.8	0.21	0.1	0.05	BDL		
	20g/L [NP], 1 hr	0.46	94.8	0.48	0.12	0.11	0.01	4%	84%
	20g/L [NP], 24 hrs	0.77	84.9	0.73	0.49	0.11	0.01	13%	76%

BDL- below detection limit of the instrument
 Solution 1 - 0.0245 M thiosulfate and 5 g/L PEI-MNPs,
 Solution 2 - 0.1 M thiosulfate and 5 g/L PEI-MNPs,
 Solution 3- 0.1 M thiosulfate and 20 g/L PEI-MNPs

The decrease in $S_2O_3^{2-}$ concentration could result either from adsorption onto PEI-MNPs as a thiosulfate anion itself or oxidation into polythionate and sulfate form. The sulfur mass balance calculations revealed that in one hour, any of the sulfur species adsorption onto PEI-MNPs was insignificant in case of Solution 1 and Solution 2. However after 24 hours, 6% -12% of sulfur mass loss was observed which may be resulted either by adsorption onto PEI-MNPs as thiosulfate or polythionates, or otherwise precipitate as gypsum ($CaSO_4 \cdot 2H_2O$) in the presence of calcium and sulfate in the solution. Concerning sample 3, where the adsorbent dosage was 20 g/L, a 4% drop in $S_2O_3^{2-}$ concentration was detected even after one hour and a further reduction to 13% was noted after 24 hours. An increase in adsorption duration obviously resulted in a higher sulfur species loading but a lower gold loading. This confirms the importance of the use of shorter immersion times to achieve higher gold adsorption.

To differentiate between sulfur species adsorption and any precipitation, a particle analysis was conducted using XRF and LECO techniques, which provide valuable information on the actual sulfur species (as total sulfur) adsorbed onto PEI-MNPs. It was determined that out of

13% sulfur mass loss, only 3% is adsorbed onto PEI-MNPs and the balance of 10% is anticipated to be precipitate as gypsum in the presence of calcium and sulfate ions in the solution. Assuming that gold was adsorbed as its respective thiosulfate complex, the net sulfur mass adsorbed as free thiosulfate or polythionates would be even lower than 3%.

5.3.3 Catalytic Degradation of Thiosulfate

A few experiments were conducted to study the effect of added copper and PEI-MNPs on thiosulfate degradation and the results are presented in Figure 5-7. Two solutions were tested; one containing only 0.1 M thiosulfate added as respective calcium salt (Solution 1) and the other solution containing 0.1 M thiosulfate, 10 mg/L gold and 20 mg/L copper, added as copper sulfate (Solution 2). Both solutions were tested in the presence and absence of PEI-MNPs.

The results showed that the presence of copper, as well as PEI-MNPs, catalyse thiosulfate degradation to a certain level. For instance, in a pure thiosulfate solution (without copper) the initial concentration of tetrathionate was 0.02 mM and the thiosulfate concentration was 88 mM. As shown in Figure 5-7B, upon the addition of PEI-MNPs, tetrathionate concentration was increased to 0.03, 0.09 and 0.16 mM over 1, 6 and 24 hours, respectively. In the presence of copper (without PEI-MNPs), the tetrathionate concentration was 0.09, 0.13 and 0.20 mM after 1, 6 and 24 hours. Upon the addition of both copper and PEI-MNPs, the tetrathionate concentration increased to 0.14, 0.23 and 0.37 mM in 1, 6 and 24 hours, respectively.

Simultaneously, in Solution 1, the thiosulfate concentration dropped to 83 mM in one hour, however the final concentration after 24 hours reached 88 mM. In the presence of both copper and PEI-MNPs, the initial thiosulfate concentrations was 92 mM which later dropped to 89 mM after 24 hours (Figure 5-7A).

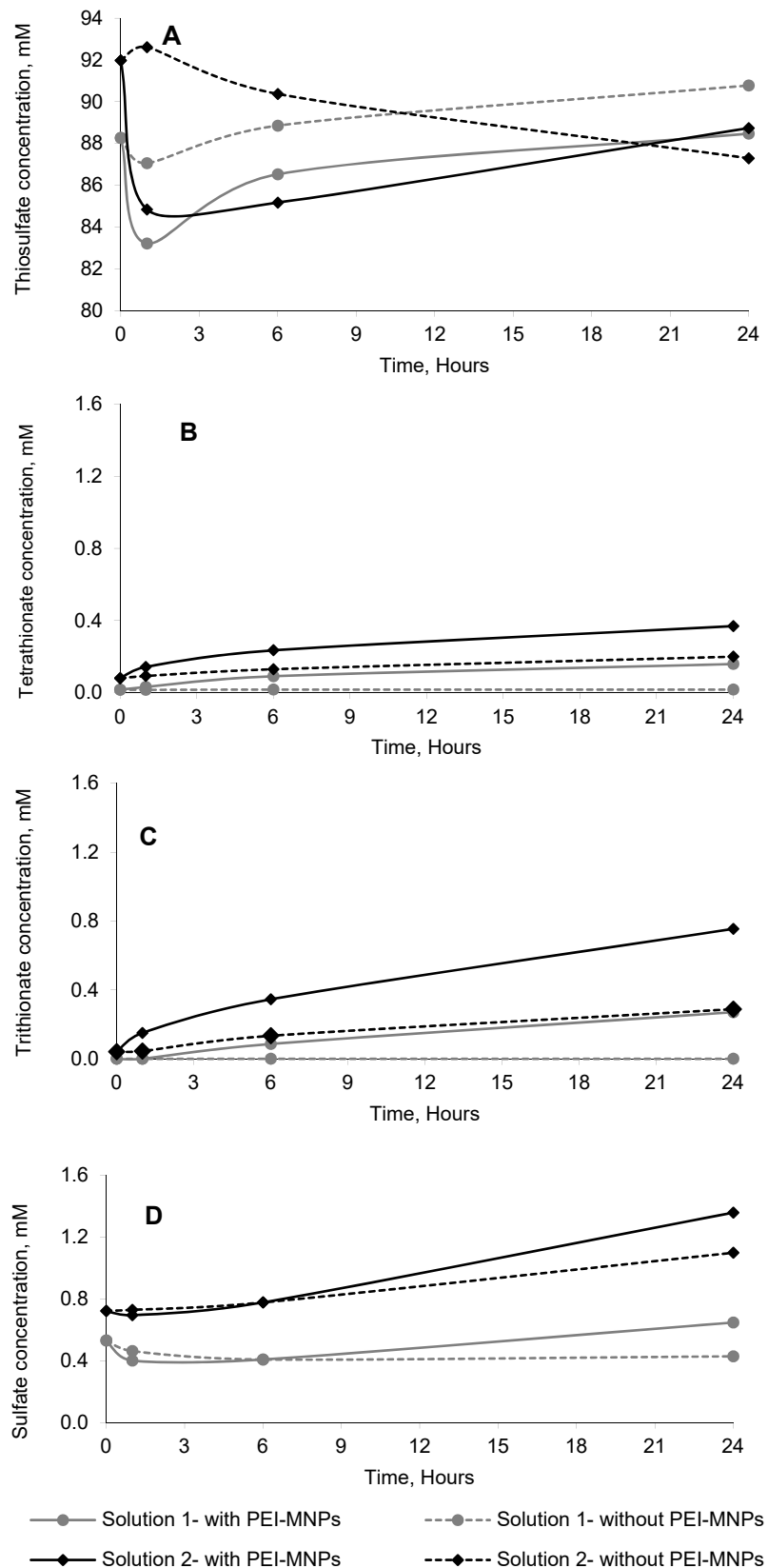


Figure 5-7. Thiosulfate degradation (A) and the formation of tetrathionate (B), trithionate (C) and sulfate (D) in pure thiosulfate solutions without copper (Solution 1) and in thiosulfate, gold and copper solutions (Solution 2)

Being metastable, thiosulfate can readily degrade in aqueous solutions. The catalytic effect of copper on the oxidative degradation of thiosulfate has been observed in earlier studies (Zhang and Nicol 2005, Xu et al. 2017). The availability of oxygen further enhanced oxidative degradation. However, the mechanism behind the catalytic effect of PEI-MNPs on thiosulfate degradation was not further investigated. It could be due either to the iron oxide core or the surface coating. If it is due to any uncoated iron oxide MNPs, a proper surface coverage by functional groups should resolve the problem. Some iron minerals such as hematite, pyrite and pyrrhotite can catalyse the oxidative degradation of thiosulfate (Benedetti and Boulègue 1991, Xu and Schoonen 1995). Feng and van Deventer (2007) found that the presence of hematite can catalyse oxidative degradation of TS, but this detrimental effect can be minimised by adding a natural guar type surfactant (Gempolym M47) to the solution.

The results showed that, polythionate and sulfate formation increased over time. Therefore, the use of shorter (less than one hour) adsorption times would be beneficial to higher gold adsorption as well as to minimise thiosulfate degradation.

5.3.4 Comparison of Gold, Copper and Sulfur Species Adsorption with IX Resin and Activated Carbon

The competitive adsorption of copper and sulfur species onto PEI-MNPs was compared with two IX resins (Purolite A500 and Amberjet 4200) and granular AC (PICAGOLD G210AS). A typical calcium thiosulfate leaching solution was used and the adsorbent dosages used were 5 and 20 g/L. The initial concentrations of gold, copper and total sulfur were 10, 21 and 5600 mg/L, respectively.

As illustrated in Figure 5-8, copper and sulfur species adsorption was higher with IX resins than with PEI-MNPs. The lower adsorption of competitive ions (sulfur species and copper) was beneficial in the case of PEI-MNPs. Sulfur species adsorption ranged from 6% to 23% for IX resins. This is a considerable amount compared to the high concentration of sulfur in the solution. The competitive adsorption of polythionates is also reported elsewhere (Muslim et al. 2009, Daenzer et al. 2016). Sulfur species adsorption was significantly lower in PEI-MNPs (2.6% to 5.8%) compared to IX resin (6% to 23%). Gold adsorption efficiency of IX resins was apparently higher than PEI-MNPs. AC did not adsorb any of the adsorbates at 5 g/L adsorbent dosage while approximately 11% of gold and 3% of sulfur species adsorption resulted at 20 g/L adsorbent dosage.

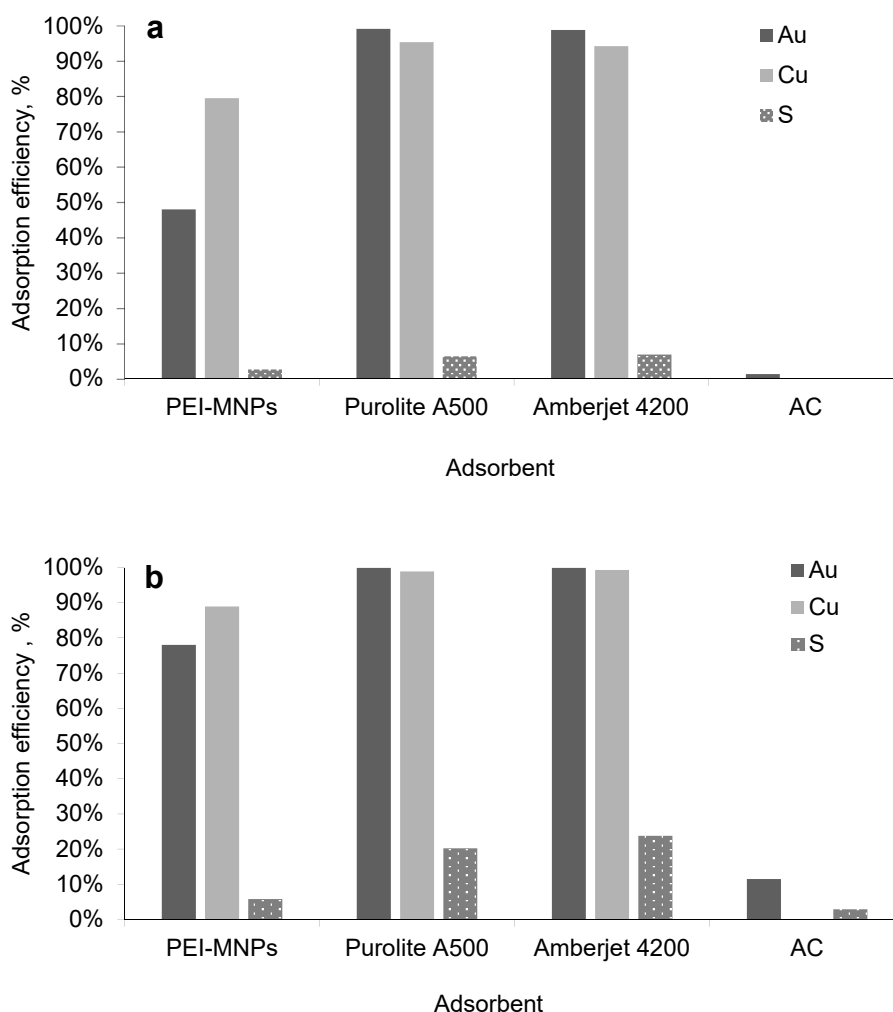


Figure 5-8. Comparison of metal adsorption efficiency of PEI-MNPs with IX resins and AC from a solution consisting of 0.1 M thiosulfate, 10 mg/L gold and 21 mg/L copper, pH 8, 50 °C, after 1 hour with an adsorbent dosage of 5 g/L (a) and 20 g/L (b).

5.4 Gold Adsorption Kinetics

5.4.1 Pure Gold Thiosulfate Solutions

Gold adsorption kinetics in pure gold thiosulfate solutions was conducted with two different adsorbent dosages, 5g/L and 20 g/L, at pH 8 and 50 °C. Sample aliquots were collected after 5, 10, 20, 30, 40, 60 and 180 minutes and the results are shown in Figure 5-9. The gold adsorption was rapid and 100% equilibrium gold adsorption was achieved within few minutes, irrespective of the adsorbent dosage. The good affinity of gold-thiosulfate complex with PEI-MNPs is prominent without any competitive ions.

The adsorption kinetics were tested in the first hour in a solution containing only gold thiosulfate complex with the first three samples collected after 1, 2 and 5 minutes. After 1

minute, almost 99.5 % gold was adsorbed onto the PEI-MNPs and that value remained almost steady throughout the first hour.

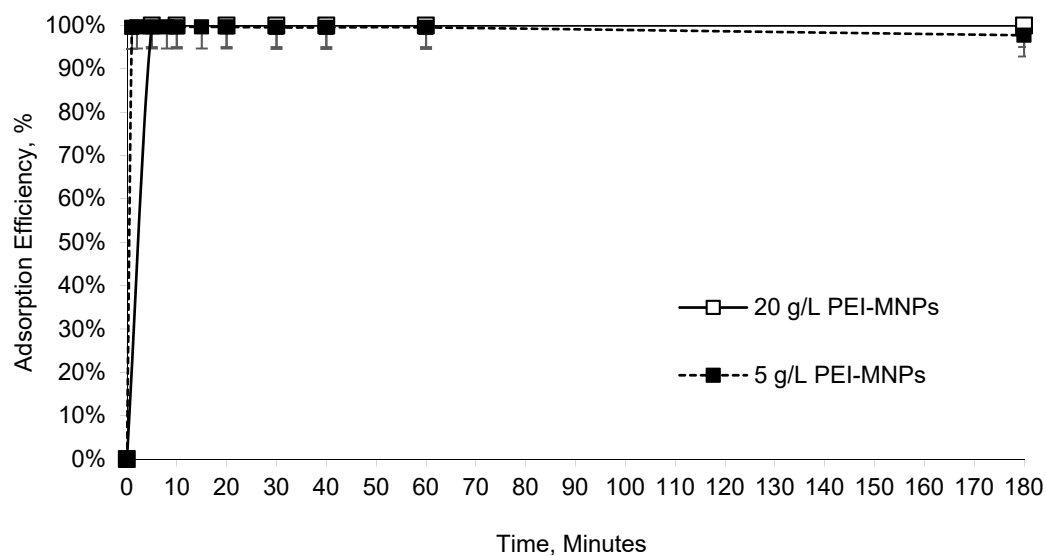


Figure 5-9. Gold adsorption kinetics in pure gold thiosulfate solution at pH 8 and 50 °C

5.4.2 Synthetic Leaching Solutions

Gold adsorption kinetics in two different solutions were evaluated. One solution consisted of gold, copper and free thiosulfate added as calcium thiosulfate (Solution 1). The other solution consisted of gold and free thiosulfate (Solution 2).

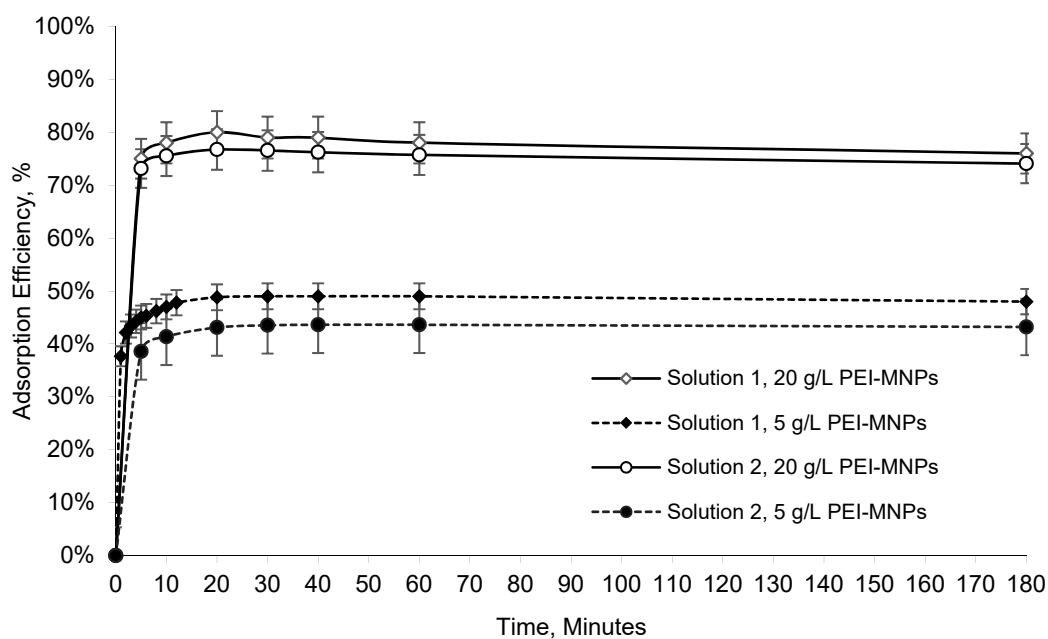


Figure 5-10. Comparison of gold adsorption kinetics in different solutions (Solution 1 = 0.09 M CaS_2O_3 + 10 mg/L Au + 20 mg/L Cu; Solution 2 = 0.09 M CaS_2O_3 + 10 mg/L Au) at pH 8 and 50 °C.

Experiments were conducted with adsorbent dosages of 5 g/L (shown as solid markers in Figure 5-10) and 20 g/L (shown as open markers in Figure 5-10). The gold adsorption kinetics were rapid in all of the solutions tested. In all cases, the gold peaked rapidly and a similar kind of kinetic pattern was observed in almost all of the experiments conducted.

In solution 1, 76% and 48% gold adsorption was observed at 20 g/L and 5 g/L PEI-MNPs dosages, respectively. In CaS₂O₃ + Au solution (Solution 2), the gold adsorption was around 74% and 43% after one hour with 20 g/L and 5 g/L adsorbent dosages, respectively. The availability of more adsorption sites and hence reduced competition could have been the reason for improved adsorption efficiency at higher adsorbent dosages.

This extremely fast kinetics is an indication of the physical adsorption behaviour of the process where activation energy is not required (Inglezakis and Pouloupoulos 2006).

5.4.3 Kinetics Model Fitting

Gold adsorption kinetics was fitted to pseudo-first-order kinetics model (Lagergren 1898), pseudo-second-order kinetics model (Blanchard et al. 1984) and intra-particle diffusion model (Weber and Morris 1963, Crank 1975). As mentioned previously, gold adsorption kinetics is fast, irrespective of the solution content, and reached equilibrium in less than 30 minutes. The adsorption efficiency results obtained from Solution 1 with a 5 g/L adsorbent dosage (in Figure 5-10) were used for kinetics model fitting. Sample aliquots were collected frequently within the first 12 minutes and then at 10 minute intervals for up to one hour to obtain enough data points for the kinetic model fitting.

Non-linearised and the respective linearised kinetics model equations are listed under equations (5-4) to (5-8). The linearised versions were used for the model fitting.

$$\text{Pseudo-first-order (non-linear)} \quad q_t = q_e(1 - e^{-k_1 t}) \quad (5-4)$$

$$\text{Pseudo-first-order (linear)} \quad \ln(q_e - q_t) = -k_1 t + \ln q_e \quad (5-5)$$

$$\text{Pseudo-second-order (non-linear)} \quad q_t = \frac{q_e^2 k_2 t}{1 + q_e k_2 t} \quad (5-6)$$

$$\text{Pseudo-second-order (linear)} \quad \frac{t}{q_t} = \frac{1}{k_2 q_e^2} + \frac{1}{q_e} t \quad (5-7)$$

$$\text{Intra-particle diffusion} \quad q_t = k_p \sqrt{t} + C \quad (5-8)$$

where, q_e and q_t are the adsorption capacity expressed in mg/g at equilibrium and at time t , respectively. k_1 , k_2 and k_p are the first-order, second-order and intra-particle diffusion rate constants, respectively. C in mg/g is a constant (the intercept of the intra-particle diffusion equation) associated with the thickness of the boundary layer.

The experimental data first fitted to the pseudo-first-order and pseudo-second-order models as shown in Figure 5-11 and Figure 5-12. The kinetic model parameters are listed in Table 5-2. The adsorption rate constants of pseudo-first order model and pseudo-second-order model are 0.2021 and 2.57, respectively. Based on R^2 values, the experimental data had a better fit with the pseudo-second-order model within the tested conditions. Significance of the difference between two correlation coefficients was tested using the Fisher R to Z transformation which also confirmed the better fit to pseudo-second-order model. The predicted equilibrium adsorption capacity ($q_{e, cal}$) matched with the experimental value ($q_{e, exp}$).

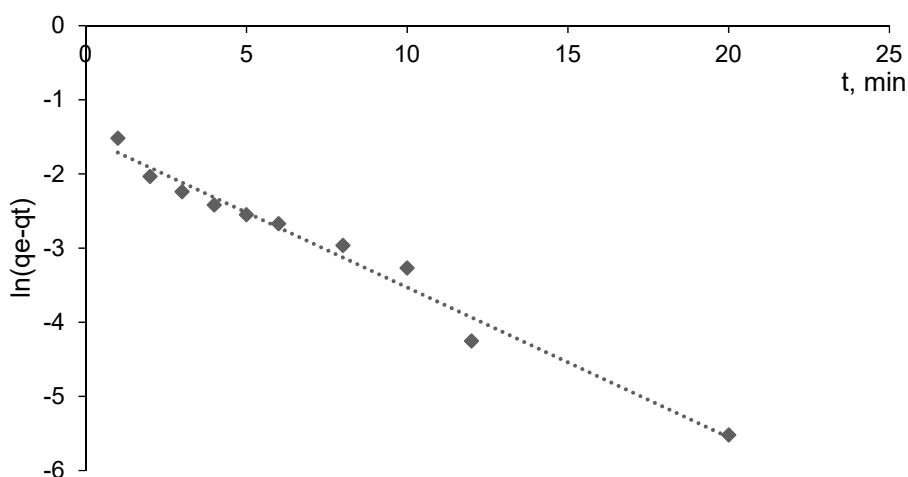


Figure 5-11. Pseudo-first-order adsorption kinetics of Au adsorption onto PEI-MNPs

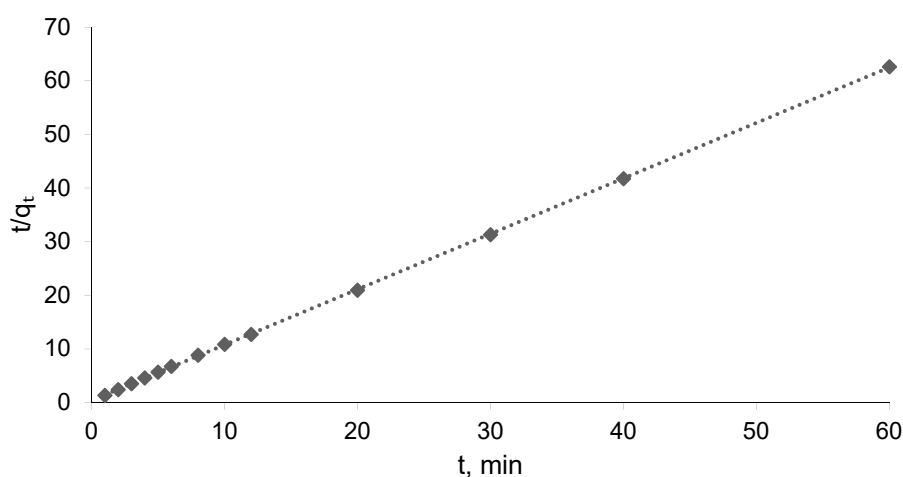


Figure 5-12. Pseudo-second-order adsorption kinetics of gold adsorption onto PEI-MNPs

Table 5-2. Kinetic parameters of pseudo-first-order and pseudo-second-order models

$q_{e, exp}$	First Order Model			Second Order Model		
	k_1 (min^{-1})	$q_{e, cal}$ (mg/g)	R^2	k_2 ($\text{g mg}^{-1} \text{min}^{-1}$)	$q_{e, cal}$ (mg/g)	R^2
0.958	0.2021	0.22	0.9775	2.57	0.966	0.9999

According to Azizian (2004), the initial adsorbate concentration (C_0) greatly influences the fitting of data to a kinetics model, where a pseudo-first-order model describes the kinetics at very high C_0 values and the data fit well to a pseudo-second-order model at low C_0 . However, only 10 mg/L (relatively low) adsorbate concentration was tested in the current study to simulate practical/real world conditions, and it should be noted that the kinetic model fit can be different for a very high or very low initial gold concentration. In many published works, the adsorption mechanism was concluded to be chemisorption by fitting the kinetics data to a pseudo-second-order model, which is incorrect as highlighted by Kajjumba et al. (2018). It is further reported that an adsorption mechanism cannot simply be determined only by fitting data to a kinetic model but can be achieved with comprehensive particle analysis techniques and thermodynamic evaluations (Lima et al. 2015, Tran et al. 2017). The adsorption mechanism will be thermodynamically assessed in Section 5.6.

The intra-particle diffusion model is frequently used to determine the rate-limiting step of the adsorption process. This model was originally developed for pure diffusion on porous solids (Crank 1975). However, currently this model is often used to describe the adsorption mechanism of adsorbates onto numerous adsorbents. The Weber and Morris model (Weber and Morris 1963) is often used to fit kinetic data. If a plot of q_t vs \sqrt{t} is linear and passes through the origin, the rate-limiting step is entirely controlled by intra-particle diffusion. In contrast, if the plot shows multiple linear sections, it implies that the adsorption is controlled by multistep stages. As shown in Figure 5-13, the graph consist of two well defined linear sections. The first section is associated with bulk-diffusion (also knowns external-diffusion), which means the adsorbate is transferred from the bulk solution to the outer hydrodynamic layer of the adsorbent. This is a rapid process. The second section of the graph (the levelled-off section) is corresponded to the surface-diffusion. This means the transfer of adsorbent into the hydrodynamic boundary layer, which is most likely to be the surface PEI layer. The presence of multiple linear regions indicates that the rate-limiting step is not only the intra-particle diffusion.

The values of k_p and C were calculated from the slope and intercept of second linear section of the graph, respectively. The value of k_p was 0.003. The value of C gives an idea on the

thickness of the boundary layer. A higher value of C resembles that a greater effect on limiting boundary layer (Tran et al. 2017). In this study the value of C was 0.94 that may imply a little effect on limiting boundary layer.

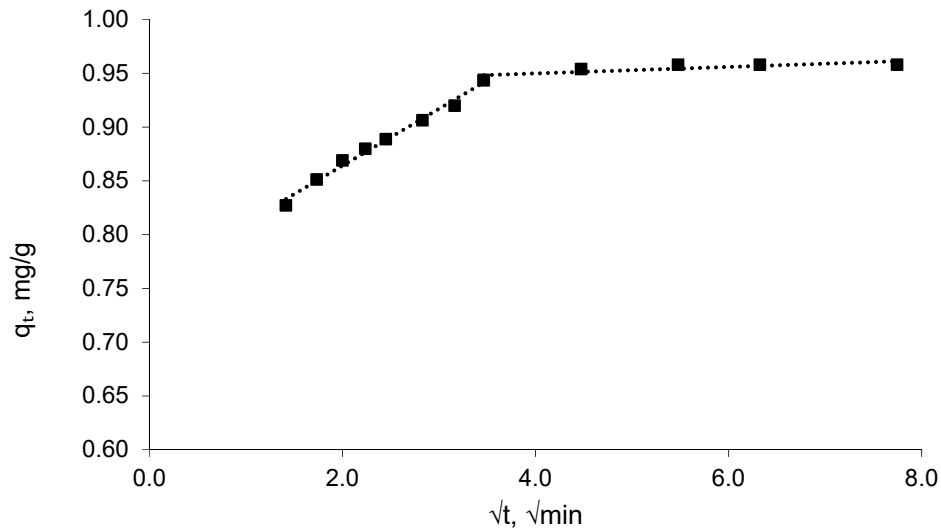


Figure 5-13. Intra-particle diffusion model for the gold adsorption onto PEI-MNPs

5.5 Gold Adsorption Isotherms

The relationship between the amount of adsorbate attached to an adsorbent surface to its concentration in the solution phase at a constant value of temperature is known as an adsorption isotherm in a solid-liquid system. Initially, the Langmuir isotherm and the Freundlich isotherm models were used for data fitting. Nonlinear forms of the Langmuir model and the Freundlich model are represented in equations (5-9) and (5-10), respectively.

$$q_e = \frac{q_m K_L C_e}{1 + K_L C_e} \quad (5-9)$$

$$q_e = K_F C_e^{1/n} \quad (5-10)$$

where, q_e is the adsorption capacity at equilibrium in mg/g, C_e is the equilibrium concentration of adsorbate in the solution in mg/L, q_m is the maximum adsorption capacity in mg/g, K_L is the Langmuir isotherm constant in L/mg, K_F is the Freundlich constant in (mg/g) (L/mg)^{1/n} and n is a dimensionless intensity parameter.

The adsorption isotherm data were fitted to non-linear Langmuir and Freundlich models. OriginPro software was used for the nonlinear curve fitting and the results are summarised in Table 5-3. Simulated leaching solutions at pH 8 were used and initial copper concentration and thiosulfate concentration was maintained at 20 mg/L and 0.1 M, respectively. Adsorbent

dosage was 5 g/L for all the experiments and the temperature was varied from 25 °C to 50 °C. Gold loading significantly improved with increasing gold concentration.

Table 5-3. Model parameters of Langmuir and Freundlich adsorption isotherms

T(°C)	Langmuir model		Freundlich model			
	q _m (mg/g)	K _L (L/mg)	R ²	K _F (mg/g)(L/mg) ^{1/n}	n	R ²
25	42.11	0.00418	0.9959	0.499	1.4710	0.9930
35	41.22	0.00411	0.9973	0.458	1.4556	0.9873
50	33.85	0.00373	0.9959	0.338	1.4304	0.9834

A coefficient of determination (R²) value was used to determine the goodness of fit. The data fitted well with both isotherm models, and this has been reported elsewhere also in some instances (Chowdhury et al. 2010, Feng et al. 2017). The selected gold concentration range could be the reason for this. However, as temperature increased, the Langmuir model showed a slightly better fit. The Langmuir adsorption isotherm assumes a monolayer adsorption. Graphically the adsorption capacity should reach a plateau although the adsorbate concentration is increased. However, as illustrated in Figure 5-14, the adsorption process doesn't seem to reach equilibrium even at very high gold concentrations. This could be due to a few reasons. One is that the adsorbent may not reach saturation, which means the existence of more vacant adsorption sites on the surface. Furthermore, it can be a multilayer/physical adsorption process. Finally, one can predict that at very high adsorbate concentrations, surface precipitation of the adsorbate could occur. The shape of the plot indicates the formation of multilayers. Therefore, the adsorption mechanism could be a physical adsorption. The maximum gold adsorption capacity derived from the Langmuir model was varied from 33.85 to 42.11 mg/g, at different temperatures.

The favourable nature of the adsorption can be expressed in terms of a dimensionless equilibrium constant known as the separation factor (R_L). R_L can be determined according to equation (5-11).

$$R_L = \frac{1}{1 + K_L C_0} \quad (5-11)$$

Where K_L is the Langmuir constant and C₀ is the initial concentration of adsorbate in the solution, expressed in mg/L. An R_L value in between 0 and 1 indicates favourable adsorption, while R_L>1 means unfavourable adsorption, R_L=1 denotes linear adsorption and R_L=0 indicates an irreversible adsorption (Hamdaoui and Naffrechoux 2007, Foo and Hameed 2010). From the data presented in Table 5-3, the calculated R_L value ranges in between 0.44

and 0.99 for the initial gold concentrations considered in this study, which denotes the favourable adsorption of gold onto PEI-MNPs.

The Freundlich fitting of adsorption data is illustrated in Figure 5-15. Intensity parameter n , in the Freundlich isotherm model is an indicator of adsorption intensity or heterogeneity of the surface (Foo and Hameed 2010). It is reported that n values of less than 1 indicates an unfavourable adsorption. According to Hamdaoui and Naffrechoux (2007), n values in between 1 and 2 denoted moderate adsorption, whilst $n > 2$ represent good adsorption. According to Choudhary et al. (2018), $0 < 1/n < 1$ indicates favourable adsorption, while $1/n > 1$, $1/n = 1$ and $1/n = 0$ denotes unfavourable, linear and irreversible adsorption, respectively. The n values of 1.43 to 1.47 in the current study indicate favourable adsorption.

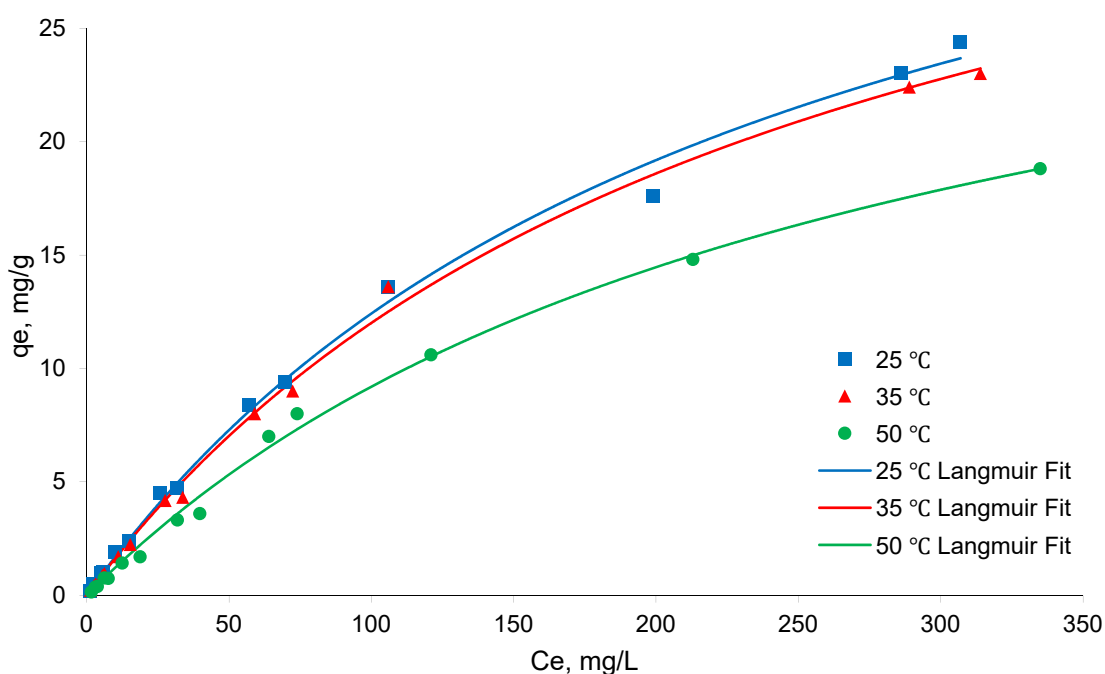


Figure 5-14. Langmuir isotherm model fitting. Synthetic leaching solutions consist of 0.1 M thiosulfate, 20 mg/L copper and different initial gold concentrations ranging from 4 to 429 mg/L. Adsorption was conducted at temperatures of 25, 35 and 50°C and a pH of 8.

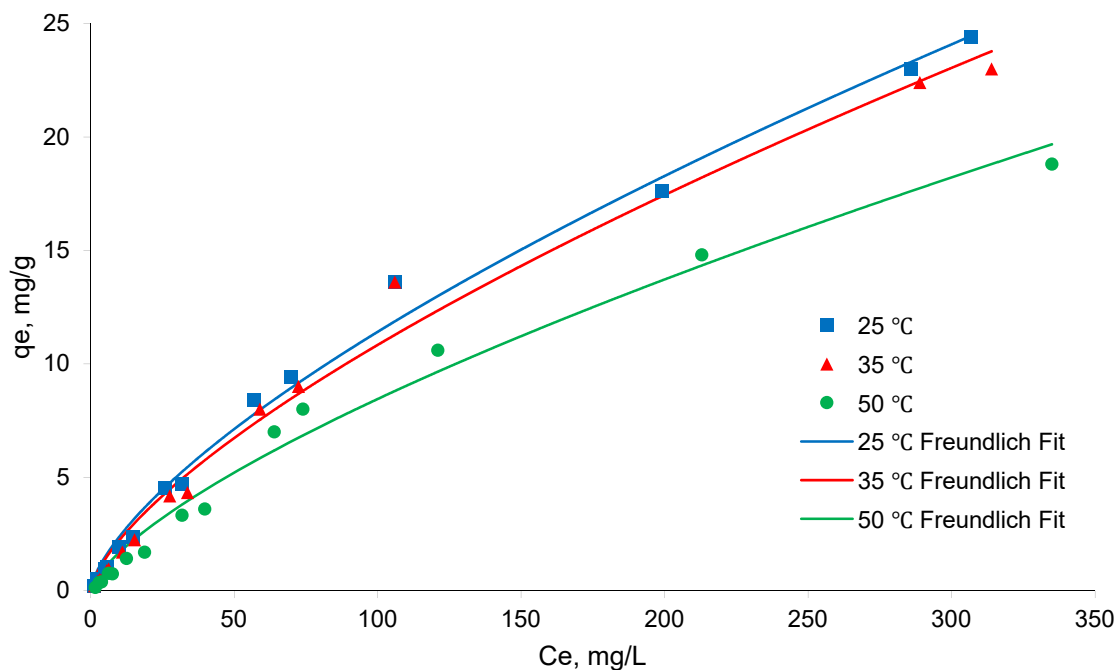


Figure 5-15. Freundlich isotherm model fitting. Synthetic leaching solutions consist of 0.1 M thiosulfate, 20 mg/L copper and different initial gold concentrations ranging from 4 to 429 mg/L. Adsorption was conducted at temperatures of 25, 35 and 50°C and a pH of 8.

5.6 Thermodynamic Studies

Thermodynamic studies can be effectively used to determine the adsorption mechanism in aqueous solutions. A series of adsorption experiments were conducted at different temperatures and at different initial gold concentrations (from 4-429 mg/L). All other parameters such as solution pH, adsorbent dosage, and solid to liquid ratio were kept constant. Once the system reached equilibrium, the residual adsorbate concentrations were analysed and the adsorbent capacity data was fitted to the Langmuir adsorption isotherm model. To calculate the thermodynamic parameters (Gibbs free energy change (ΔG°), enthalpy change (ΔH°) and entropy change (ΔS°)) according to equations (3-3) to (3-6), it is important to determine the thermodynamic equilibrium constant (K_C , dimensionless). The Langmuir constant (K_L) can be used to calculate the equilibrium constant, K_C , according to equations mentioned above. Tran et al. (2016) discusses in detail the thermodynamic equilibrium constant calculation by use of isotherm constants.

In general, two adsorption mechanisms are mainly considered. Physical adsorption (also known as physisorption) occurs from electrostatic attraction which is relatively weak. Chemical adsorption (also known as chemisorption) involves covalent bonds between the adsorbent surface and the adsorbate molecules. As a consequence, chemisorption ceases once the adsorbent's surface layer is saturated (monolayer adsorption) and additional adsorption

can occur only on the already adsorbed layer(s) by physical means. In contrast, physical adsorption can continue up to several layers. Chemisorption is accompanied with a considerable amount of activation energy, and consequently this is a comparatively slow process. By contrast, physical adsorption does not need any activation energy and therefore fast kinetics are observed more so than in chemisorption (Laidler and Meiser 1999).

The Langmuir constant, K_L was used for the calculation of equilibrium constant, K_C in order to determine the adsorption mechanism. Caution should be exercised when using the Langmuir constant for equilibrium constant calculation as inaccurate calculations can alter the values and signs (+/-) of ΔG° , ΔH° and ΔS° considerably and lead to inaccurate conclusions. K_C should be dimensionless but K_L is given in L/mg. The erroneousness of using the K_L value “as it is” to calculate ΔG° is emphasised in many articles (Liu 2009, Anastopoulos and Kyzas 2016, Ghosal and Gupta 2017, Tran et al. 2017). Instead, the equilibrium constant (K_C) should be used, and this can be derived using the value of K_L . However the calculation of K_C using K_L is contradictory in some of the existing literature. Two methods followed by Tran et al. (2016) and Ghosal and Gupta (2017) were tried in this study and the same conclusions were derived, but the values of ΔG° and ΔS° are distinct. Yet the signs are the same, which is important in concluding the spontaneity and randomness of the adsorption process. The results included below are based on the method suggested by Tran et al. (2016).

It is reported that the negative value for ΔG° implies the spontaneous and favourable nature of adsorption at a given temperature (Tran et al. 2016). The value and sign of ΔH° is a reflection of the adsorption mechanism (either physical or chemical) and endothermic/exothermic nature of the adsorption process, respectively. Moreover, ΔS° represent the randomness or state of disorder of the adsorption system. A negative ΔS° value indicates the decrease of randomness at the solid-liquid interface which corresponds to an associative mechanism. Conversely, a positive ΔS° value suggests an increase in randomness at the solid-liquid interface, which corresponds to a dissociative mechanism.

In this study, the average value of ΔG° for all the temperatures tested was approximately -27.2 kJ/mol. The calculated negative value for the Gibb's free energy change indicates the spontaneous nature of the adsorption. The enthalpy change and the entropy change were determined using the slope and intercept of the plot (Figure 5-16) of $\ln(K_C)$ vs $1/T$, respectively, in accordance with equation (3-5). The calculated thermodynamic parameters are summarised in Table 5-4. The negative value of ΔH° verifies the exothermic nature of gold adsorption onto PEI-MNPs. A decrease in the metal loading was observed when increasing the temperature, which is an indication of the exothermic nature of the adsorption process. The

adsorption process in the solid-liquid system is a combination of two processes, the desorption of already adsorbed solvent (water) molecules and the adsorption of the adsorbate. In an exothermic process, the energy absorbed in bond-breaking (adsorbent-water) is less than the energy released at bond-making (adsorbent-adsorbate). The extra energy is released as heat, making the ΔH° value negative. The calculated value for ΔH° was -11.99 kJ/mol, which implies physical adsorption (physisorption), given that typical adsorption enthalpy change values for physical adsorption vary from 2.1-20.9 kJ/mol and 80-200 kJ/mol for chemical adsorption (Saha and Chowdhury 2011). According to Inglezakis and Pouloupoulos (2006), enthalpy changes between 5 and 40 kJ/mol and 40-800 kJ/mol correspond to physisorption and chemisorption, respectively. The positive value (49.33 J/mol.K) obtained for entropy change, ΔS° was indicative of increased randomness at the solid liquid interface and affinity of the adsorbent towards the adsorbate.

It is generally expected that an increase in temperature causes a reduction in anion adsorption onto an oxide surface (Lutzenkirchen 2002). This is caused by the decrease in the point of zero charge. Consequently, at a constant pH, the cationic surface charge (in adsorbent surface) is reduced, by lowering the electrostatic attraction to anions (gold complex). A few studies have reported the temperature dependence of zeta potential and pH_{PZC} . According to Tewari and McLean (1972), the pH_{PZC} of magnetite reduced when the temperature was increased. A similar scenario can also be expected with the adsorbent used in this study. This further verifies that the gold adsorption onto PEI-MNPs is a consequence of electrostatic attraction. Any published results on the temperature dependence of the surface charge of the PEI layer could not be found.

Table 5-4. Summary of the thermodynamic parameters

Temperature (K)	K_L (L/mg)	K_C (dimensionless)	ΔG° (kJ/mol)	ΔH° (kJ/mol)	ΔS° (J/mol.K)
298	0.00418	94137.44	-26.58		
308	0.00404	72598.44	-27.39	-11.99	49.33
323	0.00291	41765.97	-27.84		

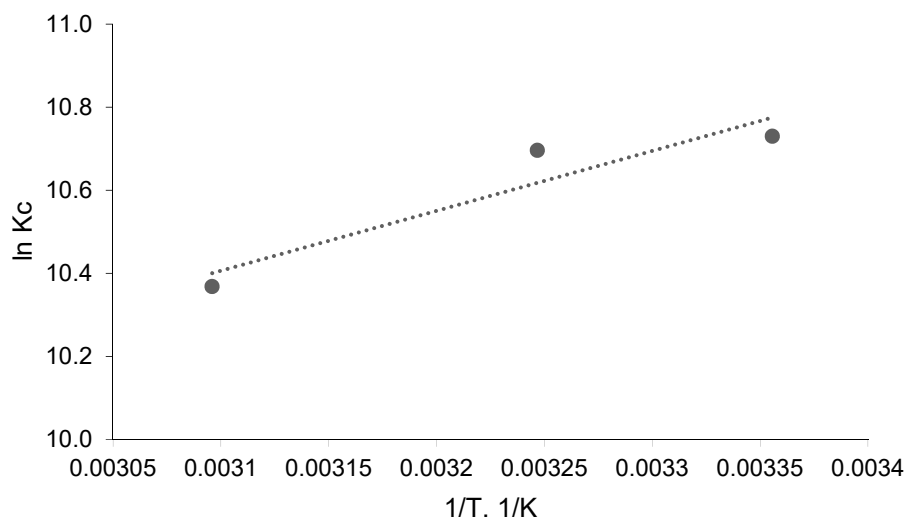


Figure 5-16. In Kc vs 1/T

5.7 Gold Adsorption from Other Thiosulfate Leaching Systems

Gold and other metals (used as oxidants) adsorption behaviour in selected different thiosulfate leaching systems other than CaS_2O_3 -air system was investigated. These experiments were conducted for the sole purpose of comparison and, detailed studies such as isotherms, kinetics and thermodynamic studies were not performed. Synthetic leaching solutions were used for all the experiments and the reagent concentrations and experiment conditions are illustrated in Table 5-5. Initial gold concentration was varied from 6.5-9.5 mg/L. The natural pH of Fe-EDTA solution was approximately pH 2, once FeCl_3 and EDTA were mixed together in DI water. This was adjusted to pH 7 before adding thiosulfate as such an acidic pH can decompose thiosulfate. Furthermore it is recommended to add thiosulfate only to the mixture of ferric ions and the ligand (either EDTA or oxalate) to prevent thiosulfate oxidation by Fe (III) (Heath et al. 2008).

Table 5-5. Conditions and content of leaching solutions of different thiosulfate systems

Oxidant-Ligand pair	$\text{Na}_2\text{S}_2\text{O}_3$ concentration	Oxidant concentration	Ligand concentration	pH	Temperature
Fe-EDTA	0.06-0.1 M	5mM, Fe (III)	5.5 mM, EDTA	7	25 °C
Fe-Oxalate	0.06-0.1 M	5mM, Fe (III)	12.5M, Oxalate	5	25 °C
Ni-NH ₃	0.06-0.1 M	5mM, Ni (II)	0.5M, NH ₃	10	25 °C
Cu-NH ₃	0.06-0.1 M	5mM, Cu (II)	0.4M, NH ₃	11.4	25 °C

The adsorption efficiency results are depicted in Figure 5-17 and Figure 5-18. Despite the solution composition, the gold adsorption was higher at 0.06 M thiosulfate concentration. At low thiosulfate concentration, the free thiosulfate concentration is lower in the solution. Free thiosulfate may competitively adsorb onto PEI-MNPs. Higher amount of gold can adsorb onto PEI-MNPs when the competitive ions are lower in the solution.

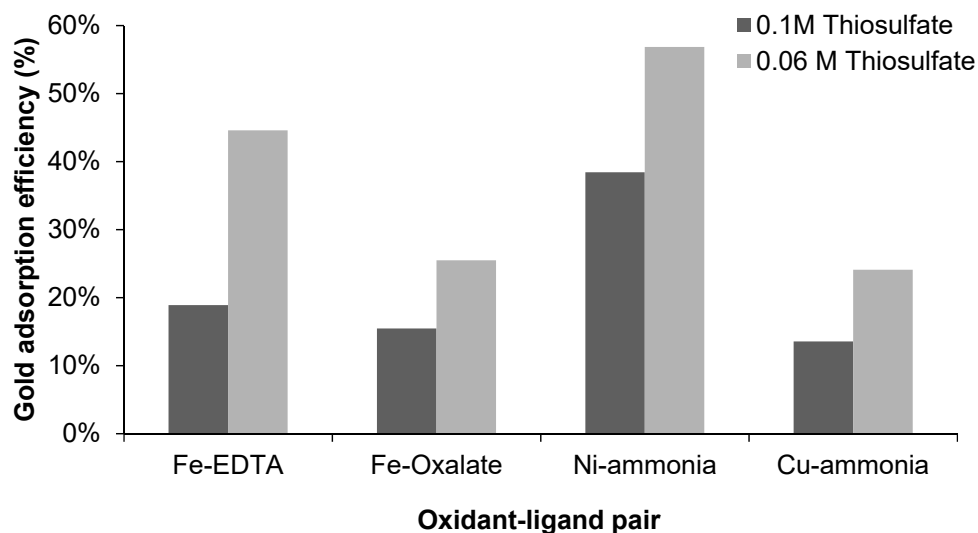


Figure 5-17. Gold adsorption efficiency in different thiosulfate leaching systems at 5 g/L adsorbent dosage

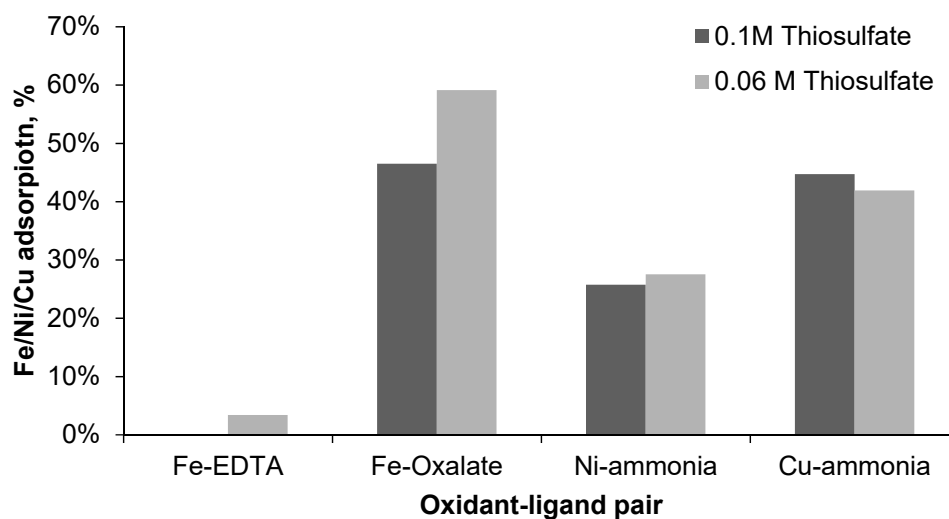


Figure 5-18. Metal adsorption in different thiosulfate leaching systems at 5g/L adsorbent dosage. The solution preparation is according to Table 5-5.

For the tested conditions, gold adsorption decreased in the order of; Ni-ammonia > Fe-EDTA > Fe-oxalate > Cu-ammonia system. Gold adsorption was enhanced when using lower thiosulfate concentrations. As the initial concentration of thiosulfate was constant for all the leaching systems, this variation could be due to the effect of individual oxidant-ligand pairs

on thiosulfate oxidation and the adsorption of the metal-ligand complex itself by the adsorbent. PEI-MNPs perform best in Ni-ammonia system where gold adsorption is highest and Ni adsorption is lowest, compared to the other oxidants. Thiosulfate concentration does not seem to be a major factor in Ni adsorption, but it is for gold adsorption. Although gold adsorption is lower in the Fe-EDTA system than in the Ni-ammonia system, ferric ion adsorption is negligible which is advantageous at the metal elution stage. Ferric ion adsorption is highest in the Fe-oxalate system. It was previously reported that oxalate ions are attracted towards natural magnetite surfaces, depending on the zeta potential values and hence solution pH (Erdemoğlu and Sarıkaya 2006). Therefore, in this study, either free oxalate anions (which have not complexed with ferric ions) or metal-oxalate complexes can adsorb preferentially onto PEI-MNPs, hindering the gold adsorption. Gold adsorption dropped dramatically in the Cu-ammonia system, which necessitated a solution analysis for sulfur speciation.

Sulfur species were analysed by High performance liquid chromatography (HPLC) for Cu-ammonia and Ni-ammonia systems to investigate the effect of polythionates and thiosulfate on gold loading onto PEI-MNPs. The synthetic leaching solution used for the adsorption experiments comprised 0.1 M sodium thiosulfate, 5 mM Copper, 0.6 M ammonia and approximately 10 mg/L gold. After 24 hours of adsorption at room temperature, no free thiosulfate was detected in the solution, possibly due to adsorption onto nanoparticles or ultimately, oxidation to polythionates or to a more stable sulfate form. With respect to the Ni-ammonia system, a slight reduction in thiosulfate concentration was observed together with an increase in tri- and tetrathionates after the adsorption. The total sulfur mass loss derived from mass balance calculations was 1.97% and 17.4% for Ni-ammonia and Cu-ammonia systems, respectively. In the Ni-ammonia system, the formation of polythionates was relatively lower.

To conclude, the adsorption results are based on a 5 g/L adsorbent dosage only. It is anticipated that higher adsorbent dosages would enhance gold adsorption efficiency. However, experiments with higher adsorbent dosages were not attempted for the aforementioned thiosulfate leaching systems, as detailed investigation of these systems is not within the scope of this study.

5.8 Chapter Summary

Gold adsorption onto PEI-MNPs, from synthetic leaching solutions was discussed in this chapter. Gold adsorption was superior in pure gold thiosulfate solutions whilst the competitive adsorption of other species such as copper and sulfur caused a drop in gold adsorption efficiency in a simulated synthetic leaching solution. The presence of copper and sulfur species

is inevitable in the particular thiosulfate leaching system considered. However, the competitive adsorption of the aforementioned species is lower than that which was observed with an IX resin. Adsorbent dosage and free thiosulfate concentration positively and negatively affected gold adsorption efficiency, respectively. The initial solution pH and copper concentration did not show any considerable effect.

According to the solution and particle analysis, not all the sulfur species calculated by solution analysis were adsorbed onto the adsorbent. For instance, a 13% total sulfur mass loss was observed by solution analysis, whilst only 3% sulfur was adsorbed onto PEI-MNPs, as confirmed by particle analysis (XRF/LECO). Copper adsorption capacity was consistent with both solution and particle analysis.

Gold adsorption kinetics were rapid, irrespective of the solution composition. Both pseudo-first-order and pseudo-second-order models fit the kinetic data having R^2 values of 0.9775 and 0.9999, respectively. With a slightly higher R^2 value, together with close approximation of equilibrium adsorption capacity, pseudo-second-order models showed a best fit to the data within the tested range.

Similarly, both the Langmuir and Freundlich isotherm models fitted the adsorption isotherm data. However, the Langmuir model showed a slightly better fit, estimating the maximum adsorption capacity within the range of 33.85 to 42.11 mg/g for the tested temperatures. Interestingly, both the separation factor (R_L) derived from the Langmuir isotherm model and the intensity parameter (n) derived from the Freundlich isotherm model, confirmed a favourable adsorption of gold onto PEI-MNPs.

Determination of possible adsorption mechanism(s) was attempted through a thermodynamic approach. The adsorption kinetic studies and the particle characterisation results supported this indeed. According to the observation thus far, the adsorption mechanism can be estimated as a physisorption. This conclusion was derived based on the following observations.

- Adsorption kinetics were extremely rapid
- The relatively low enthalpy change value (ΔH° was -11.99 kJ/mol) was indicative of physical adsorption. The value is well below the threshold value.
- Although the gold adsorption isotherm fitted well to the Langmuir model, the curve did not reach a perfect plateau even at the highest initial gold concentration tested, i.e. at 429 mg/L. This can possibly be due to the multilayer adsorption, which is certainly a physical adsorption phenomenon.

Chapter 6 Metal Elution and PEI-MNPs Reuse Studies

6.1 Introduction and Chapter Objectives

In this chapter, the approaches taken to elute the loaded gold and copper from the adsorbent are discussed. Several eluants were tested for metal elution on a trial and error basis. Copper pre-elution with EDTA and gold elution with NaOH were the most promising eluants and will be discussed in detail in the following sections. The influence of process conditions such as temperature, pH, eluant concentration and solid to liquid ratio on elution efficiency was evaluated. Furthermore, the reuse of the adsorbent for up to six cycles was also investigated. Few other eluant systems such as NaOH, diluted HCl, glycine and thiosulfate together with sodium sulfite and sodium chloride under different concentrations and process conditions were also evaluated and the results will be discussed in Appendix D. However these other systems are not very promising compared to the two step EDTA-NaOH system.

6.2 Parameters

6.2.1 Solid to Liquid Ratio

This is one of the most important parameters to be considered in an elution system. Comparison of elution efficiency values of different eluants is quite meaningless without stating a solid to liquid ratio. In addition, S/L ratio is an important parameter to consider in practical applications. Solid to liquid ratio is defined as the weight of the adsorbent in one litre of the eluant solution expressed in g/L. Higher values for the S/L ratio are preferred in order to get a concentrated metal solution after elution. In a batch desorption system, the S/L ratio cannot increase much as the solution becomes highly dense, and practical application becomes difficult. Mixing becomes problematic and contact of the eluant solution with the adsorbent is disturbed (Vilar et al. 2007). Column application is preferred in order to get a very high S/L ratio. In this study the S/L ratio was maintained in the 2.5-10 g/L range. The value used for each experiment is stated in respective sections.

6.2.2 Elution Efficiency

Elution efficiency can be defined as,

$$\text{Elution efficiency (\%)} = \frac{\text{amount of metal eluted}}{\text{amount of metal loaded}} * 100$$

The amount of metal loaded was calculated by the difference in initial and equilibrium metal concentration during the adsorption and the adsorption solution volume. The value of elution efficiency was used for comparison of the different eluants and for the selection of the best suited eluant(s) for metal elution from the PEI-MNPs.

6.3 Copper Pre-elution using EDTA

EDTA was used for selective copper elution from metal loaded PEI-MNP at relatively mild elution conditions. The influence of process parameters and reagent concentrations on elution efficiency was investigated and is discussed in the following sections. EDTA can form stable complexes with many of the base metals. The stability constant of Cu-EDTA complex is reported as 18.7 (Martell and Smith 1974, Martell and Hancock 1996). The schematic representation of the Cu-EDTA complex is illustrated in Figure 6-1. The excellent metal chelating property of EDTA was the reason for using it as a potential eluant in this study. EDTA forms a five membered chelate ring size and the smaller ionic radius of divalent copper (0.57 Å) facilitates the formation of a strong complex. No gold chelates have been reported but it can be assumed that the larger size of the Au (I) ion (1.37 Å) with respect to copper makes the complex less stable than that of the Cu-EDTA complex. EDTA can form a weak complex with silver, having a stability constant of 7.3 (Dwyer and Mellor 1964). Further it is reported that EDTA as an eluant for Au(III) resulted only a 4.4% elution efficiency from a silica gel adsorbent (Sabermahani et al. 2016). Considering these aspects, it is anticipated that EDTA can selectively elute copper without eluting gold from PEI-MNPs.

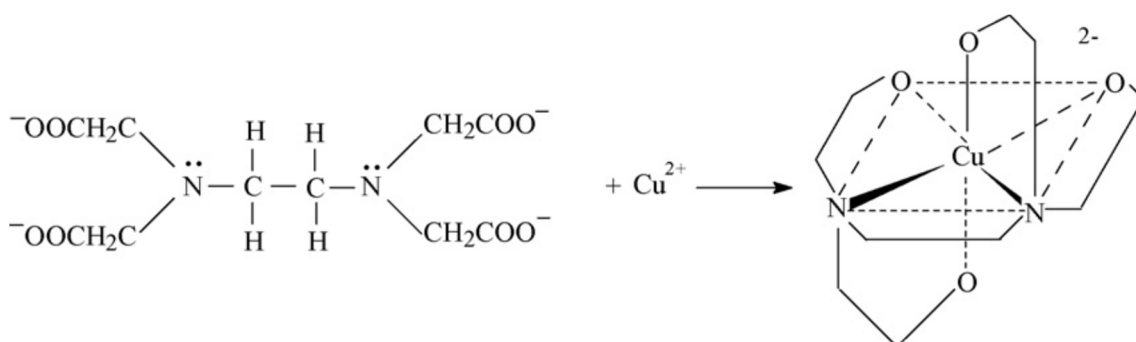


Figure 6-1. Copper complexation with EDTA forming an octahedral complex (derived from (Tseng et al. 2009) with permission)

6.3.1 Effect of EDTA Concentration

The influence of EDTA concentration on copper elution was investigated. Briefly, gold and copper loaded nanoparticles were exposed to EDTA solutions at different concentrations (0.3 mM to 20 mM) at pH 6 and 25 °C for 15 minutes. An increase in the EDTA concentration supported higher copper elution efficiency. However, gold elution was insignificant as

illustrated in Figure 6-2. These results verify the suitability of EDTA for the selective elution of copper from nanoparticles and used as the preferred copper eluant in this study. A 20 mM EDTA concentration was used for all future experiments.

With an excess of Cu (II), the Cu-EDTA complex precipitates as $\text{Cu}_2\text{EDTA}\cdot 4\text{H}_2\text{O}$ up to pH 5.6. However, this depends on concentrations of copper and EDTA, solution temperature and ionic strength (Gyliené et al. 2004). Therefore, to keep copper in the solution as the Cu-EDTA soluble complex, the use of excess EDTA is preferred.

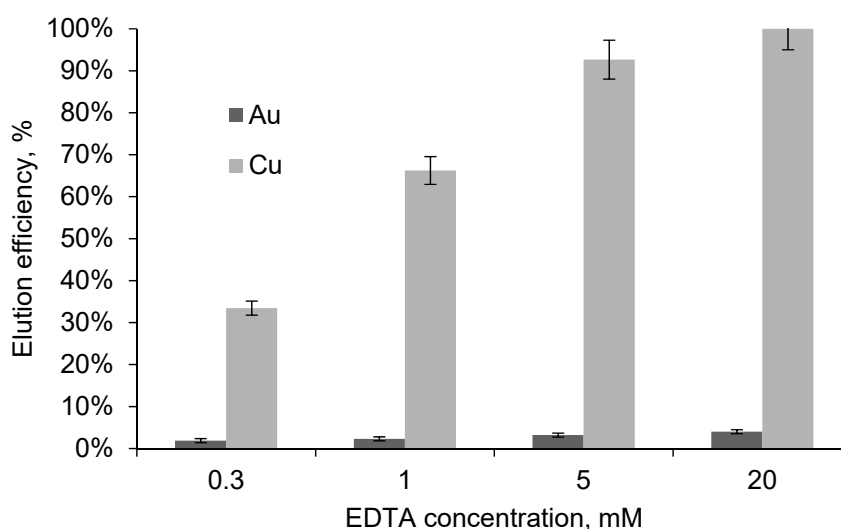


Figure 6-2. Effect of EDTA concentration on metal elution at pH 6, 2.5 g/L of S/L ratio and 25 °C for 15 minutes

6.3.2 Effect of Solution pH

The influence of solution pH on gold and copper elution efficiency in 0.02 M EDTA solutions was evaluated and the results are illustrated in Figure 6-3. Copper elution efficiency was 100% for pH 4.5, 6 and 7 while it dropped to 79% in a pH 8.5 solution. Gold elution was insignificant in pH 4.5 and 6 solutions while it reached 17% and 54% in pH 7 and 8.5 solutions, respectively. However, the reason for considerable gold elution at pH 8.5 is unclear. Perhaps the formation of an Au-EDTA complex could be the reason, but this would require further investigations. Based on the results, pH 6 was chosen for subsequent studies due to the minimal gold elution and 100% copper elution.

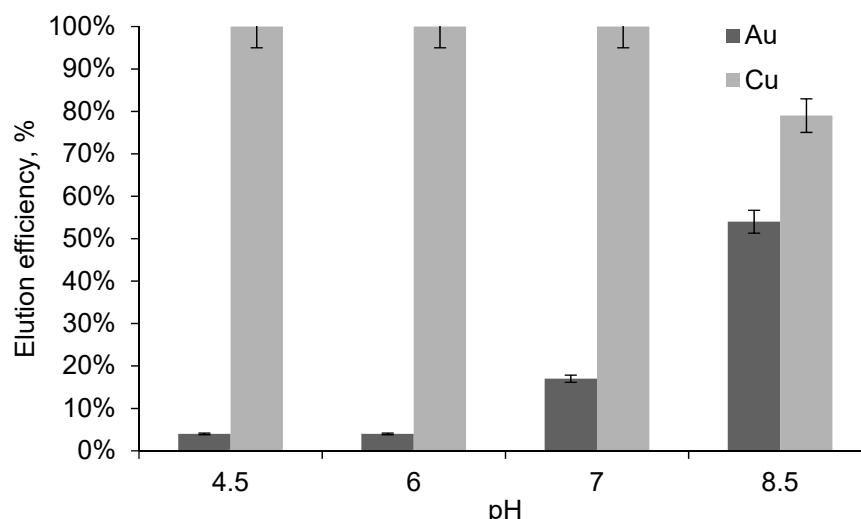


Figure 6-3. Effect of solution pH on metal elution at copper pre-elution stage with 0.02 M EDTA at 25 °C and 2.5 g/L S/L ratio for 15 minutes

6.3.3 Effect of Solution Temperature

To optimise the elution temperature, the metal elution efficiency at different temperatures was examined. The eluant solution was first heated to the desired temperature and then mixed with metal-loaded PEI-MNPs. Sample aliquots were collected at predetermined intervals of up to one hour for analysis. The influence of temperature on copper and gold elution at the copper pre-elution stage after 15 minutes was as shown in Figure 6-4. Copper elution was 98-100% at 50 and 25 °C solutions but a slight drop was observed at 40 °C. Gold elution was negligible at both 40 °C and 25 °C, however nearly 10% gold elution was observed at 50 °C. Therefore, a temperature of 25 °C was chosen for copper elution due to high copper elution efficiency and negligible gold elution.

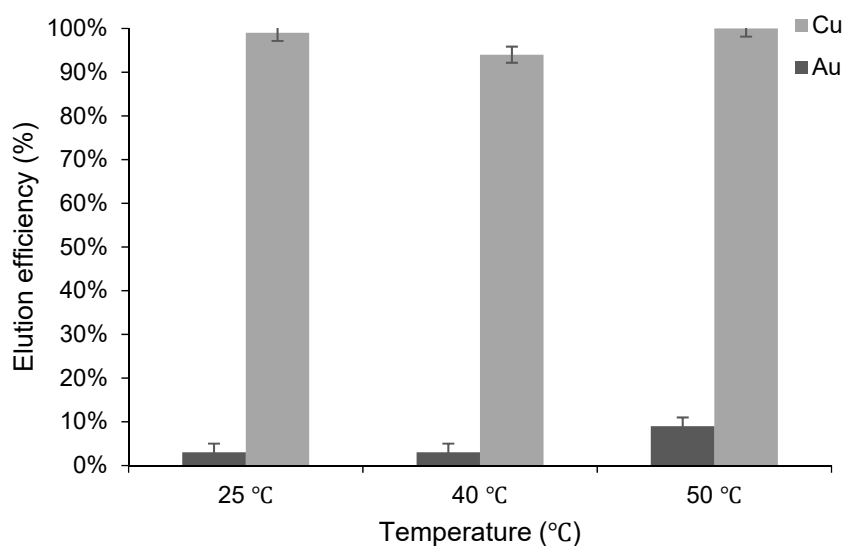


Figure 6-4. Effect of solution temperature on gold and copper elution efficiency in 0.02 M EDTA solution at 15 minutes and 2.5 g/L of S/L ratio

6.3.4 Effect of Solid to Liquid Ratio

Being one of the important parameters in elution experiments, the influence of S/L ratio on elution efficiency was investigated. This parameter did not show any significant impact on metal elution for the tested range (2.5 to 10 g/L), as displayed in Figure 6-5. Higher S/L ratio values are preferred for more concentrated metal solutions, with less volume of eluant solution. This influences the process costs as well as reduction of the volumes of spent eluants. In batch operations, the maximum S/L ratio is limited by practical implications, while higher ratios are possible in column applications.

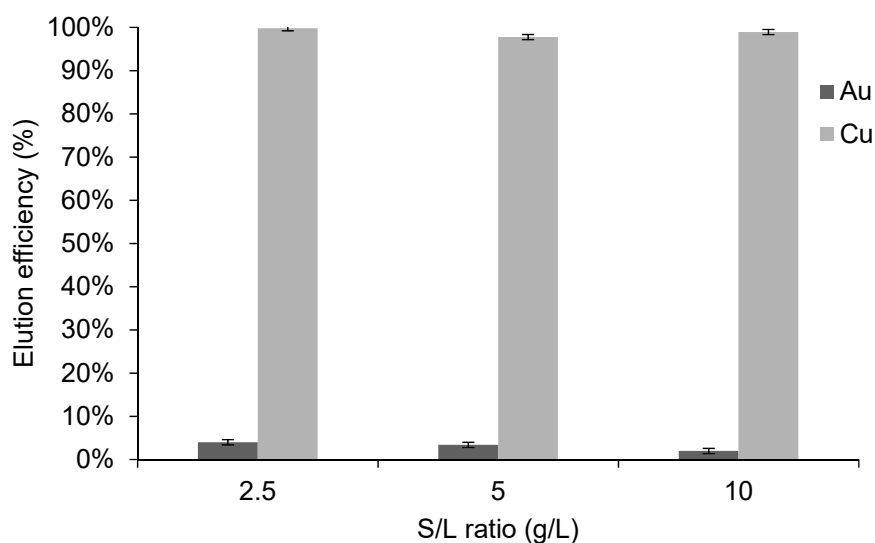


Figure 6-5. Effect of solid to liquid ratio on metal elution with 0.02 M EDTA at pH 6 and 25 °C after 15 minutes

6.4 Gold Elution using NaOH

6.4.1 Effect of NaOH Concentration

Gold elution efficiency of copper pre-eluted nanoparticles was investigated in the solutions consisting of different NaOH concentrations. The associated pH values in the solution were approximately 10, 11 and 12 for 0.0001M, 0.001 M and 0.01 M NaOH concentrations, respectively. The results are shown in Figure 6-6, and it is apparent that higher NaOH concentrations, hence higher pH values are favourable for increased gold elution efficiency. Based on the zeta potential studies, in a pH 12 solution, the adsorbent surface is negatively charged. This leads to a repulsion of the anionic gold thiosulfate complex by PEI-MNPs in 0.01 M NaOH (pH 12) solution. In a pH 11 solution (0.001M NaOH), the nanoparticle surface does not hold any charge as this is where the pH_{PZC} of PEI-MNPs. According to zeta potential analysis results, particle surface is positively charged at a pH of 10 (in a 0.0001 M NaOH solution). This explains the reason for different gold elution efficiencies at different NaOH

concentrations. Based on the selectivity and 100% gold elution efficiency, it was decided that 0.01 M NaOH would be suitable for all future elution experiments.

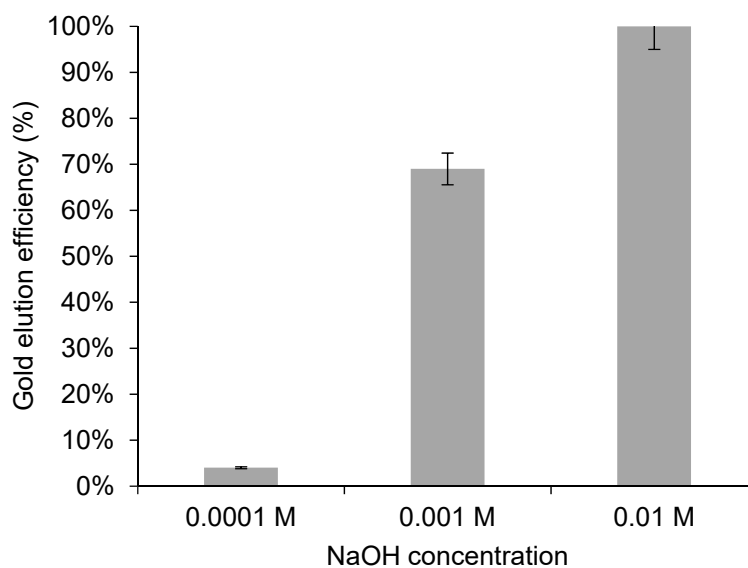


Figure 6-6. Effect of NaOH concentration on gold elution at 50 °C and 2.5 g/L of S/L ratio

6.4.2 Effect of Solution Temperature

Gold elution efficiency was evaluated at different temperatures ranging from 25 °C to 50 °C, as represented in Figure 6-7. The already copper pre-eluted adsorbent was subjected to gold elution in 0.01 M NaOH solutions at 2.5 g/L solid to liquid ratio. At a temperature of 50 °C, a 100% gold elution efficiency was achieved whilst this dropped slightly with a decrease in temperature. As mentioned in Section 5.6, the gold adsorption process was determined as exothermic, which means the lower temperatures are more appropriate for a higher gold adsorption efficiency. Therefore, higher temperatures should be useful for fast gold desorption. Sensitivity to temperature was only minor however, as 96% and 100% elution efficiency was achieved at 25 °C and 50 °C, respectively.

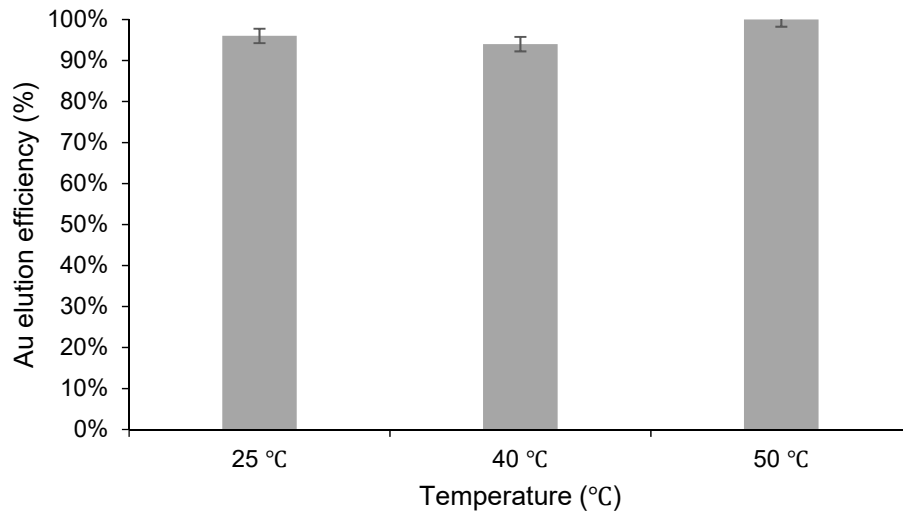


Figure 6-7. Effect of solution temperature on gold elution efficiency in 0.01 M NaOH solutions at 2.5 g/L of S/L ratio at 15 minutes.

6.4.3 Effect of Solid to Liquid Ratio

The solid to liquid ratio of the eluant solution was altered from 2.5 to 10 g/L by varying the solution volume. As represented in Figure 6-8, it was apparent that the S/L ratio does not have any influence on gold elution efficiency, as 100% gold elution was achieved irrespective of the S/L ratio for the tested range of 2.5 to 10 g/L. This confirms the possibility of using lower volumes of eluant solution which generate highly gold concentrated solutions for further processing that consume fewer amounts of chemicals and ultimately lower the processing costs.

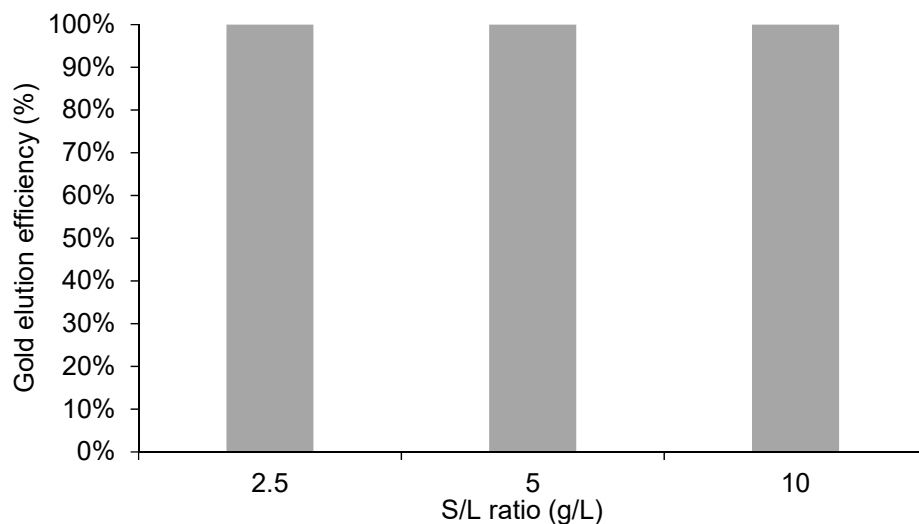


Figure 6-8. Effect of S/L ratio on gold elution efficiency in 0.01 M NaOH solutions at 50 °C

6.5 Elution Kinetics

6.5.1 Copper Elution Kinetics

Copper elution kinetics were investigated in 0.02 M EDTA solutions at different temperatures and results are shown in Figure 6-9. The S/L ratio was maintained at 2.5 g/L and sample aliquots were collected at different time intervals. Elution kinetics were fast irrespective of the temperature for 25-50 °C range. The equilibrium was achieved after 15 minutes. The elution efficiency was lower at 40 °C than at 25 °C and 50 °C.

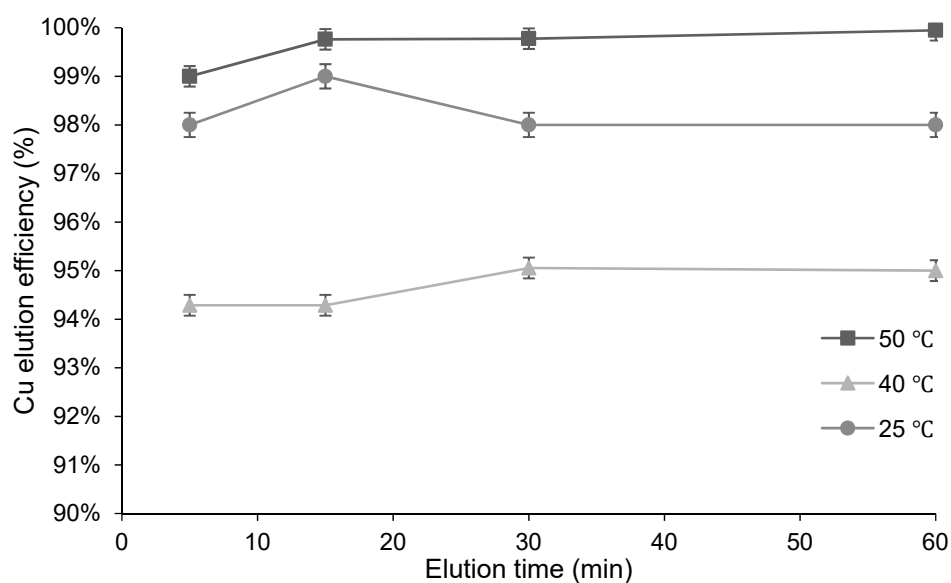


Figure 6-9. Copper elution kinetics at different temperatures (25, 40 and 50 °C), at pH 8 and 2.5 g/L S/L ratio

6.5.2 Gold Elution Kinetics

The kinetics of gold elution from already copper eluted nanoparticles were evaluated at different temperatures in diluted NaOH solutions at a pH of 12. The results are presented in Figure 6-10. It was apparent that the elution kinetics were rapid and almost 100% of adsorbed gold was eluted after only 5 minutes at 50 °C with no evidence of re-adsorption. Therefore, the time for complete elution was concluded as 15 minutes to err on the side of caution, and this time would be used for all future experiments. However, elution efficiency was higher at 25 °C than at 40 °C. This was reconfirmed by additional tests. The same behaviour was also observed in the copper elution stage.

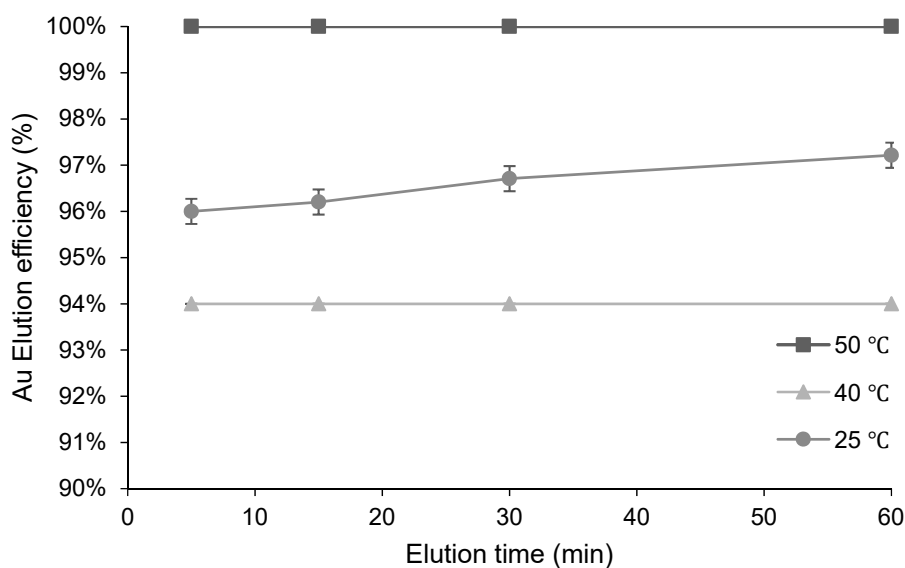


Figure 6-10. Gold elution kinetics at different temperatures (25, 40 and 50 °C), at pH 12 and 2.5 g/L S/L ratio

6.6 Reuse of the Adsorbent

Six consecutive adsorption-elution cycles were conducted to investigate the reusability of PEI-MNPs. Solution 1 was a synthetic leaching solution which consisted of free thiosulfate, gold and copper while Solution 2 was a pure gold thiosulfate solution. Metal-loaded PEI-MNPs (Solution 1) were magnetically separated, washed with deionised water and copper pre-elution was then performed, followed by gold elution. Only the gold elution step was performed for the PEI-MNPs used in Solution 2. The nanoparticles were subsequently washed with DI water, before being used for metal adsorption either in a fresh solution of Solution 1 or Solution 2. The solutions were analysed after each step and the results are shown in Figure 6-11. An approximate 12-15% drop in the adsorption efficiency was observed after six cycles in Solution 1. Interestingly, the adsorption efficiency was almost 100% in Solution 2 for up to six cycles.

According to the metal elution studies, almost 100 % gold and copper elution was achieved at the metal elution stage. The complete elution of gold and copper was also verified by particle analysis by acid digestion and XRF. No gold was found on metal eluted PEI-MNPs by acid digestion studies. The copper composition of metal eluted PEI-MNPs tested by XRF was almost same to that of bare MNPs. However, the complete elution of the sulfur species was not possible during copper and gold elution. Approximately 2 % of sulfur mass loaded remained on the adsorbent surface after the gold elution stage. The gradual loss of adsorption efficiency in Solution 1 is expected to occur as a result of the accumulation of uneluted sulfur species on the adsorbent. The preservation of adsorption efficiency in Solution 2 further

supports this conclusion. Solution 2 consists of only gold thiosulfate (no competitive ions available). Therefore, elution of 100% of gold was achieved and the PEI-MNPs does not have any uneluted species on them. But in the case of Solution 1, the competitively adsorbed sulfur can accumulate on PEI-MNPs. These uneluted sulfur will occupy the adsorption sites reducing the gold adsorption efficiency in subsequent cycles.

Moreover, a nanoparticle agglomeration phenomenon can also cause a reduction in adsorption efficiency, after several adsorption-desorption cycles. This ultimately causes a lowering of adsorption sites available, resulting in a reduction in adsorption efficiency. One may also think that, the loss of surface coating can cause a drop in adsorption efficiency in consecutive cycles. However, this is less likely to happen, as the adsorption efficiency is constant for up to six cycles in Solution 2. Considering all the facts, the main reason for the reduction in adsorption efficiency may be the accumulation of sulfur species on PEI-MNPs.

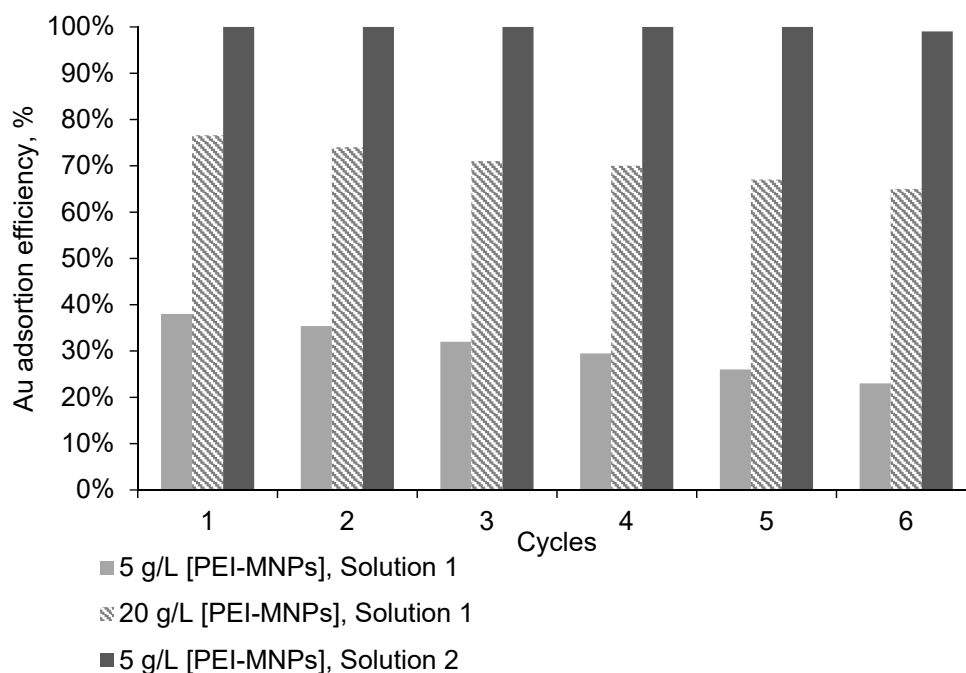


Figure 6-11. Reuse of eluted PEI-MNPs up to six cycles. The adsorption solutions consist of 10 mg/L gold, 20 mg/L copper and 0.1 M free thiosulfate (Solution 1) at 20 g/L adsorbent dosages and 10 mg/L gold thiosulfate (Solution 2) at 5 g/L adsorbent dosage at a pH value of 8 and 50 °C

6.7 Chapter Summary

Copper pre-elution was conducted by using 0.02 M EDTA solutions at pH 6, 25 °C for 15 minutes. Subsequent gold elution was successfully achieved in 0.01 M NaOH solution at pH 12, 50 °C after 15 minutes. Selective gold and copper elution was accomplished by selected eluants at low concentrations. This is one of the major positive outcomes achieved by this

study. Copper elution was anticipated to occur by formation of a Cu-EDTA complex. Physically adsorbed gold was desorbed as the adsorbent changed its surface charge to a negative state at pH 12 solutions, in the gold elution process. Both gold and copper elution was favoured by higher eluant concentration. Neither solution pH nor S/L ratio had a considerable effect on the elution of both gold and copper.

The outcome of the reuse experiments was encouraging. However there is ample room for improvement, such as finding a method to elute the sulfur species. The elution of sulfur was not considered, as any sulfur elution was not observed at the gold elution stage. This means that there is no risk of contaminating the gold eluant solution. However, sulfur elution could have been beneficial for the effective reuse of PEI-MNPs. Accordingly, it is foreseen that adsorption efficiency will be maintained for further cycles.

Chapter 7 Leaching, Metal Recovery and Elution Experiments with Gold Ore Samples

7.1 Introduction and Chapter Objectives

This chapter consists of information on the processing of real ore samples; from leaching to gold elution. As all the previously mentioned results are based on synthetic leach solutions, the investigation into the behaviour and performance of PEI-MNPs in real world conditions is important. Ore samples from Cortez ore, located in Nevada, USA were used for leaching. As this particular ore originates from the Nevada region, the characteristics should be more or less comparable to the refractory gold ores discussed in this study. The resultant leachate was utilised for subsequent adsorption experiments. Metal loaded PEI-MNPs were subjected to a two-step metal elution process identical to the method described in Section 3.12. The Central composite design (CCD) and response surface methodology (RSM) that used for adsorption experiment design and process optimisation, respectively are also briefly stated. The competitive adsorption and elution of gangue mineral/impurities was also evaluated.

7.2 Leaching

As the optimisation of leaching is not within the scope of this study, the ore sample was leached under fixed conditions comparable to the thiosulfate - air leaching system, without any changes. Calcium thiosulfate (equivalent to 0.1 M) and copper (equivalent to 20 ppm) as $\text{CuSO}_4 \cdot 5\text{H}_2\text{O}$ were dissolved in DI water and used for the leaching. The solid to liquid ratio was set to 40% and leaching was conducted at a pH of 8-8.5 and at a temperature of 50 °C for 48 hours. A slight drop in the solution pH to 7.67 was observed immediately after mixing the ore with the solution and this was again adjusted to 8.5 by using hydrated lime.

The ore sample was characterised by QXRD and XRF/LECO techniques and the analysis results are presented in Table 7-1 and Table 7-2, respectively. The gold head grade was 3.74 ppm determined by fire assay. The total carbon content of the ore derived by XRF was 3.71% and the organic carbon composition was 0.18%. This ore was considered to be mild refractory as cyanidation yielded only 86-88% of low gold recovery.

Table 7-1. Mineralogical composition of ore sample by QXRD analysis

Mineral	Quartz	Mica group	Dolomite	Plagioclase
Composition (%)	35	14	41	10

Table 7-2. Elemental composition of the ore sample by XRF and LECO combustion analysis

Element	Si	Ca	Al	C	Fe	Mg	Mn	S	As	Zn	Ni	Cu	Pb
Composition (%)	23.2	12.5	4.2	3.7	2.9	1.2	0.08	0.05	0.06	0.03	0.02	0.01	0.01

The gold content of the ore sample was 3.74 ppm according to acid digestion analysis. The concentration of elements in the leachate after 48 hours were analysed by AAS (Au and Cu only) and ICP-MS (other elements), as listed in Table 7-3. As the sole purpose of leaching is to obtain a gold containing solution for the adsorption, no attempt was made to achieve maximum leaching efficiency. Some of the gangue minerals observed in the ore sample have also been dissolved in the leaching solution. Although other elements such as As, Fe, Mg, Ni, Pb and Zn were detected in the ore sample, the concentrations in the leachate were below the detection limit (BDL) possibly due to the availability only in trace levels or an inability to leach by the thiosulfate. The decrease in copper concentration in the leachate after 48 hours was possibly due to precipitation as hydroxide, sulfide or oxide derivatives in the absence of sufficiently strong ligands to complex with copper at pH 8 (Al Subu et al. 2001, Dai et al. 2017).

Table 7-3. Concentration of elements in the filtered solution after 48 hours of leaching

Element	Au	Cu	Ca	S	Mn	Si	Na
Concentration (mg/L)	1.55	5.39	2760	5360	1.0	18	80

7.3 Adsorption

The adsorption behaviour of both gold and copper is considered here due to the presence of copper being unavoidable in this particular thiosulfate leaching system. As mentioned in Section 3.14.3, experiments were designed based on CCD. The independent variables were adsorbent dosage (X_1) in g/L, adsorption time (X_2) in minutes and the solution temperature (X_3) in °C, while the response variables were set as adsorption efficiencies (%) of gold (Y_{Au}) and copper (Y_{Cu}). The resultant gold and copper adsorption efficiencies (responses) are listed in Table 7-4, and will be discussed in Sections 7.4.1 and 7.4.2.

Table 7-4. Experiment design matrix and corresponding gold and copper adsorption efficiencies

Test run	Independent variables (coded)			Independent variables (actual)			Response variables	
	X ₁	X ₂	X ₃	X ₁	X ₂	X ₃	Y _{Au}	Y _{Cu}
1	+1	+1	+1	30	45	50	79%	86%
2	-1	+1	+1	10	45	50	52%	80%
3	+1	-1	+1	30	15	50	79%	87%
4	-1	-1	+1	10	15	50	53%	85%
5	+1	+1	-1	30	45	30	79%	90%
6	-1	+1	-1	10	45	30	54%	90%
7	+1	-1	-1	30	15	30	76%	91%
8	-1	-1	-1	10	15	30	50%	92%
9	+1.68	0	0	36.8	30	40	84%	88%
10	-1.68	0	0	3.1	30	40	28%	90%
11	0	+1.68	0	20	55	40	72%	87%
12	0	-1.68	0	20	5	40	63%	93%
13	0	0	+1.68	20	30	56.8	68%	81%
14	0	0	-1.68	20	30	23.1	69%	92%
15	0	0	0	20	30	40	70%	87%
16	0	0	0	20	30	40	70%	87%
17	0	0	0	20	30	40	70%	87%
18	0	0	0	20	30	40	69%	87%
19	0	0	0	20	30	40	70%	87%
20	0	0	0	20	30	40	70%	87%

X₁ – Adsorbent dosage given in g/L in actual values,

X₂ – Time given in minutes in actual values,

X₃ – Temperature given in °C in actual values;

Y_{Au} – Gold adsorption efficiency (%)

Y_{Cu} – Copper adsorption efficiency (%)

According to a solution analysis using ICP-MS, some impurities such as S, Si, Ca, Mn and Na will be present in the leaching solution. The competitive adsorption of those elements on to PEI-MNPs is possible if the conditions are favourable. However gangue minerals are ore-specific and would be different based on the ore composition. Particle analysis by the XRF method revealed the competitive adsorption of Si, Ca and S onto PEI-MNPs. Furthermore, sulfur adsorption was relatively higher than that of other gangue minerals. Sulfur speciation analysis was not conducted, but only the total sulfur concentration in the solution, as the solutions are unstable and speciation can rapidly change. Sulfur can be available in the leachate as thiosulfate or its oxidised products such as polythionate or sulfate. The competitive adsorption of the aforementioned anionic sulfur species is possible. In addition, there will be

availability of calcium as Ca^{2+} cations and silica as silicate in the solution is anticipated. Furthermore an intermediate product of $\text{Au}_2(\text{S}_2\text{O}_3)_2\text{Ca}$ is also possible prior to the formation of the $\text{Au}_2(\text{S}_2\text{O}_3)_2^{3-}$ complex (Senanayake 2012). In general, anionic species can be predominantly adsorbed via electrostatic attraction, whilst positively charged ions may adsorb to the electric double layer to achieve the electron neutrality.

The adsorption efficiency derived from solution analysis and particle analysis was significantly different, which implies only a partial adsorption of those impurities to the adsorbent, as summarised in Table 7-5. For instance, sulfur adsorption efficiency based on solution analysis was 10.8%, while the ultimate sulfur adsorption was only 3.25% based on the particle analysis. Likewise, calcium adsorption efficiency was 6.88% and 1.72% based on solution analysis and particle analysis, respectively. The results correspond to a test solution of 20 g/L adsorbent dosage, at a temperature of 40 °C and at a pH of 8 and 30 minutes of adsorption time. Despite the full adsorption of Si, only partial adsorption of calcium and sulfur species was observed. The difference between the particle and solution analysis may explain the possible precipitation of those elements in addition to the adsorption. Any signs of sodium or manganese adsorption onto PEI-MNPs were not detected.

Table 7-5. Adsorption efficiency of other elements available in leaching solution based on particle analysis and (XRF) and solution analysis (ICP-MS)

Adsorption efficiency (%)	Ca	S	Si	Na	Mn
Particle analysis (XRF)	1.72	3.25	100	0	0
Solution analysis (ICP-MS)	6.88	10.8	67	3	80

7.4 Response Surface Methodology

The data obtained from CCD experiments was statistically analysed using Design-Expert 11 software. The resulting analysis of variance (ANOVA) of regression analysis was used to check the significance of the model. The p-values associated with linear, quadratic and interaction variables were used to decide the significance of each term. The insignificant variables where p- value was > 0.05 were eliminated.

According to Myers et al. (2016), it is crucial to check the adequacy of the model to verify that it adequately approximates to the real system. Several techniques have been proposed to check the adequacy of the fitted model such as residual analysis, scaling residuals, F-value and adequate precision. F value compares the mean squares to the residual mean squares. Adequate precision is signal to noise ratio and it compares the range of the predicted values at the design points to the average prediction error. Adequate precision was also considered to check the

adequacy of the predicted model and a ratio higher than four is preferred. The equation of the model was derived by including the coefficients of intercept and the significant variables (p value < 0.05).

7.4.1 Gold Adsorption

Gold adsorption efficiency under different process conditions, as listed in Table 7-4, were statistically analysed using RSM. As mentioned before, Design Expert (version 11) software was employed for the model fitting, graph generation and optimisation. The statistical significance of the model and individual and interactive parameters were evaluated using variance analysis (ANOVA) and coefficient of determination (R^2). The ANOVA and regression statistics of the quadratic model for gold adsorption is represented in Table 7-6 and in Table 7-7, respectively. The R^2 value of the model is 0.979, whereas adjusted R^2 and the predicted R^2 values are in reasonable agreement where the difference is less than 0.2. The adequate precision indicates the signal to noise ratio and a value higher than four is desirable (Bilici Baskan and Pala 2010). The high value of 26.4 of the model indicates an adequate signal and hence the adequacy of the model. Furthermore, the high F value of the model (52.5) and p value less than 0.05 suggests that the model is significant. Based on the p values, only the variables X_1 and X_1^2 are significant for gold adsorption.

Table 7-6. Analysis of variance (ANOVA) for the quadratic model of gold adsorption

Source	Sum of Squares	Degree of freedom	Mean Square	F-value	p-value
Model	3217.69	9	357.52	52.53	< 0.0001
X_1 -Adsorbent dosage	2875.88	1	2875.88	422.53	< 0.0001
X_2 -Time	32.71	1	32.71	4.81	0.0531
X_3 -Temperature	0.39	1	0.3935	0.058	0.8148
$X_1 X_2$	0.00	1	0.00	0.00	1.00
$X_1 X_3$	0.50	1	0.50	0.073	0.79
$X_2 X_3$	8.00	1	8.00	1.18	0.30
X_1^2	298.66	1	298.66	43.88	< 0.0001
X_2^2	3.41	1	3.41	0.50	0.49
X_3^2	0.25	1	0.25	0.037	0.85
Residual	68.06	10	6.81		
Pure Error	0.83	5	0.17		
Corrected Total	3285.75	19			

Table 7-7. Coefficients of determination for the quadratic model of gold adsorption

Regression Statistics	
R ²	0.979
Adjusted R ²	0.961
Predicted R ²	0.844
Adequate precision	26.5

After elimination of the insignificant factors, the quadratic model for gold adsorption onto PEI-MNPs can be expressed by equation (7-1). The terms with positive coefficients in the equation increase the response variable, while negative coefficients decrease the response variable (Petrović et al. 2018). Accordingly, an increase in adsorbent dosage (X_1) gives an increase in the gold adsorption efficiency. However the negative coefficient for X_1^2 term indicates a decrease in adsorption efficiency at higher adsorbent dosages.

$$Y_{Au}(\%) = 69.78 + 14.51X_1 - 4.55X_1^2 \quad (7-1)$$

The interaction of independent variables on gold and copper adsorption is illustrated in Figure 7-1, Figure 7-2 and Figure 7-3. The axes are marked with coded values. As mentioned above and as illustrated in the figures below, the adsorbent dosage is most influential on gold adsorption efficiency. The increase in adsorption dosage clearly increased gold adsorption efficiency. As an example, an increase in adsorbent dosage from 3.1 g/L to 36.8 g/L resulted an increase in gold adsorption efficiency from 28% to 84%. The increase in adsorption dosage facilitated the increased availability of adsorption sites and hence the reduced competitiveness among the adsorbates.

The shapes of the response surfaces demonstrate that neither time (X_2), temperature (X_3) nor interaction of temperature and time (X_2X_3) have an influence on gold adsorption. In summary, the changes of adsorption in gold increased monotonically with changes in the variable.

The response surfaces corresponding to copper adsorption (Figure 7-1, Figure 7-2 and Figure 7-3 left side) show that the short adsorption times and lower temperatures support higher copper adsorption efficiencies. Furthermore, the combined effect of adsorbent dosage and temperature shows a positive effect on copper adsorption.

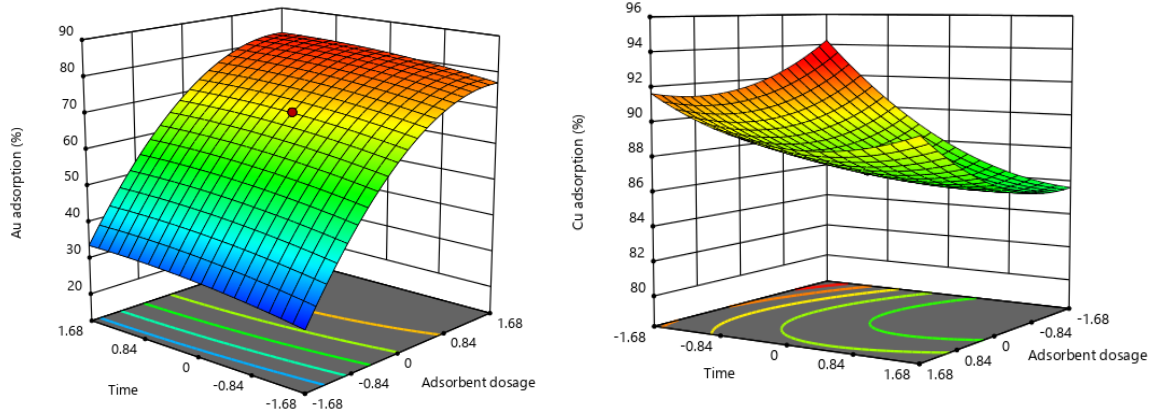


Figure 7-1. Response surfaces of interactive effect of adsorbent dosage and time on gold adsorption efficiency (left) and copper adsorption efficiency (right)

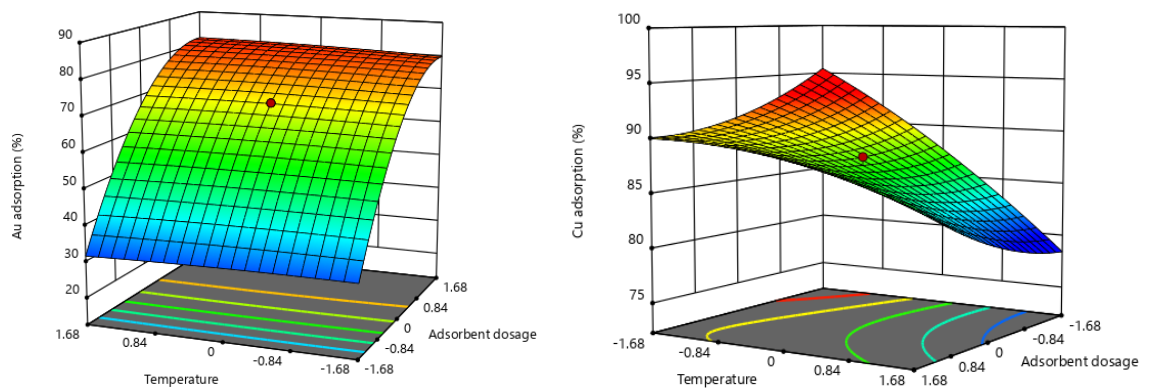


Figure 7-2. Response surfaces of interactive effect of adsorbent dosage and temperature on gold adsorption efficiency (left) and copper adsorption efficiency (right)

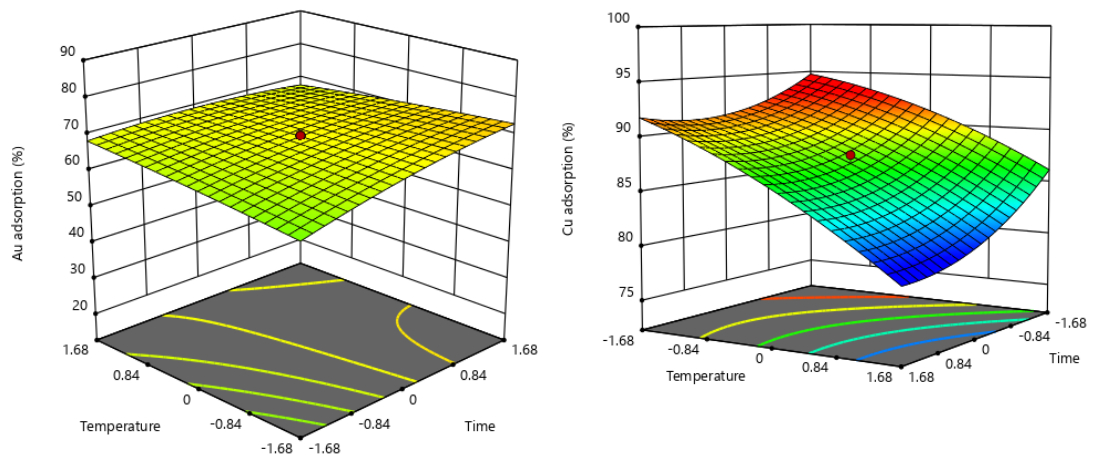


Figure 7-3. Response surfaces of interactive effects of temperature and time on gold adsorption efficiency (left) and copper adsorption efficiency (right)

Figure 7-4 represents the relationship between gold and copper adsorption efficiency values predicted by the respective quadratic models, and the experimental results. The graph shows

a close proximity of experimental and predicted values for gold adsorption, which verifies the validity of the model.

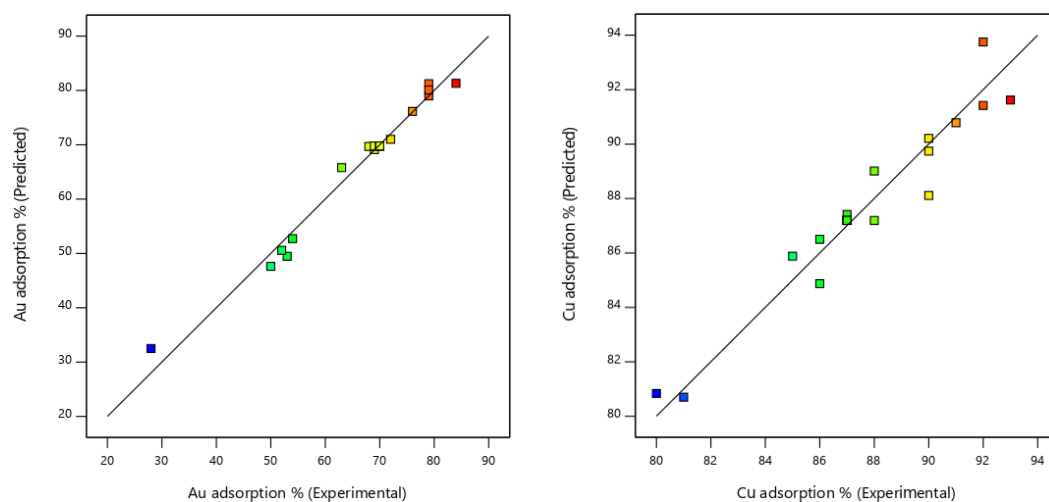


Figure 7-4. Predicted Vs actual values of gold adsorption (left) and copper adsorption (right)

7.4.2 Copper Adsorption

ANOVA and R² values for the quadratic model of copper adsorption are illustrated in Table 7-8 and

Table 7-9, respectively. Based on the model p value and F value the model is significant. The R² value of the model is 0.933. However the predicted R² value is not close to the adjusted R² value where the difference is greater than 0.2. This may indicate a large block effect. The adequate precision is 15.5 which represents the adequacy of signal.

Table 7-8. Analysis of variance (ANOVA) for the quadratic model of copper adsorption

Source	Sum of Squares	Degree of freedom	Mean Square	F-value	p-value
Model	198.05	9	22.01	15.5	< 0.0001
X ₁ -Adsorbent dosage	0.9683	1	0.97	0.68	0.427
X ₂ -Time	31.60	1	31.60	22.32	0.0008
X ₃ -Temperature	138.56	1	138.56	97.90	< 0.0001
X ₁ X ₂	3.12	1	3.12	2.21	0.17
X ₁ X ₃	10.12	1	10.12	7.15	0.023
X ₂ X ₃	1.13	1	1.13	0.795	0.397
X ₁ ²	3.37	1	3.37	2.38	0.154
X ₂ ²	6.29	1	6.29	4.44	0.061
X ₃ ²	2.31	1	2.31	1.63	0.23
Residual	14.15	10	1.42		
Pure Error	0.83	5	0.167		
Corrected Total	212.20	19			

Table 7-9. Coefficients of determination for the quadratic model of copper adsorption

Regression Statistics	
R ²	0.933
Adjusted R ²	0.873
Predicted R ²	0.510
Adequate precision	15.5

The quadratic model for copper adsorption onto PEI-MNPs can be expressed by equation (7-2).

$$Y_{Cu} = 87.19 - 1.52X_2 - 3.18X_3 + 1.125X_1X_3 \quad (7-2)$$

In contrast to gold adsorption, X_2 , X_3 and X_1X_3 significantly affect copper adsorption. In brief, lower temperatures and short adsorption durations favoured higher copper adsorption. The relationship between experimental and predicted values of copper adsorption efficiency is represented in Figure 7-4 (right). It shows that the correlation is lower than that of gold. This observation is more compatible with the lower R² values for copper adsorption than gold adsorption.

7.4.3 Optimisation of Parameters for Maximum Gold Adsorption

In optimum conditions, gold adsorption efficiency should reach maximum value. The adsorbent dosage was the only variable significantly influencing the efficiency of gold adsorption. As the interaction between the parameters is not significant for gold adsorption, higher adsorbent dosage values will enhance gold adsorption. Copper adsorption is not encouraged in this system, but it was unavoidable, as the functional amine groups in PEI and copper show an inherent attraction to each other. However, the selective pre-elution of copper could successfully resolve the potential contamination of gold by copper. In general the adsorbent dosage (X_1) itself is not a significant factor for copper adsorption, but the interaction of adsorbent dosage and temperature ($X_1 X_3$). Higher temperatures are detrimental to the copper adsorption.

The criteria followed for the optimisation is depicted in Table 7-10. Lower and upper range values were set for all the input variables, from -1.68 to + 1.68 (the coded values, mentioned in Table 3-1). As mentioned previously, the main purpose of optimisation is to maximise gold adsorption. Copper adsorption was ignored in the first criteria and set as minimal in the second. Importance was chosen as ranging from 1 to 5 and this denotes the relative priorities allocated for each variable to achieve the chosen goal (Mpinga et al. 2017). The optimum values

predicted by the inbuilt optimisation tool of Design Expert software for maximum gold adsorption (criteria 1) is 35 g/L adsorbent dosage, 55 minutes time and a temperature of 23 °C. If copper adsorption should be minimised, the optimum conditions would be 25 g/L adsorbent dosage, 46 minutes time and a temperature of 56 °C. However, several options are available based on the requirements and the option with highest desirability was selected.

Desirability function is an established method for allowing simultaneous determination of optimum values for several input variables to achieve a desired goal. It is an objective function ranging from zero to one (Myers et al. 2016). The desirability of the predicted conditions is presented in Figure 7-5. The values imply how well the variables satisfied the selected criteria. A value closer to one is recommended. The desirability of gold adsorption and copper adsorption, as well as combined desirability, is closer to 1 which verifies the meeting of selected criteria.

Table 7-10. Optimisation criteria

Parameter	Criteria 1	Criteria 2	Lower Limit	Upper Limit	Importance
Adsorbent dosage	in range	in range	-1.68	1.68	3
Time	in range	in range	-1.68	1.68	3
Temperature	in range	in range	-1.68	1.68	3
Au adsorption	maximise	maximise	50	85	5
Cu adsorption	none	minimise	80	93	4

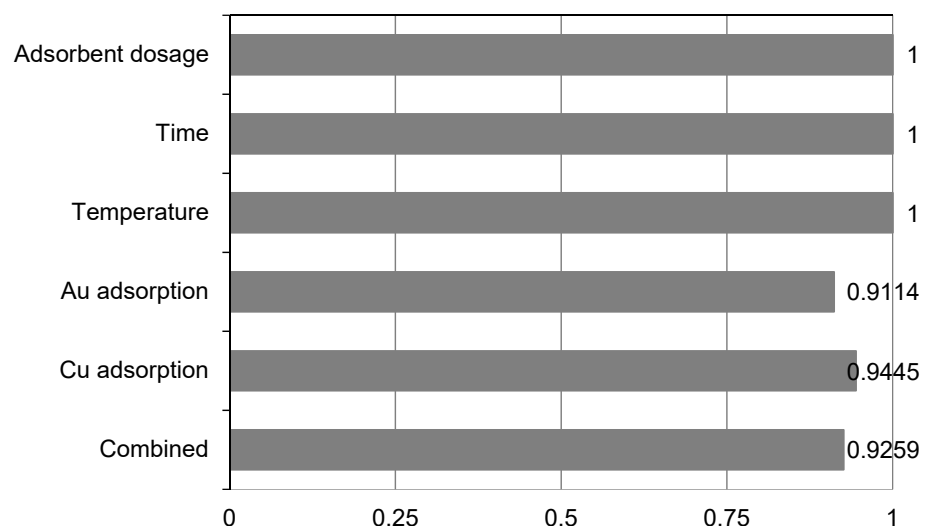


Figure 7-5. Desirability of satisfying the selected optimisation criteria 2

7.4.4 Validation Experiments

In order to verify the accuracy of the model, some additional reconfirmation experiments were carried out. The selected test conditions were slightly different to those in the CCD test runs. The results given in Table 7-11 indicate that at adsorbent dosages within the model design range (3-30 g/L), the predicted values of gold adsorption are in very close agreement with the experimental values. The deviation of copper adsorption efficiency is slightly higher than that of gold. Therefore, it can be concluded that the model is valid within the range of independent variables used for the model design.

Table 7-11. Actual vs predicted values of reconfirmation experiments

X ₁ (g/L)	X ₂ (min)	X ₃ (°C)	Au adsorption efficiency (%)		Cu adsorption efficiency (%)	
			Actual	Predicted	Actual	Predicted
5	30	25	38	38	90	94
10	30	25	50	51	90	93
10	60	50	49	50	82	80
20	15	50	64	69	86	86
30	5	30	76	74	92	91

7.5 Elution

7.5.1 Gold and Copper Elution

The same two step metal elution process, which was used to elute metal from synthetic leaching solutions tests was applied in these experiments. The competitive loading of copper necessitates a copper pre-elution step to ensure the purity of the final gold product. Almost 100% copper elution was achieved using 0.02 M EDTA for 15 minutes. Copper elution efficiency was independent of the solid to liquid ratio (S/L ratio) within the tested range of 2.5 to 10 g/L (results not shown). EDTA can form stable complexes with many of the base metals. The stability constants of Cu-EDTA complex and Ca-EDTA complex are reported as 18.7 and 10.6, respectively (Martell and Hancock 1996).

Gold elution was accomplished using 0.01 M NaOH solutions at different S/L ratios and the elution time varied from 15 minutes to 3 hours, as depicted in Figure 7-6. Gold elution efficiency was low at a higher S/L ratio and substantially increased at a S/L ratio of 2.5 g/L. The effect of time beyond 15 minutes was insignificant. Therefore, the ideal elution conditions for gold elution were set as 0.01 M NaOH (approximately pH 12) for 15 minutes and at a S/L ratio of 2.5 g/L. The mechanism behind gold elution may be proposed as the loss of

electrostatic attraction at higher pH solutions. The pH_{PZC} of PEI-MNPs used in this study was determined previously as pH 11. At pH values higher than that, the adsorbent holds a negative surface charge. This leads to desorption of gold from the PEI-MNPs surface.

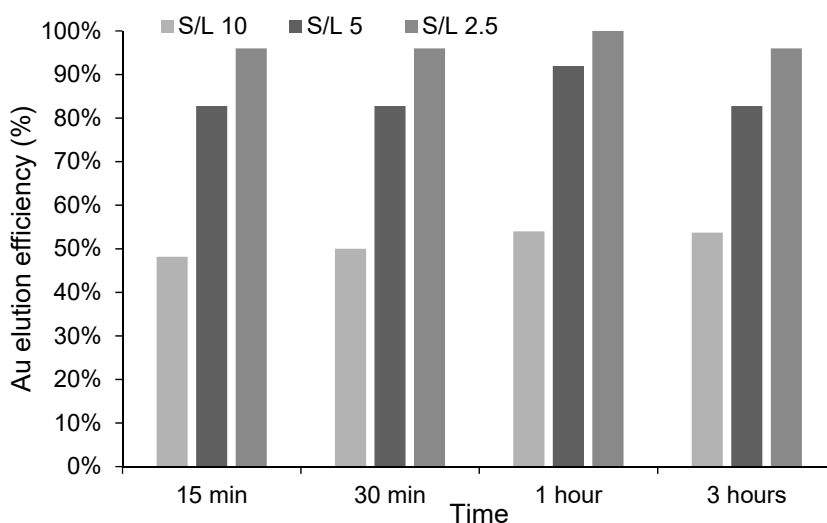


Figure 7-6. Gold elution efficiency at different S/L ratio

7.5.2 Elution of Other Elements

Other elements, which were available in the leachate and then competitively adsorbed onto PEI-MNPs are also considered and the results are presented in Table 7-12. The resultant copper elution efficiency was 98-100% at the copper pre-elution stage. According to the solution analysis with ICP-MS and particle analysis with XRF, 100% calcium elution and 68% sulfur elution was accomplished during the copper pre-elution stage. It should be noted that most importantly, the elution of many of the other species was not identified during gold elution, except for some sulfur and silica elution. It is foreseen that the corresponding species of the aforementioned two elements would not have any negative effect on the gold electrowinning process, hence the purity of the final gold product (Kasper et al. 2016).

Table 7-12. Elution efficiency of gold, copper and other competitively adsorbed elements

Element	Elution efficiency (%)		
	Cu pre elution stage ¹	Au elution stage ²	Overall
Au	0-2	98-100	100
Cu	98-100	0-3	100
Si	0	≈18	≈18
Ca	100	0	100
S	68	≈24	≈92

¹ eluant used was 0.02 M EDTA, pH 6, 15 min

² eluant used was 0.01 M NaOH, pH 12, 3 hours

7.5.3 Comparison with Synthetic Leaching Solutions

Gold elution behaviour shows a slight deviation from the conditions observed in gold elution from PEI-MNPs used for synthetic leaching solutions (Section 6.4). Gold elution was independent from the S/L ratio in synthetic leach tests, whilst it is highly dependent on the S/L ratio in gold elution from real ore sample tests. A possible explanation may be the competitive adsorption of impurities, hence the requirement of more eluant solution volume, i.e., a high S/L ratio. The performance of the copper eluant did not change in either circumstance. The stable complex formation of copper with EDTA may be the reason.

7.6 Chapter Summary

Extending the use of PEI-MNPs to recover gold from a gold ore leachate was considered in this chapter. Although the laboratory scale adsorption experiments conducted with synthetic leaching solutions showed considerable promise, the evaluation of the performance of PEI-MNPs in actual gold ore leachates was worthwhile. Compared to synthetic leaching solutions, the gold ore leachates are more complex solutions, as a consequence of complex ore mineralogy. Gangue minerals can also dissolve in the solution and there is a high chance of competitive adsorption.

The systematically designed experiments were used to investigate the effect of adsorbent dosage, along with time and temperature on gold and copper adsorption efficiency. Gold adsorption was mainly dependent on adsorbent dosage, and the other two variables did not show any considerable influence. The optimum conditions predicted by the model for maximum gold adsorption and minimum copper adsorption were 25 g/L adsorbent dosage for 46 minutes at a temperature of 56 °C. Validation experiments confirmed the suitability of the model for predicting gold and copper adsorption within the range considered.

Selective metal elution was attempted while the majority of impurities eluted at the copper pre-elution stage. Approximately 18% of silica and 24% of total sulfur was detected in the gold eluant together with 98% - 100% gold elution. According to the literature, it is foreseen that the available Si and S would not have any detrimental effect on the gold electrowinning process. The efficacy of using the same eluant system for both synthetic systems and actual ore systems is of great value.

Chapter 8 Conclusions and Recommendations

The purpose of this study was to investigate the ability of polyethylenimine functionalised magnetic nanoparticles to recover anionic gold complexes from alkaline thiosulfate leaching solutions. In order to achieve this, the nanoparticles were functionalised, characterised and used for gold adsorption. This was followed by gold elution and reuse of the adsorbent. The objectives of this study were:

- to functionalise the iron oxide magnetic nanoparticles with polyethylenimine to adsorb anionic gold thiosulfate complex in alkaline pH solutions (as described in Section 8.1)
- to characterise nanoparticles before and after surface functionalisation and after the adsorption process (as described in Section 8.2)
- to evaluate the influence of different reagent concentrations and experimental conditions on gold adsorption efficiency from thiosulfate leaching solutions, onto functionalised MNPs (as described in Section 8.3)
- to determine the gold adsorption mechanism onto functionalised MNPs through adsorption isotherm, kinetics and thermodynamic analyses (as described in Section 8.4)
- to selectively elute the gold from MNPs, and to reuse the adsorbent (as described in Section 8.2).

The extent to which the proposed objectives have been achieved and the specific conclusions that were drawn from the experiment results will be discussed below. The discussion will also cover the perceived limitations associated with the proposed technology. Furthermore, some suggestions and recommendations for any future work will also be included.

8.1 Functionalisation of Magnetic Nanoparticles

Commercially available iron oxide magnetic nanoparticles were used as the magnetic core, to be functionalised with suitable functional groups to fit the purpose. Based on a comprehensive review of the literature and some preliminary trial and error attempts, a core-shell nanoparticle coating was conducted by using citrate molecules as the intermediate layer and polyethylenimine groups as the outer layer. The prepared magnetic nanoadsorbent was

denoted as **PEI-MNPs**. The selection of functional groups was based on the conditions of the particular leaching system, which operates at alkaline pH solutions, at elevated temperatures and under oxidising conditions. Iron oxide was used as the magnetic core due to its high saturation magnetisation, biocompatibility, being environmentally benign, abundant and relatively low in cost. A trisodium citrate intermediate coating was able to provide a highly negative surface charge to the MNP surface. This was useful to deagglomerate the MNPs and to attach cationic PEI as the outer layer. The high cationic charge density, high point of zero charge, preservation of magnetisation properties of the magnetic core and biocompatibility were the main reasons for using PEI as the surface functionalisation agent to adsorb gold. The preparation process was straightforward and simple. The adsorbent was functionalised in order to promote the physical adsorption of gold, which was beneficial for subsequent gold elution processes.

The agglomeration tendency of nanosized particles, especially magnetic nanoparticles is a global issue, however it can be solved to a certain degree with various techniques. In this study, ultrasonic dispersion was attempted with the aid of an ultrasonic probe in different dispersion media at different pH values. According to the results shown in Table 8-1, dispersion was considerably better in trisodium citrate solutions than in DI water. Longer ultrasonic durations favoured better dispersion, however nanoparticle concentration was not a considerable factor. Although the well- dispersed particles can re-agglomerate after drying in the oven, ultrasonication was able to re-disperse them to an acceptable level. Provided that ultrasound is reproducible, if applied to an identical solution formulation and with identical ultrasonication process parameters, the same energy per volume can produce an identical result. That means that the scaling up from bench scale to commercial scale is simplified.

Table 8-1. Hydrodynamic sizes of nanoparticles after ultrasonic dispersion

Sample description	Intensity weighted Z-Ave (nm)	PdI
Bare MNPs, before ultrasonication	2682	0.342
Bare MNPs, 600S ultrasonication	112.3	0.389
PEI-MNPs	174.3	0.254
Metal adsorbed MNPs	208.5	0.264

8.2 Characterisation of the Adsorbent

The adsorbent was characterised to understand its properties and to check the effectiveness of the preparation process at different stages of the functionalisation and after adsorption. The SEM, TEM and DLS techniques were employed for size and morphology measures, whilst, XPS and FT-IR methods provided valuable information about surface elemental composition and functional groups. Atom probe tomography was used for the analysis of the atomic structure of the adsorbent. Further characterisation of the adsorbent was conducted by using XRD and Raman spectroscopy for crystal structure, SQUID for magnetic measurements, TGA and DSC for thermal properties and degradation, BET for specific surface area and zeta potential analysis for the surface charge.

The aforementioned characterisation methods revealed that;

- The nanoparticles demonstrated two different shapes and showed a bimodal size distribution. The approximate size of the smaller particles varied from 13-20 nm and the larger particles were in the range of 36-84 nm, in dry powder form. Only a slight particle size increase (less than 2 nm) was observed after the coating process, and this showed compatibility with other studies (Li et al. 2013). The hydrodynamic size increased slightly after coating, as a result of the attachment of functional groups.
- The zeta potential measurement depicted that the point of zero charge (pH_{PZC}) of the adsorbent significantly increased to pH 11, following the surface coating with PEI. This was beneficial for anionic gold thiosulfate adsorption from an alkaline aqueous solution.
- Based on the XRD and QXRD analysis, the crystal structure of the uncoated MNPs was a mixture of pure iron oxide mainly consisting of magnetite and maghemite. An insignificant amount (less than 1%) of hematite was also identified. No other contaminants were detected. The crystalline structure did not change after surface functionalisation which confirms non-formation of any other crystalline phases during this process.
- XPS and FT-IR studies revealed the presence of nitrogen (as amine groups) on the surface which confirms the success of the PEI coating process. The reconstructed APT images also confirmed the presence of nitrogen atoms on iron oxide surfaces.
- Furthermore, APT results revealed successful gold adsorption onto the PEI-MNPs surface. The competitive adsorption of copper and sulfur species was also confirmed.

Peaks related to gold and sulfur were observed in XPS spectra of metal adsorbed samples which verifies the adsorption of these species.

- Magnetisation measurements revealed that the saturation magnetisation reduced only slightly after the PEI coating. Saturation magnetisation was 60.5, 52.3 and 50.5 emu/g for bare MNPs, PEI-MNPs and Au-PEI-MNPs, respectively.
- TGA results indicated that 10% of weight of the adsorbent are held by functional groups.
- According to BET analysis, the specific surface area of the adsorbent was 99 m²/g.

8.3 Evaluation of the Influence of Adsorption Process Parameters on Gold Adsorption Efficiency

8.3.1 Adsorption from Synthetic Leaching Solutions

The effect of thiosulfate concentration, copper concentration, adsorbent dosage and solution pH on gold adsorption efficiency was investigated by conventional experiment design; changing one parameter at a time while keeping other parameters constant. Adsorption isotherm, adsorption kinetics and adsorption thermodynamics were also evaluated in synthetic leaching solutions.

The concentration of free thiosulfate anions was the most detrimental factor to gold adsorption, as a result of the competitive adsorption of thiosulfate anions and their oxidation products such as polythionate anions. However, sulfur adsorption, as any sulfur compound, was less than 3%. Although some copper adsorption onto PEI-MNPs was observed, the initial copper concentration was not a significant factor, at a 95% confidence level. However, copper is believed to have an indirect influence in lowering gold adsorption by oxidising thiosulfate in the solution.

An increase in adsorbent dosage enhanced gold adsorption significantly. The availability of ample adsorption sites and hence the reduced competition could be the reason for higher gold adsorption at higher adsorption dosages. The solution pH did not show any considerable effect on the final loading for the tested pH range of 5 - 8.8. Lower temperatures favoured higher gold loading, which confirms the exothermic nature of the adsorption process.

Therefore, in essence, maximum gold adsorption is facilitated by maintaining lower free thiosulfate concentration, using higher adsorbent dosages and lowering temperatures in the solutions. Shorter contact times between the adsorbent and the adsorbate solution is preferred, according to kinetics studies. This results in a higher gold loading and relatively lower adsorption of competitive ions.

8.3.2 Adsorption from Gold Ore Leaching Solutions

Gold ore samples from Cortez ore, Nevada, USA were leached and the resultant solution was used for the adsorption studies. Experiments were designed based on the Central Composite Design (CCD) and the Response Surface Methodology (RSM) approach was used for optimisation of the parameters. The adsorbent dosage, solution temperature and time were set as independent variables while gold adsorption efficiency and copper adsorption efficiency were the response variables. Adsorbent dosage was the most influential factor for gold adsorption, while the effect on copper adsorption was insignificant. Although solution temperature and adsorption time influences gold adsorption from synthetic leaching solutions, these two parameters were not of great influence on gold adsorption from real ore leachate. The optimum conditions predicted by the model for maximum gold adsorption and minimum copper adsorption were 25 g/L adsorbent dosage for 46 minutes at a temperature of 56 °C.

Therefore in brief, PEI coated iron oxide magnetic nanoparticles can be effectively used for gold adsorption from clarified thiosulfate leach solutions. An increase in adsorbent dosage clearly enhanced gold adsorption, whilst copper adsorption efficiency did not show a considerable improvement. The predicted values of gold and copper adsorption efficiency by the fitted regression model are in accordance with the experimental results. Selective elution of the metals by use of low eluant concentrations within a short period of time is an added advantage.

8.4 Determination of Adsorption Mechanism through Adsorption Kinetics, Adsorption Isotherms and Thermodynamic Analyses

Gold adsorption kinetics data were fitted with pseudo-first-order, pseudo-second-order kinetic models and intra-particle diffusion model. The adsorption kinetic parameters are summarised in Table 8-2. The R^2 values imply that the adsorption kinetics data fit better with the pseudo-second-order model. The rapid adsorption kinetics irrespective of solution type, is indicative of physical adsorption that does not require activation energy.

Table 8-2. Summary of the adsorption kinetics model parameters

Pseudo-first-order Model			Pseudo-second-order model			Intra-particle diffusion model		
k_1 (min ⁻¹)	$q_{e, cal}$ (mg/g)	R^2	k_2 (g mg ⁻¹ min ⁻¹)	$q_{e, cal}$ (mg/g)	R^2	k_p	C	R^2
0.2021	0.22	0.9775	2.57	0.966	0.9999	0.003	0.94	0.6569

Adsorption isotherm data were fitted with the Langmuir and Freundlich isotherm models. The maximum gold adsorption capacity derived from the Langmuir equation was 42.11, 41.22 and 33.85 mg/g at temperatures of 25, 35 and 50 °C, respectively, as presented in Table 8-3. The adsorption mechanism was verified using a thermodynamic approach.

Table 8-3. Summary of the adsorption isotherm model parameters

Isotherm model	Parameter (units)	25 °C	35 °C	50 °C
Langmuir isotherm	q_m (mg/g)	42.11	41.22	33.85
	K_L (L/mg)	0.00418	0.00411	0.00373
	R^2	0.9959	0.9973	0.9959
Freundlich isotherm	K_f (mg/g)(L/mg) ^{1/n}	0.499	0.458	0.338
	n	1.47	1.46	1.43
	R^2	0.9930	0.9873	0.9834

Thermodynamic studies confirmed the adsorption process to be exothermic and spontaneous. The results are shown in Table 8-4. Moreover, the value of the enthalpy change (-11.99 kJ/mol) in conjunction with fast kinetics and simple gold elution all are indicators of physical adsorption. According to the characterisation of the particles using an APT, the multilayer adsorption of gold was apparent. XPS analysis results revealed that gold exists in Au(I) state without reducing to metallic state. Therefore, it can be concluded that gold adsorption onto PEI-MNPs from thiosulfate leaching solutions is a physical adsorption process where anionic gold thiosulfate complexes are adsorbed onto PEI-MNPs by electrostatic attraction.

Table 8-4. Summary of thermodynamic parameters of gold adsorption

Temperature (°C)	25 °C	35 °C	50 °C
ΔG° (kJ/mol)	-26.58	-27.39	-27.84
ΔH° (kJ/mol)		-11.99	
ΔS° (J/mol.K)		49.33	

8.5 Metal Elution and Reuse of PEI-MNPs

Gold and copper elution was conducted in two elution steps. Due to the unavoidable adsorption of copper on PEI-MNPs and to ensure the purity of the final gold product, copper pre-elution was conducted using 0.02 M EDTA solutions. This was followed with gold elution using 0.01 M NaOH solutions. Almost 100% metal elution was achieved over durations as short as 15 minutes, with considerably low eluent concentrations. This is deemed superior when comparing the complexity and higher reagent concentrations required for gold and copper elution from IX resins. Both gold and copper elution efficiencies were independent of the solid to liquid ratio in the elution solutions for the tested range (2.5- 10 g/L) which confirms the possibility of using lower eluant volumes.

The metal-eluted PEI-MNPs were reused for adsorption, after being washed with DI water. These adsorption-elution cycles were continued for up to six cycles to evaluate the reusability of the adsorbent, which is vital for reducing the costs of the process. Some loss of adsorption efficiency was noticed at each cycle where the total loss was 12-15% after six cycles. The causes for this drop could be the accumulation of sulfur species onto the adsorbent and possibly the agglomeration of PEI-MNPs during the process. Sulfur species elution was not considered in this study. Uneluted sulfur species can occupy the adsorption sites, disturbing gold adsorption in subsequent cycles. Frequent magnetic separation could have an effect on particle agglomeration, hence a drop in specific surface area. However, intermediate particle agglomeration could have been restored by occasional ultrasonic dispersion. Nevertheless, the exploration of all these options was not possible within the time frame of this study, but is suggested for future research.

The same eluants and comparable conditions were used for gold and copper elution from PEI-MNPs used for gold adsorption in gold ore leachates. In contrast to the PEI-MNPs used in synthetic leaching solutions, gold elution efficiency was dependent on S/L ratio. Copper elution was identical in both instances, probably due to the high stability constant of the Cu-EDTA complex. Competitively adsorbed calcium (100% elution) and sulfur (68% elution) could be effectively eluted at the copper pre-elution stage with 0.02 M EDTA at a pH of 6 and at 25 °C.

8.6 Schematic representation of the process

The schematic representation of the process is given in Figure 8-1. Firstly, the adsorption of gold and copper onto PEI-MNPs is conducted after leaching. The metal adsorbed PEI-MNPs are then separated from the solution by magnetic separation and are forwarded on to the elution

process. At this stage, the adsorbent undergoes copper elution followed by gold elution. The eluant solution is then forwarded on for elemental gold recovery using a suitable process like electrowinning, and metal- eluted PEI-MNPs are redirected for metal adsorption again. Competitive adsorption of other species (except Cu) has not been considered here.

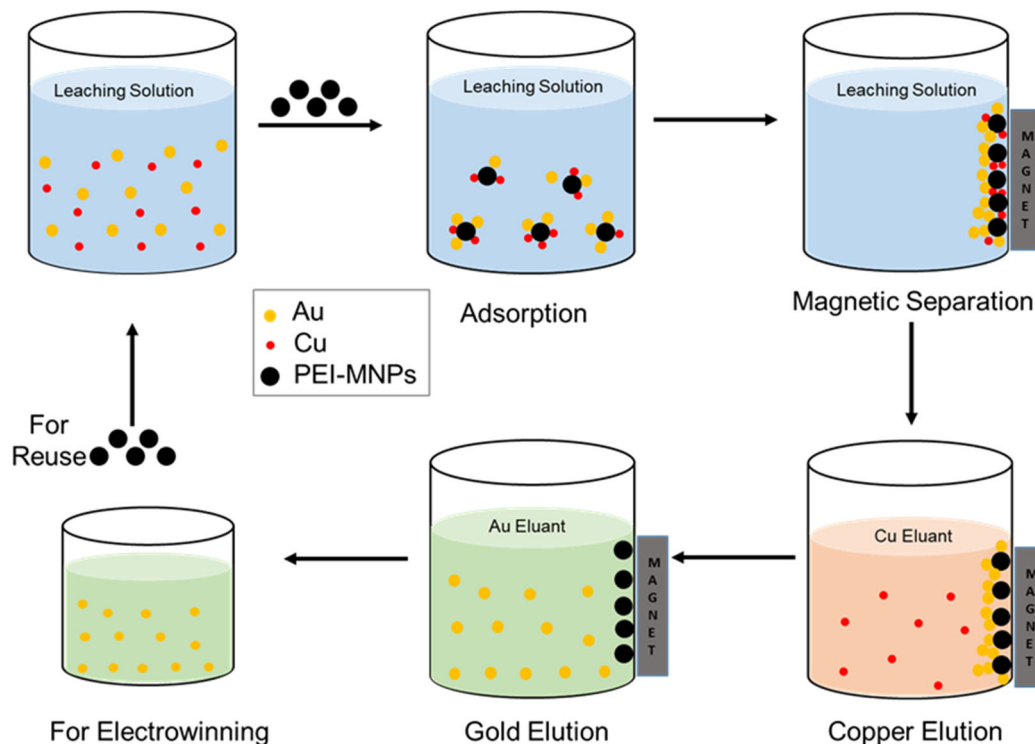


Figure 8-1. Schematic representation of the adsorption-elution-reuse cycle

In conclusion, the research shows excellent gold adsorption from pure gold thiosulfate solutions, fast kinetics and comparable adsorption capacity in simulated leaching solutions, a simple surface functionalisation process and most prominently, uncomplicated and selective metal elution characteristics. However, further improvements are still possible and essential. It should be understood that this process, in its current state, is by no means a replacement for the existing RIL process. However, compared to the IX resins, the advantages with PEI-MNPs are:

- the lower adsorption of competitive ions such as copper and sulfur species
- a simple and rapid metal elution process
- easy solid-liquid separation with the aid of an external magnetic field.

The above points are the motivation for considering this technology for gold recovery in the future. Any potential improvements that could be made to this particular adsorption system are listed in the following section.

8.7 Recommendations for Future Investigations

As far as is known, this is the first time that research has provided a basis for, as well as a preliminary understanding of, the use of functionalised magnetic nanoadsorbents to recover gold from non-ammoniacal thiosulfate leaching solutions. However, this is by no means an exhaustive study and many improvements could be made by refining the process. The following section includes some suggestions for the advancement of the adsorbent and improvements for the overall process.

- Optimisation of the functionalisation process - further adjustment of the surface functionalisation process conditions and/or use of different ligands appropriate for alkaline pH conditions could result in a better product. The use of quaternised PEI is one recommendation.
- Selectivity towards gold adsorption – Although almost 100% gold adsorption was achieved in pure gold thiosulfate solution using a low adsorbent dosage, the adsorption efficiency dropped in simulated leaching solutions in the presence of free thiosulfate and copper. Modification of the adsorbent and adsorption conditions to enhance selective gold adsorption is suggested.
- Regeneration of the adsorbent – it is foreseen that adsorption efficiency in subsequent cycles would have improved if the adsorbed sulfur species could have been eluted. Therefore, consideration of some means of sulfur species elution would be worthwhile.
- Expanding the range of use of the adsorbent - Some preliminary studies were conducted on using PEI-MNPs to recover gold from other thiosulfate leaching systems such as Cu-ammonia, Fe-EDTA, Fe-oxalate, Ni-ammonia. However, more comprehensive studies are suggested.
- Scaling up to pilot scale – This study considered gold adsorption from both synthetic and actual leach solutions on a laboratory scale. Magnetic separation was conducted with a handheld neodymium magnet. The use of HGMS, for instance using a steel wool matrix on a laboratory scale or pilot scale, would be an important part of a future study.

- Pulp application- the adsorption studies were conducted in clear solutions and the feasibility of the application in pulp would be an important area to consider. Few preliminary studies have been conducted using silica flour with PEI-MNPs, which also guarantee the recovery of MNPs without any nanoparticle loss. Further investigation in this area is required.

Some of the limitations associated with PEI-MNPs could have been overcome by some changes in the process, but only at the expense of affecting the claimed advantages. For instance, it is foreseen that, the use of quaternary PEI may improve adsorption capacity as well as a wide range of operating pH values but pay off with difficulty in metal elution process.

References

- Abbruzzese, C., Fomari, P., Massidda, R., Veglio, F. and Ubaldini, S. 1995. Thiosulphate leaching for gold hydrometallurgy. *Hydrometallurgy* 39 265-276.
- Abd Razak, N. F., Shamsuddin, M. and Lee, S. L. 2018. Adsorption kinetics and thermodynamics studies of gold(III) ions using thioctic acid functionalized silica coated magnetite nanoparticles. *Chemical Engineering Research and Design* 130 18-28.
- Adenier, A., Chehimi, M. M., Gallardo, I., Pinson, J. and Vilà, N. 2004. Electrochemical Oxidation of Aliphatic Amines and Their Attachment to Carbon and Metal Surfaces. *Langmuir* 20(19), 8243-8253.
- Aghaei, E., Alorro, R., Encila, A. and Yoo, K. 2017. Magnetic Adsorbents for the Recovery of Precious Metals from Leach Solutions and Wastewater. *Metals* 7(12), 529.
- Ahmed, M. A., Ali, S. M., El-Dek, S. I. and Galal, A. 2013. Magnetite–hematite nanoparticles prepared by green methods for heavy metal ions removal from water. *Materials Science and Engineering: B* 178(10), 744-751.
- Aksu, S. and Doyle, F. M. 2001. Electrochemistry of Copper in Aqueous Glycine Solutions. *Journal of The Electrochemical Society* 148(1), B51-B57.
- Al Subu, M. M., Salim, R., Abu Shqair, I. and Swaileh, K. M. 2001. Removal of dissolved copper from polluted water using plant leaves: I. effects of acidity and plant species. *Revista Internacional de Contaminación Ambiental* 17(2), 91-96.
- Alorro, R. D., Hiroyoshi, N., Ito, M. and Tsunekawa, M. 2010. Recovery of Precious Metals from Chloride Solution by Magnetite. *International Mineral Processing Congress (IMPC) 2010*, Brisbane, QLD, Australia.
- Ambashta, R. D. and Sillanpaa, M. 2010. Water purification using magnetic assistance: a review. *Journal of Hazardous Materials* 180(1-3), 38-49.
- Anastopoulos, I. and Kyzas, G. Z. 2016. Are the thermodynamic parameters correctly estimated in liquid-phase adsorption phenomena? *Journal of Molecular Liquids* 218 174-185.
- Andreas, K., Georgieva, R., Ladwig, M., Mueller, S., Notter, M., Sittinger, M. and Ringe, J. 2012. Highly efficient magnetic stem cell labeling with citrate-coated superparamagnetic iron oxide nanoparticles for MRI tracking. *Biomaterials* 33(18), 4515-4525.
- Arima, H., Fujita, T. and Yen, W.-T. 2002. Gold Cementation from Ammonium Thiosulfate Solution by Zinc, Copper and Aluminium Powders. *Materials Transactions* 43(3), 485-493.
- Arima, H., Fujita, T. and Yen, W.-T. 2004. Using Nickel as a Catalyst in Ammonium Thiosulfate Leaching for Gold Extraction. *Materials Transactions* 45(2), 516-526.
- Armstrong, R. J., Morrish, A. H. and Sawatzky, G. A. 1966. Mössbauer study of ferric ions in the tetrahedral and octahedral sites of a spinel. *Physics Letters* 23(7), 414-416.
- Arsalani, S., Guidelli, E. J., Silveira, M. A., Salmon, C. E. G., Araujo, J. F. D. F., Bruno, A. C. and Baffa, O. 2019. Magnetic Fe₃O₄ nanoparticles coated by natural rubber latex as MRI contrast agent. *Journal of Magnetism and Magnetic Materials* 475 458-464.

- Arsianti, M., Lim, M., Marquis, C. P. and Amal, R. 2010. Assembly of polyethylenimine-based magnetic iron oxide vectors: insights into gene delivery. *Langmuir* 26(10), 7314-7326.
- Artioli, Y. 2008. Adsorption Encyclopedia of Ecology. B. D. Fath. Oxford, Academic Press, 60-65.
- Awadalla, F. T. and Ritcey, G. M. 1991. Recovery of Gold from Thiourea, Thiocyanate, or Thiosulfate Solutions by Reduction-Precipitation with a Stabilized Form of Sodium Borohydride. *Separation Science and Technology* 26(9), 1207-1228.
- Aylmore, M. G. 2016a. Chapter 27 - Alternative Lixiviants to Cyanide for Leaching Gold Ores. *Gold Ore Processing*. M. D. Adams, Elsevier, 447-484.
- Aylmore, M. G. 2016b. Chapter 28 - Thiosulfate as an Alternative Lixiviant to Cyanide for Gold Ores. *Gold Ore Processing (Second Edition)*. M. D. Adams, Elsevier, 485-523.
- Aylmore, M. G. 2016c. Thiosulfate as an Alternative Lixiviant to Cyanide for Gold Ores.
- Aylmore, M. G. and Muir, D. M. 2001. Thiosulfate leaching of gold—A review. *Minerals Engineering* 14(2), 135-174.
- Azizian, S. 2004. Kinetic models of sorption: a theoretical analysis. *Journal of Colloid and Interface Science* 276(1), 47-52.
- Badruddoza, A. Z. M., Tay, A. S. H., Tan, P. Y., Hidajat, K. and Uddin, M. S. 2011. Carboxymethyl- β -cyclodextrin conjugated magnetic nanoparticles as nano-adsorbents for removal of copper ions: Synthesis and adsorption studies. *Journal of Hazardous Materials* 185(2), 1177-1186.
- Bakerbond (2012). BAKERBOND™ Multimode Ion Exchange Chromatography Media (Technical note). www.avantormaterials.com. Avantor Performance Materials, USA: 1-6.
- Baron, J. Y., Choi, Y. and Jeffrey, M. 2016. Chapter 50 - Double-Refractory Carbonaceous Sulfidic Gold Ores A2 - Adams, Mike D. *Gold Ore Processing (Second Edition)*, Elsevier, 909-918.
- Benedetti, M. and Boulègue, J. 1991. Mechanism of gold transfer and deposition in a supergene environment. *Geochimica et Cosmochimica Acta* 55(6), 1539-1547.
- Betancur, J. C., Montoya, P. M. and Calderón, J. A. 2019. Gold recovery from ammonia-thiosulfate leaching solution assisted by PEI-functionalized magnetite nanoparticles. *Hydrometallurgy* 189 105128.
- Biesinger, M. C., Payne, B. P., Grosvenor, A. P., Lau, L. W. M., Gerson, A. R. and Smart, R. S. C. 2011. Resolving surface chemical states in XPS analysis of first row transition metals, oxides and hydroxides: Cr, Mn, Fe, Co and Ni. *Applied Surface Science* 257(7), 2717-2730.
- Bilici Baskan, M. and Pala, A. 2010. A statistical experiment design approach for arsenic removal by coagulation process using aluminum sulfate. *Desalination* 254(1), 42-48.
- Blanchard, G., Maunaye, M. and Martin, G. 1984. Removal of heavy metals from waters by means of natural zeolites. *Water Research* 18(12), 1501-1507.
- Blaney, L. 2007. Magnetite (Fe₃O₄)- Properties Synthesis and Applications, Lehigh Preserve.
- Boussif, O., Lezoulach, F., Zanta, M. A., Mergny, M. D., Scherman, D., Demeneix, B. and Behr, J. P. 1995. A versatile vector for gene and oligonucleotide transfer into cells in culture and in vivo: Polyethylenimine. *Proceedings of the National Academy of Sciences, USA*.
- Boyer, C., Whittaker, M. R., Bulmus, V., Liu, J. and Davis, T. P. 2010. The design and utility of polymer-stabilized iron-oxide nanoparticles for nanomedicine applications. *NPG Asia Materials* 2(1), 23-30.

- Braul, P. 2013. Thiosulfate going commercial. *CIM Magazine* 8(1).
- Breuer, P., Dai, X., Zhang, H. and Hewitt, D. 2012. The increased activity in the development of thiosulfate based Processes for gold recovery. ALTA 2012, Perth, Australia, ALTA Metallurgical Services Publications.
- Breuer, P. L. and Jeffrey, M. I. 2002. An electrochemical study of gold leaching in thiosulfate solutions containing copper and ammonia. *Hydrometallurgy* 65(2-3), 145-157.
- Breuer, P. L. and Jeffrey, M. I. 2003. Copper catalysed oxidation of thiosulfate by oxygen in gold leach solutions. *Minerals Engineering* 16(1), 21-30.
- Bruvera, I. J., Zélis, P. M., Calatayud, M. P., Goya, G. F. and Sánchez, F. H. 2015. Determination of the blocking temperature of magnetic nanoparticles: The good, the bad, and the ugly. *Journal of Applied Physics* 118(18), 184304.
- Bucak, S., Jones, D. A., Laibinis, P. E. and Hatton, T. A. 2003. Protein Separations Using Colloidal Magnetic Nanoparticles. *Biotechnology Progress* 19(2), 477-484.
- Bus, T., Traeger, A. and Schubert, U. S. 2018. The great escape: how cationic polyplexes overcome the endosomal barrier. *Journal of Materials Chemistry B* 6(43), 6904-6918.
- Casaletto, M. P., Longo, A., Martorana, A., Prestianni, A. and Venezia, A. M. 2006. XPS study of supported gold catalysts: the role of Au⁰ and Au^{+δ} species as active sites. *Surface and Interface Analysis* 38(4), 215-218.
- Cervellino, A., Frison, R., Cernuto, G., Guagliardi, A. and Masciocchi, N. 2014. Lattice parameters and site occupancy factors of magnetite-maghemite core-shell nanoparticles. A critical study. *Journal of Applied Crystallography* 47(5), 1755-1761.
- Chandra, I. and Jeffrey, M. I. 2004. An electrochemical study of the effect of additives and electrolyte on the dissolution of gold in thiosulfate solutions. *Hydrometallurgy* 73(3-4), 305-312.
- Chandra, I. and Jeffrey, M. I. 2005. A fundamental study of ferric oxalate for dissolving gold in thiosulfate solutions. *Hydrometallurgy* 77(3-4), 191-201.
- Chang, J. H., Lee, J., Jeong, Y., Hyung Lee, J., Kim, I. J. and Park, S. E. 2010. Hydrophobic partitioning approach to efficient protein separation with magnetic nanoparticles. *Analytical Biochemistry* 405(1), 135-137.
- Chantrapornchai, C., Dolwithayakul, B. and Gorlatch, S. 2009. Parallel Mass Transfer Simulation of Nanoparticles Using Nonblocking Communications. *Multimedia, Computer Graphics and Broadcasting. MulGraB 2009. Communications in Computer and Information Science*, Berlin, Heidelberg, Springer.
- Cheraghipour, E., Javadpour, S. and Mehdizadeh, A. R. 2012. Citrate capped superparamagnetic iron oxide nanoparticles used for hyperthermia therapy. *Journal of Biomedical Science and Engineering* 05(12), 715-719.
- Cho, H., Waters, M. A. and Hogg, R. 1996. Investigation of the grind limit in stirred-media milling. *International Journal of Mineral Processing* 44-45 607-615.
- Choi, Y. 2013. Thiosulfate Processing: From Lab Curiosity to Commercial Application. ALTA 2013 Gold-PM Proceedings, Perth, Australia.
- Choi, Y. 2016. Selecting the Best Process for the Treatment of a Refractory Gold Ore - Barrick's Experience. ALTA 2016 Gold-PM Proceedings, Perth, Australia.
- Choi, Y. and Chefai, S. 2012. Co-current and counter current resin-in-leach in gold leaching processes. US 2012/0183433 A1.
- Choi, Y. and Chefai, S. 2017. Barrick Gold Corporation, Patent Issued for Co-Current and Counter Current Resin-In-Leach in Gold Leaching Processes. US9790572B2, 1298.

- Choi, Y. and Olvera, O. 2017. Enhanced leaching of arsenopyrite concentrates as a pretreatment for gold recovery from refractory ores. ALTA 2017, Perth, Australia ALTA Metallurgical Services Publications.
- Choi, Y., Wang, Q. and Langhans, J. W. 2015. Method for recovering precious metals and copper from leach solutions. US Patent 9051625B2.
- Choo, W. L. and Jeffrey, M. I. 2004. An electrochemical study of copper cementation of gold(I) thiosulfate. *Hydrometallurgy* 71(3), 351-362.
- Choudhary, B. C., Paul, D., Borse, A. U. and Garole, D. J. 2018. Surface functionalized biomass for adsorption and recovery of gold from electronic scrap and refinery wastewater. *Separation and Purification Technology* 195 260-270.
- Chowdhury, S. R., Yanful, E. K. and Pratt, A. R. 2010. Arsenic removal from aqueous solutions by mixed magnetite–maghemite nanoparticles. *Environmental Earth Sciences* 64(2), 411-423.
- Coates, J. 2000. Interpretation of Infrared Spectra, A Practical Approach. *Encyclopedia of Analytical Chemistry*, R.A. Meyers.
- Cornell, R. M. and Schwertmann, U. 2006. *The Iron Oxides : Structure, Properties, Reactions, Occurrences and Uses*. Hoboken, Germany, John Wiley & Sons, Incorporated.
- Crank, J. 1975. *The Mathematics of Diffusion*, Oxford University Press.
- Dąbrowski, A. 2001. Adsorption — from theory to practice. *Advances in Colloid and Interface Science* 93(1), 135-224.
- Daenzer, R., Dreisinger, D. and Choi, Y. 2016. Role of Polythionates on the stability of Gold in the leaching of double refractory ores in the Calcium Thiosulfate-Air Leaching System. ALTA 2016 Gold-PM Proceedings, Perth, Australia.
- Dai, X., Breuer, P., Hewitt, D. and Bergamin, A. 2013. Thiosulfate process for treating gold concentrates. *World Gold 2013 Conference Proceedings*, Brisbane, QLD.
- Dai, X., Sitando, O., Senanayake, G., Nikoloski, A. and Breuer, P. 2017. Enhanced gold ore leaching in a thiosulfate-oxygen system by a novel additive. ALTA 2017, Perth, Australia ALTA Metallurgical Services Publications.
- de Faria, D. L. A., Venâncio Silva, S. and de Oliveira, M. T. 1997. Raman microspectroscopy of some iron oxides and oxyhydroxides. *Journal of Raman Spectroscopy* 28(11), 873-878.
- de Sousa, M. E., Fernández van Raap, M. B., Rivas, P. C., Mendoza, Z. P., Girardin, P., Pasquevich, G. A., Alessandrini, J. L., Muraca, D. and Sánchez, F. H. 2013. Stability and Relaxation Mechanisms of Citric Acid Coated Magnetite Nanoparticles for Magnetic Hyperthermia. *The Journal of Physical Chemistry C* 117(10), 5436-5445.
- Dehghani, M. H., Maroosi, M. and Heidarinejad, Z. 2018. Experimental dataset on adsorption of Arsenic from aqueous solution using Chitosan extracted from shrimp waste; optimization by response surface methodology with central composite design. *Data Brief* 20 1415-1421.
- Ding, P. and Pacek, A. W. 2008. De-agglomeration of goethite nano-particles using ultrasonic comminution device. *Powder Technology* 187(1), 1-10.
- Ditsch, A., Laibinis, P. E., Wang, D. I. C. and Hatton, T. A. 2005. Controlled Clustering and Enhanced Stability of Polymer-Coated Magnetic Nanoparticles. *Langmuir* 21(13), 6006-6018.
- Do, D. D. 1998. *Adsorption analysis: Equilibria and Kinetics*. London, Imperial college press.
- Dong, Z., Jiang, T., Xu, B., Yang, Y. and Li, Q. 2017. Recovery of Gold from Pregnant Thiosulfate Solutions by the Resin Adsorption Technique. *Metals* 7(12).

- Donia, A. M., Atia, A. A. and Elwakeel, K. Z. 2007. Recovery of gold(III) and silver(I) on a chemically modified chitosan with magnetic properties. *Hydrometallurgy* 87(3-4), 197-206.
- Drmotič, A., Drofenik, M., Koselj, J. and Žnidaršič, A. 2012. Microemulsion Method for Synthesis of Magnetic Oxide Nanoparticles. *Microemulsions - An Introduction to Properties and Applications*, Dr. Reza Najjar (Ed.).
- Dubinina, M. M. and Radushkevich, L. V. 1947. Equation of the Characteristic Curve of Activated Charcoal. *Proceedings of the Academy of Sciences of the USSR: Physical Chemistry Section*.
- Dwyer, F. P. J. and Mellor, D. P. 1964. *Chelating agents and metal chelates*. N.Y. Academic Press.
- Easwaramoorthi, S. and Natarajan, P. 2009. Characterisation and spectral properties of surface adsorbed phenosafranin dye in zeolite-Y and ZSM-5: Photosensitisation of embedded nanoparticles of titanium dioxide. *Microporous and Mesoporous Materials* 117(3), 541-550.
- Ebrahimzadeh, H., Moazzen, E., Amini, M. M. and Sadeghi, O. 2012. Novel magnetic ion imprinted polymer as a highly selective sorbent for extraction of gold ions in aqueous samples. *Analytical Methods* 4(10), 3232-3237.
- Eksteen, J. J. and Oraby, E. A. 2015. The leaching and adsorption of gold using low concentration amino acids and hydrogen peroxide: Effect of catalytic ions, sulphide minerals and amino acid type. *Minerals Engineering* 70(Supplement C), 36-42.
- Erdemoğlu, M. and Sarıkaya, M. 2006. Effects of heavy metals and oxalate on the zeta potential of magnetite. *Journal of Colloid and Interface Science* 300(2), 795-804.
- Esdale, L. J. and Chalker, J. M. 2018. The Mercury Problem in Artisanal and Small-Scale Gold Mining. *Chemistry (Weinheim an der Bergstrasse, Germany)* 24(27), 6905-6916.
- Faure, B., Salazar-Alvarez, G., Ahniyaz, A., Villaluenga, I., Berriozabal, G., De Miguel, Y. R. and Bergstrom, L. 2013. Dispersion and surface functionalization of oxide nanoparticles for transparent photocatalytic and UV-protecting coatings and sunscreens. *Science and Technology of Advanced Materials* 14(2), 023001.
- Feijoo, S., González-García, S., Moldes-Diz, Y., Vázquez-Vázquez, C., Feijoo, G. and Moreira, M. T. 2018. Chapter 3 - The Environmental Impact of Magnetic Nanoparticles Under the Perspective of Carbon Footprint. *Environmental Carbon Footprints*. S. S. Muthu, Butterworth-Heinemann, 45-77.
- Feng, C., Aldrich, C., Eksteen, J. J. and Arrigan, D. W. M. 2017. Removal of arsenic from alkaline process waters of gold cyanidation by use of $\gamma\text{-Fe}_2\text{O}_3 @ \text{ZrO}_2$ nanosorbents. *Hydrometallurgy* 174 71-77.
- Feng, D. and van Deventer, J. S. J. 2002. The role of heavy metal ions in gold dissolution in the ammoniacal thiosulphate system. *Hydrometallurgy* 64(3), 231-246.
- Feng, D. and van Deventer, J. S. J. 2007. Effect of hematite on thiosulphate leaching of gold. *International Journal of Mineral Processing* 82(3), 138-147.
- Feng, D. and van Deventer, J. S. J. 2010a. The effect of iron contaminants on thiosulphate leaching of gold. *Minerals Engineering* 23(5), 399-406.
- Feng, D. and van Deventer, J. S. J. 2010b. Effect of thiosulphate salts on ammoniacal thiosulphate leaching of gold. *Hydrometallurgy* 105(1-2), 120-126.
- Feng, D. and van Deventer, J. S. J. 2011. The role of amino acids in the thiosulphate leaching of gold. *Minerals Engineering* 24(9), 1022-1024.

- Ferreira, R. V., Pereira, I. L. S., Cavalcante, L. C. D., Gamarra, L. F., Carneiro, S. M., Amaro, E., Fabris, J. D., Domingues, R. Z. and Andrade, A. L. 2010. Synthesis and characterization of silica-coated nanoparticles of magnetite. *Hyperfine Interactions* 195(1), 265-274.
- Fleming, C., Wells, J. and Thomas, K. G. 2002. Process for recovering gold from thiosulfate leach solutions and slurries with ion exchange resin. US Patent 6344068 B1.
- Fleming, C. A., McMullen, J., Thomas, K. G. and Wells, J. A. 2003. Recent advances in the development of an alternative to the cyanidation process: Thiosulfate leaching and resin in pulp. *Minerals & Metallurgical Processing* 20(1), 1-9.
- Fletcher, D. 1991. Fine particle high gradient magnetic entrapment. *IEEE Transactions on Magnetics* 27(4), 3655-3677.
- Foo, K. Y. and Hameed, B. H. 2010. Insights into the modeling of adsorption isotherm systems. *Chemical Engineering Journal* 156(1), 2-10.
- Fotoohi, B. and Mercier, L. 2014. Recovery of precious metals from ammoniacal thiosulfate solutions by hybrid mesoporous silica: 1-Factors affecting gold adsorption. *Separation and Purification Technology* 127 84-96.
- Friedrich, A. J., Saxey, D. W., Adineh, V. R., Fougereuse, D., Reddy, S. M., Rickard, W. D. A., Sadek, A. Z. and Southall, S. C. 2019. Direct Observation of Nanoparticulate Goethite Recrystallization by Atom Probe Analysis of Isotopic Tracers. *Environmental Science and Technology* 53(22), 13126-13135.
- Gallagher, N. P., Hendrix, J. L., Milosavljevic, E. B., Nelson, J. H. and Solujic, L. 1990. Affinity of activated carbon towards some gold(I) complexes. *Hydrometallurgy* 25(3), 305-316.
- Gan, J., Yates, S. R., Knuteson, J. A. and Becker, J. O. 2000. Transformation of 1,3-dichloropropene in soil by thiosulfate fertilizers. *Journal of Environmental Quality* 29(5), 1476-1481.
- Garro, R., Navarro, M., Primo, J. and Corma, A. 2005. Lewis acid-containing mesoporous molecular sieves as solid efficient catalysts for solvent-free Mukaiyama-type aldol condensation. *Journal of Catalysis* 233(2), 342-350.
- Gault, B. and Larson, D. J. 2018. Atom probe tomography: Looking forward. *Scripta Materialia* 148 73-74.
- Ge, F., Ye, H., Li, M.-M. and Zhao, B.-X. 2012. Efficient removal of cationic dyes from aqueous solution by polymer-modified magnetic nanoparticles. *Chemical Engineering Journal* 198-199 11-17.
- Ge, S., Agbakpe, M., Wu, Z., Kuang, L., Zhang, W. and Wang, X. 2015. Influences of surface coating, UV irradiation and magnetic field on the algae removal using magnetite nanoparticles. *Environmental Science and Technology* 49(2), 1190-1196.
- Ge, W., Encinas, A., Araujo, E. and Song, S. 2017. Magnetic matrices used in high gradient magnetic separation (HGMS): A review. *Results in Physics* 7 4278-4286.
- Generali, J. A. and Cada, D. J. 2015. Sodium Thiosulfate: Calciphylaxis. *Hospital Pharmacy* 50(11), 975-977.
- Genik-Sas-Berezowsky, R. M., Sefton, V. B. and Gormely, L. S. 1978. Recovery of precious metals from metal sulphides. US Patent 4070182 A.
- Gerber, R., Takayasu, M. and Friedlaender, F. 1983. Generalization of HGMS theory: The capture of ultra-fine particles. *IEEE Transactions on Magnetics* 19(5), 2115-2117.
- Gholamali, H., Shafiekhani, A., Darabi, E. and Elahi, S. M. 2018. Synthesis of Ag and Au nanoparticles embedded in carbon film: Optical, crystalline and topography analysis. *Results in Physics* 8 336-340.

- Ghosal, P. S. and Gupta, A. K. 2017. Determination of thermodynamic parameters from Langmuir isotherm constant-revisited. *Journal of Molecular Liquids* 225 137-146.
- Ghoul, M., Bacquet, M. and Morcellet, M. 2003. Uptake of heavy metals from synthetic aqueous solutions using modified PEI—silica gels. *Water Research* 37(4), 729-734.
- Giakisikli, G. and Anthemidis, A. N. 2013. Magnetic materials as sorbents for metal/metalloid preconcentration and/or separation. A review. *Analytica Chimica Acta* 789 1-16.
- Girginova, P. I., Daniel-da-Silva, A. L., Lopes, C. B., Figueira, P., Otero, M., Amaral, V. S., Pereira, E. and Trindade, T. 2010. Silica coated magnetite particles for magnetic removal of Hg²⁺ from water. *Journal of Colloid and Interface Science* 345(2), 234-240.
- Gómez-Pastora, J., Bringas, E. and Ortiz, I. 2014. Recent progress and future challenges on the use of high performance magnetic nano-adsorbents in environmental applications. *Chemical Engineering Journal* 256 187-204.
- Goon, I. Y., Lai, L. M. H., Lim, M., Munroe, P., Gooding, J. J. and Amal, R. 2009. Fabrication and Dispersion of Gold-Shell-Protected Magnetite Nanoparticles: Systematic Control Using Polyethyleneimine. *Chemistry of Materials* 21(4), 673-681.
- Goon, I. Y., Zhang, C., Lim, M., Gooding, J. J. and Amal, R. 2010. Controlled fabrication of polyethylenimine-functionalized magnetic nanoparticles for the sequestration and quantification of free Cu²⁺. *Langmuir* 26(14), 12247-12252.
- Grosse, A. C., Dicinovski, G. W., Shaw, M. J. and Haddad, P. R. 2003. Leaching and recovery of gold using ammoniacal thiosulfate leach liquors (a review). *Hydrometallurgy* 69(1-3), 1-21.
- Grosvenor, A. P., Kobe, B. A., Biesinger, M. C. and McIntyre, N. S. 2004. Investigation of multiplet splitting of Fe 2p XPS spectra and bonding in iron compounds. *Surface and Interface Analysis* 36(12), 1564-1574.
- Groves, W. D. and Blackman, L. 1995. Recovery of precious metals from evaporite sediments. US Patents 5405430A.
- Guerra, E. and Dreisinger, D. B. 1999. A study of the factors affecting copper cementation of gold from ammoniacal thiosulphate solution. *Hydrometallurgy* 51(2), 155-172.
- Guillem, V. M. and Aliño, S. F. 2004. Transfection pathways of nonspecific and targeted PEI-polyplexes. *Gene Therapy and Molecular Biology* 8 369-384.
- Gupta, V. K. and Nayak, A. 2012. Cadmium removal and recovery from aqueous solutions by novel adsorbents prepared from orange peel and Fe₂O₃ nanoparticles. *Chemical Engineering Journal* 180 81-90.
- Gylienė, O., Aikaitė, J. and Nivinskienė, O. 2004. Recovery of EDTA from complex solution using Cu(II) as precipitant and Cu(II) subsequent removal by electrolysis. *Journal of Hazardous Materials* 116(1), 119-124.
- Ha, V. H., Lee, J.C., Huynh, T. H., Jeong, J. and Pandey, B. D. 2014. Optimizing the thiosulfate leaching of gold from printed circuit boards of discarded mobile phone. *Hydrometallurgy* 149 118-126.
- Hamdaoui, O. and Naffrechoux, E. 2007. Modeling of adsorption isotherms of phenol and chlorophenols onto granular activated carbon: Part I. Two-parameter models and equations allowing determination of thermodynamic parameters. *Journal of Hazardous Materials* 147(1), 381-394.
- Hamzaoui, A. H., Jamoussi, B. and M'Nif, A. 2008. Lithium recovery from highly concentrated solutions: Response surface methodology (RSM) process parameters optimization. *Hydrometallurgy* 90(1), 1-7.

- Han, K. N. and Meng, X. 1994. Ammonia extraction of gold and silver from ores and other materials. US patent 5308381 A.
- Haneda, K. and Morrish, A. H. 1977. Vacancy ordering in γ -Fe₂O₃ small particles. *Solid State Communications* 22(12), 779-782.
- Hanif, S. and Shahzad, A. 2014. Removal of chromium(VI) and dye Alizarin Red S (ARS) using polymer-coated iron oxide (Fe₃O₄) magnetic nanoparticles by co-precipitation method. *Journal of Nanoparticle Research* 16(6).
- Hao, Y.M., Man, C. and Hu, Z.B. 2010. Effective removal of Cu (II) ions from aqueous solution by amino-functionalized magnetic nanoparticles. *Journal of Hazardous Materials* 184(1), 392-399.
- Harris, L. A., Goff, J. D., Carmichael, A. Y., Riffle, J. S., Harburn, J. J., St. Pierre, T. G. and Saunders, M. 2003. Magnetite Nanoparticle Dispersions Stabilized with Triblock Copolymers. *Chemistry of Materials* 15(6), 1367-1377.
- Heath, J. A., Jeffrey, M. I., Zhang, H. G. and Rumball, J. A. 2008. Anaerobic thiosulfate leaching: Development of in situ gold leaching systems. *Minerals Engineering* 21(6), 424-433.
- Hielscher, T. 2005. Ultrasonic production of nano-sized dispersions and emulsions. ENS 2005, Paris, France.
- Hiskey, J. B. and Atluri, V. P. 2007. Dissolution Chemistry of Gold and Silver in Different Lixiviants. *Mineral Processing and Extractive Metallurgy Review* 4(1-2), 95-134.
- Hiura, S., Ikeuchi, A., Shirini, S., Subagyo, A. and Sueoka, K. 2015. Effect of adsorbed H atoms on the Fe electronic states of Fe₃O₄(001) film surfaces. *Physical Review B* 91(20).
- Ho, Y. S. and McKay, G. 1998. A Comparison of Chemisorption Kinetic Models Applied to Pollutant Removal on Various Sorbents. *Process Safety and Environmental Protection* 76(4), 332-340.
- Hostetler, R. E. and Swanson, J. W. 1974. Diffusion into and adsorption of polyethylenimine on porous silica gel. *Journal of Polymer Science: Polymer Chemistry Edition* 12(1), 29-43.
- Hou, J. G., Ma, Q., Du, X. Z., Deng, H. L. and Gao, J. Z. 2004. Inorganic/organic mesoporous silica as a novel fiber coating of solid-phase microextraction. *Talanta* 62(2), 241-246.
- Hristovski, K., Baumgardner, A. and Westerhoff, P. 2007. Selecting metal oxide nanomaterials for arsenic removal in fixed bed columns: From nanopowders to aggregated nanoparticle media. *Journal of Hazardous Materials* 147(1), 265-274.
- Hu, X., Xiao, L., Jian, X. and Zhou, W. 2017. Synthesis of mesoporous silica-embedded TiO₂ loaded with Ag nanoparticles for photocatalytic hydrogen evolution from water splitting. *Journal of Wuhan University of Technology-Materials Science Edition* 32(1), 67-75.
- Hua, M., Zhang, S., Pan, B., Zhang, W., Lv, L. and Zhang, Q. 2012. Heavy metal removal from water/wastewater by nanosized metal oxides: a review. *Journal of Hazardous Materials* 211-212 317-331.
- Huang, C. and Hu, B. 2008. Silica-coated magnetic nanoparticles modified with γ -mercaptopropyltrimethoxysilane for fast and selective solid phase extraction of trace amounts of Cd, Cu, Hg, and Pb in environmental and biological samples prior to their determination by inductively coupled plasma mass spectrometry. *Spectrochimica Acta Part B: Atomic Spectroscopy* 63(3), 437-444.

- Ilankoon, N. 2014. Use of iron oxide magnetic nanosorbents for Cr (VI) removal from aqueous solutions: A review. *International Journal of Engineering Research and Applications* 4(10), 55-63.
- Illés, E. and Tombácz, E. 2006. The effect of humic acid adsorption on pH-dependent surface charging and aggregation of magnetite nanoparticles. *Journal of Colloid and Interface Science* 295(1), 115-123.
- Inglezakis, V. J. and Pouloupoulos, S. G. 2006. 2 - Adsorption, Ion Exchange, and Catalysis. *Adsorption, Ion Exchange and Catalysis*. Amsterdam, Elsevier, 31-56.
- Ishikawa, S.I., Suyama, K., Arihara, K. and Itoh, M. 2002. Uptake and recovery of gold ions from electroplating wastes using eggshell membrane. *Bioresource Technology* 81(3), 201-206.
- Jainae, K., Sanuwong, K., Nuangjamnong, J., Sukpirom, N. and Unob, F. 2010. Extraction and recovery of precious metal ions in wastewater by polystyrene-coated magnetic particles functionalized with 2-(3-(2-aminoethylthio)propylthio)ethanamine. *Chemical Engineering Journal* 160(2), 586-593.
- Jeffrey, M. I. 2011. Process for recovering metals from resins. US Patent 2011 0011216 A1.
- Jeffrey, M. I. and Brunt, S. D. 2007. The quantification of thiosulfate and polythionates in gold leach solutions and on anion exchange resins. *Hydrometallurgy* 89(1-2), 52-60.
- Jeffrey, M. I., Hewitt, D. M., Dai, X. and Brunt, S. D. 2010. Ion exchange adsorption and elution for recovering gold thiosulfate from leach solutions. *Hydrometallurgy* 100(3-4), 136-143.
- Ji, J., Fleming, C. A., West-Sells, P. G. and Hackl, R. P. 2013. Method for Thiosulfate Leaching of Precious Metal-Containing Materials. US Patent 8,597,399 B2.
- Jia, J., Wu, A. and Luan, S. 2014. Spectrometry recognition of polyethyleneimine towards heavy metal ions. *Colloids and Surfaces A: Physicochemical and Engineering Aspects* 449 1-7.
- Jiang, J., Oberdörster, G. and Biswas, P. 2008. Characterization of size, surface charge, and agglomeration state of nanoparticle dispersions for toxicological studies. *Journal of Nanoparticle Research* 11(1), 77-89.
- Kajjumba, G. W., Emik, S., Öngen, A., Özcan, H. K. and Aydın, S. 2018. Modelling of Adsorption Kinetic Processes-Errors, Theory and Application. *Advanced Sorption Process Applications*. S. Edebali, IntechOpen.
- Kalaruban, M. 2017. Nitrate Removal from Water Using Surface-Modified Adsorbents. Doctor of Philosophy, University of Technology Sydney.
- Kamiya, H. 2012. Chapter 3 - Characteristics and behavior of nanoparticles and its dispersion systems. *Nanoparticle Technology Handbook (Second Edition)*. M. Hosokawa, K. Nogi, M. Naito and T. Yokoyama. Amsterdam, Elsevier, 113-176.
- Karavasteva, M. 2010. Kinetics and deposit morphology of gold cemented on magnesium, aluminum, zinc, iron and copper from ammonium thiosulfate-ammonia solutions. *Hydrometallurgy* 104(1), 119-122.
- Karimzadeh, I., Aghazadeh, M., Doroudi, T., Ganjali, M. R. and Kolivand, P. H. 2017. Effective Preparation, Characterization and In Situ Surface Coating of Superparamagnetic Fe₃O₄ Nanoparticles with Polyethyleneimine Through Cathodic Electrochemical Deposition (CED). *Current Nanoscience* 13(2), 167-174.
- Kasper, A. C., Carrillo Abad, J., Garcia Gabaldon, M., Veit, H. M. and Perez Herranz, V. 2016. Determination of the potential gold electrowinning from an ammoniacal thiosulphate solution applied to recycling of printed circuit board scraps. *Waste Management and Research* 34(1), 47-57.

- Kasprzak, A., Popławska, M., Bystrzejewski, M., Łabędź, O. and Grudziński, I. P. 2015. Conjugation of polyethylenimine and its derivatives to carbon-encapsulated iron nanoparticles. *RSC Advances* 5(104), 85556-85567.
- Kataria, N. and Garg, V. K. 2018. Optimization of Pb (II) and Cd (II) adsorption onto ZnO nanoflowers using central composite design: isotherms and kinetics modelling. *Journal of Molecular Liquids* 271 228-239.
- Kejun, L., Yen, W. T., Shibayama, A., Miyazaki, T. and Fujita, T. 2004. Gold extraction from thiosulfate solution using trioctylmethylammonium chloride. *Hydrometallurgy* 73(1), 41-53.
- Kelland, D. R. 1985. Submicron magnetic particle separation. *Particulate Science and Technology* 3(3-4), 101-113.
- Kelland, D. R. 1993. Magnetic separation update. *IEEE Magnetics Society News Letter* 30(4), 1-2.
- Kelland, D. R. 1998. Magnetic separation of nanoparticles. *IEEE Transactions on Magnetics* 34(4), 2123-2125.
- Kerley, B. J. 1981. Recovery of precious metals from difficult ores. US Patent 4269622 A.
- Kerley, B. J. 1983. Recovery of precious metals from difficult ores. US Patent 4369061 A.
- Khandanlou, R., Ahmad, M. B., Masoumi, H. R. F., Shameli, K., Basri, M. and Kalantari, K. 2015. Rapid Adsorption of Copper(II) and Lead(II) by Rice Straw/Fe₃O₄ Nanocomposite: Optimization, Equilibrium Isotherms, and Adsorption Kinetics Study. *PLOS ONE* 10(3), 1-19.
- Kholmogorov, A. G., Kononova, O. N., Pashkov, G. L. and Kononov, Y. S. 2002. Thiocyanate solutions in gold technology. *Hydrometallurgy* 64(1), 43-48.
- Khoobi, M., Delshad, T. M., Vosooghi, M., Alipour, M., Hamadi, H., Alipour, E., Hamedani, M. P., Sadat ebrahimi, S. E., Safaei, Z., Foroumadi, A. and Shafiee, A. 2015. Polyethyleneimine-modified superparamagnetic Fe₃O₄ nanoparticles: An efficient, reusable and water tolerance nanocatalyst. *Journal of Magnetism and Magnetic Materials* 375 217-226.
- Kim, S., Choi, Y.-E. and Yun, Y.-S. 2016. Ruthenium recovery from acetic acid industrial effluent using chemically stable and high-performance polyethylenimine-coated polysulfone-Escherichia coli biomass composite fibers. *Journal of Hazardous Materials* 313 29-36.
- Kim, W., Suh, C. Y., Cho, S. W., Roh, K. M., Kwon, H., Song, K. and Shon, I. J. 2012. A new method for the identification and quantification of magnetite-maghemite mixture using conventional X-ray diffraction technique. *Talanta* 94 348-352.
- Kinno, T., Tomita, M., Ohkubo, T., Takeno, S. and Hono, K. 2014. Laser-assisted atom probe tomography of ¹⁸O-enriched oxide thin film for quantitative analysis of oxygen. *Applied Surface Science* 290 194-198.
- Kislenko, V. N. and Oliynyk, L. P. 2002. Complex formation of polyethyleneimine with copper(II), nickel(II), and cobalt(II) ions. *Journal of Polymer Science Part A: Polymer Chemistry* 40(7), 914-922.
- Kononova, O. N., Kholmogorov, A. G., Kononov, Y. S., Pashkov, G. L., Kachin, S. V. and Zotova, S. V. 2001. Sorption recovery of gold from thiosulphate solutions after leaching of products of chemical preparation of hard concentrates. *Hydrometallurgy* 59(1), 115-123.
- Kraus, A., Jainae, K., Unob, F. and Sukpirom, N. 2009. Synthesis of MPTS-modified cobalt ferrite nanoparticles and their adsorption properties in relation to Au(III). *Journal of Colloid and Interface Science* 338(2), 359-365.

- Kumar, R. and Chawla, J. 2013. Removal of Cadmium Ion from Water/Wastewater by Nano-metal Oxides: A Review. *Water Quality, Exposure and Health* 5 215-226.
- Kwak, I. S. and Yun, Y.-S. 2010. Recovery of zero-valent gold from cyanide solution by a combined method of biosorption and incineration. *Bioresource Technology* 101(22), 8587-8592.
- Laarz, E., Zhmud, B. V. and Bergström, L. 2000. Dissolution and Deagglomeration of Silicon Nitride in Aqueous Medium. *Journal of the American Ceramic Society* 83(10), 2394-2400.
- Lagergren, S. 1898. About the Theory of So-Called Adsorption of Soluble Substances. *Kungliga Svenska Vetenskapsakademiens Handlingar* 24(4), 1-39.
- Laidler, K. J. and Meiser, J. H. 1999. *Physical Chemistry*, 3rd edition. USA, Houghton Mifflin Company.
- Lam, K. F., Fong, C. M., Yeung, K. L. and McKay, G. 2008. Selective adsorption of gold from complex mixtures using mesoporous adsorbents. *Chemical Engineering Journal* 145(2), 185-195.
- Langmuir, I. 1918. The adsorption of gases on plane surfaces of glass, mica and platinum. *Journal of the American Chemical Society* 40(9), 1361-1403.
- Larraza, I., López-González, M., Corrales, T. and Marcelo, G. 2012. Hybrid materials: Magnetite–Polyethylenimine–Montmorillonite, as magnetic adsorbents for Cr(VI) water treatment. *Journal of Colloid and Interface Science* 385(1), 24-33.
- Larson, D. J. 2006. Atom probe characterization of nanomagnetic materials. *Thin Solid Films* 505(1-2), 16-21.
- Larumbe, S., Gomez-Polo, C., Perez-Landazabal, J. I. and Pastor, J. M. 2012. Effect of a SiO₂ coating on the magnetic properties of Fe₃O₄ nanoparticles. *Journal of Physics: Condensed Matter* 24(26), 266007.
- Laurent, S., Dutz, S., Hafeli, U. O. and Mahmoudi, M. 2011. Magnetic fluid hyperthermia: focus on superparamagnetic iron oxide nanoparticles. *Advances in Colloid and Interface Science* 166(1-2), 8-23.
- Laurent, S., Forge, D., Port, M., Roch, A., Robic, C., Elst, L. V. and Muller, R. N. 2008. Magnetic Iron Oxide Nanoparticles-Synthesis, Stabilization, Vectorization, Physicochemical Characterizations, and Biological Applications. *Chemical Reviews* 108(6), 2064-2110.
- Li, L., Mak, K. Y., Leung, C. W., Chan, K. Y., Chan, W. K., Zhong, W. and Pong, P. W. T. 2013. Effect of synthesis conditions on the properties of citric-acid coated iron oxide nanoparticles. *Microelectronic Engineering* 110 329-334.
- Li, R., Yang, W., Su, Y., Li, Q., Gao, S. and Shang, J. K. 2014. Ionic Potential: A General Material Criterion for the Selection of Highly Efficient Arsenic Adsorbents. *Journal of Materials Science & Technology* 30(10), 949-953.
- Lima, É. C., Adebayo, M. A. and Machado, F. M. 2015. Kinetic and Equilibrium Models of Adsorption. *Carbon Nanomaterials as Adsorbents for Environmental and Biological Applications*. C. P. Bergmann and F. M. Machado. Cham, Springer International Publishing, 33-69.
- Lin, T.L. and Lien, H.L. 2013. Effective and Selective Recovery of Precious Metals by Thiourea Modified Magnetic Nanoparticles. *International Journal of Molecular Sciences* 14(5), 9834-9847.
- Lindén, J. B., Larsson, M., Kaur, S., Skinner, W. M., Miklavcic, S. J., Nann, T., Kempson, I. M. and Nydén, M. 2015. Polyethyleneimine for copper absorption II: kinetics, selectivity and efficiency from seawater. *RSC Advances* 5(64), 51883-51890.

- Lindquist, G. M. and Stratton, R. A. 1976. The role of polyelectrolyte charge density and molecular weight on the adsorption and flocculation of colloidal silica with polyethylenimine. *Journal of Colloid and Interface Science* 55(1), 45-59.
- Liu, Y. 2009. Is the Free Energy Change of Adsorption Correctly Calculated? *Journal of Chemical & Engineering Data* 54(7), 1981-1985.
- Liu, Y., Yang, J., Xie, M., Xu, J., Li, Y., Shen, H. and Hao, J. 2017. Synthesis of polyethylenimine-modified magnetic iron oxide nanoparticles without adding base and other additives. *Materials Letters* 193 122-125.
- Lotfi Zadeh Zhad, H. R., Aboufazeli, F., Sadeghi, O., Amani, V., Najafi, E. and Tavassoli, N. 2013. Tris(2-Aminoethyl)Amine-Functionalized Fe₃O₄ Magnetic Nanoparticles as a Selective Sorbent for Separation of Silver and Gold Ions in Different pHs. *Journal of Chemistry* 2013 1-7.
- Lu, A. H., Salabas, E. L. and Schüth, F. 2007. Magnetic Nanoparticles: Synthesis, Protection, Functionalization, and Application. *Angewandte Chemie International Edition* 46(8), 1222-1244.
- Lu, W., Ling, M., Jia, M., Huang, P., Li, C. and Yan, B. 2014. Facile synthesis and characterization of polyethylenimine-coated Fe₃O₄ superparamagnetic nanoparticles for cancer cell separation. *Molecular Medicine Reports* 9(3), 1080-1084.
- Lukey, G. C. and van Deventer, J. S. J. 2004. *Fundamental Developments in Understanding the Interactions between Metal Cyanides and Functional Polymers. Fundamentals and Applications of Anion Separations.* B. A. Moyer and R. P. Singh. New York, Springer Science+Business Media, LLC.
- Lukey, G. C., Van Deventer, J. S. J., Chowdhury, R. L. and Shallcross, D. C. 1999. The effect of salinity on the capacity and selectivity of ion exchange resins for gold cyanide. *Minerals Engineering* 12(7), 769-785.
- Lungu, C. N., Diudea, M. V., Putz, M. V. and Grudzinski, I. P. 2016. Linear and Branched PEIs (Polyethylenimines) and Their Property Space. *International Journal of Molecular Sciences* 17(4), 555.
- Lutzenkirchen, J. 2002. *Surface Complexation Models of Adsorption: A Critical Survey in the Context of Experimental Data. Adsorption- Theory, Modelling and Analysis.* J. Toth.
- Machesky, M. L., Andrade, W. O. and Rose, A. W. 1991. Adsorption of gold(III)-chloride and gold(I)-thiosulfate anions by goethite. *Geochimica et Cosmochimica Acta* 55(3), 769-776.
- Mady, M. M., Mohammed, W. A., El-Guendy, N. M. and Elsayed, A. A. 2011. Effect of polymer molecular weight on the DNA/PEI polyplexes properties. *Romanian Journal of Biophysics* 21(2), 151-165.
- Mahdavian, A. R. and Mirrahimi, M. A.-S. 2010. Efficient separation of heavy metal cations by anchoring polyacrylic acid on superparamagnetic magnetite nanoparticles through surface modification. *Chemical Engineering Journal* 159(1-3), 264-271.
- Maier, J., Pfeiffer, B., Volkert, C. A. and Nowak, C. 2016. Three-Dimensional Microstructural Characterization of Lithium Manganese Oxide with Atom Probe Tomography. *Energy Technology* 4(12), 1565-1574.
- Makhova, L., Mikhlin, Y. and Romanchenko, A. 2007. A combined XPS, XANES and STM/STS study of gold and silver deposition on metal sulphides. *Nuclear Instruments and Methods in Physics Research Section A: Accelerators, Spectrometers, Detectors and Associated Equipment* 575(1), 75-77.

- Mandel, K. and Hutter, F. 2012. The magnetic nanoparticle separation problem. *Nano Today* 7(6), 485-487.
- Marghussian, V. 2015. 4 - Magnetic Properties of Nano-Glass Ceramics. *Nano-Glass Ceramics*. V. Marghussian. Oxford, William Andrew Publishing, 181-223.
- Marsden, J. O. and House, C. L. 1960. *The chemistry of gold extraction*, Second edition. Littleton, Colorado, USA., Society for Mining, Metallurgy, and Exploration, Inc. (SME).
- Martell, A. E. and Hancock, R. D. 1996. *Metal Complexes in Aqueous Solutions*. Plenum Press, New York.
- Martell, A. E. and Smith, R. M. 1974. *Critical stability constants*. Volume 1: Amino Acids. New York; London, Plenum Press.
- McCarroll, I. 2018. *Corrosion Processes: Through the lens of atom probe tomography*. Doctor of Philosophy, The University of Sydney.
- Metso (2015). High gradient magnetic separators-METSO brochure. Sweden, Metso Corporation. BrochureNo.2573-08-11-ESBL/Sala-English, www.metsominerals.com.
- Misra, S. K., Li, L., Mukherjee, S. and Ghosh, G. 2015. Anisotropic magnetic field observed at 300 K in citrate-coated iron oxide nanoparticles: effect of counterions. *Journal of Nanoparticle Research* 17(12).
- Moeser, G. D., Roach, K. A., Green, W. H., Alan Hatton, T. and Laibinis, P. E. 2004. High-gradient magnetic separation of coated magnetic nanoparticles. *AIChE Journal* 50(11), 2835-2848.
- Mohammed, F. S., Cole, S. R. and Kitchens, C. L. 2013. Synthesis and Enhanced Colloidal Stability of Cationic Gold Nanoparticles using Polyethyleneimine and Carbon Dioxide. *ACS Sustainable Chemistry & Engineering* 1(7), 826-832.
- Mohammed, L., Gomaa, H. G., Ragab, D. and Zhu, J. 2017. Magnetic nanoparticles for environmental and biomedical applications: A review. *Particuology* 30 1-14.
- Mos, Y. M., Vermeulen, A. C., Buisman, C. J. N. and Weijma, J. 2018. X-Ray Diffraction of Iron Containing Samples: The Importance of a Suitable Configuration. *Geomicrobiology Journal* 35(6), 511-517.
- Mpinga, C. N., Eksteen, J., Aldrich, C. and Dyer, L. 2017. Identification of the significant factors determining extractability of Ni and Cu after sulfation roasting of a PGM-bearing chromitite ore. *Minerals Engineering* 110 153-165.
- Muir, D. M. 2011. A review of the selective leaching of gold from oxidised copper-gold ores with ammonia-cyanide and new insights for plant control and operation. *Minerals Engineering* 24(6), 576-582.
- Murthy, D. S. R., Kumar, V. and Rao, K. V. 2003. Extraction of gold from an Indian low-grade refractory gold ore through physical beneficiation and thiourea leaching. *Hydrometallurgy* 68(1-3), 125-130.
- Muslim, A., Pareek, V. K., Tade, M. O., Jeffrey, M. I. and Zhang, H. G. 2009. Adsorption of Polythionates and Thiosulfate on Strong Base Anion Exchange Resins. In: *Engineering Our Future: Are We up to the Challenge?*, Barton, ACT, Engineers Australia.
- Myers, R. H., Montgomery, D. C. and Anderson-Cook, C. M. 2016. *Response Surface Methodology : Process and Product Optimization Using Designed Experiments*. New York, USA, John Wiley & Sons, Incorporated.
- Na, Y., Yang, S. and Lee, S. 2014. Evaluation of citrate-coated magnetic nanoparticles as draw solute for forward osmosis. *Desalination* 347 34-42.

- Nakamoto, K. 2009. *Infrared and Raman Spectra of Inorganic and Coordination Compounds : Part B. Applications in Coordination, Organometallic, and Bioinorganic Chemistry*. New York, United States, John Wiley & Sons, Incorporated.
- Navarro, P., Alvarez, R., Vargas, C. and Alguacil, F. J. 2004. On the use of zinc for gold cementation from ammoniacal–thiosulphate solutions. *Minerals Engineering* 17(6), 825-831.
- Navarro, P., Vargas, C., Alonso, M. and Alguacil, F. J. 2007. Towards a more environmentally friendly process for gold: models on gold adsorption onto activated carbon from ammoniacal thiosulfate solutions. *Desalination* 211(1–3), 58-63.
- Nedel'ko, V. V., Korsunskii, B. L., Dubovitskii, F. I. and Gromova, G. L. 1975. The thermal degradation of branched polyethylenimine. *Polymer Science U.S.S.R.* 17(7), 1697-1703.
- Neyestani, M. R., Shemirani, F., Mozaffari, S. and Alvand, M. 2017. A magnetized graphene oxide modified with 2-mercaptobenzothiazole as a selective nanosorbent for magnetic solid phase extraction of gold(III), palladium(II) and silver(I). *Microchimica Acta* 184(8), 2871-2879.
- Nguyen, V. S., Rouxel, D., Hadji, R., Vincent, B. and Fort, Y. 2011. Effect of ultrasonication and dispersion stability on the cluster size of alumina nanoscale particles in aqueous solutions. *Ultrasonics Sonochemistry* 18(1), 382-388.
- Nicol, M. J. and O'Malley, G. 2002. Recovering gold from thiosulfate leach pulps via ion exchange. *JOM* 54(10), 44-46.
- Nigam, S., Barick, K. C. and Bahadur, D. 2011. Development of citrate-stabilized Fe₃O₄ nanoparticles: Conjugation and release of doxorubicin for therapeutic applications. *Journal of Magnetism and Magnetic Materials* 323(2), 237-243.
- Nobmann, U. and Morfesis, A. 2009. Light scattering and nanoparticles. *Materials Today* 12(5), 52-54.
- Nosrati, A., Larsson, M., Lindén, J. B., Zihao, Z., Addai-Mensah, J. and Nydén, M. 2017. Polyethyleneimine functionalized mesoporous diatomite particles for selective copper recovery from aqueous media. *International Journal of Mineral Processing* 166 29-36.
- O'Grady, K. 2002. Biomedical applications of magnetic nanoparticles. *Journal of Physics D: Applied Physics* 36(13).
- O'Handley, R. C. 2000. *Modern Magnetic Materials: Principles and Applications*. Wiley, New York.
- O'Malley, G. P. 2002. *Recovery of Gold from Thiosulfate Solutions and Pulps with Anion-Exchange Resins*. Doctor of Philosophy, Murdoch University.
- Oberteuffer, J. 1974. Magnetic separation: A review of principles, devices, and applications. *IEEE Transactions on Magnetics* 10(2), 223-238.
- Odio, O. F., Lartundo-Rojas, L., Santiago-Jacinto, P., Martínez, R. and Reguera, E. 2014. Sorption of Gold by Naked and Thiol-Capped Magnetite Nanoparticles: An XPS Approach. *The Journal of Physical Chemistry C* 118(5), 2776-2791.
- Oraby, E. A. 2009. *Gold Leaching in Thiosulfate Solutions and Its environmental effects compared with cyanide*. Doctor of Philosophy, Curtin University, Australia.
- Oraby, E. A. and Eksteen, J. J. 2015a. Gold leaching in cyanide-starved copper solutions in the presence of glycine. *Hydrometallurgy* 156 81-88.
- Oraby, E. A. and Eksteen, J. J. 2015b. The leaching of gold, silver and their alloys in alkaline glycine–peroxide solutions and their adsorption on carbon. *Hydrometallurgy* 152 199-203.

- Oraby, E. A., Eksteen, J. J. and Tanda, B. C. 2017. Gold and copper leaching from gold-copper ores and concentrates using a synergistic lixiviant mixture of glycine and cyanide. *Hydrometallurgy* 169 339-345.
- Pamme, N. 2006. Magnetism and microfluidics. *Lab on a Chip* 6(1), 24-38.
- Pandey, A. P. and Sawant, K. K. 2016. Polyethylenimine: A versatile, multifunctional non-viral vector for nucleic acid delivery. *Materials Science and Engineering: C* 68(Supplement C), 904-918.
- Pang, Y., Zeng, G., Tang, L., Zhang, Y., Liu, Y., Lei, X., Li, Z., Zhang, J., Liu, Z. and Xiong, Y. 2011a. Preparation and application of stability enhanced magnetic nanoparticles for rapid removal of Cr(VI). *Chemical Engineering Journal* 175 222-227.
- Pang, Y., Zeng, G., Tang, L., Zhang, Y., Liu, Y., Lei, X., Li, Z., Zhang, J. and Xie, G. 2011b. PEI-grafted magnetic porous powder for highly effective adsorption of heavy metal ions. *Desalination* 281 278-284.
- Parker, G., Gow, R., Young, C., Twidwell, L. and Alan Hope, G. 2008. Spectroelectrochemical investigation of the reaction between adsorbed cuprous cyanide and gold thiosulfate ions at activated carbon surfaces. *Hydrometallurgy 2008: Proceedings of the Sixth International Symposium, Littleton, CO, USA*.
- Parkinson, G. S. 2016. Iron oxide surfaces. *Surface Science Reports* 71(1), 272-365.
- Patsula, V., Moskvin, M., Dutz, S. and Horák, D. 2016. Size-dependent magnetic properties of iron oxide nanoparticles. *Journal of Physics and Chemistry of Solids* 88 24-30.
- Pearson, R. G. 1963. Hard and Soft Acids and Bases. *Journal of the American Chemical Society* 85(22), 3533-3539.
- Petkov, V., Cozzoli, P. D., Buonsanti, R., Cingolani, R. and Ren, Y. 2009. Size, Shape, and Internal Atomic Ordering of Nanocrystals by Atomic Pair Distribution Functions: A Comparative Study of γ -Fe₂O₃ Nanosized Spheres and Tetrapods. *Journal of the American Chemical Society* 131(40), 14264-14266.
- Petrović, S., Rožić, L., Jović, V., Stojadinović, S., Grbić, B., Radić, N., Lamovec, J. and Vasilović, R. 2018. Optimization of a nanoparticle ball milling process parameters using the response surface method. *Advanced Powder Technology* 29(9), 2129-2139.
- Preisinger, M., Krispin, M., Rudolf, T., Horn, S. and Strongin, D. R. 2005. Electronic structure of nanoscale iron oxide particles measured by scanning tunneling and photoelectron spectroscopies. *Physical Review B* 71(16), 165409 165401-165406.
- Qi, P. H. and Hiskey, J. B. 1991. Dissolution kinetics of gold in iodide solutions. *Hydrometallurgy* 27(1), 47-62.
- Rabai, G. and Epstein, I. R. 1992. Systematic design of chemical oscillators. 83. Equilibria and kinetics of the fast interaction between copper(II) and thiosulfate ions in aqueous solution. *Inorganic Chemistry* 31(15), 3239-3242.
- Racuciu, M., Creanga, D. E. and Airinei, A. 2006. Citric-acid-coated magnetite nanoparticles for biological applications. *The European Physical Journal E* 21(2), 117-121.
- Radeva, T. and Petkanchin, I. 1997. Electric Properties and Conformation of Polyethylenimine at the Hematite–Aqueous Solution Interface. *Journal of Colloidal and Interface science* 196 87-91.
- Rahmayanti, M., Santosa, S. J. and Sutarno 2016. Mechanisms of gold recovery from aqueous solutions using gallic acid modified magnetite particles synthesized via reverse coprecipitation method. *International Journal of ChemTech Research* 9(4), 446-452.
- Range, B. M. K. and Hawboldt, K. A. 2018. Adsorption of thiosulphate, trithionate, tetrathionate using biomass ash/char. *Journal of Environmental Chemical Engineering* 6(4), 5401-5408.

- Ranjbar, R., Naderi, M., Omidvar, H. and Amoabediny, G. 2014. Gold recovery from copper anode slime by means of magnetite nanoparticles (MNPs). *Hydrometallurgy* 143 54-59.
- Ravi, S., Zhang, S., Lee, Y.-R., Kang, K.-K., Kim, J.-M., Ahn, J.-W. and Ahn, W.-S. 2018. EDTA-functionalized KCC-1 and KIT-6 mesoporous silicas for Nd³⁺ ion recovery from aqueous solutions. *Journal of Industrial and Engineering Chemistry* 67 210-218.
- Riveros, P. A. 1993. Selectivity aspects of the extraction of gold from cyanide solutions with ion exchange resins. *Hydrometallurgy* 33(1), 43-58.
- Roto, R., Yusran, Y. and Kuncaka, A. 2016. Magnetic adsorbent of Fe₃O₄@SiO₂ core-shell nanoparticles modified with thiol group for chloroauric ion adsorption. *Applied Surface Science* 377 30-36.
- Rudolph, M., Erler, J. and Peuker, U. A. 2012. A TGA–FTIR perspective of fatty acid adsorbed on magnetite nanoparticles–Decomposition steps and magnetite reduction. *Colloids and Surfaces A: Physicochemical and Engineering Aspects* 397 16-23.
- RuizMoreno, R. G., Martinez, A. I., Castro-Rodriguez, R. and Bartolo, P. 2012. Synthesis and Characterization of Citrate Coated Magnetite Nanoparticles. *Journal of Superconductivity and Novel Magnetism* 26(3), 709-712.
- Rusitzka, K. A. K., Stephenson, L. T., Szczepaniak, A., Gremer, L., Raabe, D., Willbold, D. and Gault, B. 2018. A near atomic-scale view at the composition of amyloid-beta fibrils by atom probe tomography. *Scientific Reports* 8(1).
- Sabermahani, F., Taher, M. A. and Bahrami, H. 2016. Separation and preconcentration of trace amounts of gold from water samples prior to determination by flame atomic absorption spectrometry. *Arabian Journal of Chemistry* 9 S1700-S1705.
- Saha, P. and Chowdhury, S. 2011. Insight Into Adsorption Thermodynamics. *Thermodynamics*. M. Tadashi, InTech.
- Sahoo, Y., Goodarzi, A., Swihart, M. T., Ohulchanskyy, T. Y., Kaur, N., Furlani, E. P. and Prasad, P. N. 2005. Aqueous Ferrofluid of Magnetite Nanoparticles: Fluorescence Labeling and Magnetophoretic Control. *The Journal of Physical Chemistry B* 109(9), 3879-3885.
- Sahu, S. K., Maiti, S., Pramanik, A., Ghosh, S. K. and Pramanik, P. 2012. Controlling the thickness of polymeric shell on magnetic nanoparticles loaded with doxorubicin for targeted delivery and MRI contrast agent. *Carbohydrate Polymers* 87(4), 2593-2604.
- Santhanagopalan, D., Schreiber, D. K., Perea, D. E., Martens, R. L., Janssen, Y., Khalifah, P. and Meng, Y. S. 2015. Effects of laser energy and wavelength on the analysis of LiFePO₄ using laser assisted atom probe tomography. *Ultramicroscopy* 148 57-66.
- Saraswathy, A., Nazeer, S. S., Jeevan, M., Nimi, N., Arumugam, S., Harikrishnan, V. S., Varma, P. R. and Jayasree, R. S. 2014. Citrate coated iron oxide nanoparticles with enhanced relaxivity for in vivo magnetic resonance imaging of liver fibrosis. *Colloids Surf B Biointerfaces* 117 216-224.
- Saxey, D. W., Moser, D. E., Piazzolo, S., Reddy, S. M. and Valley, J. W. 2018. Atomic worlds: Current state and future of atom probe tomography in geoscience. *Scripta Materialia* 148 115-121.
- Schleich, N., Sibret, P., Danhier, P., Ucakar, B., Laurent, S., Muller, R. N., Jerome, C., Gallez, B., Preat, V. and Danhier, F. 2013. Dual anticancer drug/superparamagnetic iron oxide-loaded PLGA-based nanoparticles for cancer therapy and magnetic resonance imaging. *International Journal of Pharmaceutics* 447(1-2), 94-101.
- Seino, S., Matsuoka, Y., Kinoshita, T., Nakagawa, T. and Yamamoto, T. A. 2009. Dispersibility improvement of gold/iron-oxide composite nanoparticles by

- polyethylenimine modification. *Journal of Magnetism and Magnetic Materials* 321(10), 1404-1407.
- Senanayake, G. 2004. Gold leaching in non-cyanide lixiviant systems: critical issues on fundamentals and applications. *Minerals Engineering* 17(6), 785-801.
- Senanayake, G. 2005a. Gold leaching by thiosulphate solutions: a critical review on copper(II)–thiosulphate–oxygen interactions. *Minerals Engineering* 18(10), 995-1009.
- Senanayake, G. 2005b. Role of copper(II), carbonate and sulphite in gold leaching and thiosulphate degradation by oxygenated alkaline non-ammoniacal solutions. *Minerals Engineering* 18(4), 409-426.
- Senanayake, G. 2005c. The role of ligands and oxidants in thiosulfate leaching of gold. *Gold Bulletin* 38(4), 170-179.
- Senanayake, G. 2012. Gold leaching by copper(II) in ammoniacal thiosulphate solutions in the presence of additives. Part I: A review of the effect of hard–soft and Lewis acid-base properties and interactions of ions. *Hydrometallurgy* 115-116 1-20.
- Shan, G., Surampalli, R. Y., Tyagi, R. D. and Zhang, T. C. 2009. Nanomaterials for environmental burden reduction, waste treatment, and nonpoint source pollution control: a review. *Frontiers of Environmental Science & Engineering in China* 3(3), 249-264.
- Sharma, G. and Jeevanandam, P. 2012. Single step thermal decomposition approach to prepare supported γ -Fe₂O₃ nanoparticles. *Applied Surface Science* 258(8), 3679-3688.
- Shaw, R. (2014). *Dynamic Light Scattering Training - Achieving reliable nano particle sizing*. Malvern Instruments, Malvern, UK.
- Shebanova, O. N. and Lazor, P. 2003. Raman study of magnetite (Fe₃O₄): laser-induced thermal effects and oxidation. *Journal of Raman Spectroscopy* 34(11), 845-852.
- Shen, Y. F., Tang, J., Nie, Z. H., Wang, Y. D., Ren, Y. and Zuo, L. 2009. Preparation and application of magnetic Fe₃O₄ nanoparticles for wastewater purification. *Separation and Purification Technology* 68(3), 312-319.
- Singh, S., Barick, K. C. and Bahadur, D. 2011. Surface engineered magnetic nanoparticles for removal of toxic metal ions and bacterial pathogens. *Journal of Hazardous Materials* 192(3), 1539-1547.
- Sitardo, O. 2017. *Gold Leaching in Thiosulfate-Oxygen Solutions*. Doctor of Philosophy, Murdoch University, Australia.
- Sitardo, O., Senanayake, G., Dai, X. and Breuer, P. 2019. The adsorption of gold(I) on minerals and activated carbon (preg-robbing) in non-ammoniacal thiosulfate solutions - effect of calcium thiosulfate, silver(I), copper(I) and polythionate ions. *Hydrometallurgy* 184 206-217.
- Sitardo, O., Senanayake, G., Dai, X., Nikoloski, A. N. and Breuer, P. 2018. A review of factors affecting gold leaching in non-ammoniacal thiosulfate solutions including degradation and in-situ generation of thiosulfate. *Hydrometallurgy* 178 151-175.
- Sivashankar, R., Sathya, A. B., Vasantharaj, K. and Sivasubramanian, V. 2014. Magnetic composite an environmental super adsorbent for dye sequestration – A review. *Environmental Nanotechnology, Monitoring & Management* 1–2 36-49.
- Slavov, L., Abrashev, M. V., Merodiiska, T., Gelev, C., Vandenberghe, R. E., Markova-Deneva, I. and Nedkov, I. 2010. Raman spectroscopy investigation of magnetite nanoparticles in ferrofluids. *Journal of Magnetism and Magnetic Materials* 322(14), 1904-1911.
- Smith, B. C. 1999. *Infrared Spectral Interpretation : A Systematic Approach*, CRC Press.

- Smith, R. M., Martell, A. E. and Motekaitis, R. J. 1985. Prediction of stability constants. I. Protonation constants of carboxylates and formation constants of their complexes with class a metal ions. *Inorganica Chimica Acta* 99(2), 207-216.
- Soler, M. A. G. and Qu, F. 2012. 14-Raman Spectroscopy of Iron Oxide Nanoparticles. *Raman Spectroscopy for Nanomaterials Characterization*, Springer, 379-416.
- Sparrow, G. J. and Woodcock, J. T. 1995. Cyanide and Other Lixiviant Leaching Systems for Gold with Some Practical Applications. *Mineral Processing and Extractive Metallurgy Review* 14(3-4), 193-247.
- Srivastava, S., Awasthi, R., Gajbhiye, N. S., Agarwal, V., Singh, A., Yadav, A. and Gupta, R. K. 2011. Innovative synthesis of citrate-coated superparamagnetic Fe₃O₄ nanoparticles and its preliminary applications. *Journal of Colloid and Interface Science* 359(1), 104-111.
- Steitz, B., Hofmann, H., Kamau, S. W., Hassa, P. O., Hottiger, M. O., von Rechenberg, B., Hofmann-Antenbrink, M. and Petri-Fink, A. 2007. Characterization of PEI-coated superparamagnetic iron oxide nanoparticles for transfection: Size distribution, colloidal properties and DNA interaction. *Journal of Magnetism and Magnetic Materials* 311(1), 300-305.
- Stephens, J. R., Beveridge, J. S. and Williams, M. E. 2012. Analytical methods for separating and isolating magnetic nanoparticles. *Physical Chemistry Chemical Physics* 14(10), 3280-3289.
- Sui, N., Wang, L., Wu, X., Li, X., Sui, J., Xiao, H., Liu, M., Wan, J. and Yu, W. W. 2015. Polyethylenimine modified magnetic graphene oxide nanocomposites for Cu²⁺removal. *RSC Advances* 5(1), 746-752.
- Sullivan, A. M. and Kohl, P. A. 1995. The Autocatalytic Deposition of Gold in Nonalkaline, Gold Thiosulfate Electroless Bath. *Journal of The Electrochemical Society* 142(7), 2250-2255.
- Sun, X., Dong, S. and Wang, E. 2005. One-step preparation of highly concentrated well-stable gold colloids by direct mix of polyelectrolyte and HAuCl₄ aqueous solutions at room temperature. *Journal of Colloid and Interface Science* 288(1), 301-303.
- Suslick, K. S. 1998. Sonochemistry. *Kirk-Othmer Encyclopedia of Chemical Technology*. New York, John Wiley and Sons Inc. 26, 516-541.
- Swaminathan, C., Pyke, P. and Johnston, R. F. 1993. Reagent trends in the gold extraction industry. *Minerals Engineering* 6(1), 1-16.
- Tahmasebi, E. and Yamini, Y. 2013. Polythiophene-coated Fe₃O₄ nanoparticles as a selective adsorbent for magnetic solid-phase extraction of silver(I), gold(III), copper(II) and palladium(II). *Microchimica Acta* 181(5-6), 543-551.
- Takayasu, M., Gerber, R. and Friedlaender, F. J. 1983. Magnetic separation of submicron particles. *IEEE Transactions on Magnetics* 19(5), 2112-2114.
- Tang, S. C. and Lo, I. M. 2013a. Magnetic nanoparticles: essential factors for sustainable environmental applications. *Water Research* 47(8), 2613-2632.
- Tang, S. C. N. and Lo, I. M. C. 2013b. Magnetic nanoparticles: Essential factors for sustainable environmental applications. *Water Research* 47(8), 2613-2632.
- Tanwar, S., Awana, V. P. S., Singh, S. P. and Pasricha, R. 2012. Magnetic Field Dependence of Blocking Temperature in Oleic Acid Functionalized Iron Oxide Nanoparticles. *Journal of Superconductivity and Novel Magnetism* 25(6), 2041-2045.
- Tauetsile, P. J., Oraby, E. A. and Eksteen, J. J. 2018. Adsorption behaviour of copper and gold glycinate in alkaline media onto activated carbon. Part 1: Isotherms. *Hydrometallurgy* 178 202-208.

- Taurozzi, J. S., Hackley, V. A. and Wiesner, M. R. 2011. Ultrasonic dispersion of nanoparticles for environmental, health and safety assessment-issues and recommendations. *Nanotoxicology* 5(4), 711-729.
- Teja, A. S. and Koh, P.-Y. 2009. Synthesis, properties, and applications of magnetic iron oxide nanoparticles. *Progress in Crystal Growth and Characterization of Materials* 55(1-2), 22-45.
- Tewari, P. H. and McLean, A. W. 1972. Temperature dependence of point of zero charge of alumina and magnetite. *Journal of Colloid and Interface Science* 40(2), 267-272.
- Thangaraj, B., Jia, Z., Dai, L., Liu, D. and Du, W. 2019. Effect of silica coating on Fe₃O₄ magnetic nanoparticles for lipase immobilization and their application for biodiesel production. *Arabian Journal of Chemistry* 12(8), 4694-4706.
- Tóth, I. Y., Nesztor, D., Novák, L., Illés, E., Szekeres, M., Szabó, T. and Tombácz, E. 2017. Clustering of carboxylated magnetite nanoparticles through polyethylenimine: Covalent versus electrostatic approach. *Journal of Magnetism and Magnetic Materials* 427 280-288.
- Tran, H. N., You, S.-J. and Chao, H.-P. 2016. Thermodynamic parameters of cadmium adsorption onto orange peel calculated from various methods: A comparison study. *Journal of Environmental Chemical Engineering* 4(3), 2671-2682.
- Tran, H. N., You, S. J., Hosseini-Bandegharaei, A. and Chao, H. P. 2017. Mistakes and inconsistencies regarding adsorption of contaminants from aqueous solutions: A critical review. *Water Res* 120 88-116.
- Tran, N. and Webster, T. J. 2010. Magnetic nanoparticles: biomedical applications and challenges. *Journal of Materials Chemistry* 20(40), 8760-8767.
- Tseng, J. Y., Chang, C. Y., Chang, C. F., Chen, Y. H., Chang, C. C., Ji, D. R., Chiu, C. Y. and Chiang, P. C. 2009. Kinetics and equilibrium of desorption removal of copper from magnetic polymer adsorbent. *Journal of Hazardous Materials* 171(1-3), 370-377.
- Tsukamoto, O., Ohizumi, T., Ohara, T., Mori, S. and Wada, Y. 1995. Feasibility study on separation of several tens nanometer scale particles by magnetic field-flow-fractionation technique using superconducting magnet. *IEEE Transactions on Applied Superconductivity* 5(2), 311-314.
- Upadhyay, S., Parekh, K. and Pandey, B. 2016. Influence of crystallite size on the magnetic properties of Fe₃O₄ nanoparticles. *Journal of Alloys and Compounds* 678 478-485.
- van Deventer, J. S. J. and van der Merwe, P. F. 1994. Factors affecting the elution of gold cyanide from activated carbon. *Minerals Engineering* 7(1), 71-86.
- Vargas, A. M. M., Martins, A. C. and Almeida, V. C. 2012. Ternary adsorption of acid dyes onto activated carbon from flamboyant pods (*Delonix regia*): Analysis by derivative spectrophotometry and response surface methodology. *Chemical Engineering Journal* 195-196 173-179.
- Vidojkovic, S. M. and Rakin, M. P. 2016. Surface properties of magnetite in high temperature aqueous electrolyte solutions: A review. *Advances in Colloid and Interface Science* 245 108-129.
- Vijayakumar, R., Koltypin, Y., Felner, I. and Gedanken, A. 2000. Sonochemical synthesis and characterization of pure nanometer-sized Fe₃O₄ particles. *Materials Science and Engineering: A* 286(1), 101-105.
- Vikram, S., Vasanthakumari, R., Tsuzuki, T. and Rangarajan, M. 2016. Investigations of suspension stability of iron oxide nanoparticles using time-resolved UV-visible spectroscopy. *Journal of Nanoparticle Research* 18(9).

- Vilar, V. J. P., Botelho, C. M. S. and Boaventura, R. A. R. 2007. Copper desorption from Gelidium algal biomass. *Water Research* 41(7), 1569-1579.
- von Harpe, A., Petersen, H., Li, Y. and Kissel, T. 2000. Characterization of commercially available and synthesized polyethylenimines for gene delivery. *Journal of Controlled Release* 69(2), 309-322.
- Wang, J., Zheng, S., Shao, Y., Liu, J., Xu, Z. and Zhu, D. 2010. Amino-functionalized Fe₃O₄@SiO₂ core-shell magnetic nanomaterial as a novel adsorbent for aqueous heavy metals removal. *Journal of Colloid and Interface Science* 349(1), 293-299.
- Wang, X., Zhou, L., Ma, Y., Li, X. and Gu, H. 2009. Control of aggregate size of polyethyleneimine-coated magnetic nanoparticles for magnetofection. *Nano Research* 2(5), 365-372.
- Wang, Y., Xu, F., Zhang, L. and Wei, X. 2012. One-pot solvothermal synthesis of Fe₃O₄-PEI composite and its further modification with Au nanoparticles. *Journal of Nanoparticle Research* 15(1).
- Weber, W. J. and Morris, J. C. 1963. Kinetics of adsorption on carbon from solution. *Journal of the Sanitary Engineering Division* 89(2), 31-60.
- Wilhelm, C. and Gazeau, F. 2008. Universal cell labelling with anionic magnetic nanoparticles. *Biomaterials* 29(22), 3161-3174.
- Wilson, D. and Langell, M. A. 2014. XPS analysis of oleylamine/oleic acid capped Fe₃O₄ nanoparticles as a function of temperature. *Applied Surface Science* 303 6-13.
- Wu, W., He, Q. and Jiang, C. 2008. Magnetic iron oxide nanoparticles: synthesis and surface functionalization strategies. *Nanoscale Research Letters* 3(11), 397-415.
- Wu, W., Wu, Z., Yu, T., Jiang, C. and Kim, W. S. 2015. Recent progress on magnetic iron oxide nanoparticles: synthesis, surface functional strategies and biomedical applications. *Science and Technology of Advanced Materials* 16(2), 023501.
- Xia, C., Yen, W. T. and Deschenes, G. 2003. Improvement of thiosulfate stability in gold leaching. *Minerals & Metallurgical Processing* 20(2), 68-72.
- Xie, S., Zhang, B., Wang, L., Wang, J., Li, X., Yang, G. and Gao, F. 2015. Superparamagnetic iron oxide nanoparticles coated with different polymers and their MRI contrast effects in the mouse brains. *Applied Surface Science* 326 32-38.
- Xin, X., Wei, Q., Yang, J., Yan, L., Feng, R., Chen, G., Du, B. and Li, H. 2012. Highly efficient removal of heavy metal ions by amine-functionalized mesoporous Fe₃O₄ nanoparticles. *Chemical Engineering Journal* 184 132-140.
- XPSsimplified. Adventitious Carbon Contamination from <https://xpssimplified.com/> (Thermo Fisher scientific Inc.).
- Xu, B., Kong, W., Li, Q., Yang, Y., Jiang, T. and Liu, X. 2017. A Review of Thiosulfate Leaching of Gold: Focus on Thiosulfate Consumption and Gold Recovery from Pregnant Solution. *Metals* 7(6).
- Xu, H., Liu, D.-d. and He, L. 2015. Adsorption of Copper(II) from an Wastewater Effluent of Electroplating Industry by Poly(ethyleneimine)-Functionalized Silica. *Iranian Journal of Chemistry and Chemical Engineering* 34(2), 73-81.
- Xu, L., Yang, L., Luo, M., Liang, X., Wei, X., Zhao, J. and Liu, H. 2011. Reduction of hexavalent chromium by *Pannonibacter phragmitetus* LSSE-09 coated with polyethyleneimine-functionalized magnetic nanoparticles under alkaline conditions. *J Hazard Mater Journal of Hazardous Materials* 189(3), 787-793.

- Xu, Y. and Schoonen, M. A. A. 1995. The stability of thiosulfate in the presence of pyrite in low-temperature aqueous solutions. *Geochimica et Cosmochimica Acta* 59(22), 4605-4622.
- Yamashita, T. and Hayes, P. 2008. Analysis of XPS spectra of Fe²⁺ and Fe³⁺ ions in oxide materials. *Applied Surface Science* 254(8), 2441-2449.
- Yang, L., Jia, F., Yang, B. and Song, S. 2017. Efficient adsorption of Au(CN)₂⁻ from gold cyanidation with graphene oxide-polyethylenimine hydrogel as adsorbent. *Results in Physics* 7 4089-4095.
- Yang, Y., Hou, J., Wang, P., Wang, C., Miao, L., Ao, Y., Xu, Y., Wang, X., Lv, B., You, G. and Yang, Z. 2018. Interpretation of the disparity in harvesting efficiency of different types of *Microcystis aeruginosa* using polyethylenimine (PEI)-coated magnetic nanoparticles. *Algal Research* 29 257-265.
- Yavuz, C. T., Mayo, J. T., Yu, W. W., Prakash, A., Falkner, J. C., Yean, S., Cong, L., Shipley, H. J., Kan, A., Tomson, M., Natelson, D. and Colvin, V. L. 2006. Low-Field Magnetic Separation of Monodisperse Fe₃O₄ Nanocrystals. *Science* 314(5801), 964-967.
- Ye, J., Liu, S., Tian, M., Li, W., Hu, B., Zhou, W. and Jia, Q. 2014. Preparation and characterization of magnetic nanoparticles for the on-line determination of gold, palladium, and platinum in mine samples based on flow injection micro-column preconcentration coupled with graphite furnace atomic absorption spectrometry. *Talanta* 118 231-237.
- Yeap, S. P., Lim, J., Ooi, B. S. and Ahmad, A. L. 2017. Agglomeration, colloidal stability, and magnetic separation of magnetic nanoparticles: collective influences on environmental engineering applications. *Journal of Nanoparticle Research* 19(11).
- Yogo, T., Nakamura, T., Sakamoto, W. and Hirano, S. 2011. Synthesis of transparent magnetic particle/organic hybrid film using iron-organics. *Journal of Materials Research* 15(10), 2114-2120.
- Yokoyama, T. 2012. Chapter 1 - Basic properties and measuring methods of nanoparticles. *Nanoparticle Technology Handbook (Second Edition)*. M. Hosokawa, K. Nogi, M. Naito and T. Yokoyama. Amsterdam, Elsevier, 3-48.
- Yu, H., Zi, F., Hu, X., Nie, Y., Chen, Y. and Cheng, H. 2018. Adsorption of gold from thiosulfate solutions with chemically modified activated carbon. *Adsorption Science & Technology* 36(1-2), 408-428.
- Yu, H. Z., Hu, F., Nie, X., Xiang, Y., Xu, P. and Jiao; Chi, H. 2015. Adsorption of the gold-thiosulfate complex ion onto cupric ferrocyanide (CuFC)-impregnated activated carbon in aqueous solutions. *Hydrometallurgy* 154 111-117.
- Yuan, Y., Rende, D., Altan, C. L., Bucak, S., Ozisik, R. and Borca-Tasciuc, D. A. 2012. Effect of surface modification on magnetization of iron oxide nanoparticle colloids. *Langmuir* 28(36), 13051-13059.
- Yuwei, C. and Jianlong, W. 2011. Preparation and characterization of magnetic chitosan nanoparticles and its application for Cu(II) removal. *Chemical Engineering Journal* 168(1), 286-292.
- Zakharov, S., Vaneckova, M., Seidl, Z., Diblik, P., Kuthan, P., Urban, P., Navratil, T. and Pelclova, D. 2015. Successful Use of Hydroxocobalamin and Sodium Thiosulfate in Acute Cyanide Poisoning: A Case Report with Follow-up. *Basic & Clinical Pharmacology & Toxicology* 117(3), 209-212.
- Zhang, H., Dai, X. and Breuer., P. 2013a. Factors affecting gold leaching in thiosulfate-O₂ solutions. *ALTA 2013 Gold-PM Proceedings*, Perth, Australia.

- Zhang, H. and Dreisinger, D. 2003a. Gold recovery from thiosulfate leaching. US 6,632,264 B2.
- Zhang, H. and Dreisinger, D. 2003b. US patent 6632264 B2, Gold recovery from thiosulfate leaching.
- Zhang, H. and Dreisinger, D. B. 2002. The adsorption of gold and copper onto ion-exchange resins from ammoniacal thiosulfate solutions. *Hydrometallurgy* 66(1-3), 67-76.
- Zhang, H., Nicol, M. J. and Staunton, W. P. 2005. An electrochemical study of an alternative process for the leaching of gold in thiosulfate solutions. *International Symposium on the Treatment of Gold Ore*, Calgary, Alberta.
- Zhang, L., Li, Y., Yu, J. C., Chen, Y. Y. and Chan, K. M. 2014. Assembly of polyethylenimine-functionalized iron oxide nanoparticles as agents for DNA transfection with magnetofection technique. *J. Mater. Chem. B* 2(45), 7936-7944.
- Zhang, S. 2004. Oxidation of refractory gold concentrates and simultaneous dissolution of gold in aerated alkaline solutions. Doctor of Philosophy, Murdoch University, Australia.
- Zhang, S. and Nicol, M. J. 2005. An electrochemical study of the dissolution of gold in thiosulfate solutions. Part II. Effect of Copper. *Journal of Applied Electrochemistry* 35(3), 339-345.
- Zhang, X., Niu, Y., Meng, X., Li, Y. and Zhao, J. 2013b. Structural evolution and characteristics of the phase transformations between α -Fe₂O₃, Fe₃O₄ and γ -Fe₂O₃ nanoparticles under reducing and oxidizing atmospheres. *CrystEngComm* 15(40), 8166.
- Zhang, Y., Wang, G., Yang, L., Wang, F. and Liu, A. 2018. Recent advances in gold nanostructures based biosensing and bioimaging. *Coordination Chemistry Reviews* 370 1-21.
- Zhang, Y., Xu, Q., Zhang, S., Liu, J., Zhou, J., Xu, H., Xiao, H. and Li, J. 2013c. Preparation of thiol-modified Fe₃O₄@SiO₂ nanoparticles and their application for gold recovery from dilute solution. *Separation and Purification Technology* 116 391-397.
- Zhao, J., Wu, Z. and Chen, J. 1997. Extraction of gold from thiosulfate solutions with alkyl phosphorus esters. *Hydrometallurgy* 46(3), 363-372.
- Zhao, J., Wu, Z. and Chen, J. 1998. Extraction of gold from thiosulfate solutions using amine mixed with neutral donor reagents. *Hydrometallurgy* 48(2), 133-144.
- Zhao, J. I. N., Wu, Z. and Chen, J. C.-Y. 1999. Separation of Gold from Other Metals in Thiosulfate Solutions by Solvent Extraction. *Separation Science and Technology* 34(10), 2061-2068.
- Zhou, J. Y. and Cabri, L. J. 2004. Gold Process Mineralogy- Objectives, techniques, and applications. *JOM* 49-52.
- Zhou, X. and Zhou, X. 2014. The unit problem in the thermodynamic calculation of adsorption using the langmuir equation. *Chemical Engineering Communications* 201(11), 1459-1467.

Every reasonable effort has been made to acknowledge the owners of copyright material. I would be pleased to hear from any copyright owner who has been omitted or incorrectly acknowledged.

Appendices

Appendix A Other Adsorbents Attempted

A few different nanomagnetic adsorbents were tested in attempts to adsorb anionic gold thiosulfate from simulated leaching solutions and from pure gold thiosulfate solutions (on some occasions only). Adsorption experiments were conducted with conditions kept consistent (pH, temperature, solution volume, stirring speed, adsorbent dosage) and these were followed by magnetic separation and solution analysis for gold. A constant adsorbent dosage (5 g/L) value was used for comparison and the effect of the adsorbent dosage was not taken under consideration. The adsorbent(s) which showed high relative adsorption efficiency was selected and others were discontinued. No comprehensive particle characterisation was conducted for those adsorbents. However all the adsorbents tested are briefly detailed in the following sections, and listed in Table App A.1.

The competence of bare MNPs to adsorb gold from alkaline pH solutions was evaluated, although it was anticipated that the adsorption efficiency would be almost zero or very low as a result of the negative surface charge of particle surfaces in alkaline solutions. The purpose therefore, was to compare the MNPs with the surface coated nanoparticles. The surface coating was carried out as mentioned in Section 3.3. The specifications of the sourced nanoparticles, surface coatings and corresponding gold adsorption efficiencies are given in Table App A.1. below.

As expected, bare MNPs were unable to adsorb gold from thiosulfate leaching solutions under the tested conditions. Therefore, to see if a change could be effected, a surface coating was carried out using trisodium citrate and PEI. It is apparent that adsorption efficiency increased when the nanoparticle size was decreased. MNP 5 evidenced very low adsorption efficiency although this improved substantially when smaller particles were used (MNP 1). Similar behaviour was displayed in MNP 4 vs MNP 2 and MNP 3.

According to gold adsorption efficiency values, MNP 1, MNP 2 and MNP 3 demonstrated high gold adsorption amongst the tested adsorbents. Of these three candidates, MNP 1 (PEI coated magnetite, 15-20 nm) was chosen as the other two adsorbents were less efficient in magnetic separation. It is well known that the saturation magnetisation of magnetite is higher than maghemite. It was later identified that MNP 1 (known as PEI-MNPs) is also a mixture of magnetite and maghemite. However, the magnetic separation was faster than with pure maghemite alone.

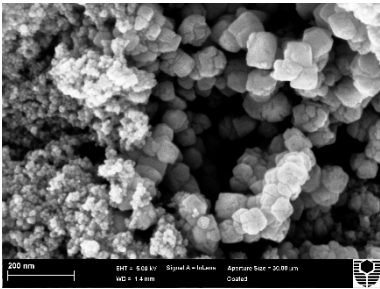
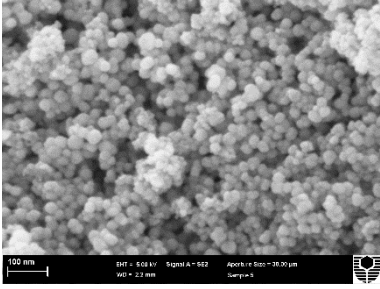
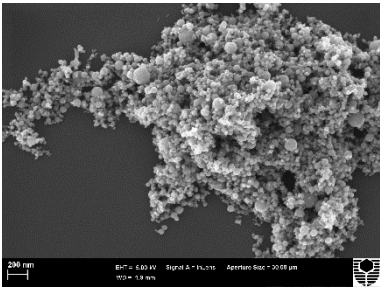
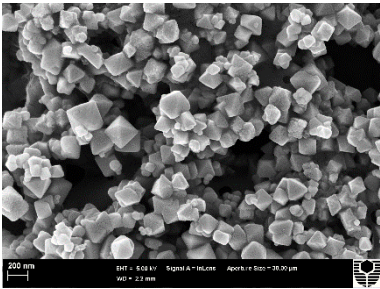
Table App A.1. Different magnetic nanoparticles attempted in the study

Reference	Magnetic core (description as per manufacturer)	Size and morphology (based on SEM)	Surface coating	Au adsorption efficiency	
				pure AuTS solution	synthetic leach solution
MNP 1	Magnetite 15-20 nm	13-84 nm, spherical/ cubodial	Uncoated (Bare MNPs)		0%
			Citrate and PEI _{25K} coated (PEI-MNPs)	100%	33%
			Citrate and PEI ₈₀₀ coated	-	10%
MNP 2	Maghemite (20 nm)	spherical	Citrate and PEI coated	96%	31%
MNP 3	Maghemite (Reade), 20-40 nm	15-60 nm, spherical	Citrate and PEI coated		32%
MNP 4	Maghemite, <50 nm (SA)	11-88 nm, spherical	Citrate and PEI coated	-	24%
MNP 5	Magnetite (black), 50-100 nm	50-300 nm, cubodial	Citrate and PEI coated	92%	8%

At a 5 g/L NP dosage, 50 °C and pH 8

After considering the adsorption efficiency and ease of magnetic separation, MNP 1 was chosen as the only adsorbent to be considered for gold adsorption studies. A comprehensive particle characterisation before and after coating, as well as after metal adsorption was conducted, as discussed in Section 4.3. MNP1 was first coated with trisodium citrate followed by polyethylenimine, as discussed in Sections 4.2.1 and 4.2.2. and designated as PEI-MNPs throughout the thesis.

An images of MNPs use are listed in Table below.

Name	Nanopowder Image	SEM image
MNP 1		
MNP 2		No SEM image available
MNP 3		
MNP 4		
MNP 5		

Appendix B Detailed Methods and Specifications of the Instruments used for Characterisation

B.1 XPS

X-ray photoelectron spectroscopy (XPS) measurements were performed on a Kratos Axis Ultra DLD spectrometer using a monochromatic Al K α (1486.6 eV) irradiation source operated at 225 W. The electron binding energy scale was calibrated for each sample by setting the main line of the C 1s spectrum to 284.8 eV. XPS spectra were collected with a pass energy of 160 eV for the survey spectra and 40 eV for the high-resolution spectra. Data files were processed using CasaXPS software and interpreted using relative sensitivity factors provided by the instrument manufacturer (Kratos) as a guide. Background subtractions using a Shirley background were applied to all high-resolution spectra. Each high-resolution spectra was fitted with a Gaussian-Lorentzian (70%-30%) line shape with the full-width half maximum (FWHM) constrained to values considered reasonable for each element.

B.2 XRD and QXRD

XRD analysis of the crystalline phase of nanopowder samples was performed with a Bruker D8 Advance Powder Diffractometer (Bruker AXS, Germany) with a Co K α radiation source ($\lambda=1.79\text{\AA}$) run at 35kV voltage and 40 mA current with a LynxEye detector. The scanning parameters were in the 5-120 degree range (2 theta), with a 0.0008 step size used for 3s each and the sample was run for 12 hours. The nanoparticles were suspended in few drops of absolute ethanol and the suspension was pipetted onto low background sample holders and allowed to air dry before the XRD measurements were taken. Crystalline phases were identified by using the Search/Match algorithm, DIFFRAC. EVA. 3.2 (Bruker-AXS, Germany) to search for the Powder Diffraction File (PDF).

The QXRD analyses were performed in a PANalytical X'Pert Pro PW3040 diffractometer at 40 kW of voltage and with a 40 mA current under Co K α radiation ($\lambda=1.79\text{\AA}$). The 2θ values ranged from 5° to 80° at a step size of 0.0167°. Mineral identification was undertaken using the X'Pert HighScore Plus search/match software.

B.3 HPLC

To analyse thiosulfate and polythionates, a Waters 2695 HPLC separation module was used with the separation being effected using a Thermo Scientific™ Dionex™ IonPac AS16 (4 mm) ion exchange column equipped with a Thermo Scientific™ Dionex™ IonPac AG16 (4 mm) guard column. All the analytes were detected using UV with a Waters 2998 Photodiode Array Detector. A pump flow rate of 1 mL/min was used (0.35 M NaClO₄·H₂O), at room temperature. The Empower™ software package (Waters Corporation) was used to control the HPLC and calculate peak areas. Thiosulfate, tetra- to hexa-thionate was integrated at 214 nm and trithionate was integrated at 192 nm.

For the analysis of the non-UV active sulfate, a Waters 2695 HPLC separation module was used, by suppressed conductivity detection (Dionex AMMS 300 suppressor and Water 432 conductivity detector). The separation was effected using a Thermo Scientific™ Dionex™ IonPac AS17 (4 mm) anion exchange column equipped with Thermo Scientific™ Dionex™ IonPac AG20 and AG17 (both 4 mm) guard columns. A step change gradient elution method using a sodium hydroxide/acetonitrile mixture (with increasing percentage of hydroxide) was chosen as the mobile phase with this column as it facilitated the separation of sulfate and sulfite ions (low percentage hydroxide) as well as providing a rapid exchange of the strongly adsorbing oxy-sulfur anion species.

Appendix C Hydrodynamic Size Data by DLS

Table App C.1. DLS size measurements

Sample description	Intensity weighted Z-Ave (nm)	average size (nm)	PdI	Pk 1	Pk 2	Pk 3
				Mean Int	Mean Int	Mean Int
				d (nm)		
PEI-MNPs, surfactant, 30S	554.8	517.7667	0.813	1194	234.7	5150
	385.3		0.569	247.6	714.5	4879
	613.2		0.679	495.8	161.3	5385
PEI-MNPs, surfactant, 300S	263.1	294.4667	0.409	254.4	2956	0
	250.2		0.432	180.9	706.4	4597
	370.1		0.688	536	170.6	4829
PEI-MNPs, surfactant, 600S	209.7	207.9667	0.335	290.1	4904	0
	209.9		0.364	271.6	4235	36.26
	204.3		0.396	188.5	1007	0
PEI-MNPs, DI water, 30S	334.3	321.7	0.404	455.6	4885	0
	325.5		0.432	356.4	4586	0
	305.3		0.397	379.8	4589	51.05
PEI-MNPs, DI water, 300S	300.2	271.6333	0.464	547.9	4016	0
	295.5		0.473	319.8	3004	0
	219.2		0.385	359.8	3949	0
PEI-MNPs, DI water, 600S	203.7	207.3	0.361	406.5	4515	0
	200.1		0.36	231.1	4316	0
	218.1		0.412	272.1	71.66	4432
Bare MNPs, citrate solution, 600S sonication	120.6	115	0.368	168.5	4640	0
	112.1		0.367	153.1	4733	0
	112.3		0.389	164.7	4463	0
PEI-MNPs	181.2	175.7333	0.231	195.9	4937	0
	174.3		0.254	192.9	4534	36.61
	171.7		0.237	202.8	4901	0
Metal adsorbed MNPs	221.1	211.8667	0.272	275.1	4735	0
	208.5		0.264	231.3	4301	0
	206		0.272	235.7	2732	0

Appendix D Different Metal Elution Systems

Different eluants were used on trial and error basis to find the most promising eluant(s) for this particular system. Few eluants were selected based on the literature review and some eluants which have been used for metal elution from IX resins were used for comparison purposes. The optimum eluant should demonstrate higher elution efficiency, should be selective, should non-damaging and preserve the adsorption capacity of the adsorbent, and cost effective. In this study, a two-step elution process comprised of a copper pre-elution step followed by gold elution was the most promising technique and discussed in Chapter 6. Other eluant systems used are briefly discussed in the following sections.

D.1 NaOH

Gold and copper loaded PEI-MNPs were mixed with NaOH solutions at pH 12 separately at 25 °C and 50 °C solution temperatures. Sample aliquots were collected at predetermined time intervals for gold and copper analysis of up to six hours. Non selective metal elution was observed while gold elution efficiency was higher than that of copper at both 25 °C and 50 °C temperatures. The possible mechanism behind this method is the loss of electrostatic attraction due to the pH change in the solution above pH_{PZC} (pH 11), which reverses the adsorption process. According to isotherm and thermodynamic studies, the gold adsorption mechanism was physical adsorption and the adsorption process was exothermic. The copper adsorption mechanism was not determined. In this study, 100% gold elution was achieved at 50 °C temperature in 5 minutes while it was only 36% at 25 °C. However, a drop in the gold elution efficiency was observed at 50 °C. As the gold adsorption mechanism was determined as physisorption, 100% gold elution was achieved at 50 °C while copper elution was around 40% at the same temperature. The adsorption mechanism for copper may be a combination of chemisorption and physisorption while only physically adsorbed copper is desorbed at this occasion. This method was discontinued due to non-selective metal elution.

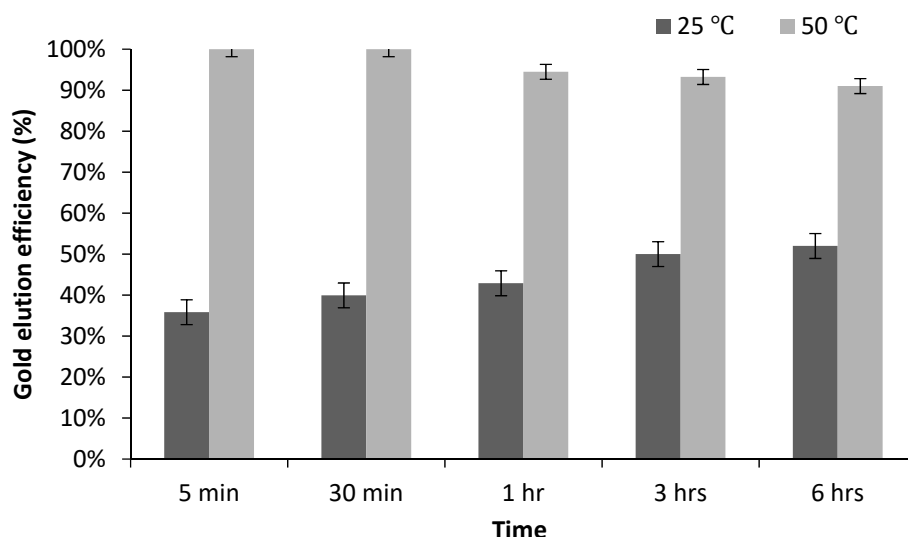


Figure App D.1 Gold elution efficiency at different temperatures by NaOH at pH 12

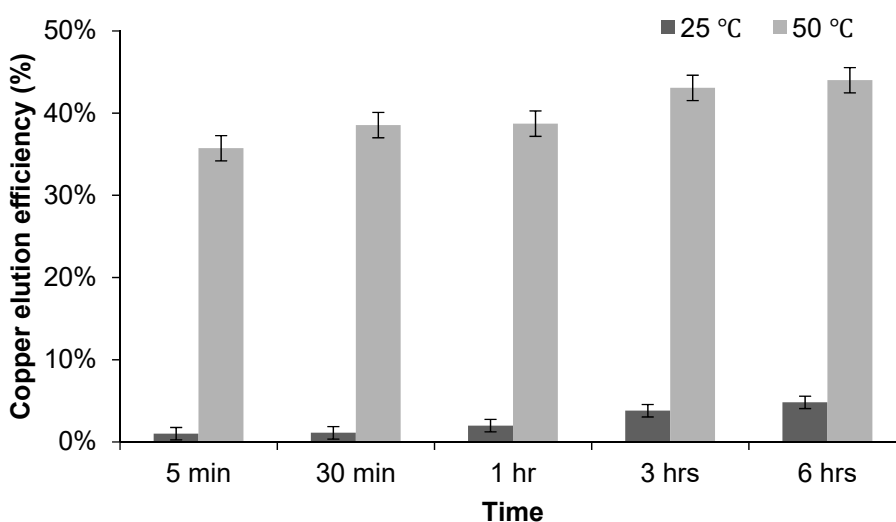


Figure App D.2 Copper elution efficiency at different temperatures by NaOH at pH 12

D.2 HCl

Diluted HCl has been reported as a promising eluant for copper desorption from magnetic nano adsorbents, as discussed in Section 2.9.3. Therefore, HCl solutions at three different concentrations were used for metal elution from PEI-MNPs at a temperature of 25 °C for up to four hours in this study. As shown in Table App D.1., at a pH of 2 (0.01M HCl) and pH 2.5 both gold and copper were eluted to some extent while no metal elution was observed at pH 3 (0.001M) HCl solution. A slight dissolution of adsorbent was noticed in pH 2 and pH 2.5 solutions, leaching Fe back into the eluant solution. In addition, non-selective metal elution and potential osmotic shock on MNPs due to sudden change in pH at subsequent gold elution step make this method undesirable.

Table App D.1. Metal elution with HCl as the eluant

Time	Elution efficiency (%)					
	pH 2		pH 2.5		pH 3	
	Au	Cu	Au	Cu	Au	Cu
30 min	14%	55%	8%	10%	0%	0%
4 hours	34%	70%	13%	20%	0%	0.5%

D.3 Glycine

Glycine solutions (0.1M) at different pH values (6, 9 and 11) and temperatures (25 and 50 °C) were investigated for metal elution. Sample aliquots were collected at 15 min, 30 min, 1 hour and 3 hours for analysis and the results are listed in Table App D.2. and Table App D.3. The ability to form strong complexes with copper is the main reason for trying glycine solutions as an eluant in this study. The stability constant of different copper-glycine complexes range from 8.15 to 15.6 (Martell and Smith 1974, Aksu and Doyle 2001). It is obvious that the elution efficiencies of both metals are negligible for the tested conditions, except approximately 40% and 50% of gold elution in a solution at pH 11 at 27 °C and 50 °C temperatures respectively, after 3 hours. These noticeable elution efficiencies at pH 11 may due to the natural desorption of adsorbed metal as a result of loss of electrostatic attraction in between adsorbates and adsorbent as the PEI-MNPs surface charge is almost zero at this pH value (pH_{pzc} is 11). The insignificant copper elution, even at higher pH values, is questionable, possibly due to the insufficient amount of glycine in the solution. However, further investigations were not carried out on the use of glycine as the eluant for nanoparticles did not seem to be very promising.

Table App D.2. Gold elution efficiencies with 0.1 M glycine solutions

Temperature	27°C			50°C		
	pH 6	pH 9	pH 11	pH 6	pH 9	pH 11
15 min	2%	4%	36%	1%	3%	52%
30 min	2%	4%	38%	1%	3%	52%
1 hour	2%	4%	39%	1%	3%	55%
3 hours	2%	4%	41%	2%	3%	50%

Table App D.3. Copper elution efficiencies with 0.1 M glycine solutions

Temperature	27°C			50°C		
	pH 6	pH 9	pH 11	pH 6	pH 9	pH 11
15 min	1%	1%	1%	1%	2%	2%
30 min	1%	1%	1%	1%	2%	3%
1 hour	1%	1%	2%	2%	2%	4%
3 hours	2%	1%	3%	5%	4%	8%

D.4 Thiosulfate, Sulfite and Chloride

Copper pre elution with ammonium thiosulfate and gold elution with a mixture of sodium sulfite and sodium chloride combinations are promising eluants for gold and copper elution from IX resins (Jeffrey et al. 2010). Although the adsorption mechanisms could be different in IX resins and MNPs, this method was tested for comparison purposes. Firstly, metal loaded PEI-MNPs were mixed with 0.5 M ammonium thiosulfate solutions for six hours at pH 9.5 at 25 °C. Samples were collected for analysis and then the particles were washed with DI water before mixing with 0.1M sodium sulfite and 1M sodium chloride at pH 9.5 and 60 °C.

An average of 84% gold elution and an average of 28% copper elution was achieved in 0.5M ammonium thiosulfate solution as the eluant at pH 9.5 and 25 °C temperature. At the next stage, with 0.1M sodium sulfite and 1M sodium chloride, at a pH of 9.5 and at a temperature of 60 °C, no gold elution was observed, while an average of 26% copper elution efficiency was achieved. The results were not as expected such that gold elution was higher with copper eluant (ammonium thiosulfate) and vice versa. Besides this, non-selective metal elution was observed, which potentially hinders the purity of final gold product. Due to these limitations, this eluant combination was considered as undesirable and no further experiments were conducted.

Appendix E Co-Author Attribution Statement

To Whom It May Concern

I, Nirmala Damayanthi Ilankoon, the primary author of the following two publications forming part of this thesis, contributed to the conception of the project, design of experimental protocol, data collection, analysis and interpretation and also drafted all of the paper manuscripts.

List of Publications

- **Ilankoon, N. D., Aldrich, C., Oraby, E. A. and Eksteen, J. J. 2020.** Use of polyethylenimine functionalised magnetic nanoparticles for gold thiosulfate recovery. *Hydrometallurgy* 195.
- **Ilankoon, N. D., Aldrich, C., Oraby, E. A. and Eksteen, J. J. 2019.** Extraction of Gold and Copper from a Gold Ore Thiosulfate Leachate by Use of Functionalized Magnetic Nanoparticles. *Mineral Processing and Extractive Metallurgy Review* 1-12.

The co-authors contributed by supervision of the research work, proof reading and suggesting the necessary amendments in the manuscript.

Name of candidate : Nirmala Damayanthi Ilankoon

Signature

I, as a Co-Author, endorse that this level of contribution by the candidate indicated above is appropriate.

Name of co-author 1 : Professor Chris Aldrich

Signature

Name of co-author 2 : Dr Elsayed A. Oraby

Signature

Name of co-author 3 : Professor Jacques Eksteen

Signature

Appendix F Permission Statements

The permissions granted to use some of the third-party copyright materials such as figures from the published journals papers are attached to this section.

1/25/2020

RightsLink Printable License

ELSEVIER LICENSE TERMS AND CONDITIONS

Jan 25, 2020

This Agreement between GPO Box U1987, Perth, WA 6845, Australia ("You") and Elsevier ("Elsevier") consists of your license details and the terms and conditions provided by Elsevier and Copyright Clearance Center.

License Number	4743871270602
License date	Jan 07, 2020
Licensed Content Publisher	Elsevier
Licensed Content Publication	Hydrometallurgy
Licensed Content Title	Leaching and recovery of gold using ammoniacal thiosulfate leach liquors (a review)
Licensed Content Author	Andrew C Grosse, Greg W Dicoski, Matthew J Shaw, Paul R Haddad
Licensed Content Date	Apr 1, 2003
Licensed Content Volume	69
Licensed Content Issue	1-3
Licensed Content Pages	21
Start Page	1
End Page	21
Type of Use	reuse in a thesis/dissertation

<https://s100.copyright.com/CustomAdmin/PLF.jsp?ref=405fbfb0-97f9-4028-b782-2b146bf35761>

1/7

1/25/2020

RightsLink Printable License

Portion figures/tables/illustrations

Number of figures/tables/illustrations 2

Format both print and electronic

Are you the author of this Elsevier article? No

Will you be translating? No

Title Adsorption of Gold from Thiosulfate Leaching Solutions using Polyethylenimine Functionalised Magnetic Nanoparticles

Institution name Curtin University

Expected presentation date Jan 2020

Portions A part of Figure 1 and the Figure 2

GPO Box U1987, Perth, WA 6845, Australia
GPO Box U1987, Perth, WA 6845, Australia

Requestor Location Bentley, WA 6102
Australia
Attn: GPO Box U1987, Perth, WA 6845, Australia

Publisher Tax ID GB 494 6272 12

Total 0.00 AUD

Terms and Conditions

INTRODUCTION

1. The publisher for this copyrighted material is Elsevier. By clicking "accept" in connection with completing this licensing transaction, you agree that the following terms and conditions apply to this transaction (along with the Billing and Payment terms and conditions established by Copyright Clearance Center, Inc. ("CCC"), at the time that you opened your Rightslink account and that are available at any time at <http://myaccount.copyright.com>).

GENERAL TERMS

<https://s100.copyright.com/CustomAdmin/PLF.jsp?ref=405fbfb0-97f9-4028-b782-2b146bf35761>

2/7

ELSEVIER LICENSE
TERMS AND CONDITIONS

Jan 21, 2020

This Agreement between GPO Box U1987, Perth, WA 6845, Australia ("You") and Elsevier ("Elsevier") consists of your license details and the terms and conditions provided by Elsevier and Copyright Clearance Center.

License Number	4743881237230
License date	Jan 07, 2020
Licensed Content Publisher	Elsevier
Licensed Content Publication	Journal of Hazardous Materials
Licensed Content Title	Kinetics and equilibrium of desorption removal of copper from magnetic polymer adsorbent
Licensed Content Author	Jyi-Yeong Tseng, Ching-Yuan Chang, Chiung-Fen Chang, Yi-Hung Chen, Chia-Chi Chang, Dar-Ren Ji, Chun-Yu Chiu, Pen-Chi Chiang
Licensed Content Date	Nov 15, 2009
Licensed Content Volume	171
Licensed Content Issue	1-3
Licensed Content Pages	8
Start Page	370
End Page	377
Type of Use	reuse in a thesis/dissertation

1/21/2020

RightsLink Printable License

Portion figures/tables/illustrations

Number of figures/tables/illustrations 1

Format both print and electronic

Are you the author of this Elsevier article? No

Will you be translating? No

Title Adsorption of Gold from Thiosulfate Leaching Solutions using Polyethylenimine Functionalised Magnetic Nanoparticles

Institution name Curtin University

Expected presentation date Jan 2020

Portions Figure 9

GPO Box U1987, Perth, WA 6845, Australia
GPO Box U1987, Perth, WA 6845, Australia

Requestor Location Bentley, WA 6102
Australia
Attn: GPO Box U1987, Perth, WA 6845, Australia

Publisher Tax ID GB 494 6272 12

Total 0.00 USD

Terms and Conditions

INTRODUCTION

1. The publisher for this copyrighted material is Elsevier. By clicking "accept" in connection with completing this licensing transaction, you agree that the following terms and conditions apply to this transaction (along with the Billing and Payment terms and conditions established by Copyright Clearance Center, Inc. ("CCC"), at the time that you opened your Rightslink account and that are available at any time at <http://myaccount.copyright.com>).

GENERAL TERMS

<https://s100.copyright.com/CustomAdmin/PLF.jsp?ref=ea9acba1-b880-49ec-bbfc-4c3f187b6e3f>

2/7

ELSEVIER LICENSE
TERMS AND CONDITIONS

Jan 25, 2020

This Agreement between GPO Box U1987, Perth, WA 6845, Australia ("You") and Elsevier ("Elsevier") consists of your license details and the terms and conditions provided by Elsevier and Copyright Clearance Center.

License Number	4743880403661
License date	Jan 07, 2020
Licensed Content Publisher	Elsevier
Licensed Content Publication	Advances in Colloid and Interface Science
Licensed Content Title	Surface properties of magnetite in high temperature aqueous electrolyte solutions: A review
Licensed Content Author	Sonja M. Vidojkovic, Marko P. Rakin
Licensed Content Date	Jul 1, 2017
Licensed Content Volume	245
Licensed Content Issue	n/a
Licensed Content Pages	22
Start Page	108
End Page	129
Type of Use	reuse in a thesis/dissertation

1/25/2020

RightsLink Printable License

Portion figures/tables/illustrations

Number of figures/tables/illustrations 1

Format both print and electronic

Are you the author of this Elsevier article? No

Will you be translating? No

Title Adsorption of Gold from Thiosulfate Leaching Solutions using Polyethylenimine Functionalised Magnetic Nanoparticles

Institution name Curtin University

Expected presentation date Jan 2020

Portions Figure 1 (reproduced)

GPO Box U1987, Perth, WA 6845, Australia
GPO Box U1987, Perth, WA 6845, Australia

Requestor Location Bentley, WA 6102
Australia
Attn: GPO Box U1987, Perth, WA 6845, Australia

Publisher Tax ID GB 494 6272 12

Total 0.00 USD

Terms and Conditions

INTRODUCTION

1. The publisher for this copyrighted material is Elsevier. By clicking "accept" in connection with completing this licensing transaction, you agree that the following terms and conditions apply to this transaction (along with the Billing and Payment terms and conditions established by Copyright Clearance Center, Inc. ("CCC"), at the time that you opened your Rightslink account and that are available at any time at <http://myaccount.copyright.com>).

GENERAL TERMS

<https://s100.copyright.com/CustomAdmin/PLF.jsp?ref=e98c299a-04b3-44db-b9af-42da5a1ada03>

2/7

ELSEVIER LICENSE
TERMS AND CONDITIONS

Jan 25, 2020

This Agreement between GPO Box U1987, Perth, WA 6845, Australia ("You") and Elsevier ("Elsevier") consists of your license details and the terms and conditions provided by Elsevier and Copyright Clearance Center.

License Number	4743881020318
License date	Jan 07, 2020
Licensed Content Publisher	Elsevier
Licensed Content Publication	Elsevier Books
Licensed Content Title	Gold Ore Processing
Licensed Content Author	M.G. Aylmore
Licensed Content Date	Jan 1, 2016
Licensed Content Pages	39
Start Page	485
End Page	523
Type of Use	reuse in a thesis/dissertation
Portion	figures/tables/illustrations
Number of figures/tables/illustrations	1

1/25/2020

RightsLink Printable License

Format both print and electronic

Are you the author of this Elsevier chapter? No

Will you be translating? No

Title Adsorption of Gold from Thiosulfate Leaching Solutions using Polyethylenimine Functionalised Magnetic Nanoparticles

Institution name Curtin University

Expected presentation date Jan 2020

Portions Figure 28.8c (reproduced)

GPO Box U1987, Perth, WA 6845, Australia
GPO Box U1987, Perth, WA 6845, Australia

Requestor Location Bentley, WA 6102
Australia
Attn: GPO Box U1987, Perth, WA 6845, Australia

Publisher Tax ID GB 494 6272 12

Total 0.00 USD

Terms and Conditions

INTRODUCTION

1. The publisher for this copyrighted material is Elsevier. By clicking "accept" in connection with completing this licensing transaction, you agree that the following terms and conditions apply to this transaction (along with the Billing and Payment terms and conditions established by Copyright Clearance Center, Inc. ("CCC"), at the time that you opened your Rightslink account and that are available at any time at <http://myaccount.copyright.com>).

GENERAL TERMS

2. Elsevier hereby grants you permission to reproduce the aforementioned material subject to the terms and conditions indicated.

3. Acknowledgement: If any part of the material to be used (for example, figures) has appeared in our publication with credit or acknowledgement to another source, permission must also be sought from that source. If such permission is not obtained then that material

<https://s100.copyright.com/CustomAdmin/PLF.jsp?ref=9795d80d-ce79-44f7-ae87-e4fceb968a16>

2/7

may not be included in your publication/copies. Suitable acknowledgement to the source must be made, either as a footnote or in a reference list at the end of your publication, as follows:

"Reprinted from Publication title, Vol /edition number, Author(s), Title of article / title of chapter, Pages No., Copyright (Year), with permission from Elsevier [OR APPLICABLE SOCIETY COPYRIGHT OWNER]." Also Lancet special credit - "Reprinted from The Lancet, Vol. number, Author(s), Title of article, Pages No., Copyright (Year), with permission from Elsevier."

4. Reproduction of this material is confined to the purpose and/or media for which permission is hereby given.

5. Altering/Modifying Material: Not Permitted. However figures and illustrations may be altered/adapted minimally to serve your work. Any other abbreviations, additions, deletions and/or any other alterations shall be made only with prior written authorization of Elsevier Ltd. (Please contact Elsevier at permissions@elsevier.com). No modifications can be made to any Lancet figures/tables and they must be reproduced in full.

6. If the permission fee for the requested use of our material is waived in this instance, please be advised that your future requests for Elsevier materials may attract a fee.

7. Reservation of Rights: Publisher reserves all rights not specifically granted in the combination of (i) the license details provided by you and accepted in the course of this licensing transaction, (ii) these terms and conditions and (iii) CCC's Billing and Payment terms and conditions.

8. License Contingent Upon Payment: While you may exercise the rights licensed immediately upon issuance of the license at the end of the licensing process for the transaction, provided that you have disclosed complete and accurate details of your proposed use, no license is finally effective unless and until full payment is received from you (either by publisher or by CCC) as provided in CCC's Billing and Payment terms and conditions. If full payment is not received on a timely basis, then any license preliminarily granted shall be deemed automatically revoked and shall be void as if never granted. Further, in the event that you breach any of these terms and conditions or any of CCC's Billing and Payment terms and conditions, the license is automatically revoked and shall be void as if never granted. Use of materials as described in a revoked license, as well as any use of the materials beyond the scope of an unrevoked license, may constitute copyright infringement and publisher reserves the right to take any and all action to protect its copyright in the materials.

9. Warranties: Publisher makes no representations or warranties with respect to the licensed material.

10. Indemnity: You hereby indemnify and agree to hold harmless publisher and CCC, and their respective officers, directors, employees and agents, from and against any and all claims arising out of your use of the licensed material other than as specifically authorized pursuant to this license.

11. No Transfer of License: This license is personal to you and may not be sublicensed, assigned, or transferred by you to any other person without publisher's written permission.

12. No Amendment Except in Writing: This license may not be amended except in a writing signed by both parties (or, in the case of publisher, by CCC on publisher's behalf).

13. Objection to Contrary Terms: Publisher hereby objects to any terms contained in any purchase order, acknowledgment, check endorsement or other writing prepared by you, which terms are inconsistent with these terms and conditions or CCC's Billing and Payment terms and conditions. These terms and conditions, together with CCC's Billing and Payment

terms and conditions (which are incorporated herein), comprise the entire agreement between you and publisher (and CCC) concerning this licensing transaction. In the event of any conflict between your obligations established by these terms and conditions and those established by CCC's Billing and Payment terms and conditions, these terms and conditions shall control.

14. **Revocation:** Elsevier or Copyright Clearance Center may deny the permissions described in this License at their sole discretion, for any reason or no reason, with a full refund payable to you. Notice of such denial will be made using the contact information provided by you. Failure to receive such notice will not alter or invalidate the denial. In no event will Elsevier or Copyright Clearance Center be responsible or liable for any costs, expenses or damage incurred by you as a result of a denial of your permission request, other than a refund of the amount(s) paid by you to Elsevier and/or Copyright Clearance Center for denied permissions.

LIMITED LICENSE

The following terms and conditions apply only to specific license types:

15. **Translation:** This permission is granted for non-exclusive world **English** rights only unless your license was granted for translation rights. If you licensed translation rights you may only translate this content into the languages you requested. A professional translator must perform all translations and reproduce the content word for word preserving the integrity of the article.

16. **Posting licensed content on any Website:** The following terms and conditions apply as follows: Licensing material from an Elsevier journal: All content posted to the web site must maintain the copyright information line on the bottom of each image; A hyper-text must be included to the Homepage of the journal from which you are licensing at <http://www.sciencedirect.com/science/journal/xxxx> or the Elsevier homepage for books at <http://www.elsevier.com>; Central Storage: This license does not include permission for a scanned version of the material to be stored in a central repository such as that provided by Heron/XanEdu.

Licensing material from an Elsevier book: A hyper-text link must be included to the Elsevier homepage at <http://www.elsevier.com>. All content posted to the web site must maintain the copyright information line on the bottom of each image.

Posting licensed content on Electronic reserve: In addition to the above the following clauses are applicable: The web site must be password-protected and made available only to bona fide students registered on a relevant course. This permission is granted for 1 year only. You may obtain a new license for future website posting.

17. **For journal authors:** the following clauses are applicable in addition to the above:

Preprints:

A preprint is an author's own write-up of research results and analysis, it has not been peer-reviewed, nor has it had any other value added to it by a publisher (such as formatting, copyright, technical enhancement etc.).

Authors can share their preprints anywhere at any time. Preprints should not be added to or enhanced in any way in order to appear more like, or to substitute for, the final versions of articles however authors can update their preprints on arXiv or RePEc with their Accepted Author Manuscript (see below).

If accepted for publication, we encourage authors to link from the preprint to their formal publication via its DOI. Millions of researchers have access to the formal publications on

ScienceDirect, and so links will help users to find, access, cite and use the best available version. Please note that Cell Press, The Lancet and some society-owned have different preprint policies. Information on these policies is available on the journal homepage.

Accepted Author Manuscripts: An accepted author manuscript is the manuscript of an article that has been accepted for publication and which typically includes author-incorporated changes suggested during submission, peer review and editor-author communications.

Authors can share their accepted author manuscript:

- immediately
 - via their non-commercial person homepage or blog
 - by updating a preprint in arXiv or RePEc with the accepted manuscript
 - via their research institute or institutional repository for internal institutional uses or as part of an invitation-only research collaboration work-group
 - directly by providing copies to their students or to research collaborators for their personal use
 - for private scholarly sharing as part of an invitation-only work group on commercial sites with which Elsevier has an agreement
- After the embargo period
 - via non-commercial hosting platforms such as their institutional repository
 - via commercial sites with which Elsevier has an agreement

In all cases accepted manuscripts should:

- link to the formal publication via its DOI
- bear a CC-BY-NC-ND license - this is easy to do
- if aggregated with other manuscripts, for example in a repository or other site, be shared in alignment with our hosting policy not be added to or enhanced in any way to appear more like, or to substitute for, the published journal article.

Published journal article (JPA): A published journal article (PJA) is the definitive final record of published research that appears or will appear in the journal and embodies all value-adding publishing activities including peer review co-ordination, copy-editing, formatting, (if relevant) pagination and online enrichment.

Policies for sharing publishing journal articles differ for subscription and gold open access articles:

Subscription Articles: If you are an author, please share a link to your article rather than the full-text. Millions of researchers have access to the formal publications on ScienceDirect, and so links will help your users to find, access, cite, and use the best available version.

Theses and dissertations which contain embedded PJAs as part of the formal submission can be posted publicly by the awarding institution with DOI links back to the formal publications on ScienceDirect.

If you are affiliated with a library that subscribes to ScienceDirect you have additional private sharing rights for others' research accessed under that agreement. This includes use for classroom teaching and internal training at the institution (including use in course packs and courseware programs), and inclusion of the article for grant funding purposes.

Gold Open Access Articles: May be shared according to the author-selected end-user license and should contain a [CrossMark logo](#), the end user license, and a DOI link to the formal publication on ScienceDirect.

Please refer to Elsevier's [posting policy](#) for further information.

18. For book authors the following clauses are applicable in addition to the above:

Authors are permitted to place a brief summary of their work online only. You are not allowed to download and post the published electronic version of your chapter, nor may you scan the printed edition to create an electronic version. **Posting to a repository:** Authors are permitted to post a summary of their chapter only in their institution's repository.

19. Thesis/Dissertation: If your license is for use in a thesis/dissertation your thesis may be submitted to your institution in either print or electronic form. Should your thesis be published commercially, please reapply for permission. These requirements include permission for the Library and Archives of Canada to supply single copies, on demand, of the complete thesis and include permission for Proquest/UMI to supply single copies, on demand, of the complete thesis. Should your thesis be published commercially, please reapply for permission. Theses and dissertations which contain embedded PJAs as part of the formal submission can be posted publicly by the awarding institution with DOI links back to the formal publications on ScienceDirect.

Elsevier Open Access Terms and Conditions

You can publish open access with Elsevier in hundreds of open access journals or in nearly 2000 established subscription journals that support open access publishing. Permitted third party re-use of these open access articles is defined by the author's choice of Creative Commons user license. See our [open access license policy](#) for more information.

Terms & Conditions applicable to all Open Access articles published with Elsevier:

Any reuse of the article must not represent the author as endorsing the adaptation of the article nor should the article be modified in such a way as to damage the author's honour or reputation. If any changes have been made, such changes must be clearly indicated.

The author(s) must be appropriately credited and we ask that you include the end user license and a DOI link to the formal publication on ScienceDirect.

If any part of the material to be used (for example, figures) has appeared in our publication with credit or acknowledgement to another source it is the responsibility of the user to ensure their reuse complies with the terms and conditions determined by the rights holder.

Additional Terms & Conditions applicable to each Creative Commons user license:

CC BY: The CC-BY license allows users to copy, to create extracts, abstracts and new works from the Article, to alter and revise the Article and to make commercial use of the Article (including reuse and/or resale of the Article by commercial entities), provided the user gives appropriate credit (with a link to the formal publication through the relevant DOI), provides a link to the license, indicates if changes were made and the licensor is not represented as endorsing the use made of the work. The full details of the license are available at <http://creativecommons.org/licenses/by/4.0>.

CC BY NC SA: The CC BY-NC-SA license allows users to copy, to create extracts, abstracts and new works from the Article, to alter and revise the Article, provided this is not done for commercial purposes, and that the user gives appropriate credit (with a link to the formal publication through the relevant DOI), provides a link to the license, indicates if changes were made and the licensor is not represented as endorsing the use made of the work. Further, any new works must be made available on the same conditions. The full details of the license are available at <http://creativecommons.org/licenses/by-nc-sa/4.0>.

CC BY NC ND: The CC BY-NC-ND license allows users to copy and distribute the Article, provided this is not done for commercial purposes and further does not permit distribution of the Article if it is changed or edited in any way, and provided the user gives appropriate

credit (with a link to the formal publication through the relevant DOI), provides a link to the license, and that the licensor is not represented as endorsing the use made of the work. The full details of the license are available at <http://creativecommons.org/licenses/by-nc-nd/4.0>. Any commercial reuse of Open Access articles published with a CC BY NC SA or CC BY NC ND license requires permission from Elsevier and will be subject to a fee.

Commercial reuse includes:

- Associating advertising with the full text of the Article
- Charging fees for document delivery or access
- Article aggregation
- Systematic distribution via e-mail lists or share buttons

Posting or linking by commercial companies for use by customers of those companies.

20. Other Conditions:

v1.9

Questions? customercare@copyright.com or +1-855-239-3415 (toll free in the US) or +1-978-646-2777.